
**Doctoral Programme in Biomedicine and Pharmacy**

# Advanced Systems for Skin Delivery of Cyanocobalamin: A Model Molecule for > 1 kDa Drugs

*PhD Thesis*
**Antonio José Guillot García**

*Thesis Supervisors*
**Ana Melero Zaera**
**Teresa Mª Garrigues Pelufo**

**Valencia, 2022**

VNIVERSITAT DE VALÈNCIA

**Doctorado en Biomedicina y Farmacia**

# Advanced Systems for Skin Delivery of Cyanocobalamin: A Model Molecule for > 1 kDa Drugs


Tesis Doctoral presentada por:

**Antonio José Guillot García**

Directoras de la tesis:

**Dra. Ana Melero Zaera**

**Dra. Teresa Mª Garrigues Pelufo**



Valencia, 2022

VNIVERSITAT DE VALÈNCIA

**Doctorado en Biomedicina y Farmacia**

**Ana Melero Zaera**, Doctora en Farmacia, Profesora Titular de Universidad del Departamento de Farmacia y Tecnología Farmacéutica y Parasitología de la Universidad de Valencia, y **Teresa Mª Garrigues Pelufo**, Doctora en Farmacia, Catedrática de Universidad del Departamento de Farmacia y Tecnología Farmacéutica de la universidad de Valencia,

**CERTIFICAN:**

Que el trabajo presentado por el Gdo. en Farmacia **Antonio José Guillot García**, titulado **"Advanced Systems for Skin Delivery of Cyanocobalamin: A Model Molecule for > 1 kDa Drugs"**, para obtener el grado de Doctor con mención internacional, ha sido realizada bajo nuestra dirección y asesoramiento.

Concluido el trabajo experimental y bibliográfico, autorizamos la presentación de la Tesis, para que sea jugado por el tribunal correspondiente. Para que conste, firman el presente documento, en Valencia a 6 de junio de 2022.

Ana Melero Zaera Teresa Mª Garrigues Pelufo

7th February 2022

To Whom it May Concern

I certify that Antonio José Guillot García, with Spanish Passport number PAF384877, was at the Leicester School of Pharmacy at De Montfort University for his research stay, from the 13th September to 13th December 2021.

Antonio worked on the research project "Liposome-loaded microneedles for topical drug delivery", under the supervision of Dr. Ana Sara Cordeiro, Senior Lecturer in Pharmaceutical Sciences.

Yours sincerely

Antony D'Emanuele BPharm PhD MRPharmS CChem FRSC

Professor of Pharmaceutics and Head of the Leicester School of Pharmacy

**Leicester School of Pharmacy, De Montfort University**, The Gateway, Leicester LE1 9BH, UK
**Tel** +44 (0)116 257 7074 **| Email** antony.demanuele@dmu.ac.uk **|** Web http://www.dmu.ac.uk

This work has been funded by the following grants:

- “Atracció de Talent” fellowship of the university of Valencia (No. UV-INV-PREDOC-18F2-743816).

- University of Valencia 2019 grant (No. UV-19-INV-AE19).

- “Proyecto Emergente” from Conselleria d’Educació, Cultura i Esport (No. GV2015-054).

- This thesis is part of the grant PID2020-114530GA-I00 funded by MCIN/AEI/10.13039/501100011033.

# Agradecimientos

Todo lo que tiene un principio, tiene un fin. Y en ocasiones hay finales que, aun siendo conocidos con antelación, son difíciles de gestionar. Entre otras cosas, por saber que hay muchas personas que te han ayudado a llegar hasta este momento y resulta imposible agradecer directamente su contribución. Por tanto, todo aquel que sea olvidado a lo largo de estas líneas, pero sienta que un trozo de esta tesis es suyo, mis más sinceras disculpas.

En primer lugar, a mis directoras. Mi eterno agradecimiento a Ana, por creer siempre en mí, su guía científica, pero, sobre todo, por su preocupación e influencia a nivel personal. A Teresa, por su personalidad y entusiasmo arrollador, que han permitido mejorar constantemente el trabajo realizado.

A Sara, por dejarme entrar en su laboratorio, confianza y, literalmente, permitirme campar a mis anchas. Sin duda, la estancia ha sido una de las paradas más valiosas de este viaje. A las profesoras Mª Carmen Montesinos, Rosa Giner y Mª Carmen Recio, por el empuje farmacológico final de esta tesis. A la Universidad de Valencia por su mecenazgo y posibilitar que, mediante la beca “Atracció de Talent”, unos estudios se convirtieran en un trabajo. Lo siguiente que se me viene a la cabeza son, inevitablemente, mis amigos de la carrera. Aunque creo que siempre tuve bastante claro que este era mi camino, los momentos duros han sido mucho más llevaderos gracias a Pablo, Ausias, Tesa, Ana, Esther, David, Borja y Chema. Por extensión, a mis compañeros del máster, Asun, Josep, Silvia, Arturo, Lucía y Gabriela. Por vuestra amistad y por ese primer año de clases, prácticas y días de laboratorio que acababan con un denominador común, en un antro a altas horas de la madrugada y muchas cervezas sobre la mesa. Tampoco puedo olvidarme de los neurocientíficos del laboratorio de al lado, Javi, Jesús, Sandra y Claudia, porque me han hecho sentir uno más de ellos.

A mi madre y mi tía, por su apoyo y comprensión, aunque muchas veces no entendieran nada sobre lo que les estaba hablando. Por último, a quienes el recuerdo mantiene vivos, mis abuelos, porque gracias a su esfuerzo permitieron a los que vinimos detrás poder vivir tranquilos y dedicarnos a aquello que más nos interesa, sin tener que preocuparnos por nada más.

**Resumen**

**Chapter 2: Motivation and impact, aims and contributions**



**Chapter 3. State of the art: lipid vesicles and microneedle arrays**

**Chapter 5. Design, development, and characterisation of cyanocobalamin lipid vesicles**

# Resumen

## 1. Introducción

La piel ofrece una vía muy atractiva para la administración de fármacos por varias razones. En primer lugar, presenta varias ventajas sobre las principales vías de administración, como la oral o la parenteral. La administración transdérmica de fármacos tiene una buena aceptación y cumplimiento por parte de los pacientes, suele ser indolora y no necesita condiciones de asepsia y personal médico especializado para su administración. En segundo lugar, su gran superficie -aproximadamente 20.000 $cm^2$ en individuos adultos- la convierten en la mayor vía de entrada de sustancias exógenas al organismo. Por último, las dosis de fármaco administradas se pueden reducir, ya que se evita el primer paso hepático y degradación a nivel gástrico, evitando diversos efectos secundarios o adversos no deseados. Además, otras rutas alternativas como las mucosas sublingual, bucal y rectal son más erráticas y presentan limitaciones.

### 1.1. Administración tópica de fármacos

El proceso de absorción de fármacos a través de la piel está, claramente influido por las propiedades de la molécula bajo estudio, lo que condiciona en gran medida la posibilidad de administración tópica o transdérmica. En este sentido, se han definido como características ideales para que un fármaco difunda a través de la piel un coeficiente de reparto intermedio entre vehículo y membrana, un bajo grado de ionización y un peso molecular inferior a 500 Da. Asimismo, la integridad de la piel tiene un papel clave en la absorción cutánea, ya que los tejidos dañados facilitan enormemente el proceso de absorción.

Como resultado de la estructura anatomo-fisiológica de la piel, la administración de fármacos sobre la misma puede tener dos objetivos: terapia local o administración transdérmica con fines sistémicos. En concreto, esta administración del fármaco sobre la piel puede perseguir diferentes objetivos: a) permanecer sobre la piel para proteger el organismo o hacer frente a entidades vivas existentes en la superficie de la piel (por ejemplo, filtros solares, repelentes o productos

antifúngicos/antibacterianos); b) tratar diferentes trastornos de los anejos cutáneos (antitranspirantes o antiinfecciosos); c) tratar diversas afecciones del *estrato córneo* y de la epidermis viable (emolientes, exfoliantes, antiinflamatorios, antihistamínicos, etc.); d) modificar la función barrera de la piel para mejorar la absorción de otros fármacos; y, e) conseguir efectos sistémicos.

De entre todos estos objetivos, el más complejo, desde el punto de vista tecnológico, es el logro de una acción sistémica, a consecuencia de la mencionada acción barrera que la piel ejerce frente a la entrada de sustancias exógenas al cuerpo. Esta función barrera se debe principalmente a la presencia de la capa más superficial de la piel, el *estrato córneo*, debido a su carácter lipófilo y a la gran cohesión entre las células. Hay varios ejemplos bien conocidos de tratamientos que siguen este enfoque o estrategia terapéutica, específicamente terapias hormonales (estradiol), analgésicas (fentanilo) y deshabituación tabáquica (nicotina).

## 1.2. Sistemas de Administración transdérmica de fármacos

Los sistemas de administración transdérmica de fármacos (SAT) son un conjunto amplio de estrategias, recursos y herramientas que, mediante la modificación de la función barrera de la piel o el cambio de las propiedades fisicoquímicas de los fármacos, tienen como objetivo aumentar la absorción transdérmica de aquellos fármacos que no son buenos candidatos por sí mismos para difundir en cantidades adecuadas a través de la piel. El SAT ideal debe presentar las siguientes propiedades: a) ser atóxico, no irritante ni alergénico; b) proporcionar una acción rápida y con una duración del efecto predecible; c) ser farmacológicamente inerte; d) permitir una fácil retirada tras su uso; e) permitir la restauración rápida de las propiedades de la piel después de su eliminación; f) ser compatible con excipientes y fármacos; g) ser cómodo y cosméticamente aceptable; y, h) ser económico. Desafortunadamente, ningún SAT presenta todas estas propiedades juntas.

## 1.3. Liposomas, transfersomas y etosomas

La nanotecnología tiene como objetivo desarrollar una gran variedad de sistemas y partículas de tamaño nanométrico (de 1 a 1000 nm), donde puedan incorporarse diferentes fármacos. Uno de los campos de aplicación más importantes de estos sistemas es la nanomedicina y, más concretamente, en mejorar la biodisponibilidad y administración de fármacos. En la década los 60, los liposomas se diseñaron como nanovehículos con funciones programadas específicas, y se convirtieron en los precursores de varias nanopartículas utilizadas hoy en día. No mucho tiempo después, aparecieron variaciones en los componentes estructurales de estos liposomas, como es el caso de los transfersomas y etosomas, con el fin de mejorar sus propiedades, lograr una mayor eficacia y mejores resultados. Actualmente, estas variaciones estructurales siguen siendo diseñadas y estudiadas de forma habitual para satisfacer las necesidades y demandas de la industria farmacéutica y la práctica clínica.

Las vesículas lipídicas son partículas formadas por biomembranas no tóxicas y biodegradables obtenidas artificialmente, que han evolucionado gradualmente con el tiempo. Se han utilizado con éxito como transportadores de fármacos para la administración controlada y dirigida de fármacos. Su uso resulta muy atractivo, ya que su naturaleza lipófila permite incorporar fármacos poco solubles en medios acuosos y mejorar las propiedades de penetración de los fármacos a través de la piel. También se han documentado otras ventajas, como una mayor estabilidad de moléculas fotosensibles, menor degradación del fármaco y la posibilidad de conseguir un efecto depósito que libere paulatinamente su contenido.

## 1.4. La cianocobalamina como fármaco para el tratamiento de enfermedades de la piel con carácter inflamatorio

La cianocobalamina (B12) es una vitamina hidrosoluble que se almacena en el hígado y juega un papel clave en el metabolismo de las proteínas, en la formación de glóbulos rojos y en la homeostasis del sistema nervioso central. Por un lado, como vitamina es un nutriente

esencial que debe obtenerse a partir de la dieta, y su deficiencia tiene un impacto negativo en la salud. Por otro lado, su actividad como neutralizador del óxido nítrico hace que pueda aplicarse potencialmente con otros fines terapéuticos.

La deficiencia de B12 es la causa más común de ciertas patologías hematológicas, síntomas neuropsiquiátricos y otras enfermedades. Los bajos niveles de adenosil-B12 o metil-B12 en el organismo son consecuencia habitual de la deficiencia de B12. Esto produce alteraciones en los procesos de metilación y metabolismo del metilmalonato, un metabolito derivado del catabolismo de aminoácidos y ácidos grasos. En particular, los niveles bajos de adenosil-B12 producen una acumulación de ácido metilmalónico, que puede asociarse a la aparición del síndrome neurológico. Por su parte, la deficiencia de metil-B12 conduce a una acumulación de homocisteína, que puede inducir el estrés celular, la apoptosis y homocisteinilación de proteínas.

La deficiencia de B12 tiene principalmente tres etiologías o causas: trastornos de carácter autoinmune, malabsorción o baja ingesta dietética. La deficiencia autoinmune es una patología en la que la producción de anticuerpos anti-factor intrínseco bloquea su actividad, produciendo una incapacidad para absorber la vitamina. Las causas de malabsorción están asociadas con una producción ineficiente de factor intrínseco por parte de las células parietales en el estómago. Esta patología es muy frecuente en casos de bypass gástrico o enfermedades del íleon (cirugías, enfermedad de Crohn o infecciones por *Diphyllobothrium latum*). Por último, estilos de vida con una creciente implantación en la sociedad, como el veganismo, pueden conducir a una situación carencial al cabo de algunos años. Otras condiciones menos frecuentes como la deficiencia genética de transcobalamina-II y el uso de ciertos medicamentos (anticonceptivos orales, terapias de reemplazo hormonal, metformina, inhibidores de la bomba de protones y antagonistas histamínicos H2) también pueden ser causa de la deficiencia de B12. Su prevalencia en áreas desarrolladas,

como América del Norte y Europa, varía de 2.9-25.7%, dependiendo del punto de corte de los valores séricos (<148 y <256 pmol/L de B12, respectivamente). Además, varios estudios sugieren que aumenta con la edad y es más frecuente en mujeres que en hombres (3,3% frente 2,4% respectivamente, para niveles séricos <148 pmol/L). Además, el impacto en áreas en desarrollo, como África, América del Sur y Asia, es significativamente mayor y no se limita solo a grupos de mayor edad, superando el 40% de prevalencia en ciertas subpoblaciones (niños, adultos jóvenes y mujeres embarazadas).

El abordaje terapéutico de la deficiencia de B12 depende de diferentes factores como la etiología y la gravedad, y varía en función de su duración y vía de administración. Consiste, principalmente, en la reposición de los depósitos vitamínicos mediante inyecciones intramusculares o dosis orales de cianocobalamina. En caso de un funcionamiento anómalo de la vía del factor intrínseco se pueden administrar 1000 µg de cianocobalamina por vía intramuscular diariamente durante 1-2 semanas. Reducir la posología durante el mes siguiente a una vez por semana, y continuar con una inyección de mantenimiento mensual. Sin embargo, la vía intramuscular presenta ciertas desventajas, como la generación de molestias y dolor, necesidad de material y técnicas asépticas, costos asociados a su administración por personal capacitado, no ser aplicable en pacientes con baja masa muscular, y propiciar complicaciones médicas como formación de trombos, lesión de nervios -en inyecciones femorales y glúteas- o reacciones de hipersensibilidad. Como alternativa, es posible recibir B12 por vía oral, pero los principales problemas son su baja biodisponibilidad (1-4%) y su ineficacia en las etiologías relacionadas con el factor intrínseco.

En cuanto al uso de B12 como fármaco para patologías no relacionadas directamente con su déficit, se está estudiando su potencial aplicación en el tratamiento de enfermedades inflamatorias crónicas de la piel. El eccema o dermatitis atópica y la psoriasis son los más comunes, ya

que los mecanismos moleculares subyacentes de las mismas brindan una oportunidad para el uso de B12 como una posible terapia. La dermatitis atópica o de contacto se caracteriza por prurito, piel seca, y lesiones eccematosas. El inicio de la dermatitis atópica ocurre comúnmente durante la infancia y se asocia con una morbilidad significativa y calidad de vida reducida. Su prevalencia ha aumentado en los últimos 30 años, y su incidencia se ha duplicado o triplicado en los últimos años. Aproximadamente, el 20% de los niños y el 1-3% de los adultos se ven afectados por este trastorno. Aunque la patogénesis de la dermatitis no se comprende por completo, se ha asociado a varios factores: alteración de la función de barrera de la piel, desregulación inmunitaria, infecciones y procesos ambientales. Las alteraciones en la función de barrera de la piel pueden deberse a: niveles bajos de ceramidas y proteínas involucradas en la diferenciación de queratinocitos y la prevención de la pérdida transepidérmica de agua. Varios factores genéticos, como las mutaciones en los genes de la filagrina, pueden causar esta situación. La función defectuosa de la barrera permite la penetración de alérgenos y agentes irritantes que desencadenan la inflamación a través de respuestas Th2 (con aumento de citoquinas IL-4, IL-5, IL-13) en casos agudos, y respuestas Th1 (con aumento de IFN-gamma e IL- 12) en lesiones crónicas. Además, el rascado de las lesiones, el cual es habitual en la mayoría de los pacientes, estimula la liberación de citocinas inflamatorias por los queratinocitos, como TNF-alfa, IL-1 e IL-6, que perpetúan la inflamación crónica. En última instancia, el mal estado de la piel contribuye a su colonización por bacterias, lo que empeora aún más el trastorno.

La psoriasis es una enfermedad inflamatoria crónica de la piel con un marcado componente inmunológico. Su signo más característico es la presencia de placas eritematosas habitualmente diseminadas por amplias zonas del cuerpo. La prevalencia a nivel mundial varía entre el 1-8%, dependiendo del área geográfica. Aunque puede comenzar a cualquier edad, su inicio se produce con frecuencia en la edad adulta, presentándose en uno de cada tres casos durante la infancia. Una característica

importante en los mecanismos moleculares causantes de la psoriasis es la activación del sistema inmunitario de forma alterada, lo que conduce a la hiperplasia de los queratinocitos, alteración de la función de las células T y angiogénesis. Además, el estrés oxidativo también tiene un papel destacable en la patogénesis de esta afección.

Los principales objetivos de los tratamientos de estas patologías son restaurar la barrera cutánea, limitar el picor, disminuir la inflamación y controlar las alteraciones a nivel inmunitario. Para conseguirlo es posible utilizar una gran variedad de fármacos, siendo los agentes inmunosupresores sistémicos, corticoides e inhibidores de la calcineurina tópicos (ICT) los fármacos de primera línea en el manejo farmacológico de la dermatitis y la psoriasis. Sin embargo, los tratamientos sistémicos no están exentos de posibles efectos secundarios adversos severos, como disfunción renal y hepática o mielo-supresión, que complican en gran medida el abordaje terapéutico de los casos graves. Los efectos secundarios locales asociados al uso crónico de esteroides tópicos e ICT son relativamente comunes, como atrofia de la piel, equimosis, erosiones, estrías, retraso en la cicatrización de heridas, púrpura, hematomas fáciles y acné. Además, la FDA ha relacionado el riesgo de sufrir cáncer de piel y linfomas con el uso de algunos ICT.

Sin embargo, el motivo principal para utilizar la B12 en este contexto radica en que las citocinas proinflamatorias implicadas en la dermatitis y la psoriasis estimulan la expresión de la enzima óxido nítrico sintasa inducible en los queratinocitos. En consecuencia, estas lesiones cutáneas presentan niveles elevados de óxido nítrico, los cuales pueden ser reducidos y, por tanto, controlados gracias a las propiedades neutralizantes de la B12.

La B12 oral y tópica ya se ha utilizado como alternativa para prevenir o mejorar la dermatitis y la psoriasis. Aunque los primeros ensayos datan de los años 60, no se han realizado muchos otros estudios hasta la actualidad. Januchowski et al. (2009) utilizando la escala SCORAD compararon el efecto de una crema de B12 con una base hidratante en el

tratamiento del eccema infantil en un ensayo aleatorizado doble ciego. Las comparaciones intraindividuales mostraron diferencias significativas en la reducción de los valores SCORAD entre la crema de B12 y el placebo. En particular, la B12 tópica mejoró significativamente la piel tratada más que el placebo a las 2 y 4 semanas. Más recientemente, la psoriasis leve-moderada en forma de placas fue tratada con pomadas tópicas de B12 durante 12 semanas en dos ensayos clínicos aleatorizados. Stücker et al. (2001) compararon el efecto de la B12 con el del calcipotriol (análogo de la vitamina D3), obteniendo reducciones similares en la puntuación PASI tras el periodo estudiado. Además, también se observó una marcada reducción de la eficacia del calcipotriol después de 4 semanas de tratamiento, mientras que la eficacia de la vitamina B12 se mantuvo prácticamente constante durante todo el estudio. Del mismo modo, se obtuvo un resultado positivo al comparar los efectos de la B12 y una crema emoliente en el estudio realizado por Del Duca et al. (2017). Las diferencias en la reducción de la puntuación PASI se reflejaron en la semana 2 y aumentaron durante las siguientes 10 semanas. Dos semanas después de finalizar el tratamiento, las lesiones psoriásicas evolucionaron positivamente, especialmente aquellas tratadas con B12. A pesar de estos prometedores resultados, el peso molecular (1355 Da) y la hidrofilia de la B12 limitan su difusión a través de la piel humana. Es por ello por lo que, el abordaje nanotecnológico o con microagujas puede suponer una mejora sustancial respecto a los resultados obtenidos hasta la fecha.

### 1.5. Estructura de las vesículas lipídicas y clasificación

Dependiendo del método de producción y composición, es posible obtener diferentes tipos de vesículas lipídicas. Según la carga superficial que confieren los fosfolípidos, las vesículas lipídicas se pueden clasificar en aniónicas, catiónicas o neutras. Además, el tamaño y número de bicapas lipídicas es la otra característica habitual para diferenciarlas. Las vesículas multilamelares (MLV) son aquellas que presentan más de una bicapa, que encierran el mismo número de compartimentos acuosos. Por

tanto, las vesículas unilaminares tienen una sola bicapa y un núcleo acuoso central. Estos dos ambientes tan diferentes hacen de las vesículas lipídicas un sistema de formulación muy versátil, ya que pueden albergar fármacos disueltos en el núcleo acuoso o insertados dentro de la estructura de la bicapa lipídica. Los MLV suelen presentar un tamaño relativamente grande, oscilando entre la escala nanométrica hasta 1 µm. Cuando el número de bicapas es inferior a cuatro, se denominan vesículas oligolamelares. Se ha demostrado que su eficacia de encapsulación del fármaco suele ser superior a la de las MLV. Un caso especial son las vesículas multivesiculares, que presentan una gran bicapa que confina múltiples vesículas en su interior. Las vesículas unilamelares se subclasifican a su vez en vesículas unilamelares pequeñas (SUV) y vesículas unilamelares grandes (LUV). Los SUV suelen presentar una forma esférica, distribución de tamaños homogénea, y un tamaño inferior a 100 nm, por lo que la eficacia de encapsulación de los fármacos hidrófilos es limitada. Por el contrario, las LUV son vesículas más grandes (100-1000 nm) con un núcleo acuoso con mayor volumen, lo que aumenta la capacidad de encapsular moléculas hidrosolubles.

## 1.6. Mecanismos de acción de los liposomas y vesículas ultraflexibles

Se ha demostrado previamente que los liposomas pueden interactuar eficazmente con las células por diferentes métodos: a) absorción por interacción específica con componentes de la superficie celular, fuerzas electrostáticas e hidrofóbicas; b) endocitosis por células fagocíticas, por ejemplo, macrófagos y neutrófilos; c) fusión mediante la inserción de las bicapas de las vesículas con las membranas celulares; y, d) intercambio de los componentes de las bicapas.

Sin embargo, los mecanismos de acción cuando las vesículas lipídicas se aplican sobre la piel todavía no están totalmente claros. En general, se acepta que los liposomas convencionales no logran penetrar las capas de la piel y permanecen en su superficie, actuando como una especie de formulación de depósito. Los liposomas pueden interactuar

directamente con la piel e intercambiar el fármaco mediante un fenómeno conocido como “proceso de transferencia del complejo de colisión”, el cual ha sido observado en otros sistemas biológicos, o bien podrían liberar al medio exterior el fármaco contenido desde donde puede difundir a través de la piel de forma natural. En este último caso, los liposomas no solo realizan una función de depósito, sino que pueden inducir cambios estructurales en el *estrato córneo* facilitando, de este modo, la absorción del principio activo. Todas estas teorías excluyen la penetración de la estructura del liposoma intacta, que ya ha sido ampliamente evaluada en diferentes estudios. Por ejemplo, Dreier et al. (2016) combinaron la microscopía STED y la espectroscopía RICS para estudiar el mecanismo de acción de los liposomas convencionales destinados a la vía transdérmica. Las imágenes obtenidas a partir de las muestras de tejido cutáneo incubadas con liposomas radiomarcados mostraron que no permanecen intactos una vez han penetrado las diferentes capas de la piel, sugiriendo que los liposomas no actúan directamente como transportadores que llevan su carga directamente a través de la piel. La limitada eficacia de los liposomas convencionales también se ha observado cuando son utilizados para superar otras barreras biológicas, como el epitelio intestinal. En el estudio de Dreier et al. (2016), se comparó la penetración de los liposomas convencionales con vesículas ultraflexibles y, como era de esperar, las vesículas ultraflexibles marcadas con fluorescencia liberaron su contenido a una mayor profundidad dérmica. Este hallazgo apoya la existencia de un mecanismo adicional involucrado para los transfersomas y demás vesículas ultraflexibles. Desde su concepción, se ha sugerido que este tipo de vesículas lipídicas pueden atravesar la estructura de la piel en un proceso que tiene un gradiente osmótico como fuerza motriz, que aparece debido a la diferencia en la concentración de agua entre la superficie de la piel (cerca del 15% en el *estrato córneo*) y las capas viables de la epidermis (alrededor del 75%). En concreto, estas condiciones son suficientemente fuertes como para empujar entre 0,1 y 0,5 mg de material lipídico por hora y $cm^2$, que es un

flujo sustancialmente más alto que el producido típicamente por los gradientes de concentración. Como parece que ocurre con los liposomas convencionales, el mecanismo exacto mediante el cual los transfersomas mejoran la absorción transdérmica es el resultado de la combinación entre la vectorización del fármaco, la disrupción del *estrato córneo* y las características de deformabilidad concretas de cada tipo de vesículas ultraflexibles. Teniendo en cuenta que la desestabilización del *estrato córneo* que producen los transfersomas es más intensa debido a la acción de los emulgentes incorporados en las vesículas. Una confirmación de estos mecanismos de acción es el estudio realizado por Cevc et al. (2002) En su estudio evaluaron la ruptura de los liposomas al ser forzados a pasar través de una barrera semipermeable, detectando una capacidad notable de los transfersomas para mantener su integridad tras el proceso de extrusión en comparación con vesículas convencionales. Además, mediante CLSM y cromatografía de exclusión molecular se confirmó, en un modelo *in vivo*, la presencia de vesículas ultraflexibles intactas en el torrente sanguíneo. Hallazgos similares han sido obtenidos en varios estudios realizados por otros investigadores con diferentes tipos de vesículas ultraflexibles, como Niu et al. (2019) y Manconi et al. (2011).

Los etosomas se consideran como otro tipo de vesícula ultraflexible, ya que presentan también capacidad de penetrar a través de las capas epidérmicas manteniendo su estructura y tamaño originales. Los mecanismos de acción subyacentes son similares a los transfersomas con algunas pequeñas diferencias. Además de fluidificar la bicapa lipídica, el etanol también es un promotor químico de la absorción, puesto que promueve la desestabilización del *estrato córneo* por su interacción con los grupos polares de los fosfolípidos de la piel. Sin embargo, se ha observado que la mejora en la absorción producida por una formulación de etosomal es mayor que la producida por soluciones etanólicas de fármacos. Además, la evaporación del etanol una vez aplicado sobre la superficie de la piel, puede aumentar el efecto del gradiente de concentración en el proceso de absorción transdérmica.

## 1.7. Métodos de producción de vesículas lipídicas

Existen múltiples métodos de preparación de vesículas lipídicas, y cada uno de ellos presenta ciertas ventajas, desventajas y confiere características específicas a las vesículas producidas. Su selección depende de diferentes parámetros como: a) las propiedades fisicoquímicas del fármaco encapsulado y los componentes de la vesícula lipídica; b) la concentración mínima eficaz del fármaco y su toxicidad; c) el tamaño de vesícula deseado, índice de polidispersión (PDI) y carga superficial; y, d) la reproducibilidad de los lotes y producción en escala.

### *1.7.1. Métodos de producción de liposomas y transfersomas*

El mecanismo molecular específico de formación de liposomas depende en gran medida del método de producción utilizado, aunque el principio básico subyacente son las interacciones hidrofóbicas/hidrofílicas entre los lípidos y las moléculas de agua, independientemente de la metodología elegida. La aplicación y transferencia de energía en forma de calor, agitación o sonicación contribuye a la disposición de las moléculas de lípidos en bicapas.

El método de Bangham, también conocido como método de hidratación de la película lipídica o “thin-film”, es el primer procedimiento descrito para obtener artificialmente vesículas lipídicas. Presenta tres pasos claros: 1) preparación de una mezcla orgánica de fosfolípidos/colesterol/surfactante; 2) eliminación del disolvente orgánico usando un rotavapor con el objetivo de producir una película delgada sobre la pared del matraz; 3) rehidratación con una solución acuosa calentando por encima de la temperatura de transición de fase de los fosfolípidos utilizados. A pesar de la simplicidad del método, la baja eficiencia de encapsulación en muchos casos y la producción de poblaciones heterogéneas de MLV hace que sean necesarios procedimientos adicionales para obtener vesículas lipídicas útiles para fines transdérmicos. Además, a lo largo de los años se han ido desarrollando diferentes métodos para superar las limitaciones del método original.

### *1.7.2. Métodos de producción de etosomas*

Touitou et al. (2000) publicó por primera vez un método con el que obtener vesículas lipídicas con etanol como excipiente, proporcionando ventajas adicionales a las vesículas. El método propuesto consiste en preparar una fase etanólica al 20-50% p/p, calentar a 30ºC bajo agitación (700 rpm). La adición gota a gota de una fase acuosa a una velocidad constante de 12 ± 0.5 mL/h conduce a la formación de los etosomas espontáneamente. La incorporación de los principios activos se puede realizar en la mezcla orgánica o en la solución acuosa, dependiendo de sus propiedades fisicoquímicas. Una vez se ha incorporado el volumen adecuado de agua, la dispersión de etosomas se mantiene en agitación durante 5 min y se homogeneiza mediante diferentes métodos para conseguir vesículas de tamaño y PDI deseados. Este procedimiento de producción de etosomas se conoce como método clásico en frío, y una de sus principales ventajas es que se realiza casi a temperatura ambiente, lo que permite preparar vesículas lipídicas cargadas con fármacos termolábiles.

## 1.8. Propiedades y parámetros clave en el diseño de vesículas lipídicas con fines de administración transdérmica

Para lograr una permeabilidad transdérmica altamente eficiente de los fármacos, las vesículas lipídicas deben presentar algunas propiedades clave, a saber: tamaño, morfología, PDI, potencial zeta, eficiencia de encapsulación, grado de deformabilidad, liberación del fármaco, estabilidad y biocompatibilidad. Estas propiedades están conectadas entre sí y, por lo tanto, los cambios en una de ellas provocan variaciones en las otras. En consecuencia, parece casi imposible conseguir la vesícula perfecta o ideal y el verdadero reto se centra en el desarrollo de un prototipo con un equilibrio adecuado entre todos estos parámetros clave.

A modo de regla general, se ha establecido que, a menor tamaño, mayor es la absorción transdérmica proporcionada por las vesículas lipídicas. En este sentido, la deformabilidad de las partículas también juega

un papel relevante y, a mayor grado de deformabilidad, mayor es el efecto potenciador de la absorción. Respecto a los valores de PDI, resultados inferiores a 0,3 garantizan poblaciones suficientemente homogéneas.

## 1.9. Microagujas

Las microagujas (MNA) son dispositivos que contienen proyecciones microscópicas en forma de aguja que pueden perforar el *estrato córneo* creando conductos que facilitan el flujo de moléculas con gran tamaño molecular (> 500 Da), proteínas y nanopartículas a través de la piel. El campo de las microagujas ha experimentado un crecimiento constante desde el registro de la primera patente de Gastrel y Place en 1971. Sin embargo, hubo que esperar hasta el año 2000 para ver la aparición de MNA solubles y las principales aplicaciones actuales que tienen las MNA, que incluyen la vacunación, el diagnóstico y las aplicaciones cosméticas. Las MNA son un campo claramente emergente dentro de la investigación farmacéutica, dado el creciente número de artículos publicados desde la aparición del concepto de “microagujas”. En concreto, el número de artículos sobre MNA era moderado hasta antes del año 2000, pero después, se ha producido un aumento progresivo del número de trabajos publicado año tras año. Un estudio ARIMA, que extrapola tendencias futuras a corto-medio plazo en base a datos previos, identificó y predijo una tendencia creciente que se está cumpliendo en la actualidad. El número de patentes registradas en los últimos años también muestra un crecimiento continuo del uso de MNA como sistemas de administración de fármacos. El interés en los sistemas basados en MNA está altamente relacionado con algunas de sus ventajas más notables, como, por ejemplo, la liberación controlada de fármacos y su facilidad de uso, ya que pueden autoadministrarse y retirarse fácilmente. Además, pueden considerarse un sistema de liberación transdérmica indoloro, porque el tamaño de las proyecciones de las MNA es suficiente para traspasar las primeras capas de la piel evitando el contacto con las terminaciones nerviosas presentes en la dermis.

## 1.10. Seguridad y eficacia de MNA

Al igual que cualquier formulación farmacéutica, las MNA deben cumplir los requisitos mínimos e indispensables de seguridad y eficacia para ser aceptadas como una verdadera alternativa a las tecnologías clásicas de administración de fármacos. Tres acontecimientos adversos no deseados pueden tener lugar después de la inserción de las MNA: dolor, infecciones y reacciones cutáneas locales (inflamación, eritema, irritación, etc.).

### *1.10.1. Dolor*

La aceptación del paciente y el cumplimiento de la pauta terapéutica de un tratamiento con MNA depende, en gran medida, del dolor que generan en comparación con inyecciones convencionales. Varios estudios han demostrado que el dolor producido por las MNA depende de la longitud y el número de agujas en cada dispositivo. Gill et al. (2007) observaron que la inserción de las MNA es menos dolorosa que una producida por una aguja hipodérmica de calibre 26 G, estableciendo una correlación entre el nivel de dolor con el número y longitud de las MNA. En particular, los autores estudiaron el dolor producido por agujas de 480, 700, 960 y 1450 μm de longitud y demostraron que los niveles de dolor que producían variaban entre el 5-37% en comparación con los producidos por agujas hipodérmicas. Además, el aumento en el número de proyecciones produjo un aumento relativamente pequeño del dolor, del 5 -25%. Bal et al. (2008) testaron el dolor generado por MNA de menos de 550 μm de longitud, encontrando niveles de dolor muy bajos en todos los casos, sin diferencias significativas entre ellas. Sin embargo, la rotura de las MNA durante la inserción puede producir dolor y reacciones cutáneas, lo que está especialmente asociado con el uso de determinados materiales, como el vidrio y la cerámica.

### *1.10.2. Infecciones*

Los canales creados por MNA pueden convertirse potencialmente en una puerta para la entrada de patógenos al organismo puesto que, el

desarrollo de procesos infecciosos está directamente relacionado con la alteración de la función de barrera de la piel. A su vez, el tiempo que los microcanales permanecen abiertos depende en gran medida de algunas características de las MNA, como la longitud de las puntas, según Kalluri et al. (2011), que estudiaron *in vivo* la cinética del cierre de los canales. Los investigadores observaron que este proceso dura entre 15-72 h dependiendo, entre otros factores, de las condiciones y del efecto de oclusión, resultando similar al estimado para un canal producido por una aguja hipodérmica. La función de barrera de la piel también se evaluó mediante los niveles de pérdida de agua transepidérmica (TEWL), y se concluyó que la piel solo necesita 4 h para recuperar su función de barrera después del tratamiento con microagujas de 550 µm de longitud. Bal et al. (2008). demostraron que el uso de microagujas más largas produce un mayor aumento en los valores de TEWL, ya que se observó una diferencia significativa en la respuesta entre agujas con 400 y 200 µm de longitud. Además, el estudio de Donnelly et al. (2009) mostró que la inserción con MNA conllevó una colonización bacteriana significativamente menor a la producida por una inyección hipodérmica convencional. En concreto, ningún microorganismo accedió a la epidermis viable en la piel perforada con MNA, a diferencia de los resultados obtenidos con agujas hipodérmicas. Por tanto, se puede afirmar que la correcta aplicación de MNA en la piel no parece provocar infecciones locales ni sistémicas, en circunstancias normales y pacientes inmunocompetentes.

### *1.10.3. Biocompatibilidad, inmunogenicidad y reacciones cutáneas locales*

La presencia de objetos extraños o la incompatibilidad biológica de cualquier componente de las MNA puede desencadenar una inflamación, irritación o eritema en la piel durante o después del tratamiento. Bal et al. (2008) comprobaron el posible impacto de la longitud de las MNA en la irritación, y examinaron el enrojecimiento de la piel y el flujo sanguíneo. Ambos métodos permiten medir el eritema, que es uno de los indicadores fundamentales de la inflamación. Por un lado, se observaron cambios en

el enrojecimiento tras la aplicación de MNA sólidas de tipo metálico, que llegó a alcanzar los valores máximos de irritación a los 15 min, retornando a los valores basales en aproximadamente 90 min. Por otro lado, un aumento en la longitud de las MNA (200, 300 y 400 µm) se traduce en un aumento en el enrojecimiento, aunque solo las diferencias entre la menor longitud (200 µm) y el resto fueron estadísticamente significativas. Además, el tratamiento con MNA de varias longitudes no produjo diferencias significativas en el flujo sanguíneo. Por su parte, Vicente-Pérez et al. (2017) no encontraron en su estudio ninguna evidencia significativa de un aumento en los biomarcadores séricos de inflamación e irritación (TNF-α e IL-1β) después de un uso prolongado de MNA de tipo polimérico.

La baja biocompatibilidad o las respuestas alérgicas no son frecuentes en los enfoques basados en MNA, especialmente en el caso de las compuestas por polímeros, ya que los materiales de fabricación se transfieren desde otros campos de la tecnología farmacéutica donde se ha garantizado la biocompatibilidad previamente. Sin embargo, otros tipos de MNA, como las sólidas y huecas ("hollow"), pueden dar lugar a algunos de estos problemas. Por ejemplo, las MNA de acero inoxidable pueden corroerse con el tiempo, una característica que se ha mejorado notablemente con el uso de titanio para su fabricación.

## 1.11. Métodos *in vitro*, *ex vivo* e *in vivo* para evaluar la penetración y la permeabilidad transdérmica de fármacos

Aunque los métodos *in vivo* son los procedimientos ideales para evaluar los efectos de cualquier sistema de administración de fármacos, muchos estudios muestran que las concentraciones sistémicas y locales del fármaco pueden estimarse y predecirse utilizando parámetros de permeabilidad de la piel. Por ejemplo, el coeficiente de permeabilidad, el coeficiente de difusión, el periodo de latencia y el flujo transdérmico, todos ellos calculados por métodos *in vitro* y *ex vivo*.

### *1.11.1. Métodos in vitro: Células de difusión*

Las Células de Difusión de Franz (FDC) de tipo estático y vertical son el sistema más habitual en los estudios de permeabilidad transdérmica. Están compuestas por dos compartimentos separados mediante una membrana o tejido. La formulación del fármaco se administra al compartimento dador, y el receptor se llena con un medio acuoso adecuado que permita disolver el fármaco tras su paso a través de la barrera en estudio, en este caso la piel, para garantizar las condiciones sumidero ("sink"). Para imitar las condiciones *in vivo* este compartimento receptor se agita utilizando un imán y se regula a la temperatura fisiológica de la piel (32-37ºC), introduciéndolo en un baño de agua templada o utilizando un sistema calefactor adicional que rodea la célula. La cámara receptora incluye un puerto de muestreo que permite la toma de muestras a los puntos temporales preestablecidos. Posteriormente, las muestras se analizan mediante un método analítico adecuado según la naturaleza del fármaco y cantidades permeadas.

### *1.11.2. Métodos ex vivo: Tape-stripping y stripping diferencial*

La profundidad de penetración del fármaco en la piel y la farmacocinética cutánea suelen estimarse mediante métodos *ex vivo*. El tape-stripping destaca por ser una técnica mínimamente invasiva que elimina el *estrato córneo*. Consiste en colocar una biopsia de piel en un portaobjetos de vidrio, la cual se cubre con una máscara de aluminio dejando al descubierto el área de aplicación de la formulación. Posteriormente, se administra una cantidad conocida de la formulación bajo estudio y se incuba el montaje a 32ºC durante un período de tiempo comprendido entre 2 y 6 h. Después de la incubación, se aplican secuencialmente entre 20-25 tiras de cinta adhesiva sobre la piel, en condiciones estandarizadas de presión, con la intención de eliminar progresivamente las capas de corneocitos y el fármaco contenido en ellas. Finalmente, dicho fármaco se extrae de las tiras adhesivas sumergiéndolas en un medio adecuado donde el fármaco es altamente soluble, para luego

cuantificarlo mediante un método analítico apropiado. Esta técnica, además, al ser mínimamente invasiva se puede realizar *in vivo* muy fácilmente.

El stripping diferencial es una técnica que consiste en una combinación de la técnica del tape-stripping con una biopsia en superficie de la piel con cianocrilato. Se considera la técnica más sencilla para determinar cuantitativamente la captación folicular de fármacos. Después de llevar a cabo un procedimiento de stripping convencional, tal y como se describe anteriormente, se aplica una cantidad adecuada de adhesivo instantáneo de cianocrilato sobre la piel previamente desprovista de corneocitos. Tras la polimerización del adhesivo, la capa o biopsia de cianocrilato se despega para generar un molde folicular y se procesa de manera similar a las cintas adhesivas del tape-stripping convencional.

### *1.11.3. Métodos in vivo: Microdiálisis*

La microdiálisis es el método de referencia para obtener un estudio completo de los procesos farmacocinéticos en la piel. Consiste básicamente en colocar una sonda de diálisis semipermeable en la estructura y profundidad de la piel que se desea estudiar. Esta membrana de intercambio se encuentra conectada a una bomba de perfusión, que introduce un líquido receptor fisiológico. A causa de los procesos osmóticos y de difusión, el líquido perfundido es capaz de recoger el fármaco que ha permeado a través de la piel, y permite caracterizar con gran precisión el proceso de absorción. Sin embargo, los métodos *in vivo* conllevan grandes requerimientos de carácter ético, dificultades técnicas y elevado coste económico.

## 2. Objetivos

El objetivo principal de esta tesis es el desarrollo y caracterización de diferentes sistemas de administración transdérmica para mejorar la penetración y absorción cutánea de B12, con la intención de ofrecer una alternativa factible a las terapias actuales para tratar la deficiencia de B12 y la dermatitis atópica o de contacto.

Para lograr este objetivo, el proyecto se dividió en los siguientes subobjetivos:

- **Objetivo 1:** Desarrollo de un método analítico por cromatografía líquida de alta eficacia que fuera exacto y preciso para la detección y cuantificación de B12.
- **Objetivo 2:** Desarrollo y caracterización de vesículas lipídicas de B12 (liposomas, transfersomas y etosomas), con énfasis en el estudio de su biocompatibilidad, estabilidad y otras propiedades predictoras de una óptima penetración y permeabilidad cutánea del fármaco (eficiencia de encapsulación, tamaño, flexibilidad y liberación del fármaco).
- **Objetivo 3:** Desarrollo y caracterización de MNA solubles de B12, evaluando especialmente sus capacidades para superar el *estrato córneo* y propiedades de liberación del fármaco.
- **Objetivo 4:** Evaluación *ex vivo* e *in vitro* de la penetración y permeabilidad de B12 a través de la piel proporcionada tanto por vesículas lipídicas como MNA solubles, estableciendo una comparativa entre estos resultados y los obtenidos a partir de una solución de B12 como referencia estándar.
- **Objetivo 5:** Comprobar la eficacia de uno de los sistemas diseñados en un modelo *in vivo* de hipersensibilidad de tipo retardado que simule una enfermedad de la piel con carácter inflamatorio, en este caso dermatitis de contacto o atópica.

## 3. Métodos

Los métodos empleados para la realización de esta tesis doctoral se resumen a continuación.

### 3.1. Cromatografía líquida de alta eficacia

La B12 se cuantificó en todos los experimentos mediante cromatografía líquida de alta eficacia (HPLC) o espectroscopia UV-Vis.

Para ello, se utilizó un HPLC PerkinElmer Series 200® equipado con un inyector automático y un detector UV-vis (PerkinElmer; Waltham, MA, EE. UU). La fase móvil consistió en una mezcla isocrática de metanol:agua (30:70). La fase estacionaria utilizada fue una columna de HPLC Kromasil® C18 de 5 µm de tamaño de partícula, tamaño de poro 100 Å, L x I.D. 150 mm x 4,6 mm (Dr. Maisch GmbH; Ammerbuch, Alemania). El volumen de inyección fue de 50 µL y para la detección se utilizó una longitud de onda de 360 nm. El flujo para introducir la fase móvil en el equipo se reguló a 0,7 mL/min y el análisis de las muestras se realizó a temperatura ambiente. El método fue validado en términos de linealidad, sensibilidad, precisión y exactitud.

### 3.2. Preparación de liposomas, transfersomas y etosomas

Se prepararon varias formulaciones de liposomas y transfersomas por el método de Bangham. Brevemente, se disolvió en metanol el Phospholipon 90G® (P90G), el colesterol (Chol) -relación molar P90G:Chol 17:1- o los tensioactivos (P90G:Tween 15% p/p), y la B12. El disolvente se evaporó utilizando un rotavapor bajo agitación, en condiciones de temperatura y presión de 50°C y 100 mbar respectivamente (BUCHI R-210, Büchi AG; Flawil, Suiza). La película de fosfolípidos resultante se hidrató mediante la adición de una solución salina amortiguadora de fosfatos (PBS) pH 7,4 o de una solución B12 y, a continuación, se agitó durante 1 h a 50°C para obtener una dispersión de MLV.

Los etosomas se prepararon por el método de Touitou, disolviendo el P90G y la B12 en etanol. A continuación, se añadió una cantidad

adecuada de agua a un flujo de 12 ± 0,5 mL/h en un vaso de precipitados sellado bajo agitación (710 ± 5 rpm). El sistema se mantuvo en agitación durante 5 min tras la adición del agua.

Una vez obtenidos los MLV, se redujo su tamaño mediante sonicación y extrusión. En el caso de los liposomas y transfersomas, primero se sonicaron a 50°C durante 2 h (Elmasonic S60H, Elma; Singen, Alemania). Luego se enfriaron a 4°C y se extruyeron a través de una membrana de 200 µm, utilizando un LiposoFast-Basic Extruder (Avestin; Ottawa, Canadá). Los etosomas se trataron con ultrasonidos durante 1 h a temperatura ambiente y se extruyeron al igual que las otras vesículas lipídicas. Tras la reducción de tamaño, las muestras se purificaron por centrifugación (12800 xg, 30 min) o se lavaron en 2 L de PBS a 4°C durante 24 h. Los lotes se almacenaron a 4°C protegidos de la luz en todo momento.

### 3.3. Preparación de MNA solubles

Se prepararon varios prototipos de MNA solubles utilizando alcohol polivinílico (PVA) y polivinilpirrolidona (PVP) como polímeros. Para ello, en primer lugar, se disolvieron los polímeros en agua para preparar mezclas madre, las cuales se utilizaron para preparar los geles con la concentración de polímero final deseada. Estos geles se mezclaron con vesículas lipídicas o B12 hasta lograr una homogeneidad completa de la mezcla. A continuación, se centrifugaron las mezclas (3500 rpm, 15 min) para eliminar las burbujas de aire y se vertieron 0,25 g en moldes de polidimetilsiloxano, que se colocaron en una cámara de presión positiva a 3-4 bar durante 45 min (Protima®, TÜV Rheinland; Colonia, Alemania). Por último, para poder desmoldar las MNA, se secaron a temperatura ambiente durante 24-48 h.

### 3.4. Determinación del tamaño, PDI y potencial zeta de las vesículas

El tamaño de las partículas (diámetro medio) y PDI se midieron mediante un Nano zetasizer (Malvern Panalytical; Malvern, Reino Unido). Se utilizó el modo DLS para medir el tamaño de las vesículas y PDI,

mientras que el modo LDE se empleó para determinar el potencial zeta. Cada formulación se analizó por triplicado (n=3).

### 3.5. Determinación del contenido en fosfolípido de las vesículas

Se utilizó el método de Rouser et al. (1970) para determinar la cantidad de fosfatidilcolina incorporada a las diferentes vesículas. Brevemente, 100 µL de las suspensiones liposomales se calentaron a 270ºC hasta la completa evaporación del agua. Luego se añadieron 450 µL de ácido perclórico (70 % v/v) y la mezcla se calentó a 250ºC durante 30 min. Tras dejarla enfriar, se añadieron 3,5 mL de agua, 500 µL de molibdato de amonio (2,5 % p/v) y 500 µL de ácido ascórbico (10 % p/v). La mezcla resultante se agitó e incubó a 100ºC durante 7 min. Una vez enfriados los tubos, se midió la absorbancia a 820 nm (espectrofotómetro HITACHI U-2900, Hitachi High-Tech Corp.; Tokio, Japón). Todas las formulaciones se analizaron por triplicado (n=3).

### 3.6. Determinación de la eficiencia de encapsulación de las vesículas

La eficiencia de encapsulación se determinó directamente calculando la cantidad de B12 encapsulada en las dispersiones de vesículas lipídicas.

Para ello, se incubaron 0,5 mL de dispersión de vesículas lipídicas durante 1 h con una mezcla de agua:metanol:dodecil sulfato sódico 1% (45:45:10) para disolver todos los componentes de la vesícula. La mezcla final se filtró y el contenido de B12 se analizó por HPLC. Todas las formulaciones se analizaron por triplicado (n=3).

### 3.7. Evaluación de la flexibilidad de las vesículas

La flexibilidad de las diferentes vesículas lipídicas se estimó indirectamente por extrusión en frío a través de una membrana de 100 nm. Para ello, se extruyeron 500 µl de cada formulación 9 veces a temperatura ambiente. También se registró el volumen final de dispersión recogido y se calculó la relación de disminución de tamaño de las nanopartículas mediante DLS. Todas las formulaciones se analizaron por triplicado (n=3).

### 3.8. Morfología de las vesículas

Las imágenes de las diferentes vesículas lipídicas se obtuvieron mediante microscopía electrónica de transmisión (TEM). Para ello, se diluyó una gota de las dispersiones vesiculares (1:1000). Esta dilución se depositó en una rejilla de cobre y se secó durante 4 min. Se eliminó el exceso de dispersión y se aplicó una gota de solución de ácido fosfotúngstico (2 %). A continuación, se visualizaron las vesículas utilizando un JEOL JEM 1010 -100kV- (Jeol Ltd.; Tokio, Japón).

### 3.9. Estudios de estabilidad de las vesículas

La estabilidad de las vesículas se comprobó semanalmente durante 60 días en términos de tamaño y PDI mediante DLS. Los fenómenos de coalescencia, floculación, cremado, sedimentación y clarificación se estudiaron durante las 24 h posteriores a la formulación de las suspensiones con un analizador de estabilidad TurbiscanTM LAB (Formulaction SA; Toulouse, Francia). La estabilidad química de la B12 se evaluó semanalmente mediante la determinación del contenido del principio activo.

### 3.10. Liofilización de las vesículas

Las vesículas lipídicas se liofilizaron en ausencia y presencia de lactosa y sorbitol como agentes crioprotectores. Las soluciones de lactosa se prepararon con una relación molar 1:10 (fosfolípido:azúcar), mientras que las soluciones con sorbitol se prepararon al 2,5% v/v. Los etosomas no se liofilizaron, ya que el etanol puede ser eliminado con el procedimiento de liofilización. En todos los casos, se utilizaron 100 µL de muestra junto con 400 µL de crioprotector. Las muestras se congelaron a -80 °C durante 24 h (Ultra Low Temperature Freezer U570, New Brunswick Scientific; Enfield, CT, USA), y se liofilizaron durante 48 h utilizando un liofilizador LyoQuest HT-40 (Telstar; Barcelona, España) bajo condiciones controladas de temperatura y presión (-50 °C y 0,08 mbar). Las muestras liofilizadas se hidrataron con PBS y se comprobó la estabilidad de las vesículas en términos de tamaño y PDI mediante DLS.

3.11. Estudios de toxicidad de las vesículas en cultivo celular

Para los estudios de toxicidad, se utilizó la línea celular RAW 264.7 (ECACC; Salisbury, Reino Unido). Las células se mantuvieron en medio de Eagle modificado de Dulbecco (DMEM) suplementado con 10% de suero bovino fetal (FBS), penicilina (100 UI/mL) y estreptomicina (100 µg/mL), bajo una atmósfera humidificada con 5% de $CO_2$ y a una temperatura de 37ºC.

Para los ensayos de proliferación y viabilidad celular se sembraron suspensiones de células a una densidad de $1 \cdot 10^6$ células/mL en placas de 96 pocillos (200 µl/pocillo) con medio DMEM suplementado al 10% con FBS, penicilina (100 UI/mL) y estreptomicina (100 µg/mL). Tras una incubación de 2 h, el medio se sustituyó por el mismo volumen de medio DMEM suplementado con 0,5% de FBS y se expuso durante 24 h a 10 µl de cada tipo de formulación de vesículas lipídicas a diferentes concentraciones. A continuación, se descartó el medio y se añadieron 100 µl de solución de MTT (0,5 mg/mL). Se eliminó el sobrenadante después de 1 h y los depósitos azules correspondientes al metabolito coloreado se disolvieron en 100 µL de DMSO. Se midió la absorbancia a 510 nm utilizando un lector de placas VICTOR3 Multilabel (PerkinElmer; Waltham, MA, USA).

3.12. Estudios de liberación del fármaco y ajuste cinético

Los estudios de liberación *in vitro* con las vesículas lipídicas se llevaron a cabo utilizando FDC con un área de difusión efectiva de 1,76 $cm^2$. Se añadieron 500 µl de cada formulación al compartimento dador, mientras el receptor se llenó con 12 mL de PBS pH 7,4 (n=6). Se utilizó una membrana de difusión Spectra/Por® para separar los compartimentos dador y receptor. Tanto el compartimento dador como el puerto de muestreo se cubrieron con Parafilm M® para garantizar la oclusión, evitar fugas y la evaporación del disolvente. Se recogieron muestras de 400 µL a las 1, 2, 3, 4, 5, 6, 7, 8, 9, 10, 24, 48 y 72 h, reponiendo el volumen tomado por PBS atemperado.

La B12 liberada se cuantificó por HPLC y se calcularon las cantidades acumuladas de B12 frente al tiempo. Los perfiles de liberación se ajustaron a diferentes modelos cinéticos matemáticos: Higuchi, Korsmeyer-Peppas, Kim, Peppas-Sahlin, de orden cero y de primer orden.

Para los estudios de liberación *in vitro* de las MNA, estas se colocaron en una placa de 12 pocillos llena con 5 mL de PBS atemperado a 37ºC. Las muestras de 200 µL se recogieron a los 5, 10, 15, 20, 30, 40, 50, 60, 90, 120, 180, 240 min, reponiendo el volumen tomado por PBS atemperado. Finalmente, se determinó la cantidad de B12 liberada mediante espectrofotometría UV-vis.

### 3.13. Morfología de las MNA

La morfología de las MNA se observó mediante microscopia electrónica de barrido (SEM) (EVO LS 15 SEM, Carl Zeiss; Jena, Alemania). Para ello, las MNA se recubrieron con una capa conductora de oro (Q150 RS sputter coater, Quorum Technologies, Lewes, Reino Unido).

### 3.14. Resistencia mecánica y propiedades de inserción de las MNA

La resistencia mecánica de las MNA se evaluó utilizando un analizador de texturas TA-TX plus (Stable Microsystem; Haslemere, Reino Unido). Para ello, las MNA se visualizaron antes de la prueba utilizando un microscopio óptico para determinar la longitud de sus proyecciones (Leica ICC50 HD, Leica Microsystems; Wetzlar, Alemania). Seguidamente, se aplicó el modo de compresión del analizador con una fuerza de 32 N/MNA durante 30 seg para comprimir las MNA contra una superficie de acero inoxidable. Finalmente, se observaron de nuevo las MNA para determinar la disminución del tamaño de las proyecciones.

### 3.15. Ensayo termogravimétrico

El análisis termogravimétrico (TGA) se llevó a cabo utilizando un TG 209 F3 Tarsus (Netzsch; Waldkrainburg, Alemania). Los barridos de temperatura se realizaron de 25 a 200 °C a una velocidad de barrido de 10 °C/min. Se utilizó el software Netzsch Proteus Thermal Analysis 8.0

(Netzsch; Waldkrainburg, Alemania) para crear las líneas de base y termogramas.

### 3.16. Calorimetría diferencial de barrido

El análisis calorimétrico (DSC) se llevó a cabo utilizando un DSC 214 Polyma (Netzsch; Waldkrainburg, Alemania). Los barridos de temperatura se realizaron de 25 a 225 °C a una velocidad de barrido de 10 °C/min (575). Se utilizó el software Netzsch Proteus Thermal Analysis 8.0 (Netzsch; Waldkrainburg, Alemania) para crear las líneas de base y termogramas.

### 3.17. Distribución de fármaco en las capas de piel

La penetración del fármaco contenido en los diferentes tipos de vesículas lipídicas en las distintas capas de la piel se evaluó mediante la técnica de tape-stripping. Todos los estudios *ex vivo* e *in vitro* se realizaron con muestras de piel porcina y fueron aprobados por el Comité Ético de la Universidad de Valencia, bajo el número de protocolo H1540295606992 (Anexo III). Para el tape-stripping se separó la piel del tejido conectivo y se colocó en un portaobjetos, con la cara externa de la piel hacia arriba. Se colocó una máscara de aluminio sobre ella, y se dejó la zona de aplicación de las formulaciones al descubierto. Se administraron 100 µl de las formulaciones correspondientes, y el sistema se incubó a 32ºC durante 2, 4 y 6 h. Cada prueba se realizó por triplicado (n=3). Tras la incubación, se aplicaron secuencialmente 20 tiras de cinta adhesiva (strips) sobre la piel utilizando un rodillo siguiendo un procedimiento estandarizado y, luego, se retiraron cuidadosamente con una pinza. La cantidad de *estrato córneo* eliminado se determinó mediante densitometría infrarroja (SquameScanTM 850A, Hailand electronic GmbH; Wetzlar, Alemania) y, seguidamente, las tiras se agruparon siguiendo la secuencia 1, 2, 3-5, 6-10, 11-15, 16-20. La cantidad de B12 presente en cada muestra se extrajo de los strips utilizando una mezcla de metanol:agua (50:50 v/v) como disolvente de extracción, ya que ofrece un ratio de recuperación de B12 óptimo dentro del intervalo establecido (100 ± 20%). Posteriormente, la B12 fue cuantificada por HPLC sin interferencias con el método analítico.

3.18. Permeabilidad *in vitro* de fármaco a través de la piel

La permeabilidad cutánea de la B12 obtenida con las vesículas lipídicas y MNA solubles se evaluó utilizando un sistema de FDC con un área de difusión efectiva de 1,76 $cm^2$. La permeabilidad cutánea obtenida para los diferentes sistemas vesiculares se comparó con la permeabilidad cutánea de una solución de B12 al 0,5% (p/v). Para los experimentos con las vesículas lipídicas se utilizó piel porcina intacta o pre-tratada con MNA de tipo sólido sin dermatomizar. En el caso de las MNA solubles, la permeabilidad de la piel se evaluó utilizando piel porcina dermatomizada (600 µm). En el montaje del sistema de FDC, la piel se colocó horizontalmente entre las compartimento dador y receptor con el *estrato córneo* hacia arriba. Para el tratamiento de la piel con las MNA sólidas y solubles, se aplicó firmemente una presión similar en todos los casos durante 30 seg.

En el caso de las vesículas lipídicas, se añadieron 500 µL de cada formulación al compartimento dador. El compartimento receptor se llenó con 12 mL de PBS pH 7,4 y la temperatura se mantuvo a 32 ± 1ºC durante todo el experimento (n = 6). Se tomaron muestras de 200 µL en tiempos prefijados, dependiendo de la formulación ensayada y de la piel utilizada. En cada muestreo, el volumen recogido se reemplazó por el mismo volumen de PBS atemperado. La B12 liberada se cuantificó mediante el método HPLC descrito anteriormente, y se calcularon las cantidades acumuladas de B12 en función del tiempo. Los parámetros de permeabilidad se calcularon por regresión lineal del estado estacionario: *Jmax* (µg/$cm^2$/h), *Kp* (cm/h) y tL (h) como simplificación del modelo de difusión de Scheuplein.

3.19. Visualización de los microcanales creados por MNA de tipo sólido

La piel porcina tratada con MNA de tipo sólido se tiñó con una solución de azul de metileno (1% p/v) durante 1 minuto. A continuación, se limpió el lugar de inserción con agua para eliminar el exceso de colorante y se tomaron imágenes mediante microscopía óptica.

## 3.20. Estudios in vivo

### *3.20.1. Animales y condiciones de estabulación*

Para los experimentos del modelo de hipersensibilidad de tipo retardado (DTH) se utilizaron un total de 42 ratones BALB/c. Los animales se mantuvieron en las instalaciones de la Universidad de Valencia durante 10 días antes de empezar los ensayos para su acondicionamiento. Posteriormente, se asignaron aleatoriamente los grupos experimentales. Todos los procedimientos se ajustaron a los principios de cuidado de los animales de laboratorio y fueron aprobados por el Comité Ético de Experimentación y Bienestar Animal (Anexo III).

### *3.20.2. Inducción de un modelo de hipersensibilidad de tipo retardado y evaluación del edema auricular*

Para inducir la inflamación en el modelo DTH se utilizó oxazolona (OXA) disuelta en acetona al 1 y 3% p/v. Se afeitó el abdomen de los animales (día -1) y un día después se les sensibilizó mediante una única aplicación percutánea de 150 µl de solución de OXA al 3% p/v (día 0). En el día 5, se desencadenó la reacción de hipersensibilidad mediante la aplicación de 10 µl de solución de OXA al 1% p/v en cada lado de la oreja. En este estudio, se aplicaron 20 µl de cada formulación (10 µl/lado) en la oreja derecha tras la administración de OXA, 24 y 48 h después. Se aplicó también propionato de clobetasol tópico disuelto en acetona (0,025 mg/oreja), como tratamiento de referencia. El grosor de la oreja se midió antes de desencadenar la reacción de hipersensibilidad y a las 24, 48 y 72 h, utilizando un micrómetro (Absolute Digimatic 2®, Mitutoyo GmbH; Neuss, Alemania). Finalmente, los animales fueron sacrificados mediante dislocación cervical y se tomaron las orejas para los estudios histológicos.

### *3.20.3. Imágenes de bioluminiscencia*

Para la obtención de imágenes de bioluminiscencia (BLI) se utilizó un equipo IVIS Lumina X5 (PerkinElmer; Waltham, MA, USA). Los ratones se trataron con 0,2 mL de luminol (200 mg/kg i.p.; disuelto en PBS), y se obtuvieron imágenes 30 min después de la inyección bajo un protocolo

anestésico adecuado (inhalación de isoflurano). Se determinaron las emisiones totales de fotones a diferentes tiempos (3, 6 y 24 h).

### *3.20.4. Estudio histológico*

Las biopsias se fijaron en solución de paraformaldehído al 4% p/v y luego se embebieron en parafina. Posteriormente, se tiñeron las secciones de piel (de 5 µm de grosor) para visualizar las estructuras cutáneas. Para la tinción con hematoxilina y eosina, las muestras se sumergieron en una solución de hematoxilina de Harris y se lavaron para eliminar el exceso de colorante. A continuación, se trataron secuencialmente con una solución de diferenciación y una solución etanólica de eosina (50% v/v). Por último, se deshidrataron con una secuencia de soluciones alcohólicas, se montaron con líquido DPX. Los cortes histológicos también se tiñeron con el reactivo tricrómico de Masson. Para ello, las muestras se fijaron en reactivo de Bouin durante 12 h y luego se enjuagaron con agua destilada. Las secciones histológicas se tiñeron secuencialmente con hematoxilina de Mayer, solución etanólica de ácido clorhídrico (0,5% p/v), ponceau ácido, solución acuosa de ácido fosfomolíbdico (1% p/v), azul de anilina y alcohol etílico (95% p/v). Por último, las muestras se hialinizaron con dimetilbenceno y se sellaron con un bálsamo neutro.

## 3.21. Análisis estadístico

Todo el procesamiento de los datos se realizó con Microsoft Excel 2016® (Redmond, WA, EE. UU.) y SPSS versión 22.0® (IBM Corp., NY, EE. UU.). Los datos se expresaron como la media ± desviación estándar (SD). a menos que se indique lo contrario. Como requisito previo para las pruebas estadísticas, se verificó la normalidad, homocedasticidad y esfericidad en caso de ser necesario. La distribución normal de cada conjunto de datos se evaluó mediante la prueba de Shapiro-Wilk. La homogeneidad de las varianzas se confirmó mediante la prueba de Levene. Las varianzas de las diferencias entre todas las combinaciones de grupos relacionados se comprobaron mediante la prueba de esfericidad de Mauchly. El análisis estadístico se llevó a cabo mediante la prueba t-

student para comparaciones simples, ANOVA de una vía para pruebas con dos variables y ANOVA de dos vías para pruebas con tres variables. Todas las pruebas de ANOVA fueron complementadas por la prueba post hoc adecuada en cada caso. En concreto, se utilizó la prueba no paramétrica de Games-Howell en caso de heterogeneidad de varianzas. En caso de cumplirse el requisito de homocedasticidad, se utilizaron las pruebas de Bonferroni o Tukey cuando el número de comparaciones era bajo o alto respectivamente. La prueba de Gabriel se empleó si el número de muestras era diferente entre los grupos a comparar. Las diferencias estadísticas se consideraron significativas si los valores p eran inferiores al 5% ($p < 0,05$).

## 4. Resultados y discusión

### 4.1. Validación del método analítico para la detección de B12

El análisis de B12 mediante HPLC en las condiciones descritas dio lugar a un pico cromatográfico único y bien definido con un tiempo de retención de 3,5 minu. La relación entre las áreas cromatográficas y las concentraciones de B12 se evaluó en el rango de concentraciones comprendido entre 10-0,039 µg/mL. La linealidad del método quedó demostrada por los coeficientes de determinación que fueron superiores a 0,999 en todos los casos. Los límites de detección y cuantificación del método calculados, a partir de los valores obtenidos para tres curvas diferentes ensayadas en tres días distintos, fueron de 0,033 µg/mL y 0,11 µg/mL respectivamente. La precisión y exactitud del método se evaluó mediante el coeficiente de variación y el error relativo. En términos generales, la validación del método fue completamente satisfactoria, ya que todos los cálculos se mantuvieron por debajo del umbral del 10%, como recomiendan las directrices de la OCDE para la validación de un método bioanalítico. La validación del método de espectroscopia UV-vis, también ofreció una validación adecuada, ya que ambos comparten el mismo principio de detección.

4.2. Preparación de vesículas lipídicas. Evaluación del tamaño de partícula, PDI, potencial zeta y eficiencia de encapsulación

Las mediciones de tamaño estuvieron dentro del intervalo esperado para los diferentes tipos de vesículas lipídicas. Aproximadamente 290 nm los liposomas convencionales, 180 nm los transfersomas y 150 nm los etosomas. Los datos obtenidos fueron similares para los descritos por Wu et al. (2019), cuyos liposomas convencionales tuvieron un tamaño comprendido entre 236-374 nm, dependiendo del porcentaje de colesterol incluido en la formulación. Los tamaños de los transfersomas obtenidos fueron similares a preparados anteriormente por Carreras et al. (2020), mientras que los lotes de etosomas reprodujeron exactamente el tamaño descrito por Touitou et al (2000).

Cabe destacar que el tamaño tiene un impacto relevante en la permeabilidad del fármaco a través de la piel. Concretamente, las nanopartículas lipídicas con un diámetro de 300 nm o inferior pueden mejorar considerablemente la permeabilidad transdérmica de fármaco, ya que cuanto menor es el tamaño, mayor es la absorción obtenida. Basándose en este criterio, todas las vesículas formuladas en este trabajo deberían ser capaces de promover el acceso de la B12 a la epidermis y dermis y, en consecuencia, permitir su absorción sistémica. En concreto, los transfersomas y los etosomas fueron los candidatos más prometedores debido a su tamaño y propiedades teóricas de flexibilidad. Además, las nanopartículas con un tamaño en torno a los 210 nm, como las vesículas ultraflexibles obtenidas, pueden también penetrar en la piel por la vía transfolicular.

Los valores de PDI, como medida de la variabilidad del tamaño de las poblaciones de partículas, fueron inferiores a 0,3 en todos los casos, que es el valor de corte sugerido para considerar homogéneas las poblaciones en términos de tamaño con fines de administración transdérmica de fármacos. Los valores de potencial zeta de todas las formulaciones fueron negativos debido, principalmente, a la carga negativa

de los fosfolípidos. Los liposomas mostraron la carga más negativa, probablemente debido al mayor tamaño y mayor cantidad de fosfolípidos. Otra posible explicación a este resultado es que la carga superficial disminuye al aumentar el nivel de colesterol en una membrana de fosfolípido, como se ha demostrado previamente por otros investigadores. En cuanto a los transfersomas y etosomas, éstos presentan menor tamaño, probablemente debido a la presencia del tensioactivo, lo que implica una menor concentración en fosfolípidos, y reduce a su vez la carga negativa del sistema. Estos resultados son consistentes con los intervalos descritos por Ahad et al. (2017) y Touitou et al. (2000), quienes obtuvieron resultados similares para el mismo tipo de transfersomas y etosomas. Sin embargo, ninguno de los prototipos presentó un valor inferior a -30 mV, lo que predice una baja estabilidad a largo plazo de las vesículas lipídicas.

Una de las etapas clave en el proceso de producción de las vesículas lipídicas es la purificación de estas, en gran medida, porque para determinadas aplicaciones resulta fundamental la eliminación de la fracción de fármaco no encapsulada. La tasa de recuperación de fosfolípidos tras el proceso de producción demostró que la centrifugación es un método que solamente es adecuado para los liposomas convencionales. Por lo tanto, este método fue descartado para las vesículas ultraflexibles. Como alternativa, el método de diálisis se empleó con éxito para la purificación de los transfersomas. Sin embargo, este método tampoco parece ser adecuado para los etosomas debido a que el etanol también puede difundir fuera de las vesículas por su alta solubilidad en agua. Ante esta situación y debido a que las vesículas lipídicas pueden incrementar la permeabilidad de tanto la fracción encapsulada como de la no encapsulada, los etosomas empleados en los demás estudios no fueron purificados previamente.

En cuanto a la eficacia de encapsulación, hay que tener en cuenta que los compuestos hidrofílicos suelen mostrar menores tasas de encapsulación que los lipofílicos. Esto se debe a que el proceso de carga del fármaco es más eficiente si el compuesto queda retenido en las bicapas

de fosfolípidos, lo que depende principalmente de su afinidad primaria. Teniendo en cuenta esta premisa, aunque los resultados de eficacia de encapsulación no superaron el 50%, se encuentran en cualquier caso dentro en el intervalo esperado.

### 4.3. Morfología de las vesículas

En las imágenes obtenidas mediante TEM, se observaron vesículas multilamelares, ya que el método de Bangham tiende a producir MLV relativamente heterogéneas. Éstas presentaron forma esférica-ovoide, aunque con ciertas irregularidades debido al proceso de secado de la muestra. El tamaño de las partículas se ajustó satisfactoriamente a los resultados obtenidos mediante DLS. Sin embargo, las ligeras variaciones de tamaño pueden deberse a la preparación de las muestras que requieren procesos de deshidratación y secado.

### 4.4. Evaluación de la flexibilidad de las vesículas

La tasa de reducción del tamaño de las vesículas y la pérdida de volumen tras la extrusión en frío se utilizó como medida indirecta de la capacidad de deformación de las vesículas. Como era de esperar, se obtuvieron diferencias significativas entre los liposomas convencionales y las vesículas ultraflexibles. Mientras que los liposomas quedaron retenidos en los filtros de 100 nm y se vieron obligados a dividirse en partículas más pequeñas para pasar los poros, los transfersomas y los etosomas (cuyo tamaño inicial era superior a 100 nm) mantuvieron su tamaño durante el paso a través de la membrana porosa gracias a su flexibilidad.

Asimismo, el volumen final recogido tras la extrusión en frío está inversamente relacionado con la flexibilidad de la vesícula. Mientras que no se observaron diferencias en los lotes de transfersomas o etosomas, todos los prototipos liposomales presentaron una reducción significativa respecto a sus volúmenes iniciales. De este modo, ambas técnicas confirmaron la flexibilidad de los transfersomas y los etosomas en comparación con los liposomas convencionales.

4.5. Estudios de estabilidad de las vesículas

Las cinéticas de desestabilización global indicaron los índices de estabilidad sobre las vesículas de B12 (liposoma convencional < etosoma < transfersoma). Los transfersomas resultaron ser la formulación más estable, ya que no se registraron fenómenos característicos de inestabilidad, mientras que los etosomas, experimentaron un fenómeno de claro de floculación reversible, que también fue documentado previamente por Cristiano et al. (2019). Por el contrario, las vesículas liposomales experimentaron un proceso de sedimentación muy marcado.

La estabilidad física y química a largo plazo se monitorizó midiendo semanalmente el tamaño de la vesícula y PDI durante 2 meses, y el porcentaje de encapsulación durante 3 meses. No se encontraron diferencias significativas en el tamaño en función del tiempo de almacenamiento a 4ºC, excepto para los liposomas convencionales transcurridas 4 semanas. Respecto al PDI, no se observó ningún cambio significativo durante el periodo de tiempo estudiado, lo que apunta a una evolución homogénea del tamaño de las poblaciones de vesículas.

Respecto al contenido de fármaco en relación con la cantidad inicialmente formulada, se detectaron cambios significativos en él en todos los prototipos entre las semanas 7 y 8. Esta pérdida o fuga de fármaco es relativamente habitual, especialmente en aquellas vesículas que contienen fármacos hidrofílicos. Teniendo en cuenta estos resultados, las vesículas lipídicas de B12 parecen mostrar una estabilidad a corto y medio plazo (al menos 1 mes para todos los parámetros comprobados), lo que las hace una herramienta prometedora para su aplicación clínica. Sin embargo, con el objetivo de aumentar su estabilidad para que pudieran ser almacenadas durante largos periodos de tiempo, se investigó la liofilización como método de preservación, ya que se ha demostrado que es un método excelente para garantizar la estabilidad de múltiples formulaciones farmacéuticas.

## 4.6. Liofilización, estudio calorimétrico y termogravimétrico de las vesículas

La estabilidad a largo plazo es uno de los mayores retos para la producción de liposomas y vesículas lipídicas modificadas, ya que las partículas basadas en lípidos pueden oxidarse fácilmente. Como se pudo observar, cuando se dispersan en una solución acuosa, pueden permanecer estables entre 2 y 3 meses, aunque los cambios de tamaño de partícula pueden darse a partir del primer mes de almacenamiento.

Tras la liofilización de las vesículas lipídicas, la inspección visual denotó que el uso de sorbitol no evitó el colapso de la muestra, dando lugar a un producto final subóptimo en términos de calidad. De este modo, el sorbitol se consideró como un crioprotector inadecuado para el tipo de muestra en estudio. Por el contrario, la lactosa logró preservar un producto uniforme sin evidencia de daños, y fue capaz de mantener estables los valores de tamaño y PDI previos a la liofilización. La calidad de los polvos liofilizados obtenidos se evaluó mediante la determinación del contenido de agua residual que fue en todos los casos de alrededor del 1%, un resultado adecuado teniendo en cuenta que el contenido máximo recomendado es del 3%.

## 4.7. Estudio de liberación de B12 a partir de las vesículas

Los estudios de liberación de fármacos *in vitro* se utilizan regularmente en el proceso de optimización de las formas farmacéuticas. Todas las formulaciones de vesículas lipídicas mostraron una liberación controlada del fármaco. Al contrario que la solución acuosa de B12, que se utilizó como control, ya que representa el perfil de difusión del fármaco sin las limitaciones producidas por la formulación en cuestión. Concretamente, después de 3 h de liberación, la cantidad de B12 detectada en el medio receptor fue significativamente mayor para la solución que para los liposomas, los transfersomas y los etosomas, tal como se esperaba. Además, también se observaron diferencias entre la liberación a partir de liposomas convencionales y vesículas ultraflexibles. La diferencia resultó

ser mayor en el caso de los liposomas, probablemente debido a su mayor rigidez, puesto que aquellas bicapas lipídicas que presentan poca flexibilidad se oponen en mayor media al transporte o difusión del fármaco.

Los datos experimentales de liberación se ajustaron a diferentes modelos cinéticos para comprender mejor los perfiles de liberación: Higuchi, Korsmeyer-Peppas, Kim, Peppas-Sahlin, de orden cero y de primer orden. Este punto es muy recomendable, ya que la modelización matemática puede ayudar a comprender el posterior rendimiento *in vivo* de las formulaciones. En general, el modelo de Korsmeyer-Peppas presentó los valores AIC más bajos para casi todas las formulaciones, lo que es indicativo de un ajuste preciso.

Al contrario de lo que se esperaba para las vesículas ultraflexibles, el modelo de Korsmeyer-Peppas señaló que presentan un mecanismo de liberación mixto. Sin embargo, a tenor de los resultados, parece que la relajación o erosion tiene una mayor influencia durante las primeras horas de libración y su peso se diluye con el transcurrir del tiempo, en favor de la difusión pasiva como mecanismo de liberación de la B12.

### 4.8. Biocompatibilidad celular de las vesículas

Las vesículas lipídicas permiten mejorar la administración transdérmica de fármacos sin considerables efectos adversos producidos por ellas mismas. Esto se debe a su excelente biocompatibilidad y a su facilidad para mezclarse con los lípidos de la piel, al contrario que otras nanopartículas. En algunos casos, incluso presentan una mejor biocompatibilidad que las disoluciones farmacológicas equivalentes.

Los datos obtenidos en los ensayos de proliferación celular mostraron una relación directa entre la viabilidad celular y la combinación dosis de B12-portador lipídico. Las formulaciones blancas (solo el vehículo sin fármaco) no solo no resultaron tóxicas, sino que se observó un efecto proliferativo, especialmente marcado en los liposomas y transfersomas. Teniendo en cuenta, por un lado, que las vesículas con una carga de

fármaco elevada pueden provocar efectos citotóxicos en las células, y, por otra parte, que las formulaciones blancas fueron completamente biocompatibles, parece claro que una dosis excesiva de B12 fue la principal responsable de la muerte celular observada en los casos en los que las vesículas lipídicas se suministraron a las células en cultivo sin ser debidamente diluidas. Sin embargo, cabe mencionar que los etosomas no mostraron ningún signo de toxicidad con la dosis inicial de B12 (1,3 mg/mL) tras su producción. Los transfersomas demostraron ser portadores citotóxicos intermedios, ya que la viabilidad celular observada fue más alta que la producida por liposomas convencionales administrados a la misma concentración de fármaco. Por último, hay que tener en cuenta que las concentraciones de B12 que pueden acceder a la piel son presumiblemente inferiores a las ensayadas en este experimento y, por tanto, no serían de esperar problemas de biocompatibilidad con las formulaciones de vesículas lipídicas de B12 desarrolladas en caso de ser administradas en cualquier modelo *in vivo*.

### 4.9. Preparación de MNA solubles

Para la preparación de MNA se utilizaron dispersiones acuosas de diferentes polímeros biocompatibles, solos o combinados, para preparar los prototipos finales de MNA solubles. En concreto, se emplearon tres polímeros diferentes: PVP y PVA (de bajo y alto peso molecular). Dos de las formulaciones diseñadas no sirvieron para producir MNA. Una de ellas contenía una mezcla de polímeros excesivamente viscosa que no permitió el vertido del gel en los moldes de polidimetilsiloxano. La segunda de estas mezclas, que contenía las vesículas lipídicas liofilizadas y PVA de bajo peso molecular (15% p/p), no pudo retener las vesículas lipídicas en la red polimérica después de la centrifugación previa al vertido del gel en los moldes. Además, cabe destacar que las vesículas lipídicas migraron a la fracción superior de la mezcla, como consecuencia de la baja densidad del polvo liofilizado. El resto de las formulaciones produjeron mezclas

poliméricas homogéneas, y las MNA resultantes presentaron proyecciones puntiagudas y afiladas al ser observadas al microscopio.

Las MNA mostraron un comportamiento flexible discreto tras ser desmoldadas. Una semana después, las MNA eran completamente resistentes a la deformación y alcanzaron su máxima resistencia y propiedades de inserción. Este hecho fue determinado mediante el análisis TGA que mostró que las MNA perdieron un porcentaje menor de peso (atribuible al agua residual) siete días después de la producción, en comparación con las MNA recién desmoldadas.

Las MNA se caracterizaron mediante DSC a partir de sus materiales constitutivos para estudiar las posibles interacciones polímero-polímero o polímero-fármaco y caracterizarlas para posteriores procesos de escalabilidad. Dependiendo del componente polimérico principal, los termogramas mostraron un perfil característico común.

## 4.10. Morfología de las MNA

Las imágenes obtenidas mediante SEM se emplearon para observar la morfología de las MNA y confirmar la longitud de sus proyecciones determinadas previamente mediante microscopía óptica. A nivel topológico, se observaron principalmente dos diferencias entre ellas. En primer lugar, la formulación de MNA que contenía B12 presenta una topografía lisa, mientras que las vesículas lipídicas liofilizadas interactúan con la superficie de las MNA dando lugar a un relieve irregular. En segundo lugar, la longitud de las proyecciones de los prototipos de MNA formulados con vesículas lipídicas fue significativamente menor que la de los otros prototipos de MNA. Este hecho se debe probablemente a que el alto contenido de la vesícula lipídica (10% p/p) produce un comportamiento diferente del polímero, con una mayor tendencia a la contracción tras la pérdida del agua contenida en las MNA, en comparación con la producida por el fármaco libre (1% p/p).

4.11. Resistencia mecánica y propiedades de inserción de las MNA

La evaluación de la resistencia mecánica se llevó a cabo para determinar la capacidad de las MNA para resistir la fuerza de compresión que es ejercida cuando se insertan en la piel. La resistencia mecánica de las MNA se determinó en base al porcentaje de reducción de la longitud de las proyecciones tras la aplicación de una fuerza de 32 N/MNA. La compresión de las MNA produjo una reducción significativa de la longitud de dichas proyecciones en todos los casos. Sin embargo, el porcentaje específico de compresión dependió de la combinación y concentración del polímero. Las MNA preparadas utilizando sólo PVP como polímero exhibieron las máximas reducciones de longitud y deformación de las proyecciones, lo que representa unas propiedades mecánicas insuficientes. Del mismo modo, el prototipo elaborado únicamente con PVA de bajo peso molecular también mostró una considerable reducción de la longitud de las MNA. Por el contrario, los prototipos formulados con una combinación de PVA y PVP exhibieron comportamientos de mayor resistencia a la compresión, especialmente aquellos que se formularon con PVA de alto peso molecular. Además, la incorporación de partículas lipídicas liofilizadas redujo la resistencia mecánica del prototipo en cuestión. Estos hallazgos concuerdan adecuadamente con los resultados previamente publicados, donde la combinación de PVP y PVA aumentó las propiedades mecánicas de las formulaciones debido a las interacciones de los puentes de hidrógeno establecidos entre los grupos -OH del PVA y los grupos C=O del PVP.

La potencial inserción de los prototipos se evaluó mediante un modelo artificial con Parafilm® M. Los resultados de inserción corroboraron las propiedades mecánicas de las MNA, ya que las mejores tasas de inserción fueron aquellas proporcionadas por los MNA formulados con la mayor concentración de la mezcla polimérica PVP-PVA de alto peso molecular.

4.12. Estudio de liberación de B12 a partir de las MNA solubles

El uso de diferentes polímeros para producir MNA que dio lugar a diferentes propiedades mecánicas y químicas, también influyó en el proceso de liberación del fármaco y en el mecanismo por el cual se produce. Aunque la liberación de principios activos a partir de MNA solubles se rige principalmente por la disolución de la matriz, otros mecanismos adicionales también son posibles. En general, los resultados de liberación volvieron a coincidir con las tendencias obtenidas en las pruebas de resistencia mecánica e inserción. La formulación basada únicamente en PVP mostró una liberación más rápida del fármaco que las combinaciones basadas en PVA-PVP. Por su parte, el prototipo basado en PVA de bajo peso molecular también mostró una liberación más lenta en comparación con la combinación de dos polímeros (PVA-PVP). Por el contrario, la adición de las vesículas lipídicas liofilizadas en el MNA dio lugar a estructuras poliméricas menos cohesionadas que liberaron su carga con mayor facilidad. Además, como las vesículas lipídicas presentan una limitación en cuanto a la carga de fármaco que pueden albergar en comparación las MNA que contienen el fármaco libre, su dosis de B12 fue considerablemente menor, aunque también se consiguió una liberación total del fármaco. Los prototipos elaborados con PVA de alto peso molecular fueron los únicos que conservaron la matriz polimérica una vez finalizado el proceso de liberación, lo que denota un mecanismo de liberación por relajación-hinchamiento del polímero alternativo y coexistente con la disolución de la matriz.

4.13. Penetración en piel *ex vivo* de B12 a partir de las vesículas

El espesor total del *estrato córneo* determinado mediante densitometría infrarroja fue de alrededor de 20 µm, coincidiendo con los valores estándar de entre 17-28 µm previamente obtenidos por Jacobi et al. (2007). Los estudios de penetración cutánea se realizaron con las formulaciones más prometedoras de liposomas, transfersomas y etosomas (L1, L2, T1d, T2d, E1 y E3). Además, se utilizó como referencia una

solución acuosa de B12 al 0,5 % p/v, ya que representa la difusión libre de fármaco sin los posibles efectos potenciadores de la absorción proporcionados por el vehículo.

Como tiempos de incubación se seleccionaron 2, 4 y 6 h, que abarcan aproximadamente el mayor tiempo que una formulación tópica puede mantenerse sobre la piel. Además, generalmente, las cantidades de B12 detectadas en las capas más profundas de la piel aumentan en función del tiempo de incubación, lo que facilita la interpretación de los resultados. En cualquier caso, la solución de B12 presentó la mayor cantidad de B12 extraída en el primer strip. No obstante, tras el tiempo máximo de incubación, la solución de B12 no fue capaz de penetrar más allá de 6 µm de profundidad, lo que confirmó la dificultad que presenta la B12 para difundir a través de la piel intacta. Sin embargo, las vesículas lipídicas (prototipos L1, T1d, T2d y E3) permitieron que la B12 alcanzara la dermis (más de 25 µm de profundidad).

### 4.14. Permeabilidad transdérmica *in vitro* de B12 a partir de las vesículas y MNA solubles

Al igual que los resultados de penetración a través de la piel, la permeabilidad de la B12 administrada en una solución acuosa fue prácticamente despreciable, ya que las concentraciones del fármaco que se obtuvieron en el medio receptor de la FDC, tras 32 h de estudio, se encontraron por debajo del límite de cuantificación mediante el análisis por HPLC. Por un lado, el uso de las vesículas lipídicas desarrolladas aumentó notablemente la permeabilidad de la B12 a través de la piel, siendo las vesículas ultraflexibles las que proporcionaron los mayores flujos transdérmicos de fármaco. Por otro lado, estos flujos fueron mayores a partir de aquellas formulaciones que presentaron menores porcentajes de eficacia de encapsulación, pero que, a su vez, contienen mayores dosis de fármaco. Por tanto, se puede concluir que la capacidad de mejorar la difusión de la B12 por parte de las vesículas lipídicas aumenta dependiendo de su flexibilidad y de la dosis incorporada.

La constante de permeabilidad (*Kp*) se calculó correlacionando el flujo con la dosis aplicada como medida de la eficiencia de cada vesícula y, de nuevo, los transfersomas y los etosomas fueron las formulaciones más eficaces. La comparación de *Jmax* y *Kp* pone de manifiesto el rol que juega la dosis de fármaco contenida en las vesículas, ya que condiciona su actividad y eficacia final, como puede observarse en la comparación de los flujos entre los diferentes liposomas y transfersomas formulados con diferentes dosis. Por último, las vesículas ultraflexibles ofrecieron una disminución significativa del periodo de latencia, lo que produjo un inicio más temprano de la absorción y contribuyó a un aumento de la permeabilidad.

El pre-tratamiento de la piel con MNA de tipo sólido potenció en gran medida los resultados de permeabilidad obtenidos, ya que las MNA fueron capaces de abrir canales en la epidermis de mayor profundidad que el espesor del propio *estrato córneo*. A pesar de ello, el tiempo que dichos microporos permanecen abiertos en condiciones *in vivo* es objeto de controversia y discusión, por lo que se desarrollaron MNA solubles de B12 que no presentan esta limitación. Los resultados de permeabilidad de este tipo de MNA evidenciaron que, al igual que las MNA de tipo sólido, aumentan notablemente la absorción del fármaco. En cuanto a los perfiles de permeabilidad de estas MNA poliméricas, cabe destacar la existencia de dos fases bien diferenciadas. Una primera fase, correspondiente al efecto de inserción de las MNA que permite superar el *estrato córneo*; y una segunda, que tiene lugar tras la transición sólido-gel, tras la cual la B12 tiene mayor facilidad para difundir a través de la piel debido al estado líquido de la formulación.

4.15. Modelo *in vivo* DTH. Evaluación del edema auricular, estudios de bioluminiscencia e histopatológico

El aumento del grosor del pabellón auricular se considera una medida indirecta del edema de la piel de la oreja y de la permeabilidad vascular, ya que se encuentra típicamente aumentada en los procesos de dermatitis atópica y de contacto. Para estos experimentos, se seleccionaron los transfersomas y etosomas, ya que fueron los tipos de vesículas lipídicas que mostraron los mejores resultados en cuanto a la penetración y permeabilidad de la B12 a través de la piel. Es decir, se descartaron los liposomas convencionales y la solución acuosa de B12 como medida de reducción de animales en cumplimiento del principio de las 3 R.

El grosor del pabellón auricular aumentó en los grupos sensibilizados con OXA en comparación con los no sensibilizados (grupo control sano). Este aumento del grosor de la piel asociado al edema no se observó cuando los animales fueron tratados con clobetasol (1,25 mg/ml), lo que demuestra la idoneidad del modelo, ya que el proceso patológico puede ser plenamente revertido mediante un tratamiento con el fármaco adecuado. En concreto, se produjo una ligera disminución del grosor de las orejas, probablemente como consecuencia del adelgazamiento y la atrofia de la piel habitualmente inducida por el tratamiento con un esteroide.

El grupo no tratado (grupo OXA) mostró un aumento del grosor de la oreja de 308 µm después de 24 h, que remitió espontáneamente al resolverse el proceso inflamatorio, ya que los animales no fueron expuestos de nuevo al agente desencadenante. Los transfersomas cargados con B12 redujeron 182 µm el aumento del grosor de la oreja en comparación con el grupo no tratado a las 24 h. Las vesículas lipídicas sin fármaco también mostraron una reducción no significativa del edema o grosor cutáneo en comparación con el grupo no tratado, que puede ser atribuida a las propiedades emolientes de los componentes lipídicos y al efecto refrescante producido por el vehículo acuoso. Estos resultados

confirmaron la eficacia de la B12 como neutralizador del óxido nítrico. Sorprendentemente, los etosomas no produjeron un efecto significativo satisfactorio, a pesar de que en los estudios *in vitro* de penetración y permeabilidad fueron una de las formulaciones con mejores resultados. Una posible explicación es que la irritación producida por el etanol contrarrestó los efectos neutralizadores de la B12.

El modelo DTH utilizado genera una respuesta inflamatoria a través de neutrófilos, macrófagos y células T. Por lo tanto, se llevó a cabo un ensayo BLI con luminol para confirmar los hallazgos anteriores y estudiar si los neutrófilos están implicados en el proceso patológico desencadenado por la administración de OXA. En este ensayo se descartaron los grupos tratados con etosomas debido a los escasos resultados obtenidos en la reducción del grosor de las orejas. También se descartó el grupo de control sano, puesto que se utilizó la oreja izquierda como control intraindividual en cada animal. La sensibilización a OXA generó una emisión de fotones significativo entre las orejas derecha e izquierda, con una señal máxima después de 24 h, lo que confirmó la existencia de un cierto grado de infiltración leucocitaria. Como era de esperar, la BLI inducida por el luminol se normalizó completamente con el tratamiento con clobetasol, ya que los neutrófilos y los macrófagos son susceptibles típicamente de los efectos de supresión inmunitaria en tratamientos con corticoesteroides. Sin embargo, al contrario que en los estudios de edema en la oreja, el T1d (transfersoma de cianocobalamina) también mostró una atenuación total de la emisión de fotones, lo que sugiere una mitigación eficaz de la infiltración leucocitaria y de su actividad en la zona inflamada. Como se observó anteriormente, las vesículas de transfersomas blancos redujeron los niveles de BLI en comparación con el grupo no tratado, mostrando de nuevo un cierto grado de efecto producido por el vehículo acuoso.

En el estudio histopatológico se compararon las diferencias anatómicas en la estructura de la piel de los animales tratados con transfersomas con los animales sanos y no tratados. Al igual que en el

ensayo de BLI, se observó una clara infiltración celular como respuesta al daño inflamatorio tras la sensibilización con OXA, la cual se revirtió claramente con el tratamiento con trasnfersomas de cianocobalamina (T1d). Las estimaciones del grosor de los cortes histológicos estimados por medición digital coincidieron con las obtenidas directamente en el procedimiento *in vivo*, y mostraron las mismas tendencias en cuanto a la reducción del grosor. Sin embargo, fue posible observar que este engrosamiento de la piel no está causado únicamente por el edema, ya que la epidermis y la dermis también mostraron un grosor considerablemente mayor en los animales no tratados.

## 5. Resumen de los aspectos más destacados de la tesis y los hitos alcanzados

**Hito 1:** Se desarrolló un método analítico de HPLC para detectar y cuantificar la B12.

- Los parámetros calculados demostraron la sensibilidad, exactitud, precisión y robustez del método.
- Los límites de detección y cuantificación del método estuvieron por debajo de las concentraciones habituales de las muestras en los diferentes estudios realizados, por lo que el método analítico fue adecuado para los propósitos de este trabajo.

**Hito 2:** Se diseñaron, produjeron y caracterizaron tres tipos de vesículas lipídicas: liposomas, transfersomas y etosomas.

- El tamaño y el PDI de las vesículas lipídicas desarrolladas fueron óptimos para fines de administración transdérmica, siendo < 300 nm y < 0,3 respectivamente.
- La flexibilidad de los transfersomas y etosomas fue confirmada por reducción de tamaño y ratios no significativos de pérdida de volumen tras la extrusión en frío.

- La eficiencia de encapsulación obtenida se encontró dentro del intervalo esperado para un fármaco hidrofílico. La carga útil final del fármaco fue inversamente proporcional a la eficiencia de encapsulación.
- Los valores de potencial zeta no fueron predictivos de estabilidad a largo plazo (liposomas < transfersomas < etosomas). Sin embargo, para preservar las vesículas durante largos periodos de tiempo de almacenamiento, se aplicó con éxito la liofilización a los liposomas convencionales y a los transfersomas cuando se utilizó lactosa como agente crioprotector.
- Como consecuencia de la estabilidad de las formulaciones vesiculares a corto plazo, se concluyó que la centrifugación es el método óptimo para purificar los liposomas convencionales, mientras que los transfersomas se purificaron satisfactoriamente mediante diálisis. Por último, los etosomas no se centrifugaron ni se dializaron, ya que, por un lado, no sedimentaron tras la centrifugación y, por otro lado, el etanol puede eliminarse mediante diálisis como consecuencia de su alta afinidad por un medio acuoso.
- Los estudios de liberación concluyeron que, dentro de las 10 h iniciales, la relajación o erosión del sistema vesicular es el principal mecanismo de la liberación. No obstante, la difusión contribuye a la liberación en mayor medida después de este período de tiempo.
- La biocompatibilidad de las vesículas lipídicas se evaluó utilizando la línea celular RAW 264.7. Los etosomas mostraron una alta biocompatibilidad en comparación con los transfersomas, y éstos, a su vez, mayor que los liposomas.

**Hito 3:** Se diseñaron once prototipos de MNA solubles cargadas con vesículas lipídicas liofilizadas con B12 y B12 libre. PVA y PVP fueron los polímeros utilizados en diferentes concentraciones para producir dichos prototipos. Se elaboraron y caracterizaron con éxito nueve de ellos.

- Las MNA cargadas con vesículas lipídicas mostraron una longitud de las proyecciones más corta que las que incorporaron B12 libre, como resultado de la mayor contracción del polímero por la presencia de la alta proporción de vesículas lipídicas liofilizadas.
- La fuerza mecánica se evaluó a través de la resistencia de las MNA a la compresión, siendo las formulaciones con alta concentración de polímero y combinación PVP-PVA aquellas que mostraron mayor resistencia mecánica.
- Las propiedades de inserción de las MNA en un modelo de piel artificial se correlacionaron con sus propiedades mecánicas, alcanzando una profundidad de al menos 276 µm en todos los casos.
- La liberación del fármaco dependió, en gran medida, del componente polímerico principal de la formulación. Las MNA fabricadas con polímeros de bajo peso molecular (PVA 9-10 kDa y PVP 40 kDa) se disolvieron completamente en la prueba de liberación *in vitro*, mientras que las MNA elaboradas con PVA 38-50 kDa mantuvieron la integridad de la matriz. En consecuencia, los mecanismos que rigen principalmente la liberación son la difusión/disolución y el hinchamiento/relajación de la matriz polimérica, respectivamente.

**Hito 4:** Las vesículas lipídicas y MNA solubles aumentaron la penetración y permeabilidad de la B12 a través de la piel, que es casi inapreciable cuando el fármaco se administra como solución acuosa.

- La penetración de la B12 mejoró notablemente gracias a las diferentes vesículas lipídicas. Como se esperaba, las cantidades de B12 detectadas en las capas más profundas de la piel aumentan en función del tiempo de incubación y del uso de vesículas ultraflexibles.
- Los resultados de la permeabilidad de la B12 mostraron la misma tendencia que en los estudios de penetración, lo que indica que los

transfersomas y los etosomas son las vesículas más eficientes para transportar el fármaco hasta la dermis, donde puede ser absorbido hacia la circulación sistémica.

- La permeabilidad de B12 a través de la piel aumenta cuando la piel se trata previamente con MNA de tipo sólido. Los microcanales creados en el *estrato córneo* anulan en gran medida su función de barrera y, en consecuencia, aumentan notablemente la tasa de permeabilidad de B12 en las diferentes formulaciones vesiculares.
- Las MNA solubles cargadas con B12 mejoraron también la permeabilidad del fármaco. Los perfiles de absorción mostraron dos etapas diferenciadas. En la primera, el proceso que limita la difusión del fármaco es su liberación de la forma farmacéutica. En la segunda, el perfil de permeabilidad cambia y se alcanza el estado estacionario de la absorción.
- Según los resultados obtenidos, las vesículas lipídicas son los sistemas más adecuados para tratar los trastornos de la piel, mientras que las MNA son ideales para lograr un suministro sistémico de B12.

**Hito 5:** Los transfersomas cargados con B12 redujeron el edema e inflamación asociada a un modelo *in vivo* murino DTH.

- Los transfersomas cargados con B12 produjeron una reducción significativa de 172 ± 50 µm en el aumento del grosor del pabellón auricular en comparación con el grupo de control no tratado.
- El grupo tratado con transfersomas cargados con B12 no recuperó los niveles basales de grosor de la oreja observados en los controles sanos, pero la diferencia entre los grupos no fue estadísticamente significativa. Estos resultados demuestran que, aunque los transfersomas no pudieron recuperar totalmente el tejido del proceso patológico, contribuyeron a reducir el daño de manera considerable.

- Las formulaciones sin B12 produjeron una reducción no significativa de la variación del grosor de la oreja, probablemente debido a las propiedades emolientes de los lípidos constituyentes de las vesículas y a la capacidad refrescante del vehículo acuoso.
- La implicación de los leucocitos en el proceso patológico desencadenado por la sensibilización con OXA se confirmó mediante el ensayo BLI. El grupo tratado con transfersomas cargados con B12 mostró una mitigación similar a la del grupo tratado con clobetasol. Por su parte, el vehículo sin fármaco también produjo una reducción parcial de la infiltración celular.
- El estudio histopatológico de las secciones de la piel confirmó la disminución del edema, la reducción del engrosamiento de las capas de la piel y el no aumento de la infiltración de leucocitos cuando la dermatitis de contacto se trata con transfersomas cargados con B12.

## 6. Conclusiones

Las conclusiones más relevantes derivadas de los datos obtenidos en este trabajo son:

- **Conclusión 1:** La B12 puede detectarse y cuantificarse de forma precisa y exacta mediante HPLC y espectrofotometría UV-vis.
- **Conclusión 2:** Las vesículas lipídicas pueden ser producidas y cargadas con B12, y presentar propiedades óptimas para fines de administración tópica y transdérmica.
- **Conclusión 3:** La B12 y las vesículas lipídicas liofilizadas se pueden combinar con éxito con dispositivos de MNA solubles, que presentan propiedades mecánicas y de inserción adecuadas para eludir eficazmente el *estrato córneo* y administrar el fármaco directamente en la dermis.
- **Conclusión 4:** La penetración y la permeabilidad *ex vivo* e *in vitro* de B12 a través de la piel se pueden mejorar considerablemente utilizando sistemas de administración transdérmica: MNA solubles

> combinación de vesículas lipídicas con MNA de tipo sólido > transfersomas > etosomas > liposomas convencionales > solución acuosa

- **Conclusión 5:** La dermatitis de contacto y el eccema pueden mejorarse mediante la administración de transfersomas cargados con B12, que potencian las propiedades neutralizantes del óxido nítrico de la B12 al mejorar su acceso a las capas más profundas de la piel.

# Abbreviations list

**AD:** Atopic Dermatitis

**AFM:** Atomic Force Microscope

**ARIMA:** Autoregressive Integrated Moving Average

**AIC:** Akaike Information Criterion

**ATR-FTIR:** Attenuated Total Reflection-Fourier Transform Infrared

**AUC:** Area Under Curve

**B12:** Vitamin B12 or Cyanocobalamin

**BCOP:** Bovine Corneal Opacity and Permeability

**BLI:** Bioluminescence Imaging

**CAM:** Chorioallantoic membrane

**CC:** Calibration Curve

**CLSM:** Confocal Laser Scanning Microscopy

**DL:** Detection Limit

**DLS:** Dynamic Light Scattering

**DMEM:** Dulbecco's Modified Eagle's Medium

**DSC:** Differential Scanning Calorimetry

**DTH:** Delayed-type Hypersensitivity

**E:** Ethosomes

**EE:** Entrapment Efficiency

**Er:** Relative Error

**ESEM:** Environmental Scanning Electron Microscopy

**FBS:** Foetal Bovine Serum

**FDA:** Food and Drugs Administration

**FDC:** Franz Diffusion Cell

**GUV:** Giant Unilamellar Vesicles

**HET-CAM:** Hen's Egg Test Chorioallantoic Membrane

**HPLC:** High Performance Liquid Chromatography

**H-RMN:** Magnetic Resonance Spectroscopy

**iNOS:** Nitric Oxide Synthase

**IS:** Irritation Score

**Jmax:** Maximal Flux

**Kp:** Permeability Coefficient

**L:** Liposomes

**LDE:** Laser Doppler Electrophoresis

**LDH:** Lactate Dehydrogenase

**LUV:** Large Unilamellar Vesicles

**MCD:** Microdialysis

**MNA:** Microneedle Arrays

**MPO:** Myeloperoxidase

**MTT:** 3-(4,5-dimethylthiazol-2-yl)-2,5-diphenyltetrazolium bromide

**MLV:** Multilamellar Vesicles

**MVV:** Multivesicular Vesicles

**P90G:** Phospholipon 90G®

**PASI:** Psoriasis Area Severity Index

**PC:** Phosphatidyl Choline

**PDI:** Polydispersity Index

**Phox:** NADPH Oxidase

**PMN:** Polymorphonuclear leukocyte

**PVA:** Poly (vinyl alcohol)

**PVP:** Poly (vinyl pyrrolidone)

**RICS:** Raster Image Correlation Spectroscopy

**QL:** Quantification Limit

**R-MCD:** Retro-microdialysis

**S:** B12 aqueous solution

**SEM:** Scanning Electron Microscopy

**SCORAD:** Scoring of Atopic Dermatitis

**SD:** Standard Deviation

**STED:** Stimulated Depletion Microscopy

**SUV:** Small Unilamellar Vesicles

**T:** Transfersomes

**TEM:** Transmission Electron Microscopy

**TCI:** Topical Calcineurin Inhibitor

**TDD:** Transdermal Delivery of Drugs

**TDS:** Transdermal Delivery Systems

**TEWL:** Transepidermal Water Loss

**TGA:** Thermogravimetric Analysis

**TSI:** Turbiscan Stability Index

**UHPLC:** Ultra-High-Performance Liquid Chromatography

**UHPLC-MS:** UHPLC-Mass Spectrometry

**VC:** Variation Coefficient

# Tables list

# Figures list

Note: All illustrations were created using Biorender.

# Abstract

The bioavailability optimisation of drugs provides them with a second opportunity, which for several reasons, cannot exert an optimal therapeutic effect. This approach is frequently omitted in the pharmaceutical research industry as the discovery of novel therapeutic agents is always more welcome rather than the utilisation of previously available treatments. On this matter, several molecules are rejected as a consequence of the adverse effects they produce when administered systemically or because of their low availability. In consequence, local or organ-targeted therapies have attracted attention as they contribute to overcome these kinds of troubles. The skin has been used as a platform to deliver drugs since ancient times. Nowadays, it is still considered one of the main alternatives to the oral route, as it allows both the treatment of local disorders and systemic drug absorption because of its anatomical structure. However, as an interface between the body and the environment, the outer skin layer (*stratum corneum*) prevents the entrance of substances. This opposition is of major importance for large molecules, and 500 Da is considered the maximum size which can diffuse through the skin structure naturally. Therefore, switching the route of administration is often not enough to solve all the inconveniences mentioned above. Reformulation of drugs in advanced drug delivery systems (ADDS) is commonly needed to bypass the *stratum corneum* barrier and produce an optimised therapeutic effect.

The main objective of this thesis is to develop different ADDS that allow the diffusion of large molecules through the skin. As a model molecule, cyanocobalamin (B12) was selected, due to its high molecular weight (1355 Da) and hydrophobicity, which hinders its transdermal absorption. For this, lipid vesicles and polymeric microneedles were used to encapsulate and increase cyanocobalamin permeability through the skin.

Among all the lipid vesicles developed over the years, conventional liposomes, transfersomes and ethosomes were chosen and characterised towards those properties predictive of an enhanced diffusion. Specifically,

transfersomes and ethosomes showed the best features, as they were homogeneous populations of small size (< 200 nm) and flexible structures. Freeze-drying was used to solve the long-term stability issues that usually affect lipid vesicles, and, as an intermediate step that allows their incorporation in an alternative delivery system, the dissolving microneedles. As microneedles are devices that contain micrometric needle-like projections which bypass the *stratum corneum* directly, they were especially characterised in terms of mechanical strength and insertion capacity. The combination of PVA and PVP polymers conferred the optimal mechanical and insertion properties, as a consequence of the interaction between the hydroxyl and carbonyl functional groups.

*In vitro* and *ex vivo* studies confirmed the increase in drug absorption when cyanocobalamin was incorporated in the ADDS when compared to a standard aqueous solution, which provided an almost neglectable diffusion. As a consequence of their conception, microneedles were able to deliver the drug transdermally after a moderate period, suggesting their suitability to be used as an alternative to parenteral administration. Lipid vesicles, which showed longer latency times to achieve quantifiable dermal concentrations of drug, were able to localise the drug delivery in the outer skin layers improving the penetration in comparison to the standard solution.

B12 nitric oxide scavenger behaviour makes it possible to ameliorate skin inflammatory disorders such as atopic dermatitis or eczema when applied topically. The feasibility of lipid vesicles for topical treatments was assessed by *in vivo* delayed-type hypersensitivity model. B12-loaded transfersomes significantly reduced the increase in ear thickness in comparison to the untreated group, proving their effectiveness in oedema reduction. In addition, histological findings such as reduced epidermal hyperplasia, dermis thickening, and leukocyte infiltration confirmed the skin restoring effect of transfersomes.

# Chapter 1

## General introduction: topical and transdermal drug delivery

Chapter adapted from **Skin Drug Delivery Using Lipid Vesicles: A Starting Guideline for the Development of Liposomes, Transfersomes and Ethosomes.** Guillot AJ, Garrigues TM, Melero A. *Submitted to Advanced Drug Delivery Reviews.*

The skin offers a very attractive alternative route for the administration of drugs for several reasons (1). Firstly, it has several advantages over the main delivery routes such as oral or parenteral. Transdermal Delivery of Drugs (TDD) has good acceptance and compliance by patients (2), it is usually painless and does not need aseptic materials, techniques, nor specialised personnel for its administration (3). Secondly, its large surface available -an area of approximately 20.000 $cm^2$ in adults- make it the biggest entrance to the body (4). Finally, drug doses can be reduced as the first hepatic passage and the acidic stomachal environment are bypassed, avoiding several undesired effects (5). In comparison, other alternative routes like sublingual, buccal and rectal mucosae have been shown as unpredictable routes with many more limitations (6).

As a result of skin structure, the application of drugs on the skin may have two aims: local therapy or transdermal delivery of drugs (7). The application of a drug onto the skin can pursue different goals: a) remain on the skin to protect the organism or fight against alive entities existent on the skin surface (e.g. sunscreens, repellents or antifungal/antibacterial products) (8); b) treat different skin appendage disorders (antiperspirant or infections) (9); c) treat different affections of the *stratum corneum* and viable epidermis (emollients, exfoliants, anti-inflammatories, antihistaminic drugs, etc.) (10); d) modify the skin barrier function to improve the penetration of other drugs (11); and e) transdermal drug delivery (1).

## 1.1. A Brief Review of Skin Functions and Structure

For a better comprehension of this chapter, it is essential to define the structure and functions of the skin. The skin is the interface which separates the body and the environment. In consequence, the main function of the skin is to offer a robust barrier against the penetration of external xenobiotics, substances, allergens, and microorganisms (12). In addition, the skin plays other important roles, such as homeostasis maintenance -preventing the dehydration of the body- (13), and protection from the harmful effects of ultraviolet radiation (14). Finally, this tissue presents different types of receptors sensitive to pressure changes, pain and temperature, which are essential to achieve a proper interaction with the environment (15,16).

As mentioned above, the skin is the largest human organ that represents 10% of the total weight. Its thickness varies from 0.05 to 2 mm depending on the anatomical region (17). It can be divided into three differentiated layers: Epidermis, Dermis and Hypodermis.

The Epidermis is the external layer of the skin, and it can be subdivided into four stratums: basale, spinosum, granulosum and corneum. The main features of each stratum are summarised in Table 1.1. Keratinocyte is the main cell-type present in the Epidermis layer, it is created in the *stratum basale* and migrates progressively to the next layers, giving rise to a permanent cellular renewal process (18). Keratinocytes are surrounded by a medium with a low content of water. This amount of water decreases as keratinocyte differentiation progresses, and at the end, the most superficial layer is constituted by superposed dead cells -called corneocytes- (19). For drug penetration and transdermal purposes, the *stratum corneum* is the most important layer as it exerts the greatest opposition to drug diffusion through the skin (20).

The Dermis is the vascularised and innerved layer located just below the Epidermis (21,22). It is a network of proteins (mainly elastin and collagen) with notable elastic properties (23–25). Fibroblast (26),

macrophages and leukocytes are the cells present in this layer (27). The irrigation of this layer provides the nutrients to the dermal and epidermal cells and removes metabolites (28). This process allows the systemic absorption of drugs after its administration, since every substance that reaches the dermis microcirculation is susceptible to absorption. The Hypodermis is the deepest skin structure and is often not considered part of the skin. It consists of a matrix made of fatty and connective tissues that connects the skin with underlying tissues and organs (29,30). Its composition and extension vary depending on a range of factors such as gender, age, anatomical site, nutritional conditions and endocrine status (31).

The skin appendages are dermal-associated structures, such as sweet and sebaceous glands, hair and hair follicles (32). All of them are the target of local therapies, for example, acne and alopecia affections (33,34). The transfollicular route has often been ignored because hair follicles only occupy approximately 0.1% of total skin surface (35). It has been demonstrated more recently that hair follicles can have an important impact on the transdermal diffusion of drugs, because their structure offers a thinner barrier between the external environment and dermal microcirculation (36). In this sense, certain types of nanostructures can reach the bottom of the follicle and remain there as a drug deposit (37).

**Table 1.1.** Main features of the different skin layers.

| | Skin Layer | Properties | Function | Ref. |
|---|---|---|---|---|
| **Epidermis** | ***Stratum corneum*** | -20 to 25 layers of dead and cornified cells | -Prevention of external entities entrance to the body | (20,38) |
| | ***Stratum granulosum*** | -Thin layer composed of keratinocytes which contains keratin granules<br>-Cells are rich in ceramides | -Contains important proteins and enzymes (Filaggrin, Involucrine, Loricrine)<br>-Waterproof task | (39) |
| | ***Stratum spinosum*** | -Thicker layer of cells<br>-Contains Langerhans cells | -Immunological response | (40) |
| | ***Stratum basale*** | -Single layer of keratinocytes which contains stem cells<br>-Contains melanocytes and Merkel cells | -Responsible for keratinocyte division and proliferation (peeling process)<br>-UV protection by melanin production<br>-Sensory perception | (41) |
| | **Dermis** | -Fibroblast is the main cell type in this layer<br>-Composed of collagen and elastin<br>-Vascularised and innervated<br>-Location of skin appendages | -Mechanical support of the skin<br>-Contribution to skin elasticity<br>-Supplies nutrients to the dermis<br>-Thermoregulation | (25,26) |
| | **Hypodermis** | -Connective and adipose tissue<br>-Not considered part of the skin | -Anchors skin to the different tissues and organs<br>-Protective structure and insulator | (29,30) |

## 1.2. Topical administration of drugs

The access of any substance from the surface to the deeper skin layers follows a passive diffusion process. Two possible routes have been theorised as pathways: the appendageal and the transepidermal routes (Figure 1.1) (42). In the first one, the drug uses the hair follicles and glands to diffuse near the dermal vessels. The main limitation of this route is that those structures represent a minimum proportion of the total skin area and are limited to particles with an appropriate size (< 500 Da) (36,43). The transdermal route is subdivided into two variations: the transcellular route (the molecule passes through the cell and intracellular matrix) and the intercellular route (the molecule diffuses through the lipidic matrix) (44). Although the intercellular path is longer compared to the transcellular one, it is generally accepted as the main route (45).

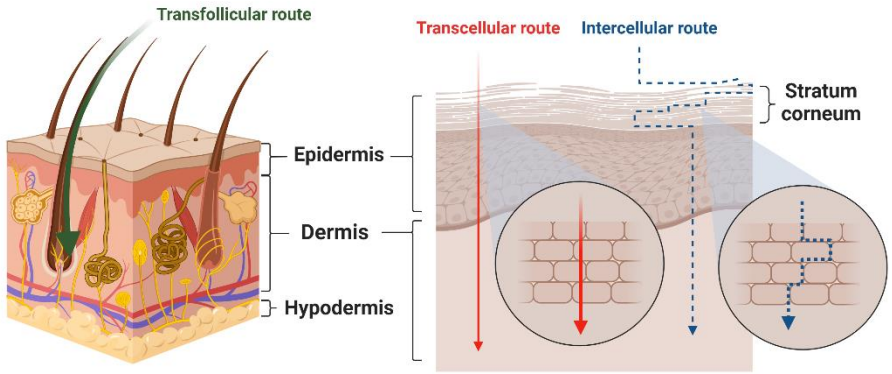


**Figure 1.1.** Illustration of the drug diffusion routes through the skin.

This diffusion process is obviously affected by the molecule properties, which conditions its suitability as a candidate for TDD. In these terms, an intermediate partition coefficient between vehicle and membrane (46), a low degree of ionisation (47), and a molecular weight less than 500 Da have been defined as the ideal characteristics (48). Furthermore, the integrity of the skin has a key role in cutaneous absorption, since damaged tissues facilitate the absorption process enormously.

Transdermal absorption of substances is a multistep process, where five stages are distinguished (2): i) Partition of the drug from the vehicle into the *stratum corneum* ii) Penetration of a molecule into the *stratum corneum*; iii) Diffusion from the *stratum corneum* into the viable epidermis; iv) Partition from the viable epidermis to the dermis; v) Access to the systemic circulation. As a consequence of this complex process, it is difficult to suggest a biophysical model that considers all the events involved. Nevertheless, diffusion through the *stratum corneum* or full-thickness epidermis process can be modelled to estimate parameters that characterise the process (49). The typical plot of a permeation study presents two phases: non-steady and steady states (Figure 1.2).

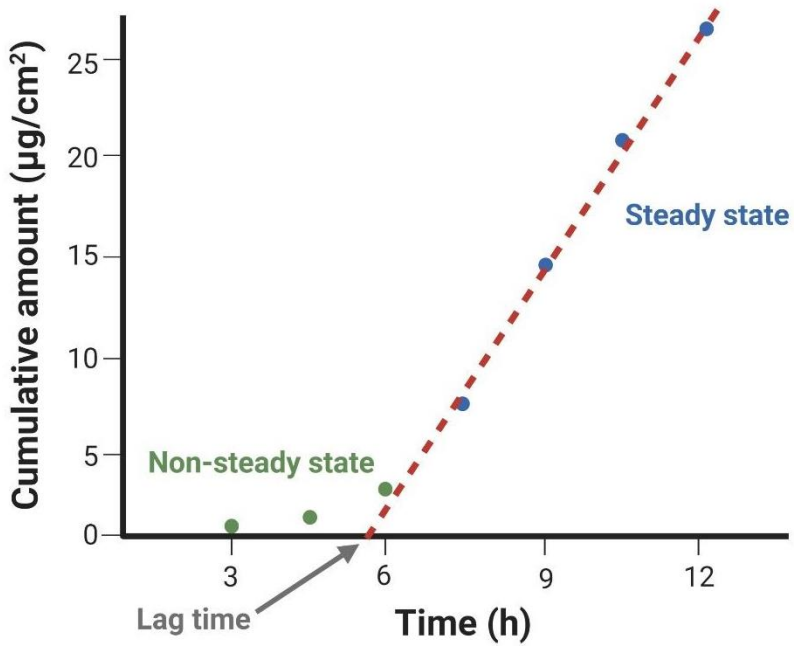


**Figure 1.2.** Typical plot obtained from a drug permeation through the skin *in vitro* study in Franz diffusion cell set-up, with infinite dose.

Fick's diffusion laws describe the process in the steady state, and they establish that the change of the concentration as function of time is proportional to the gradient variation (2), according to the following equation (equation 1.1):

*Equation 1.1:*

$$\left(\frac{\delta c}{\delta t}\right) = D\left(\frac{\delta^2 c}{\delta x^2}\right)$$

The Scheuplein equation is an approximation, often used when *in vitro* models are performed under infinite dose and skin conditions. The amount of the drug that diffuses through the barrier is described by the following equation (equation 1.2) (50,51):

*Equation 1.2:*

$$Q(t) = A \cdot P \cdot L \cdot C \cdot \left[D \cdot \frac{t}{L^2} - \frac{1}{6} - \frac{2}{\pi^2} \cdot \sum_{n=1}^{\infty} \frac{(-1)^n}{n^2} \cdot \left(\frac{-D \cdot n^2 \cdot \pi^2 \cdot t}{L^2}\right)\right]$$

Where *Q(t)* is the amount of the drug which diffuses at a given time (t); *A* is the diffusion surface area ($cm^2$); *P* represents the partition coefficient of the permeant between the membrane and the donor vehicle; *L* is the membrane thickness; *D* is the diffusion coefficient of the permeant drug in the membrane; and *C* is the concentration of the permeant (µg/mL) in the vehicle (or the donor).

Equation 1.2 can be transformed to determine permeability coefficient (*Kp)* and lag time (*tL)* by substituting *P·D/L* and $L^2/6D$ for *Kp* and *tL*, respectively (equation 1.3):

*Equation 1.3*

$$Q(t) = A \cdot Kp \cdot C \cdot \left[t - tL - \frac{12 \cdot tL}{\pi^2} \cdot \sum_{n=1}^{\infty} \frac{(-1)^n}{n^2} \cdot \left(\frac{-n^2 \cdot \pi^2 \cdot t}{6 \cdot tL}\right)\right]$$

The linear regression of the experimental cumulative amount data versus time offers the estimation of *Kp* and *tL*. Lag time is calculated as the intercept of the slope to the abscissae axis. Permeability coefficient and maximal flux per surface unit, *Jmax* (µg/$cm^2$/h), can be calculated from the linear regression of the slope according to the equations (equations 1.4 and 1.5):

*Equation 1.4:*

$$J = \frac{m}{A}$$

*Equation 1.5:*

$$Kp = \frac{J}{C}$$

Where *m* is the slope of the linear part from the cumulative amount versus time; *A* is the diffusion surface area ($cm^2$); *C* is the concentration of the drug in the donor drug site.

## 1.3. Common *in vitro*, *ex vivo* and *in vivo* methods to evaluate drug transdermal permeability and penetration

Even though *in vivo* methods are the ideal procedures to evaluate the effects of any drug delivery system, many studies show that systemic and local drug concentrations can be estimated and predicted using skin permeation parameters, such as the permeability coefficient (*Kp*), the permeation coefficient (P), the diffusion coefficient (D), the lag time (tL) and the transdermal flux (*Jmax*), all of them calculated by *in vitro* and *ex vivo* methods.

### 1.3.1. *In vitro* methods: Diffusion cells

Since their conception, diffusion cells have become the reference method for assessing transdermal drug permeation parameters. Specifically, Franz diffusion cells (FDC) of static and vertical type are widely used in a huge number of studies (52). FDC are composed of two compartments, also called chambers. They are clamped together incorporating a membrane or tissue in between. The donor chamber harbours the drug formulation, and the receptor chamber is filled with an acceptor medium to receive the drug after its passage through the barrier under study, in this case, the skin (Figure 1.3). To mimic the *in vivo* conditions, as a surrogate method, this receptor compartment is stirred using a magnetic bar and warmed to the physiological temperature of the skin (32-37ºC) introducing it in a tempered water bath or using and

additional jacket system surrounding the cell (53). The receptor chamber includes a sampling port that allows the sampling procedure at preset intervals of time. Afterwards, the samples are analysed by a suitable analytical method according to the drug nature and its permeated amounts.

As an essential premise for optimal FDC studies, they should be conducted under conditions that ensure the real performance of the formulations. Finite dose condition is an approach based on the use of an insufficient drug dose that causes a final equilibrium between donor and receptor drug concentrations (54). This method is closer to the *in vivo* and clinic practice conditions. However, it requires complex calculations and complicates the interpretation of the results (55). On the other hand, infinite dose conditions entail the existence of a sufficiently high drug concentration in the donor chamber that produces a concentration gradient between chambers and the maintenance of the skin conditions (56). These conditions ensure a constant thermodynamic dragging force over the drug and results in a practical simplification that makes the perception of the absorption process easier. In these terms, it is accepted that in the acceptor medium, the drug concentration should not increase above 10% of the drug solubility in the medium or decrease beyond 10% of the initial concentration in the donor medium (57,58). However, not only a high drug solubility in the acceptor medium is important towards the maintenance of the sink conditions. Temperature, pH, stirring and degasification have an undeniable influence on the experimental variability. In fact, FDC studies often show a lack of reproducibility, which can be minimised when validated conditions and procedures are followed. Acid or basic drugs solubility is directly correlated with the pH and denotes the importance of selecting the proper acceptor medium to avoid the breakage of sink conditions (57). It has also been reported that an increase in temperature of around 10ºC leads to a 2-fold transdermal flux as a consequence of its marked impact in drug diffusivity and solubility (58). Although it seems that stirring and stirrer-type could have a trivial role in the outcome from permeability studies, they determine the correct mixing and homogenization of drug in the receptor

chamber and, hence, the correct sampling procedure and maintenance of the sink conditions. In general, the use of a common magnetic stirrer with a low stirring speed (200 rpm) does not offer proper mixing conditions and higher speed rates are needed (800 rpm) (57). Nevertheless, speeds as high as this can produce air bubbles on top of the receptor chamber that notably reduce the effective diffusional area at the membrane. Therefore, the evaluation of the suitability of the stirrer-speed combination must be assessed in each case, since there are examples where a simple PTFE cylindrical magnetic bar (12x4.5 mm) operating at 200 rpm demonstrated to be optimal (58). As mentioned, degassing must be carried out in any study by tilting the FDC and letting the bubbles come out through the sampling arm, but it must be done as quick as possible in order to avoid temperature fluctuations.

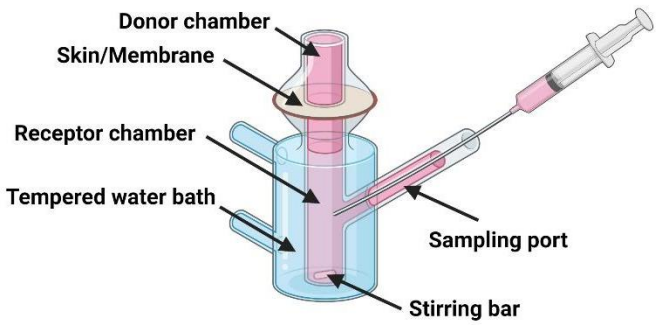


**Figure 1.3.** Schematic illustration of a jacketed-FDC set-up.

Excised human skin is considered the self-standard as a diffusional barrier for *in vitro* experiments (59). However, ethical and supply issues restrict its use. Moreover, in the case of obtaining human skin samples, they frequently present considerable inter-individual variations, as a consequence of the difficulties to obtain donors with a similar profile (age, gender, ethnic group, general state, etc.) (60–62). Thus, animal skin is used as an alternative, since it is easier to obtain and there is higher homogeneity in the population (62). Porcine skin is, from a histological point of view, the most similar to human (63–65). Rat skin is structurally the most similar

among all rodents, but several studies point that it is more permeable in comparison to human skin (66–68). The thickness of the skin, and particularly the *stratum corneum*, has a notable influence on drug penetration and determination of transdermal absorption parameters (69). This thickness varies depending on the species and the anatomical region chosen, as shown in Table 1.2. Standard experimental protocols and guidelines for *in vitro* skin permeation studies allow the use of full-thickness skin, dermatomed-skin, heat separated epidermis, and *stratum corneum* sheets (59). Heat separated epidermis can be easily obtained by the Kligman method, which consists of plunging the skin for 90-120 sec in a 60ºC water bath and then removing the epidermal layer using a forceps (70). For *stratum corneum* layer isolation, the epidermis is immersed for 24 h in a 0.0001% w/v trypsin solution (pH 8.0-8.6) (70).

**Table 1.2.** Skin thickness among species and anatomical region. Taken and modified from Todo, 2017 (59).

| Animal specie | Anatomical region | *Stratum corneum* (µm) | Epidermis (µm) | Whole skin (µm) |
|---|---|---|---|---|
| Human | Forearm | 17 | 36 | 1.5 |
| Pig | Back | 26 | 66 | 3.4 |
| Pig | Ear | 10 | 50 | 1.3 |
| Mouse | Back | 5 | 13 | 0.8 |
| Rat | - | 18 | 32 | 2.09 |

Even though *in vitro* permeation through human skin presents high variability in general, animal skin samples are not exempt from it. Artificial cellulose and sulfone based-membranes have been used as diffusional barriers (71–73). Nonetheless, they do not replicate the structure and characteristics of the skin and its use has been relegated to drug delivery mechanistic studies. As a real alternative, reconstructed skin models and 3D-bioprinted tissues have been set-up in recent decades (74). These

artificially generated tissues replicate, either partially or completely (epidermal and dermal layers), the native histological skin structure, but they are rather expensive due to the equipment involved (75). For example, histological architecture is mimicked sandwiching a fibroblast layer between two collagen-based layers and, eventually, including immune cells as well (76). EpiSkin®, EpiDerm® or Labskin® are other artificial commercially available skin models.

### 1.3.2. *Ex vivo* methods: Tape-stripping, differential-striping, and confocal laser scanning microscopy

Drug depth-penetration in the skin and dermatopharmacokinetics are usually estimated using *ex vivo* methods (77). Tape-stripping stands out for being a minimally invasive technique that removes the *stratum corneum* (78). Briefly, a skin biopsy is placed onto a glass slide and covered with an aluminium mask, leaving the application area uncovered. A feasible amount of drug formulation is applied, and the set-up is incubated at 32ºC for between 2 h and 6 h (79). Longer incubation times can cause the disintegration of the epidermis as a consequence of excessive exposure to occlusive conditions (50). After incubation, 20-25 strips of adhesive tape are applied sequentially to the skin under standardised conditions of pressure to progressively remove the corneocyte layers (Figure 1.4) (80). For this purpose, the percentage of *stratum corneum* removed can be monitored through infrared densitometry devices, differential weighing methods, microscopic measures or transepidermal water loss (TEWL) measurements (80,81). The drug is extracted from the strips, immersing it overnight in an extractive medium where the drug is highly soluble, and then quantified using an appropriate analytical method. To avoid drug concentrations under the quantification limit, strips can be grouped in different pools, for example: 1, 2, 3-5, 6-10, 11-15, 16-20, 21-25. Eventually, tape-stripping can be performed under *in vivo* conditions (82,83). High performance liquid chromatography (HPLC, and UHPLC) (84), Attenuated total Reflection-Fourier transform infrared (ATR-FTIR) (85), Differential scanning calorimetry (DSC) (86,87), and Raman

microscopy have been successfully coupled with tape stripping as analytical methods (88,89). Although the tape-stripping method is widely used to study the barrier activity of skin, it is a technique associated with considerable variability and errors if it is not done under standardised conditions. Therefore, a standardised protocol which specifies the material, pressure, and operating conditions reduces considerably the associated variability (90). Additionally, to reduce the variability, the first strip can be discarded since immediate drug availability in the first layer, or deficient cleaning of the skin surface before the stripping step, can introduce an overestimation (91).

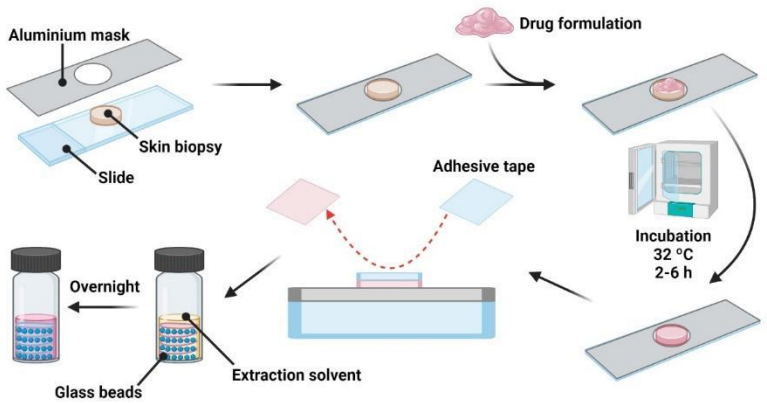


**Figure 1.4.** Schematic illustration of the tape-stripping technique steps.

Differential-stripping is a technique that consists of a combination of the tape-stripping technique with a cyanoacrylate skin surface biopsy (92). It is considered the most straightforward technique to quantitatively determine the follicular uptake (93). For this technique, human skin is not recommended because hair follicles are contracted after the skin excision. Therefore, pig ear skin is considered here as the gold standard, as the ear cartilage prevents the closure of hair follicles and because they are anatomically quite similar (density and follicular diameter) to human skin (94). Briefly, after carrying out a tape-stripping procedure, as described above, a suitable amount of instant quick-drying cyanoacrylate adhesive is

applied onto the pre-stripped skin (93). Upon the glue polymerisation, the cyanoacrylate layer is peeled off to recover the follicular cast and is then processed similarly to common strips. A mass balance study is highly recommended in both techniques to assure complete drug extraction by the method, where 100 ± 20% is considered a satisfactory final balance (95).

Confocal laser scanning microscopy (CLSM) has been applied to skin research for multiple purposes, for example, the determination of vesicle pathway, vesicle-skin interactions or the effect of different penetration enhancers (96,97). The CLSM approach is based on linking covalent fluorescent dyes (e.g. rhodamine) to the xenobiotic in order to track the system diffusion (98,99). It allows the virtual depth-sectioning of the skin, slicing horizontal planes, and then reconstructing them to obtain an image of the skin structure (100). The main advantage of CLSM is its low invasiveness (101), and its drawbacks are the interferences as a consequence of skin autofluorescence and short periods of analysis (102).

### 1.3.3. *In vivo* methods: Microdialysis, skin biopsies, *in vivo* plasma level-time profiles and pharmacodynamic response-correlation studies

Microdialysis (MCD) is the reference method to obtain a complete study of drug pharmacokinetic processes in the skin (103). Unlike the tape-stripping technique, MCD is not only restricted to the *stratum corneum* structure, and *in vivo* conditions provide more realistic outcomes. MCD set-up consists basically of a semipermeable dialysis probe lodged in the skin structure and connected to a perfusion pump, which infuses a physiological receiver fluid (Figure 1.5) (104). The main difficulties of MCD are those related with the surgical procedure to install the dialysis probe (anaesthetic pre-treatment and need of trained personnel) (104), the perfusion conditions like flow or drug concentration in retro-microdialysis (R-MCD) variation (105), the requirement of a highly sensitive analytical method for sample analysis (106), and a compulsory calibration before and after the experiment (107). When an optimal equilibrium of the system is achieved, an exchange of molecules takes place by diffusion, as an effect of the

concentration gradient. The drug molecules, previously released by the drug formulation and permeated until the extracellular fluid in the dermis, diffuse to the receiver fluid and are collected for analysis (108). R-MCD variation uses the same principles, however, the drug under study is dissolved in the perfusion fluid and diffuses from the dialysis probe to the dermis (Figure 1.5) (105). Beyond the information about drug diffusive properties provided by R-MCD, its application seems more limited, as it overlooks the *stratum corneum* effect on drug absorption.

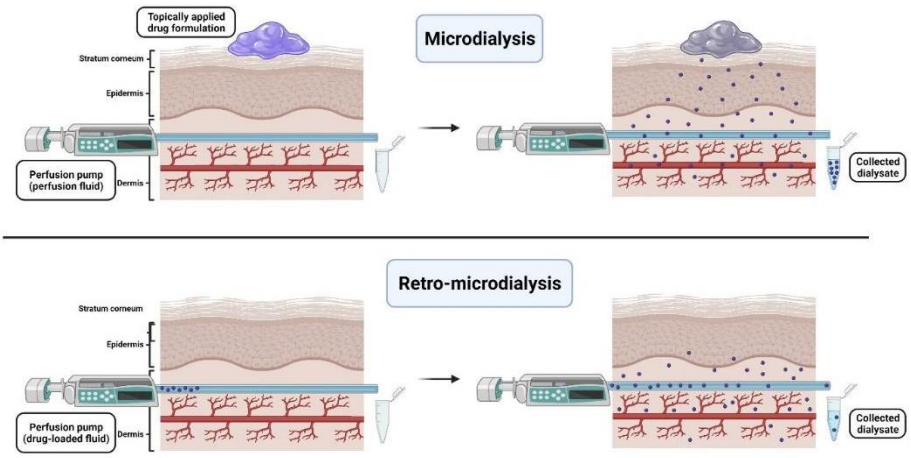


**Figure 1.5.** Schematic illustration of skin microdialysis and retro-microdialysis basic set-up.

When a drug is applied topically with systemic purposes, *in vivo* plasma concentrations-time profiles offer a direct measurement of the absorption, distribution and elimination processes from blood or plasma samples (109), obtained at pre-set times via tail vein, retro-orbital puncture, jugular cannulation, or other ethically approved bleeding techniques (110). In these experiments, topical formulations are compared to oral, parenteral, or subcutaneous as reference administration routes, to determine the feasibility of topical application as an effective alternative by comparison of certain parameters, such as the area under curve (AUC), maximal plasmatic concentration (Cmax), time of the peak plasma concentration (Tmax) and elimination half-life ($t_{1/2}$) (109). Local or systemic

pharmacological effects and safety of topical treatments usually require the use of animal models which trigger the pathologic condition under study. Atopic dermatitis, psoriasis and melanoma models are often employed since there is currently a great interest in these skin diseases (111–113). Diabetes, hypertension and pain are other focus points of pharmaceutical research nowadays (114–116).

The obtention of skin biopsies is an extremely-invasive approach, where skin samples are removed (under anaesthetic procedure) using a punching device or a controlled-deep blade (117). It is used for the study of certain skin affections, such as skin tumours or immuno-inflammatory skin diseases, like atopic dermatitis or psoriasis (118,119). The tissues are further processed to extract the drug and determine drug concentration or the metabolite of interest in the skin. Afterwards, the tissue is homogenised and the drug is extracted from the homogenate to release the interstitial and extracellular analytes (117). Homogenisation is performed usually using either a fast-rotating device that shreds or grinds the skin into smaller pieces or a mortar to pulverise a frozen skin sample (120). Additionally, to ensure a complete release of the intracellular and interstitial content, skin samples can be solubilised using chemical agents (for example hydrogen peroxide 30% and ammonium hydroxide (121), or enzymatic digestion (collagenase) (122). The extraction procedure is performed similarly to the *ex vivo* methods, with a drug-affine medium, or using a precipitation protocol in the case of proteins (123).

# Chapter 2

## Motivation and Impact, Aims and Contributions

## 2.1. Motivation and Impact

Cyanocobalamin is a hydro-soluble vitamin (B12) which is stored in the liver and plays important roles in protein metabolism, red blood cell formation and central nervous system homeostasis (Figure 2.1). As a vitamin, it is an essential nutrient that needs to be obtained from the diet, and its deficiency negatively impacts health. On the other hand, its activity as a nitric oxide scavenger has recently drawn attention to it for its potential therapeutic applications.

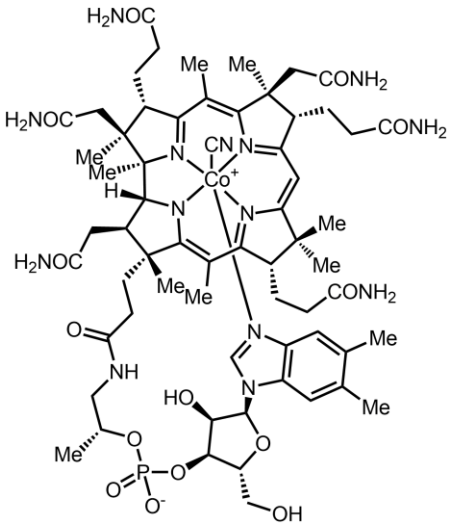


**Figure 2.1.** Chemical structure of the cyanocobalamin.

B12 deficiency is the most common cause of certain haematologic pathologies, neuropsychiatric symptoms and other illnesses (124–128). The lack of adenosyl-B12 or methyl-B12 is the usual consequence of vitamin B12 deficiency. It produces impaired methylation processes and methylmalonate metabolism, derived from the amino acids and fatty acids catabolism (129). Low levels of adenosyl-B12, in particular, produce methylmalonic acid accumulation, which can be associated with neurologic syndrome (130). Methyl-B12 deficiency leads to an accumulation of homocysteine, which can induce cellular stress, apoptosis and protein homocysteinylation (128,131).

B12 deficiency has three main aetiologies: autoimmune disorder, malabsorption and low dietetic intake (132). Autoimmune deficiency is a condition in which anti-intrinsic factor antibody production blocks its activity, resulting in an inability to absorb the vitamin (133). The causes of malabsorption are associated with an inefficient production of intrinsic factors by parietal cells in the stomach (134,135). This condition is very frequent in gastric bypass or ileum illness (surgeries, Crohn's disease or *Diphyllobothrium latum* infections) (136–140). Lastly, lifestyles with a growing implantation in society, such as veganism, could lead to a deficiency situation after some years (141–143). Other less frequent conditions like transcobalamin-II genetic deficiency (144), and the use of certain drugs (oral contraceptives, hormonal replacement therapies, metformin, proton pump inhibitors and H2-histaminic antagonists) could also be a cause of B12 deficiency (145,146). Its prevalence in developed areas, such as North America and Europe, varies from 2.9 - 25.7%, depending on the cut-off of the serum level values (<148 and <256 pmol/L of B12, respectively) (129,147,148). Moreover, several studies suggest that it increases with age and is more frequent in women than men (3.3% versus 2.4% respectively, for <148 pmol/L serum levels). Additionally, the impact on developing areas, like Africa, South America and Asia, is significantly higher, and it is not only confined to older age groups, exceeding 40% of prevalence in certain subpopulations (children, young adults and pregnant women) (129).

The management of B12 deficiency depends on different factors like aetiology and severity, and varies as a function of its duration and administration route. It consists of vitamin deposits repletion by intramuscular injections or cyanocobalamin oral doses (149–151). In case of an anomalous functioning of the intrinsic factor way, it is possible to administer 1000 µg of cyanocobalamin by intramuscular injections daily for 1-2 weeks, reduce the posology during the following month to once a week, and continue with a monthly maintenance injection (152,153). However, the intramuscular route presents certain disadvantages, such as: discomfort

and pain generation; the need for aseptic material and techniques; the costs associated with its administration by trained personnel; the restriction to patients with low muscular mass; and medical complications such as thrombus formation, nerves injuries -in femoral and gluteal injections- or hypersensitivity reactions (154–156). As an alternative, it is possible to take cyanocobalamin orally, but the main issues are its low bioavailability (1-4%) and inefficiency in intrinsic factor-related aetiologies (151).

Concerning B12 use as a drug, it has been proposed to treat chronic inflammatory skin diseases. Eczema or atopic dermatitis (AD) and psoriasis are the most common ones, and the molecular mechanisms underneath provide an opportunity for the use of B12 as a possible therapy. AD is characterised by pruritus, dry skin, eczematous injuries and lichenification (157). The onset of AD commonly occurs during childhood, and it is associated with significant morbidity and reduced quality of life. The prevalence of AD has increased over the past 30 years and its incidence has increased two to three-fold in recent years. Approximately 20% of children and 1-3% of adults are affected by this disorder (158). Although the pathogenesis of AD is not completely understood, it has been associated with various factors: alteration of the skin barrier function, immune dysregulation, infections, and environmental processes. The alterations in the skin barrier function may be caused by deficient levels of ceramides and proteins involved in keratinocyte differentiation and prevention of transepidermal water loss (159,160). Several genetic factors, such as mutations in filaggrin genes could cause this situation (161). The defective barrier function allows the penetration of allergens and irritant agents that trigger inflammation through Th2 responses (with increased IL-4, IL-5, IL-13 cytokines) in the acute phase and Th1 responses (with increased IFN-gamma and IL-12) in chronic injuries (162). In addition, the usual action of patients scratching themselves stimulates keratinocytes to release other inflammatory cytokines like TNF-alpha, IL-1, and IL-6, which perpetuate chronic inflammation. Ultimately, the modified state of the skin contributes to bacteria colonisation, which further worsens the disorder (162).

Likewise, psoriasis is a chronic inflammatory skin disease with a marked immune component. Its most characteristic sign is the presence of erythematous plaques, often spread over large areas of the body. The worldwide prevalence varies from 1-8%, depending on geographical areas. Although it can begin at any age, its onset frequently occurs in adulthood, with one out of three cases occurring during childhood (163). A major characteristic in psoriasis pathogenesis is the inappropriate activation of the immune system, which leads to keratinocyte hyperplasia, altered T-cell function, and angiogenesis, among others (164–166). Furthermore, oxidative stress and increased expression of insulin-like growth factor-1 and epidermal growth factor also participate in the pathogenesis (167).

The main goals of the treatment of these pathologies include restoring the skin barrier, limiting itching, decreasing inflammation, and controlling immune alterations. To achieve them, a wide plethora of drugs may be used, with systemic immunosuppressive agents, topical corticosteroids and topical calcineurin inhibitors (TCIs) being the first-line drugs in the pharmacological management of AD and psoriasis (168). However, systemic treatments are not exempt from potential adverse side-effects, such as kidney and liver dysfunction or myelosuppression, which complicate the management of severe cases (169–171). Local side-effects associated with long-term use of topical steroids and TCIs are relatively common, such as skin atrophy, ecchymosis, erosions, striae, delayed wound healing, purpura, easy bruising, and acne (172). In addition, the Food and Drug Administration (FDA) has reported warnings about the use of some TCIs due to the potential risk of skin cancer and lymphomas (173).

The proinflammatory cytokines involved in AD and psoriasis stimulate the expression of inducible nitric oxide synthase (iNOS) in keratinocytes. In consequence, skin lesions of AD and psoriasis present high levels of nitric oxide, which has been implicated in the pathogenesis of atopic eczema and psoriasis (174,175).

Oral and topical B12 have been used as an alternative for preventing or ameliorating AD and psoriasis, since it has been described as a nitric oxide scavenger (176). Although the first trials date back to the 60s, not many studies have been carried out since then (177). Januchowski et al. (2009) compared the effect of B12 cream (0.07%) with a moisturiser base for the treatment of childhood eczema in a double-blinded randomised trial using the SCORAD scale (Scoring of atopic dermatitis). Intraindividual comparisons showed significant differences in reduction of SCORAD values between B12 cream and the placebo. Particularly, topical B12 significantly improved treated skin more than the placebo at 2 and 4 weeks. Recently, mild-to-moderate plaque psoriasis has been treated with topical B12 ointments for 12 weeks in two randomised clinical trials (178). Stücker et al. (2001) compared the effect of B12 with calcipotriol (vitamin $D_3$ analogue), obtaining similar decreases in the PASI score (Psoriasis Area Severity Index) after the studied period. Moreover, there was a noticeable reduction in the efficacy of calcipotriol after 4 weeks of therapy, whereas the efficacy of B12 remained largely constant over the whole observation period, making it more suitable for long-term use (179). Similarly, a positive outcome was obtained when comparing B12 and an emollient cream in the study done by Del Duca et al. (2017). The differences in PASI reduction were noticeable at week 2 and increased during the following 10 weeks. Two weeks after the end of the treatment, the psoriatic lesions evolved positively (especially the ones treated with B12), proving the potential role of cyanocobalamin-based formulation in the treatment of epidermal disorders (180). Despite these promising results, the molecular weight (1355 Da) and hydrophilicity of B12 limit its diffusion through intact human skin given that one of the main functions of the skin is to prevent the penetration of exogenous substances to the body (181). As the barrier function is recovered during treatment, B12 permeability might be gradually reduced. Research on cutaneous permeability has shown that skin diffusion may be improved by using a suitable formulation, and it can even be used for systemic administration (182).

## 2.2. Aims

The main objective of this thesis is the development and characterisation of pharmaceutical formulations to enhance B12 penetration and absorption through the skin to offer a feasible alternative in the AD and vitamin B12 deficiency therapies.

To achieve this goal, the project was divided into the following sub-objectives:

**Objective 1:** Development of an accurate and precise analytical HPLC method for B12 detection and quantification.

**Objective 2:** Development and characterisation of B12 lipid vesicles (liposomes, transfersomes and ethosomes), emphasising the biocompatibility, stability and other properties that work as predictors of optimal drug penetration and permeability (entrapment efficiency, size, flexibility, and drug release).

**Objective 3:** Development and characterisation of B12 dissolving microneedles, specially evaluating their cargo delivery properties and ability to overpass the *stratum corneum*.

**Objective 4:** *Ex vivo* and *In vitro* evaluation of B12 penetration and permeability through the skin provided by lipid vesicles and microneedle arrays, and results comparison with B12-solution as standard reference.

**Objective 5:** Challenge one of the designed drug delivery systems in an *in vivo* Delayed-type Hypersensitivity (DTH) model of inflammatory skin disease.

## 2.3. Contributions

During this PhD I have contributed to the field of drug delivery and pharmaceutical technology in the form of research papers, review articles, oral communications, poster presentations, and outreach activities. As part of the “Atracció de Talent” fellowship of the University of Valencia, I have also carried out 240 hours of teaching tasks and actively supervised BSc theses.

### 2.3.1. Research papers

**1)** Carolina Oliveira dos Santos L, Spagnol CM, Guillot AJ, Melero A, Corrêa MA. Caffeic acid skin absorption: Delivery of microparticles to hair follicles. **Saudi Pharmaceutical Journal**. 2019 Sep 1;27(6):791–7.

**2)** Carreras JJ, Tapia-Ramirez WE, Sala A, Guillot AJ, Garrigues TM, Melero A. Ultraflexible lipid vesicles allow topical absorption of cyclosporin A. **Drug Delivery and Translational Research**. 2020 Apr 1;10(2):486–97.

**3)** Christfort JF, Guillot AJ, Melero A, Thamdrup LHE, Garrigues TM, Boisen A, et al. Cubic Microcontainers Improve In Situ Colonic Mucoadhesion and Absorption of Amoxicillin in Rats. **Pharmaceutics**. 2020 Apr;12(4):355.

**4)** Melero A, Guillot A, Carneiro C, Nuñez-Sanchez H, Rodríguez-Martí L, Chiari-Andréo BG, et al. Caffeine analysis and extraction from a topical cream intended for UV-skin protection. **Journal of Dispersion Science and Technology**. 2020 Nov 27;0(0):1–7.

**5)** Guillot AJ, Jornet-Mollá E, Landsberg N, Milián-Guimerá C, Montesinos MC, Garrigues TM, et al. Cyanocobalamin Ultraflexible Lipid Vesicles: Characterization and In Vitro Evaluation of Drug-Skin Depth Profiles. **Pharmaceutics**. 2021 Mar;13(3):418.

**6)** Guillot AJ, Petalas D, Skondra P, Rico H, Garrigues TM, Melero A. Ciprofloxacin self-dissolvable Soluplus based polymeric films: a

novel proposal to improve the management of eye infections. **Drug Delivery and Translational Research**. 2021 Apr 1;11(2):608–25.

**7)** Mirabet V, García D, Roca A, Quiroz AR, Antón J, Rodríguez-Cadarso M, et al. Cranioplasty with Autologous Bone Flaps Cryopreserved with Dimethylsulphoxide: Does Tissue Processing Matter. **World Neurosurgery**. 2021 May 1;149:e582–91.

**8)** Chiari-Andréo BG, Marto J, Ascenso A, Carneiro C, Rodríguez L, Guillot AJ, et al. The Impact of Titanium Dioxide Type Combined with Coffee Oil Obtained from Coffee Industry Waste on Sunscreen Product Performance. **Dermato**. 2021 Sep;1(1):2–17.

**9)** Mirabet V, Arrébola M, Briones J, Bosch MP, Ocete MD, Melero A, et al. Microbiological assessment of arterial allografts processed in a tissue bank. **Cell Tissue Bank**. 2021 Dec;22(4):539–49.

**10)** Di Filippo LD, Duarte JL, Borba CA, Pavan FR, Meneguin AB, Chorilli M, Melero A, Guillot AJ, Spagnol CM, Correa M. In vitro skin co-delivery and antibacterial properties of chitosan based microparticles containing ascorbic acid and nicotinamide. **Life**. 2022 July;12(7):1049.

**11)** Guillot AJ, Merino P, Bocchino A, O'Mahony C, Giner RM, Recio MC, et al. Exploration of Microneedle-assisted Skin Delivery of Cyanocobalamin formulated in Ultraflexible Lipid Vesicles. **European Journal of Pharmaceutics and Biopharmaceutics**. 2022 Aug, 177:184–98.

**12)** Pironi AM, Melero A, Eloy JO, Guillot AJ, dos Santos KC, Chorilli M. Solid dispersions included in poloxamer hydrogels have favorable rheological properties for topical application and enhance the in vivo antiinflammatory effect of ursolic acid. **Journal of Drug Delivery Science and Technology**. 2022 Aug, 72: 103602.

### 2.3.2. Review articles

**1)** Guillot AJ, Cordeiro AS, Donnelly RF, Montesinos MC, Garrigues TM, Melero A. Microneedle-Based Delivery: An Overview of Current Applications and Trends. **Pharmaceutics**. 2020 Jun;12(6):569.

**2)** de Oliveira RS, Fantaus SS, Guillot AJ, Melero A, Beck RCR. 3D-Printed Products for Topical Skin Applications: From Personalized Dressings to Drug Delivery. **Pharmaceutics**. 2021;13(11): 1946.

**3)** Guillot AJ, Garrigues TM, Melero A. Skin Drug Delivery Using Lipid Vesicles: A Starting Guideline for the Development of Liposomes, Transfersomes and Ethosomes. **Submitted to Advanced Drug Delivery Reviews**

### 2.3.3. Conferences

- **Biological Barriers 2018**. Design of a protective cream to prevent radio-induced skin damage at three levels of absorption. ***Poster***.
- **III QuimBioQuim 2018**. Development of a new cream to prevent the skin damage in radiotherapy treatments. ***Oral Communication***.
- **CISDEM 2018**. "Cubosome and liposome drug release profiles: comparison of two model drugs". ***Poster***.
- **ESLAV-AAALAC-SECAL 2018**. "A radiodermatitis rat model design of a protective cream to prevent radio-induced skin damage at three levels of absorption". ***Poster***.
- **SEFM-SEPR 2019**. "Diseño de un modelo animal de radiodermitis y evaluación de la liberación absorción y acción de una crema radio protectora y mitigadora". ***Poster***.
- **SEFIG 2019**. "First steps in the development of a new radioprotective cream, and Use of cubosomes to improve topical administration of naproxen". ***Poster***.

- **2nd SPLC-CRS Young Scientist Meeting 2019**. "*In vitro* human skin permeability of ursolic acid from solid dispersions carried in poloxamer-based hydrogels". ***Poster***.
- **CRS Annual Meeting 2019**. "*In vitro* human skin permeability of ursolic acid from solid dispersions carried in poloxamer based hydrogels". ***Poster***.
- **7th Galenus Workshop 2019**. "Ciprofloxacin loaded ocular films to treat eye infections". ***Poster***.
- **13th SPLC Conference on Controlled Drug Delivery 2020**. "Polymeric films: a novel proposal to improve the management of eye infections". ***Oral Communication***.
- **CRS Annual Meeting 2020 (Virtual)**. "Ultraflexible liposomes as topical carriers for Vitamin B12 through the skin". ***Poster***.
- **Biological Barriers 2021**. "Adenosine-loaded liposomes: a new potential tool for the treatment of inflammatory diseases". ***Poster***.
- **SEFIG 2021**. "B12 ultraflexible lipid vesicles: characterization and *in vitro* evaluation of drug-skin depth profiles". ***Poster***.
- **14th SPLC Conference on Controlled drug delivery 2022**. "Ultraflexible lipid vesicles allow *in vitro* skin permeability of cyanocobalamin: a potential treatment for vitamin B12 deficiency". ***Poster-Flash Presentation***.

2.3.4. Engagement, outreach, and divulgation activities

- **2nd Research Networking at UV faculty of pharmacy: Mentoring in research**. 2018.
- **Teaching and Research Exchange at the Faculties of Pharmacy**. 2022.
- **Aligning faculties of pharmacy teaching with sustainable development goals Webinar**. 2022.

2.3.5. Event Organisation

- **8th Galenus International Workshop.** Organising committee, scientific committee, and chair tasks.

# Chapter 3

## State of the art: lipid vesicles and microneedle arrays.

---

Chapter adapted from **Skin Drug Delivery Using Lipid Vesicles: A Starting Guideline for the Development of Liposomes, Transfersomes and Ethosomes.** Guillot AJ, Garrigues TM, Melero A. *Submitted to Advanced Drug Delivery Reviews*; and **Microneedle-Based Delivery: An Overview of Current Applications and Trends,** Guillot AJ, Cordeiro AS, Donnelly RF, Montesinos MC, Garrigues TM, Melero A. *Pharmaceutics, 2020***.**

When talking about drug delivery via the skin, the most challenging aim from a technological point of view is the achievement of a systemic action. There are several well-known examples of treatments that follow this approach, specifically hormonal (estradiol) (183,184), pain (fentanyl) (185), and smoking cessation (nicotine) therapies (186,187). However, as mentioned before, the main skin function is to prevent the entry of exogenous substances into the body. This barrier function is mainly achieved by the *stratum corneum*, due to its lipophilicity and the great cohesion between the cornified cells (188). Transdermal Delivery Systems (TDS) are a plethora of strategies and resources that aim to increase transdermal drug absorption by modifying the skin barrier function or changing the physicochemical properties of molecules to make them optimal for this goal (189,190). Transdermal drug permeability enhancement can be achieved by two approaches: physical and chemical methods (191). The ideal TDS must present the following properties (44,192,193): a) non-toxic, non-irritant or non-allergenic; b) quick action and predictable duration; c) pharmacologically inert; d) ease removal; e) allow rapid restorage of skin properties after its removal; f) compatible with excipients and drugs; g) comfortable and cosmetically acceptable; and h) inexpensive. Unfortunately, no TDS presents all these properties together to date. The main advantages and disadvantages of TDS are summarised in table 3.1. Nanotechnology aims to develop a huge variety of systems and entities ranging in the nanoscale, from 1 to 1000 nm (194). One of the most important fields of application is nanomedicine, and more specifically, drug delivery (195). In the 1960s, liposomes were designed as nanovehicles with specific programmed functions and precursors of several current nanoparticles (196,197). Not long after, variations in structural components were suggested, as in the case of transfersomes and ethosomes, in order to improve their properties and achieve better results (198,199). Nowadays, these structural variations are still emerging to fulfil the needs and demands of the pharmaceutical industry and the clinical practice (200–202).

**Table 3.1.** Advantages and Disadvantages of TDS to enhance TDD.

| | TDS | Advantages | Disadvantages | Ref. |
|---|---|---|---|---|
| **Chemical methods** | Alkanes, Azone, Pyrrolidone, Urea, Fatty acids, Esters, Alcohols, Surfactants, Terpenes | High efficiency in combination with low sized molecules | -Inability to locate their effects only on the *stratum corneum*<br>-Skin reactions (irritation, inflammation, and erythema)<br>-Low efficiency in combination with macromolecules | (203–205) |
| | Prodrugs | -Higher drug stability<br>-No degradation in the skin | Size increase can reduce its permeability through the skin | (42,206) |
| **Physical methods** | Iontophoresis, Sonophoresis, Electroporation and thermal methods | -Rapidly responsive molecular transport<br>-Control of transport magnitude | -Expensive devices<br>-Inability to locate the effects only on the *stratum corneum*<br>-Intense skin reactions (irritation, inflammation, and erythema) | (207–211) |
| | Jet Injectors | -Control of drug depth deposition | -Possible incorrect dosage and skin damage, pain, and infections | (212,213) |
| | Microneedles | Bypass the *stratum corneum* | -Expensive production compared to other methods<br>-Difficult use for local skin treatments<br>-Time that micropores remains open still unclear | (214,215) |
| | Microsystems and Nanosystems | Possibility to achieve drug release in the first layers of the skin or a transdermal drug delivery | High-sized systems cannot improve drug diffusion through the skin | (216) |

## 3.1. Lipid vesicles: Liposomes, Transfersomes and Ethosomes

Lipid vesicles are non-toxic and biodegradable biomembranes obtained artificially, that have gradually evolved over time and been successfully applied as drug carriers for controlled, targeted, and enhanced drug delivery (217). Their application to TDD is highly attractive, because their lipophilic nature allows them to incorporate poorly soluble drugs in aqueous media and improve the penetration properties of drugs through the skin (218,219). Other advantages have also been documented, such as increased stability of photosensitive molecules (220), lower drug degradation (221), and depot release (222).

### 3.1.1. Composition and structure of Lipid-based vehicles

#### *3.1.1.1. Components of lipid vesicles for transdermal delivery of drugs*

Liposomes, transfersomes and ethosomes are mainly composed of phospholipids, and they present a lipid bilayer structure, similar to cellular membranes (223). The amphiphilic character of phospholipids, as a result of their hydrophobic tails and hydrophilic heads, allow them to spontaneously disperse in aqueous medium and incorporate both hydrophilic and lipophilic drugs (Figure 3.1) (224). Variations in polar head and nonpolar tail functional groups lead to a broad variety of phospholipids that can be used in vesicles production. Phosphatidic acids (DMPA, DPPA, DSPA and DMPG), Phosphatidyl glycerols (DPPG, DSPG, POPG, DMPE), Phosphatidyl ethanolamines (DPPE, DSPE, DOPE, DLPC) and Phosphatidyl cholines (DMPC, DPPC, DSPC, DOPC) are the common types used in drug delivery, which condition to a certain degree the properties of the developed systems (225). For example, phosphatidyl cholines tend to form permeable, but less stable, bilayers, whereas acyl chains-based phospholipids form more stable bilayers but more rigid structures (226). Lipid vesicle composition often includes stabilising agents to produce systems like cell bilayers, with cholesterol being the stabiliser *par excellence*. The phospholipid/cholesterol ratio varies from 0 to 25% w/w and depends on the vesicle application purposes (227). On one hand, it is

well documented that the entrapment efficiency of lipophilic drugs decreases if the percentage of cholesterol increases, since they occupy the same space in the lipid bilayers (228). On the other hand, the increase in cholesterol content produces an increase of vesicle size and Polydispersity Index (PDI), probably as a consequence of the capacity of stabilising higher structures (227). Finally, cholesterol can influence vesicle rigidity and, consequently, drug release and leakage. In general, the higher the cholesterol content, the higher the bilayer rigidity and lower the vesicle flexibility (229), and therefore the more flexible the vesicles, the higher the drug release and leakage (79).

The other key factor for deformability of the lipid vesicles is to include edge-activators in their composition, which leads to the obtention of transfersomes (230). The most common edge-activators are surfactants: tweens®, spans®, bile salts (sodium cholate and sodium deoxycholate), and dipotassium glycyrrhizinate (230–233). Usually, those components are a single chain surfactant which causes a destabilisation of the lipid bilayers and increases its fluidity and elasticity by lowering the interfacial tension (234). These surfactants produce micelles if they are present in concentrations greater than the micellar critic concentration (235). However, when the molar relation phospholipid/surfactant is optimal, which happens at low surfactant concentrations, they are incorporated in the lipid vesicle structure, conferring interesting properties to the ultraflexible or ultradeformable vesicles. For instance, 15% w/w has been revealed to be the more efficient proportion in the case of non-ionic surfactants as tween or span for transdermal delivery purposes (236,237). In addition, 25% w/w seems the most appropriate concentration in the case of sodium deoxycholate (237).

Ethosomal systems are composed of phospholipids, water, and ethanol, or other volatile alcohols at high concentrations (up to 50% w/w) (238). However, the most suitable concentration of ethanol would range between 20-30% w/w to ensure the formation of closed multilamellar

vesicles with good transdermal delivery results (199). Characterisation properties are also affected since size decreases with the increase in ethanol concentration (239).

The new designs of lipid vesicles are based on the incorporation of other components in an attempt to give additional properties to the formulations. Glycerosomes are vesicles with considerable amounts of glycerol (10-30% in the water phase) (240). Their objective is to confer extra flexibility to the bilayers and hydrate the skin at the same time, due to the humectant properties of glycerol (241). Inspired by the features that hydrogels can offer to liposome delivery, such as an extra control of release, hyaluronosomes aim to incorporate a gelled nucleus made of hyaluronic acid, avoiding the possible inconveniences that polymeric matrices could produce, like an excessive retention of active ingredients or long-term stability issues (242).

*3.1.1.2. Structure of lipid vesicles and classification*

Depending on the production method and composition, it is possible to obtain different types of lipid vesicles. According to the superficial charge given by the phospholipids, they can be classified as anionic, cationic, or neutral vesicles (243,244). Moreover, the size and number of lipid bilayers are the usual parameters to characterise them. Multilamellar vesicles (MLV) are those that present more than one bilayer, which enclose the same number of aqueous compartments. Unilamellar vesicles have just one bilayer and a central aqueous core (245). These well-differentiated environments make lipid vesicles a versatile TDS, as they can shelter drugs dissolved in the aqueous core or inserted within the lipid bilayer structure (Figure 3.1) (246). MLV are usually bigger in size, ranging between the nanometric scale up to 1 µm. When the number of bilayers is less than 4, they are called oligolamellar vesicles, and the drug entrapment efficiency is commonly higher than MLV (247,248). A special case is multivesicular vesicles, where a large bilayer confines multiple vesicles inside it (MVV) (249). Unilamellar vesicles are subclassified as small unilamellar vesicles

(SUV) and large unilamellar vesicles (LUV). SUV present a size lower than 100 nm, spherical shape and a homogeneous size distribution (250). The entrapment efficiency of hydrophilic drugs is limited. On the contrary, LUV are larger vesicles (100-1000 nm) with a bigger aqueous core, which increases the capacity of encapsulating hydrophilic molecules (251).

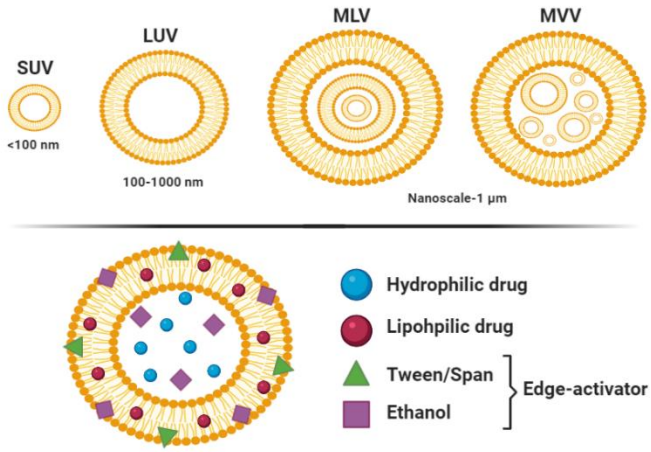


**Figure 3.1.** Lipid vesicle classification according to size and number of lipid bilayers. Location of liposomes, transfersomes or ethosomes components in the lipid vesicle structure.

### 3.1.2. Mechanisms of action of liposomes and ultraflexible vesicles

It has been reported that liposomes can effectively interact with cells by different methods (252): a) absorption by specific interaction with cell-surface components, electrostatic and hydrophobic forces, b) endocytosis by phagocytic cells like macrophages and neutrophils; c) fusion and cytoplasm delivery by insertion of liposome bilayers into cell membranes; and d) exchange of bilayers components.

However, the mechanisms of action when applied on the skin for transdermal delivery purposes remain unclear. It is generally accepted that conventional liposomes fail to penetrate the skin layers and remain on the skin surface (253), acting as a kind of depot formulation (254). The liposomes could directly interact with the skin and exchange the drug by the “collision complex transfer process” observed in other biological systems,

or could release the free drug which is available to penetrate through the skin (255). In the last case, liposomes perform not only a depot function, but they can induce structural changes in the *stratum corneum*, thus facilitating the drug absorption (256–258). In the same way, a very similar mechanism based on the liposome insertion into the outer lipid layers of the *stratum corneum* can also explain the enhancement effect (98). All these theories exclude the penetration of the intact liposome structure, which has been extensively assessed in different studies. For example, Dreier et al. (2016) combined the stimulated emission depletion microscopy (STED) and raster image correlation spectroscopy (RICS) to study the mechanism of action of conventional liposomes once applied to the skin. The images of tissue samples incubated with radio-labelled liposomes, obtained by skin cryo-section, revealed that liposomes do not remain intact beneath the skin surface and suggest that the liposomes do not act as carriers that transport their cargo directly through the skin barrier (259). This poor performance of conventional liposomes has also been observed when crossing other biological barriers, such as the intestinal epithelia (260). In Dreier's et al. (2016) study, the penetration of conventional liposomes was compared to sodium cholate-based vesicles. As expected, the conclusion points out that fluorescent-labelled ultraflexible vesicles were able to deliver their content deeply. The improvement in the delivery obtained from transfersomes supports the existence of extra mechanisms involved for transfersomes. From its conception, transfersomes designers support that they can pass through the skin in a squeezing process helped by an osmotic gradient as a driving force, created by the difference in the water concentration between the skin surface (near to 15% in *stratum corneum*) and the viable epidermis layers (around 75%) (198). Specifically, this skin environment is strong enough to push between 0.1-0.5 mg of lipidic material per hour and $cm^2$, which is substantially higher than the typical flux produced by concentration gradients (198,261). As may occur with liposomes, the exact mechanism of transfersomes is the result of the combination of drug vectorisation, *stratum corneum* disruption and penetration features of transfersome vesicles,

bearing in mind that the destabilisation of *stratum corneum* produced by transfersomes is more intense due to the action of surfactants incorporated in the vesicles. One confirmation of these squeeze-mediated mechanisms is the study done by Cevc et al. (2002) (96). In their study they assessed the fracture of liposomes during the transport through a semipermeable barrier, while transfersomes maintained their initial sizes. They also present the liposome and transfersome behaviour after its application on a murine skin model using CLSM, and confirmed the presence of intact vesicles in the blood stream of transfersome-treated mice by size exclusion chromatography. Similar findings have been obtained in several studies performed by other researchers in different types of ultraflexible vesicles, as Niu et al. (2019) and Manconi et al. (2011) (102,262).

Ethosomes are considered a variation of transfersomes because they have the same ability to penetrate intact through the epidermal layers. The underlying mechanisms of action are essentially similar, with little differences. Besides being a bilayer fluidiser, ethanol is also a chemical enhancer that promotes *stratum corneum* disruption by its interaction with the polar groups of skin phospholipids (263,264). Nevertheless, it has been reported that the enhancement produced by an ethosomal formulation is greater than those produced by ethanolic drug solutions (265,266). Moreover, the ethanol evaporation once applied on the skin surface could increase the effect of concentration gradient in the transdermal absorption process.

### 3.1.3. Production methods of lipid vesicles

A wide variety of lipid vesicle preparation methods are available, and each of them has certain advantages and disadvantages, and confer specific characteristics to the vesicles (267). Its selection depends on different parameters, such as: a) physicochemical properties of the encapsulated drug and lipid vesicle components; b) effective therapeutic drug concentration and its toxicity; c) desired vesicle size, polydispersity

index and surface charge according to its further applications; and d) batch reproducibility and scale up production.

*3.1.3.1. Liposomes and Transfersomes production methods*

The specific molecular mechanism of liposome formation depends to a large extent on the production method used. The basic underlying principle is the hydrophobic/hydrophilic interactions between lipid and water molecules, regardless of the chosen methodology (268). The application and transference of energy in form of heating, stirring, shaking or sonication contributes to the arrangement of the lipid molecules into bilayer vesicles.

The Bangham's method, also known as film method, is the first described procedure to obtain lipid vesicles (196). It presents three clear steps, consisting of the preparation a phospholipid/cholesterol/edge activator organic mixture; removal of organic solvent using a rotary evaporator to produce a thin-film on the round-bottom flask wall; re-hydration with an aqueous solution above the phospholipid transition temperature to produce the lipid vesicles. Despite the method simplicity, the low entrapment efficiency in many cases, and the production of MLV heterogeneous populations makes further procedures to obtain useful lipid vesicles for transdermal purposes necessary (269). Furthermore, different methods have emerged over the years to overcome the limitations of the original method (Table 3.2).

*3.1.3.2. Ethosome production methods*

Touitou et al. (2000) introduced for the first time a lipid vesicle with ethanol as an edge-activator (199). The proposed method consists of preparing a 20-50% w/w ethanolic phase at 30ºC and stirred at 700 rpm and its dropwise addition into an aqueous phase, using a constant rate of 12 ± 0.5 mL/h. The incorporation of the active ingredients can be done in the organic blend or in the aqueous solution, depending on its physicochemical properties. Then, when the proper volume of water is incorporated, the ethosomal dispersion is kept under stirring for 5 min and

homogenised in terms of size and PDI by different methods. This procedure is defined as a classical cold method, and one of its main advantages is that it is done almost at room temperature, so it allows the preparation of thermo-sensitive drug-loaded lipid vesicles (263). Alternative methods can be used to produce ethosomes in a more efficient way (Table 3.2), as it is for conventional lipid vesicles.

**Table 3.2.** Main lipid vesicle production methods.

| Method | Procedure | Outcome | Ref. |
|---|---|---|---|
| **Thin-Film (Bangham's method)** | It can be used for preparing ethosomes if the thin-film is rehydrated with an ethanolic solution | MLV | (270) |
| **Ultrasonication** | Strong ultrasound pulses applied to an aqueous phospholipid dispersion | SUV<br>LUV | (271) |
| **Reverse-phase evaporation** | Phospholipids are hydrated by mixing the aqueous and organic phases. When organic solvent is removed, a gel is produced, which turns into a vesicle dispersion | MLV<br>LUV | (247,252, 272) |
| **Eter/Ethanol injection** | Phospholipids are dissolved in an organic phase which is injected through a syringe system into the aqueous phase | SUV<br>LUV | (273,274) |
| **Hot method** | Drug is dissolved in ethanol and propylene glycol mixture. Then it is added to a 40ºC phospholipid aqueous dispersion and mixed for 5 min. | SUV<br>LUV | (275) |

### 3.1.4. Purification methods of lipid vesicles

A mandatory step in the production process to obtain homogeneous final products is to remove the excess of vesicle components (252). In addition, the elimination of non-entrapped drug fraction, these purification methods can remove the rest of non-incorporated components guaranteeing a high-quality formulation (276). As the molecular weight of lipid vesicles is considerably higher than drugs and edge-activators, most of the methods are based on this size difference.

Even though these methods allow the vesicles purification, they have drawbacks in most cases, such as vesicle dilution or decreased product yield (277). These difficulties explain why large-scale purification is limited and the purification process remains nowadays a challenge. According to the drug physicochemical properties and lipid vesicle final application, researchers must choose the appropriate method in each case. The most used purification methods are dialysis, centrifugation, ultrafiltration, and size exclusion chromatography (Figure 3.2).

#### *3.1.4.1. Dialysis method*

Dialysis removes non-entrapped molecules from liposomal dispersions with the use of a semi-permeable membrane, whose pores allow molecules to pass through, while the diffusion of large structures is restricted (278). The simplicity of the process, the possibility to purify large volumes of vesicle formulations and its low cost are the main advantages of this technique. The success of this method resides in the use of an appropriate dialysis bag and dialysis media. Both free drug and other molecules should be highly soluble in the dialysis media for an adequate extraction (279). Moreover, osmotic pressure must be considered to preserve the vesicles' integrity and avoid the forced leakage of entrapped drugs (227). This operation is generally successful for hydrophilic molecules, since an aqueous media generally fulfils these requirements, and it is usually performed at low temperatures, around 4ºC (79,280,281). The time required to complete the process is one of the main disadvantages

of this method, as it takes at least 24 h to ensure complete free-drug removal (79,280). However, an excessive dialysis time can lead to an encapsulated drug depletion as a consequence of the drug affinity for the media (282). Dialysis of lipophilic molecules is often more complex as drugs do not pass to aqueous media, and double-way flow of organic media through the pores in the diffusion process could make the vesicle structure unstable. Nevertheless, if the volume ratio between vesicle dispersion and aqueous dialysis media is considerably balanced in favour of the media, the concentration gradient for drug diffusion remains active and the dialysis of lipophilic components is possible (281).

*3.1.4.2. Centrifugation method*

The application of a centrifugal force to heterogeneous dispersion produces the separation of its components according to their size and density. It can be used in lipid vesicle purification, leveraging the obvious differences regarding size, weight and density between non-encapsulated components and lipid vesicles. Under the centrifugal force, free drugs remain in the supernatant, while lipid vesicles tend to accumulate in the bottom of the centrifuge tube or Eppendorf. The optimal rotor speed depends on different factors, such as the density of the medium or vesicles size and stability, but as a general rule, the rotating speed to achieve an effective separation should be up to 10000 rpm and applied between 30-90 min at 4ºC (79,283,284). Differential high-speed centrifugation precipitates vesicles under forces up to 100000 xg. However, excessive forces may cause particle aggregation and the bilayer fusion, with the subsequent drug entrapment loss.

*3.1.4.3. Ultrafiltration method*

Ultrafiltration is a method that combines the centrifugation and the pass of free molecules through a semipermeable membrane (285). As with dialysis, the pore size plays a key role in the purification process. Usually, to achieve an effective purification, the pore size used is ranged at least one tenth of the vesicle size (between 50-300 kDa) (285–288), and

centrifugation force around 4000 rpm or 2000 xg (286,287,289). High weight structures are retained in the membrane while water and other smaller components freely pass through the membrane pores. The method divides the formulation in two fractions: the ultrafiltrate which contains the extra-vesicle components in the vesicle dispersion medium, and the sediment which contains the lipid vesicles (286). Thus, ultrafiltration is especially useful for hydrophilic drugs and its main advantages are that drug leakage is partially avoided as the liposomes do not immerse in a purification media, and it reduces the time to complete the purification (around 1-2 h) in comparison with the dialysis method (288).

*3.1.4.4. Size exclusion chromatography method*

Size exclusion chromatography is based on the separation of the components of a blend as a consequence of their interaction with the porous beads contained in chromatographic columns, which leads to a different retention time (290). The non-entrapped drug and other free components with low molecular weight and size are capable of interacting with the pores, whereas lipid vesicles or other large components do not enter the pores (291,292). Consequently, the elution of vesicles is relatively quick, while the free drug is retained in the column for a longer period. To achieve an efficient elution, the type and diameter of gel particles and pores is essential. Sephadex, Sepharose and Sephacryl columns are the most used. For example, Sephadex G-25, G-50 and G-100; Sepharose 2B, 4B and 6B; and Sephacryl S200 and S1000 usually offer good results in liposomes purification (252,276,291,293,294). The time needed to complete the purification process is intermediate, no more than 6 h (276). The inconveniences of this method are possible reactions between vesicles and reactive groups of gel particles, drug leakage (286), and issues in removing lipophilic compounds as the eluent solutions are usually of a hydrophilic character, like HEPES buffer (295).

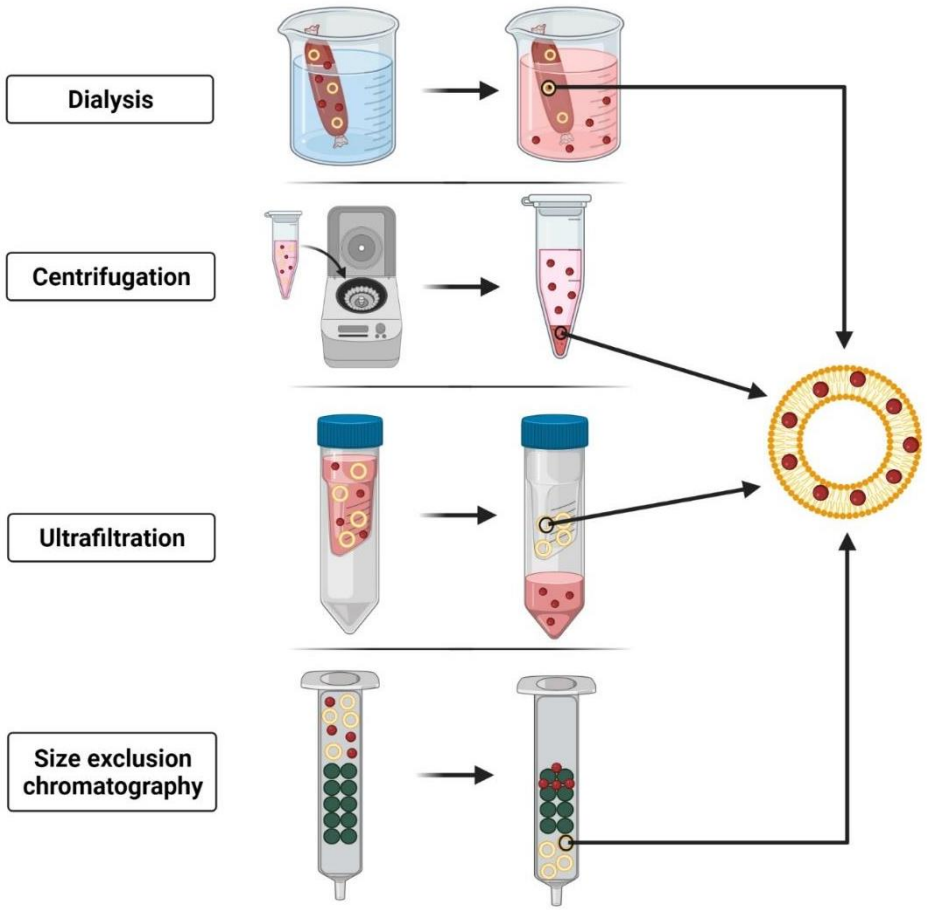


**Figure 3.2.** Purification methods of lipid vesicles: dialysis, centrifugation, filtration and size exclusion chromatography.

### 3.1.5. Size reduction procedures of lipid vesicles

MLV formation is often spontaneous after using most of the lipid vesicle production methods (296,297). Nevertheless, the topical and transdermal application mostly requires the use of vesicles with a smaller and specific size (SUV and LUV). The reduction of the size and lamellarity is possible once the vesicles are obtained by different methods. Usually, the techniques used for those purposes are sonication, extrusion, and homogenisation.

Lipid bilayers present different structural states depending on the temperature (298). There is an ordered phase, also called gel state, which exhibits high rigidity at lower temperatures. On the other hand, beyond the transition phase temperature, which is specific for each lipid type, they become a disordered phase, known as liquid-crystalline state. At this phase, lipids have soft mechanical properties making the bilayers more fluid (298,299). In that way, it is important to work above the phospholipid transition temperature (298,300), while reducing size vesicles, to prevent a sharp drop in the efficiency process (301).

*3.1.5.1. Sonication*

Sonication provides energy to the vesicle systems by high frequency ultrasound. Usually, it allows the obtention of a homogeneous population of SUV from the sonicated MLV (302). The obtained SUV show a size not larger than 200-100 nm (303,304). In particular, ultrasounds can be applied in short intervals (around 30 sec) or pulses of a few seconds to the vesicles (303–306). The number of pulses (from 3 to 8 cycles) depends on their energy and frequency (ranging up to 600W and 450kHz) (303,306,307). The main limitations of the sonication technique are the oxidative reactions that phospholipids could suffer and the loss of encapsulated drugs, especially if they are hydrophilic, as a result of the reduced aqueous volume entrapped within the bilayers (247).

*3.1.5.2. Extrusion*

Extrusion converts MLV into homogeneous LUV and SUV vesicle populations (308,309). The technique consists in the passage of the vesicle dispersion through polycarbonate or polyethersulfone extrusion membranes with uniform pore networks (310–313). The pore size ranges usually between 0.1 and 5 μm (309,311,313). Variables that define the lower size attainable are pore size, number of extrusion cycles, applied pressure, extrusion temperature and vesicle flexibility (313). Different protocols have been proposed, but around 20 passages, combined with the appropriate extrusion membranes, have commonly been performed to

achieve sizes lower than 300 nm (281,314). However, Ribeiro et al. (2018) demonstrated that after 6 passages, the particle size of liposomes was reduced significantly from 569 ± 61.2 nm to 162.5 ± 1.4 nm, accompanied with a reduced PDI lower than 0.150 (308).

*3.1.5.3. Industrial methods*

Homogenisation, French press, and micro-fluidification methods can be considered an evolution of the extrusion technique. They are the preferred methods in the industrial context (301). Operating at high pressure levels, the first two consist of pumping the vesicle formulation through a stainless holed wall, while a microfluidiser aims to provoke vesicle collisions between them (315–318). The main drawbacks of all of them is their own working high pressure and the equipment costs, but on the other hand, the reproducibility in downsizing and the possibility of processing higher vesicle formulation volumes makes them ideal methods for scale-up process (301).

3.1.6. Drug-loading strategies

Drug encapsulation in lipid vesicles is probably one of the critical steps in vesicle production, as their pharmacological activity is subjected to achieve drug concentrations within the therapeutic range after the drug release process. Two loading strategies can be distinguished: active and passive loading.

Passive strategies just rely on the spontaneous capacity of vesicles to capture a certain aqueous volume (where a water-soluble molecule is dissolved) during their formation (319,320). As hydrophilic drugs are located in aqueous core of vesicles, their entrapment efficiency is affected by the vesicle size and lamellarity, and these, in turn, by phospholipid concentration and production methods (321). Regarding lipophilic molecules that are embedded within the lipid bilayer, the entrapment efficiency mainly depends on phospholipid concentration and vesicle number, regardless of the size or morphology (322).

Active loading consists of the incubation of empty vesicles with a drug solution to push the cargo through bilayers if they are permeable enough. In the simplest case, a concentration gradient is the pushing force to complete the loading until the equilibrium between the interior of vesicles and the surrounding medium is achieved (323). In consequence, this type of loading is restricted to hydrophilic and small molecules, with the packaging structure of bilayer components being the main opposition to the loading (324). Efficient and quick loadings can be achieved using other pushing impulses, such as pH gradient (325). It involves the preparation of liposomes using a pH buffer around 4.0 and then adjusting the external pH to more than 7.0, adding a basic character compound or directly exchanging the surrounding medium by the optimal buffer solution (326).

Freeze-thaw cycles is also a processing technique to encapsulate drugs into vesicles or to improve the entrapment efficiency (327,328). It works as an extra force to achieve the equilibrium in drug concentrations inside and outside the vesicles (329). The optimal number of freeze-thaw cycles reported in the literature is highly variable (up to 10 in some cases) (330), because of the different types of drugs involved. Zhao et al. (2009) showed that 4 cycles are optimal in the case of protein-loaded vesicles (331). However, Costa et al. (2014) reported that 2 freeze-thaw cycles resulted in the maximum predicted entrapment efficiency of Tenofovir, a polar anti-HIV nucleoside with low permeability (329).

### 3.1.6. Key properties and parameters in the design of lipid vesicles for transdermal delivery purposes

In order to achieve a highly efficient transdermal permeability of drugs, lipid vesicles should present some key properties, namely: size, morphology, PDI, zeta-potential, entrapment efficiency, deformability degree, drug release properties, stability, and biocompatibility. These properties are connected with each other, and therefore, changes in one of them lead to variations in the other. Consequently, it seems almost impossible to get the perfect or ideal vesicle and the real challenge focuses

on the development of a prototype with a suitable balance between all the key parameters.

*3.1.6.1. Entrapment efficiency*

The drug-to-lipid ratio influences the drug therapeutic index for any lipid vesicles application (332,333). Hence, high entrapment efficiencies are desirable since they contribute directly to achieving significant effects after vesicles administration. In turn, entrapment efficiency is dependent on various factors such as physicochemical properties of drugs, vesicle size and lamellarity, and vesicle production method.

Firstly, hydrophilicity or lipophilicity of drugs have a huge influence in the encapsulation process when vesicles are loaded through passive strategies. Lipophilic drugs attain a high encapsulation ratio, around 90% or above, as a consequence of their intercalated location between lipids of vesicle bilayers, while hydrophilic drugs present low entrapment rates, between 10-50% (334–336). Encapsulation of water-soluble drugs depends on the fact that an important proportion of drug dissolved into the water phase remains outside the vesicles, decreasing the encapsulation ratio. This is the reason why size conditions, especially the entrapment efficiency of water-soluble drugs: LUV, in comparison to SUV, have larger amounts of water in their core (272). In the same way, the increase in the number of lipid bilayers in MLV plays in favour of lipophilic drug entrapment, as the concentrical membranes increase the available space for hydrophobic drugs. Moreover, MLV also improve encapsulation of hydrophilic drugs since the several bilayers tend to retain inside this type of drugs (321).

Secondly, as each production method provides different types of vesicles regarding size, it can be considered that the entrapment efficiency is also subjected to the selection of the manufacturing technique (337).

Finally, the drug loading method is the last factor which has a notable influence on entrapment efficiency. Active loading strategies have an excellent uptake response from vesicles which can improve the entrapment

efficiency, since it is independent of the lipid composition and presents high drug retention properties (338).

Entrapment efficiency can be directly or indirectly calculated. The indirect method consists of determining the amount of drug present in the outer medium of vesicles to estimate the entrapped fraction of drug by difference to the initial amount of drug formulated (339). For this, usually vesicle dispersions are centrifuged to isolate them and analyse the supernatant, which contains the non-entrapped drug fraction (339). The direct estimation of the entrapped amount of drug requires the destabilisation of vesicles to force the release of their content (340). It is achieved by adding high amounts of methanol or surfactants like sodium dodecyl sulphate or Triton X-100 (79,334,340,341).

*3.1.6.2. Determination of phospholipid concentration*

The efficiency of lipid vesicle fabrication and their percentage in phospholipids in establishing the drug-to-lipid ratio can be estimated through different methods (342). Chemical methods like Steward, Rouser and Barlett assays are frequently used, as they are relatively simple and cost-effective. In Steward's assay, the vesicle solutions are mixed with chloroform, $FeCl_3$ 0.1 M, $NH_4SCN$ 0.4 M in a ratio 0.5:3:2:2 and vortexed for 20 s. After centrifugation (1000 rpm) for 5 min, 2 mL of the lower chloroform fraction is carefully transferred into a quartz cuvette, and absorbance is measured at 485 nm (343). Rouser's method consists of heating 100 µL of vesicle solutions at 270ºC until complete liquid evaporation, followed by the addition of 450 µL of $HClO_4$ (70% v/v). After, the blend is heated to 250ºC for 30 min. Then, 3.5 mL of water, 500 µL of ammonium molybdate (2.5% w/v) and 500 µL of ascorbic acid (10% w/v) are added. Finally, the mixture is vortexed and incubated at 100ºC for 7 min and cooled down again. The absorbance is measured at 820 nm (344). In Bartlett's method, up to 2 mL of samples and 0.5 mL of $H_2SO_4$ 10 N are mixed and heated at 150-160ºC for at least 3 h. Subsequently, 2 drops of $H_2O_2$ (30%) are added and maintained at 150-160ºC again for 1.5 h to

ensure a complete combustion and decomposition of all the peroxide. Then, 4.6 mL of ammonium molybdate (0.22% w/v) or 4.4 mL of water, plus 0.2 mL of ammonium molybdate (5% w/v) and 0.2 mL of Fiske-SubbaRow reagent are added, mixed, and heated for 7 min in a boiling water bath. The optical density is measured at 830 nm (345).

Alternatively, enzymatic assays have been suggested to determine phosphatidylcholines in liposomes (346). For example, a colouring reagent solution is prepared by adding 45 mL of buffer solution (Tris buffer 50 mM, calcium chloride 5 mg/dL, and phenol 0.05%) to the dry colouring reagent (phospholipase D 20 U, choline oxidase 90 U, peroxidase 240 U, 4-aminoantipyrine). Microwell plates are filled with 50 µL of vesicle dispersion and 250 µL of the colouring agent and warmed to 37ºC for 5 minutes. The quantification is performed measuring the absorption at 492 nm. Other techniques have seldom been applied based on phospholipid and its degradation product determination purposes, such as gravimetric assays (347), magnetic resonance spectroscopy (H-RMN) (343), and ultra-high-performance liquid chromatography-mass spectrometry (UHPLC-MS) (348).

*3.1.6.3. Size and morphology*

The particle size of lipid vesicles is probably one of the parameters with a stronger influence on the transdermal delivery. Generally, the smaller the vesicles, the higher the transdermal flux is achieved, even though it is dependent on other parameters (349). Vesicles with a diameter of 300 nm or below enable the delivery of their ‘cargo’ to the deeper skin layers, especially when they are flexible. Verma et al. (2003) used CLSM to visualise the effect of the size penetration ability of liposomes, loaded with the fluorescent molecule. The maximum levels of fluorescence in the cryo-sectioned skin samples were observed with < 70 nm diameter, while liposomes with a size of 120 nm diameter also showed statistically enhanced skin penetration as compared to larger ones (350). On the contrary, vesicles sized 600 nm or above remain on the *stratum corneum*

layers where they release their cargo (351,352). Absorption through the skin of vesicles ranging between 200-600 nm is possible, but their performance is more influenced by other aspects, such as edge-activators composition or the deformable behaviour of vesicles (353).

The exact mechanism that nanovesicles follow in the skin permeability process is still under discussion, however, it also seems to be linked to vesicles size. Small nanovesicles may be absorbed through transepidermal routes including aqueous pores (354), whereas larger entities up to 210 nm also follow the transfollicular route as an extra option (43,355). As mentioned before, size and morphology can be controlled choosing the appropriate vesicle production method, and are commonly assessed by Dynamic Light Scattering (DLS) and microscopy techniques respectively (356,357).

DLS is a reliable method for determining the size of nano and micro particles (308,358). It is based on the property of vesicle dispersions to produce a variable light scattering over time because of the constant changing position of vesicles as result of a Brownian motion. DLS measures this intensity and its fluctuations to establish a correlation function. An exponentially decaying function is correlated with decay times, which are related to diffusion coefficients and particle radius by the Stokes-Einstein equation (359).

Microscopy techniques offer the possibility to visualise the lipid vesicles and estimate their preliminary size. These techniques are not a surrogate of DLS since vesicles can show certain variations in size due to the sample preparation protocol. Optical microscopy is a basic tool unable to provide complete information about lipid vesicles and their bilayer in comparison with other microscopy techniques (360). Nevertheless, it can be used to obtain a quick image of lipid vesicles and general information, although not precise, about the size, shape, and homogeneity of big vesicle types such as Giant Unilamellar Vesicles (GUV) and even MLV (361–363).

Electron microscopy is the most extended method for the visualisation of lipid vesicles. It offers a high magnification and super-resolution images that allow us to obtain a clear view of vesicles (364). This technique focuses a beam of electrons onto the vesicles' surface, which are scattered by the sample. These electrons are refocused and magnified to produce a projected image (357). Scanning electron microscopy (SEM) utilises an electron beam that is scattered across the surface of the sample to produce a magnified image of an object (365). SEM is now not usually used for imaging lipid vesicles because it requires the sample to be fixed or air-dried prior to imaging, which can cause damage to the particle's integrity due to the surface tension of the evaporating water (364,366). However, special drying techniques, such as the critical point drying, or paper absorption, followed by ethanol concentration gradients, have been successfully used to prepare the sample before SEM analysis (364,367). Also, freeze-dried powders of lipid vesicles can be analysed using this technique to study the morphology of the vesicles (365,368).

Environmental scanning electron microscopy (ESEM) is an improved imaging system that does not require the use of fixing, staining or freezing of vesicles to visualise wet systems (369). ESEM allows the presence of vapour in the sample chamber, since a multiple-aperture vacuum system lets the imaging chamber be maintained in a partial vacuum environment, unlike other parts of the equipment (370).

Transmission electron microscopy (TEM) is probably the most frequently used imaging technique for lipid vesicle imaging (281,371). It provides a better contrast and contour of vesicle structures than other microscopy techniques, thus it easily denotes information about structure and surface modifications of vesicles (357). In contrast to scanning-based microscopy, the electron beams cross the samples and are refocused by different lenses to form an image. It requires sample-preparation procedures prior to visualisation, specifically negative staining, freeze-fracture and cryo-TEM (372–374). The negative staining is a fast

preparation technique and allows the use of hydrated samples. It consists of embedding the vesicles in electron-dense materials, typically heavy metal salts like phosphotungstic acid or uranyl acetate, which enhances the contrast between them and the background (375). The most relevant inconvenience is the difficulty in evaluating the vesicle morphology. The possibility to introduce artefacts that may be mistaken for vesicle structure and entities (376), and the changes in the structure of vesicles as a consequence of vacuum atmosphere and dehydration of the samples are other important limitations (370). The freeze–fracture technique involves vitrification by quick freezing using cold liquids such as propane or nitrogen (377). Then, samples are fractured and surfaces etched to get a negative replica of the fracture sample (378). The main advantages of freeze-fracture TEM are that it can provide information about the internal structure and does not require any drying pre-treatment. However, it requires the use of organic solvents to clean the replicas of the samples that are removed prior to visualisation (357). Cryo-TEM is the most evolved technique of microscopy currently available (379,380). The native state of lipid vesicles can be evaluated through it, receiving complete information about size, shape, internal structure, and lamellarity (381,382). The aqueous films are vitrified in liquids such as ethane, and the quick freezing of samples prevents the crystallisation of drugs and vesicle components and minimises the appearance of artefacts (357).

As a variation of the scanning microscopy technique, atomic force microscopy (AFM) is an interesting alternative to visualise nanoparticles and analyse their surface modifications and ligands detection, thanks to its high resolution in the order of fractions of a nanometer (383–386). AFM consists of a sharp tip attached to a cantilever and connected to an optical sensor with a laser beam that records and quantifies the cantilever deflection (387). The system explores the sample surface and it moves up and down the cantilever as a result of the surface relief. The main advantage of AFM is that it can operate in a liquid or air environment, and it does not need a vacuum condition (357). On the other hand, the main

limitations are the need to adsorb the nanoparticles onto mica or silicon surfaces, which can potentially modify the size and shape of the lipid vesicles (388), and their displacement and dragging as result of their contact with the tip and cantilever (357).

*3.1.6.4. Polydispersity index*

As mentioned before, vesicle size has an important impact on transdermal permeability as well as on therapeutic efficacy. Successful formulations should be efficient, stable and safe, which demands homogeneous populations in the case of pharmaceutical nanoparticles (389–391). PDI is the parameter that evaluates the size distribution of a population of particles (392,393). As for size, PDI is accurately determined using DLS. It is scaled to the unit, so that its values are ranged from 0 to 1. In general, values lower than 0.5 refer to monodisperse systems, whereas results above 0.7 indicate high polydisperse populations. In drug delivery, PDI values of 0.3 and below are considered acceptable for lipid-based carriers, and indicate homogeneous populations of phospholipid vesicles (349). Size reduction methods like sonication, extrusion, and high-pressure homogenization have been reported to reduce excessive PDI values (394–397).

*3.1.6.5. Vesicle flexibility*

The degree of deformability is the differential feature of flexible lipid vesicles in comparison to common liposomes. It seems to be the key aspect that allows the improvement in drug permeation and permeability by transfersomes and ethosomes (398). The flexibility of a lipid vesicle depends on the composition and the incorporation of the edge-activators. Different simple methods have been proposed for the determination of this degree of deformability to compare the flexibility of different vesicle batches. Essentially, two techniques based on the extrusion procedure are used. The first one consists of the measurement of the vesicle suspension volume recovered after extrusion, which is directly proportional to the flexibility. Thus, the more deformable the vesicles are, the more freely they will pass

through extrusion membranes without saturating the extrusion membrane and leading to a minimum volume loss (79,281,399). The alternative method compares the size before and after the extrusion process. The reduction in size is inversely proportional to the flexibility, as the more flexible vesicles can squeeze through the membrane pores maintaining their size (400,401). A deformability index has been proposed using the following equation (equation 3.1) (402):

*Equation 3.1:*

$$D = J \cdot \left(\frac{rv}{rp}\right)^2$$

Where *J* is the volume of formulation extruded; *rv* is the particle size after the experiment; *rp* is the membrane pore size.

*3.1.6.6. Drug release*

The design and optimisation processes of lipid vesicles imply the analysis of drug release mechanisms that constitutes the first and indispensable step after *in vivo* administration. The *in vitro* methods to study drug release are similar to the purification ones, such as the centrifugation/filtration and dialysis method, but applied under completely different experimental conditions (403). Dialysis methods are commonly used since they are simple and cost-effective (227). The solubility requirements of drugs in the acceptor medium and the maintenance of sink conditions are the main limitations (404). Even though drugs released from vesicles must cross an extra barrier (the dialysis membrane), it does not interfere if first and zero order kinetics are representative of the process, and the release rate from vesicles is higher than or equal to the diffusion rate through the dialysis membrane. Thus, the limiting step here is the release process. The experimentally obtained data reflects the release behaviour in all cases (79,227). The dialysis methods are usually carried out using FDC set-ups or dialysis tubes systems in a physiologically tempered environment at 32-37ºC (405,406).

Rigidity and structure of vesicles can modify the release patterns of drugs. MLV present a higher number of barriers that drugs should overcome, which increases drug retention inside the structures and delays the diffusion process through the membranes (321). Vesicle composition modulates the rigidity because cholesterol acts as a membrane stabiliser, diminishing the fluidity of phospholipids and increasing the rigidity. In fact, it has been reported that rigidity increases the resistance to drug transport and therefore diminishes drug release (229,407). On the other hand, the hydrophilic or lipophilic character of molecules is the other main factor that influences drug release, as hydrophilic drugs present higher and faster release processes in aqueous media in comparison to lipophilic substances (227,408).

Release data is often fitted to different kinetic models that propose the underlying release mechanisms and allow quantitative release rate comparisons. Theoretical models such as zero and first order kinetics have been used, but empirical models generally offer more complete information (409). Higuchi, Korsmeyer-Peppas, and Peppas-Sahlin are the semi-empirical mathematical models usually applied to the drug release from vesicular systems. Among them, the Higuchi model seems to be the most limited as it assumes that the process is carried out exclusively by passive diffusion (410). The Korsmeyer-Peppas and Peppas-Sahlin models consider both a relaxation mechanism and passive diffusion with different impact in the whole release process (411–413). A modification of the Korsmeyer-Peppas model, also called the Power-law model, was introduced by Kim and it considers a possible burst effect during the initial moments of drug release (414). However, burst effects can be attributed to free drugs present in the media when vesicles are not adequately purified or if the drug has been released from the TDS during the storage.

The suitability and accuracy of the different fitting models to the experimental data is commonly evaluated by the correlation coefficient ($R^2$) and the Akaike information criterion (AIC) (equation 3.2) (415–417). The

AIC is very useful to compare models with a different number of parameters, since it compensates for the statistical versatility of equations with lower degrees of freedom using a penalising factor. The correlation coefficient is usually reported as an indicator of the proportion of the results variability that is explained by the model.

*Equation 3.2:*

$$AIC = n \cdot Ln\,(SSr) + 2 \cdot p$$

Where *n* is the number of experimental data; *SSr* is the residual sum of squared; and *p* is the number of parameters in the mathematical model considered.

*3.1.6.7. Stability*

The stability of lipid-vesicles formulations is a key issue in drug delivery, as it determines the feasibility of any pharmaceutical product to be commercially available (418). Stability-related phenomena can be classified into two groups: immediate or long-term changes. In general, zeta-potential works as a good predictive stability parameter of colloidal particles such as lipid vesicles (419). High values above ± 30 mV assure a great repulsion between the surface charged particles, which produces an electrical stabilisation of the particles and leads to a low aggregation or flocculation (420). Temperature clearly affects the stability of vesicles, for which they are stored at 4ºC until their use (421). However, they still present some stability issues, which are in fact one of the main limitations of lipid-vesicles (221).

*3.1.6.7.1. Immediate or short-term stability*

Physical stability refers to phenomena occurring in the days or weeks following lipid-vesicles production. Creaming-clarification, aggregation, coalescence, sedimentation, and flocculation are typical events of instability that vesicles can show relatively often (Figure 3.3). These phenomena are easily detected by size and PDI measurements carried out with DLS (Table

3.3) (422). Additionally, Turbiscan® is a complementary tool to check the phenomena that vesicles experience during the early storage period. It records the variation of transmitted and backscattered light by the sample over the time (Table 3.3). In addition, it offers the Turbiscan Stability Index (TSI), which expresses a global idea about the stability of the formulation.

**Table 3.3.** Possible changes of lipid vesicles observed in a short-term period by DLS and Turbiscan®. ΔBS: variation of backscattering. ΔT: variation of fransmitance.

| | Vial Bottom | | Vial Middle | | Vial Top | | | |
|---|---|---|---|---|---|---|---|---|
| | **ΔBS** | **ΔT** | **ΔBS** | **ΔT** | **ΔBS** | **ΔT** | **Size** | **PDI** |
| **Sedimentation** | ↑ | ↓ | - | - | ↓ | ↑ | ↑ | ↑ |
| **Creaming** | ↓ | ↑ | - | - | ↑ | ↓ | ↑ | ↑ |
| **Flocculation** | - | - | ↑/↓ | ↑/↓ | - | - | ↑ | ↑ |
| **Coalescence** | - | - | ↑/↓ | ↑/↓ | - | - | ↑ | ↑ |

Coalescence and flocculation lead to an increase in particle size. Coalescence is irreversible as it entails the fusion of vesicles, while flocculation is an aggregation of particles without the creation of single drops (423,424). Flocculates are often easily dispersible, unless they coagulate. Moreover, flocculation can lead to coalescence at some point. Creaming is rarely observed in lipid-vesicle storage. It takes place when the dispersed phase has lower density than the continuous phase and goes up to the top of the vial sample. Creaming can be coupled with coalescence, flocculation and even phase separation. On the other hand, sedimentation is a similar process. The density of the dispersed phase is higher than the density of the continuous phase, and the fraction of particles migrate to the bottom of the vial sample (425). Clarification is an associated phenomenon that implies particle depletion of a part of the sample.

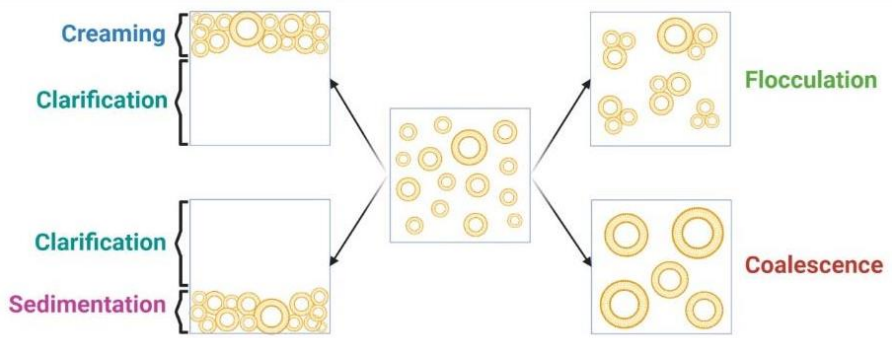


**Figure 3.3.** Short-term instability phenomena that lipid-vesicles can show during the storage period: flocculation, coalescence, clarification, creaming and sedimentation.

*3.1.6.7.2. Long-term stability*

It has been reported that lipid-vesicles may be stable for 2-3 months (426,427). During this period, the phenomena described above can continue. Additionally, if vesicles suffer the destabilisation of lipid bilayers or changes in storage conditions, they can disintegrate. Nevertheless, the main issue during the long-term storage is drug leakage, which takes place especially in vesicles loaded with hydrophilic drugs, as a consequence of their affinity for the media where the vesicles are dispersed (428). Rigid vesicles, with high amounts of cholesterol, can control drug leakage, but will slow down in drug release.

*3.1.6.7.3. Freeze-drying*

Freeze-drying or lyophilisation is the easiest method to preserve lipid vesicles during long periods of storage. It removes the aqueous content of the formulation and therefore avoids chemical reactions, such as oxidation, which can affect the vesicle structure (429,430). Moreover, drug leakage is prevented since there is not a media to which to diffuse.

Freeze-drying is a complex process that has three main steps: freezing, sublimation, and secondary drying. There is not a general recipe

that works with all formulations, and each one requires the development of a specific protocol of temperature, pressure, and time according to its own characteristics. It is particularly important to attain the whole sample freezing prior to the vacuum phase to get an optimal result. Therefore, it is essential to determine the critical collapse temperature for the preparation, which is the maximum temperature that can be used during drying (431). As amorphous structures, lipid vesicles substances have a glass transition temperature instead of an eutectic point (432), and the collapsing temperature is usually a few degrees higher (433,434). The use of organic solvents is also a problem, as lower temperatures are required to freeze, and they can easily bypass the condenser during the following phases and damage the equipment. On this matter it seems impossible to proceed to ethosomes lyophilisation, as ethanol is also removed from the formulation as a consequence of its high volatility and vesicles would be reconstituted in water (435). The next step dries the sample by removing the bulk of the water via sublimation, and it is divided into two steps (Figure 3.4).

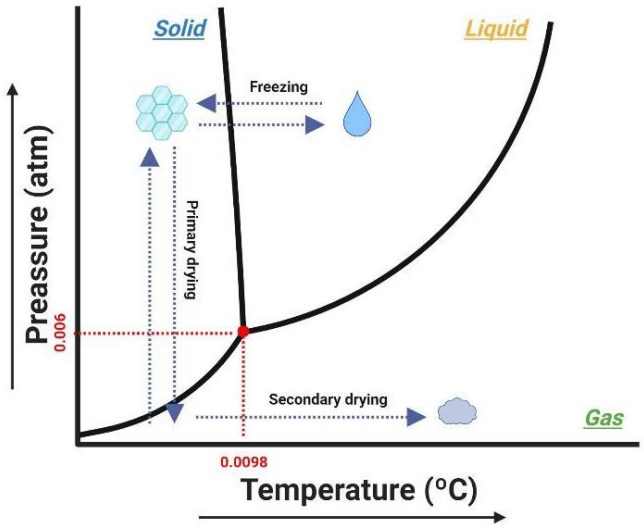


**Figure 3.4.** Standard phase diagram of water. The process starts with the freezing of the formulation, and the drying steps take place by dropping down the pressure level and increasing the temperature.

Primary drying is a slow phase, conducted at cooler temperatures than the critical collapse temperature of the freeze-dried formulation. The

product temperature depends on its vapour pressure, which in turn, is determined by the heat transfer to the product (controlled by the shelf temperature) and the vacuum level. Provided the optimal temperature of the formulation is identified, the parameters to control during the primary drying are the shelf temperature and the vacuum level (436). The amounts of residual water still bound to the formulation after this process is desorbed in the secondary drying by increasing the temperature (437,438). This increase must be controlled and slowed to avoid the collapse of the formulation.

Depending on the further applications of the formulations, the final water content varies from 0.5 to 3%, but in most cases, the driest products will have a longer shelf life. Thermogravimetric analysis (TGA) can be used to set up the freeze-drying conditions and as a control of the final product, since it measures the mass loss and its rate as a function of temperature. In thermograms, different steps of mass loss can be detected and the first one is used to correspond with the moisture content of the sample (Figure 3.5) (439,440).

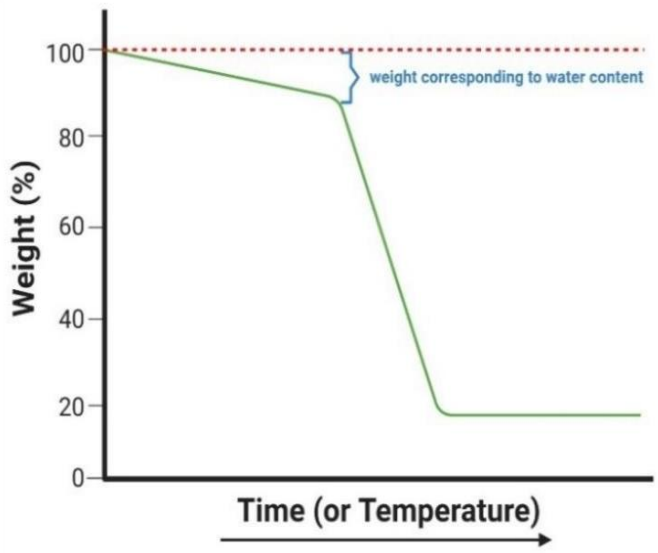


**Figure 3.5.** Standard profile of a thermogravimetric analysis. The first phase of weight loss corresponds to the water content which must range between 1-3% for freeze dried products.

Lyophilisation of lipid vesicles can be achieved with just the primary drying step (441,442). Vesicles must be previously frozen around -80ºC for at least 6-12 h to assure a complete freezing of the sample. For the primary drying (24-48 h), shelf temperature must be set around -40ºC, condenser temperature -55/-60ºC, and pressure 1-6 Pa. In the case of a multiple step drying, a constant rate of 0.25ºC/min or additional cycles of 5 h with a decreasing shelf temperature are used, for instance -30ºC, -16ºC and 20ºC (443). The final products can be stored during long periods at 4ºC prior to use. An optimal lyophilisate should be a cake composed of a uniform, fine and smooth powder, easily hydratable and dispersible in water.

Different phenomena can lead to changes in the lyophilised cake appearance with critical, major, or minor consequences in the product efficacy and safety. The most common are collapse, melt-back, and puffing. Collapse is usually a consequence of a drying (primary or secondary) above the collapse temperature of liposomal formulation and results in a viscous flow and loss of the microstructure previously established by the freeze process (444). Melt-back takes place due to traces of ice remaining at the end of primary drying or in the early moments of secondary drying (445,446). Consequently, it happens if primary drying occurs above the eutectic point or if primary drying is incomplete. Both are undesirable in all cases since they have an important impact on the final product quality and attributes. Puffing consists of the presence of bubbles on the top surface of the dried product. Different reasons can cause its appearance, such as minimum collapse or small melting during drying. During the freezing process small bubbles of air are included, which can migrate to the surface and, if they are stable enough to withstand the drying, remain in the final product (444,447). Contrary to collapse and melt-back, puffing does not imply in all cases critical consequences in the quality of the final product and is acceptable when it is observed as a characteristic of the formulation in all vials within a batch without any impact on the product attributes. In case of observing it in a few vials of a batch, the product showing puffing evidence should be discarded (444).

The use of cryoprotective agents is generally recommended to preserve the starting characteristics and vesicle integrity. Amino acids and complex polysaccharides have been used as cryoprotecting agents (448,449); however, simple saccharides are generally considered the first-choice excipients. Their mechanism of action is not completely understood, and different theories have been proposed which are not exclusive and may work together. On one hand, the water replacement theory suggests that the H-bonds interactions between water and polar head groups of phospholipids are replaced by those with the carbohydrates, stabilising the vesicle structure (450). On the other hand, the vitrification model proposes that sugars produce a phase with high viscosity and low mobility, which allows to maintain the distance among vesicles acting as a barrier between adjacent bilayers. This matrix protects the bilayers from damages caused by ice formation and prevents the fusion of vesicles. In consequence, sugar avoids the increase of Tm and the possible leakage of hydrophilic drugs induced by the effect of extra-vesicular ice (451). For example, glucose, lactose, sucrose, mannitol and maltose have been used in a 5-10:1 molar ratio (cryoprotectant: lipid) (Table 3.4) (452). Sorbitol has been prepared at 0.7-2.5% (v/v) solutions and then mixed in a 1:4 ratio (vesicle sample: cryoprotective solution) (281). After the reconstitution of freeze-dried vesicles, parameters such as size and PDI are maintained in most cases. Nevertheless, some reports show that the use of sugars can produce a tiny but significant size decrease after lyophilisation, which is higher when sugar concentrations are increased (441,453). As an explanation of this, several reasons have been accounted for, but the loss of water content in the membrane for preventing vesicle damage as a consequence of kosmotropic effects seems to be the most reliable cause (454).

**Table 3.4.** Glass transition temperature (Tg) of some common cryoprotecting sugars. Taken and modified from Levine and Slade, 1988 (455).

| Cryoprotectant | Tg (ºC) |
|---|---|
| **Glucose** | -43 |
| **Lactose** | -28 |
| **Sucrose** | -32 |
| **Mannitol** | -40 |
| **Maltose** | -29.5 |

*3.1.6.7.4. Differential scanning calorimetry*

DSC has been widely used to characterise solid components and stability (456). The technique supplies heat at a constant rate to a sample and a reference material -usually between 1-20ºC/min from 25 to 300ºC range- (457–460), with the aim of comparing and determining the difference in the heat flow needed to keep both at the same temperature (461). Thermal analysis represents the heat flow difference between the samples and the reference material, which is plotted versus temperature (Figure 3.6). It allows the identification and determination of different material state transitions like glass transition temperature (*Tg*), degradation temperature (*Td*), melting temperature (*Tm*) or crystallisation temperature (*Tc*). First-order transitions, such as crystallisation, melting and degradation, imply an abrupt absorption or release of latent heat and are depicted as well-defined peaks in thermograms (462). Second-order transitions, like glass transitions, do not involve a change in volume or latent heat, since they are just associated with variations in molecular mobility (463). Consequently, it is observed as a slight change in the slope that may take place in a large range of temperatures. These parameters and phase transitions are essential for a complete understanding of the relationship between the properties and the structure of materials. As a result, DSC provides a characterisation of the solid materials or powders (including lyophilised lipid vesicles), providing key information about the interaction of their constituent components and its evolution over the time.

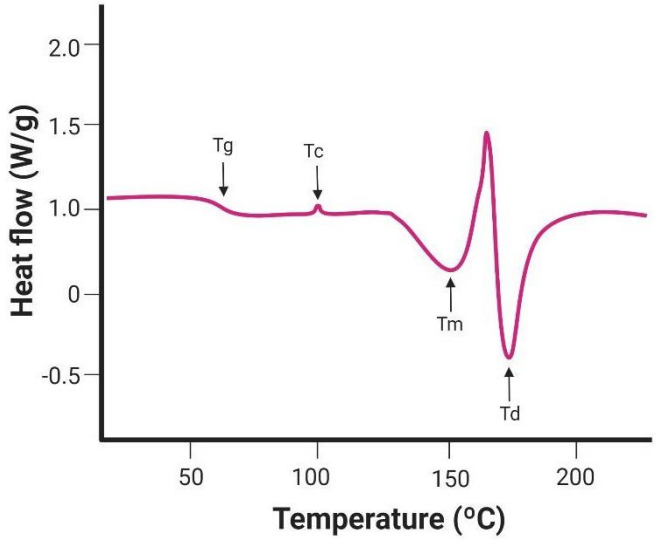


**Figure 3.6.** Standard DSC analysis profile. Glass transition temperature (Tg) is observed as a slight change in the slope that can take place in a wide range of temperatures. Crystallisation (Tc), melting (Tm), and degradation (Tg) temperatures are observed as well-defined peaks.

The main limitations of DSC are, on one hand, the analysis of multicomponent samples that generate thermograms with complex signals, which can be different from those provided by pure constituents that make the correct identification of transitions and thermodynamic changes difficult. On the other hand, the overlapping thermogram profiles are also dependent first, on the heat rates used and second, on the fact that melting and degradation can occur in a narrow range of temperatures (461).

*3.1.6.8. Biocompatibility*

Lipid nanocarriers are composed predominantly by phospholipids, which are considered by regulatory agencies as safe components (464). However, the chemical modifications in its structure and the inclusion of other additional components may potentially lead to an increase of the toxicity of the resulting liposomes. Even though lipid vesicles increase the therapeutic index of many drugs by decreasing drug accumulation in other organs and healthy tissues, they can produce toxic effects in the target tissues or elicit immune responses (465). In particular, the interaction with proteins and vesicular systems can trigger the innate immune responses

such as the activation of complement cascade, cytokine production, and hypersensitivity reactions. In the same way as the other aspects related to lipid vesicles, the final biocompatibility or toxicity is the result of the combination of different properties and features such as size, surface charge, and composition (465,466). Thereby, *in vitro* and *in vivo* evaluation of lipid vesicle biocompatibility has become a compulsory step in their design and development.

*In vitro* toxicity is assessed as viability tests on cell lines such as diploid fibroblast strain MLD and 3T3 mouse fibroblast (467,468), NEB-1, SCC, HaCaT and HEK as representative of keratinocyte lines (469–471), B16F10 murine melanoma cells (472), and RAW 264.7 murine macrophages (473,474). These assays include 3-(4,5-dimethylthiazol-2-yl)-2,5-diphenyltetrazolium bromide (MTT) or lactate dehydrogenase (LDH) tests (475–477). Cell viability results are generally expressed as percentage of viability, and those above 80% are considered non-toxic, between 80-40% as weak-moderate and below 40% as cytotoxic (478). The main limitation of these protocols is the possible *per se* interference of lipid vesicles as a consequence of their lipidic nature, since certain vesicle components can induce and stimulate cell growth (479).

For the *in vivo* evaluation of side effects, the Buehler test has been used extensively. It is considered a conservative test with relevance to the clinical condition (480). In the Buehler sensitisation test, a single occlusive patch containing a minimally irritating concentration of the tested formulation is applied to the shaved flanks of guinea pigs for 6 h. This procedure is repeated 2 times more on the same site once a week. After a 2-week rest period, the animals are challenged with an occlusive patch with the highest non-irritating concentration of the test material at a naive skin site. The patch challenge test sites are evaluated 24 h and 48 h after removal for the presence of erythema using a scale of 0-3, in which 3 represents intense erythema. Additional control groups of animals are

needed and similarly challenged. The incidence of severity of responses in the test group is calculated relative to that in the control group.

If the point of application is the eye, the Draize test was the most used assay to assess the irritating properties of the formulation (481,482). However, there are many ethical concerns related to animal testing and the scientific community is searching for alternative methods. This test is based on the blinking produced by 0.1 mL of the studied formulation in the rabbit eye compared to a saline-treated control eye. Irritation levels are registered at 24, 48, 72 h and 4, 7, 14 and 21 days following application using a score from 0 (non-irritative) to 100 (maximally irritative) (483). As an *in vitro* alternative for testing ocular irritation, the Bovine corneal opacity and permeability (BCOP) test has been proposed. After *in vitro* experiments where cornea or sclera are used, ocular tissues are visually inspected looking for any damage or appearance modification that indicates irritation (484–486). However, in many cases this test is not considered strong enough to assess the complete safety of formulations and other tests are needed. Hen's Egg Test Chorioallantoic Membrane (HET-CAM test) is probably one of the most accepted alternatives to the Draize test (487,488). In order to conduct it, fertilised eggs are placed and maintained for 8 days in the incubator at 37 ± 0.5ºC with 40 ± 5% environmental humidity. They are turned 3-5 times per day to prevent the attachment of the embryo to one side of the egg. At the end of the 8th day, eggs are placed with the large end facing up for 24 h to ensure the moving of the embryo to the bottom of the egg. On day 9, eggshells are cut in the air chamber area without damaging the membrane, which is moistened for 30 min with 2 mL of 0.9% NaCl solution before removing it to expose the chorioallantoic membrane (CAM). Around 200 µL are deposited in the CAM and eggs are observed for bleeding, vascular lysis, and coagulation of the CAM vessels for 300 sec (489). The irritation score (IS) is calculated according to the following equation (equation 3.3) (490):

*Equation 3.3:*

$$IS = \frac{(301 - tH) \cdot 5}{300} + \frac{(301 - tL) \cdot 7}{300} + \frac{(301 - tC) \cdot 9}{300}$$

Where *tH* is the haemorrhage time (s), *tL* is the lysis time (s) and *tC* is the coagulation time (s). Substances are classified as no irritation (IS < 1), weak irritation (1 ≤ IS < 5), moderate irritation (5 ≤ IS < 9), and severe irritation (9 ≤ IS < 21) (483).

Luckily, topical application of lipid vesicles does not entail frequent side effects in *in vitro* studies, since cells are often insensitive to the toxic effects of vesicles showing higher compatibility than the corresponding drug solutions, and well tolerated in *in vivo* models when they are given topically (491). On this matter, the administration of liposomes containing a high proportion of negatively charged phospholipids has been related to the drying effect on the skin, and stearylamine to irritation if applied topically in the eye (480).

## 3.2. Microneedle arrays

Microneedle arrays (MNA) are devices that contain microscopic needle-like projections that can perforate the *stratum corneum*, creating ducts that facilitate the flow of large molecules (> 500 Da), proteins and nanoparticles through the skin (492). Different types of MNA have been designed, including solid, coated, hollow, dissolving, and hydrogel-forming microneedles. The microneedle field has been growing constantly since the registration of the first patent (solid and hollow microneedles) by Gastrel and Place in 1971, and shortly after, the second one (coated microneedles) by Paul in 1975. However, we had to wait until the year 2000 for the emergence of dissolving microneedles and the current main applications of MNA, which include gene delivery, vaccination, diagnosis, and cosmetic applications (493). MNA are a clearly emerging field within pharmaceutical research, given the rising number of articles being published since the appearance of the “microneedle” concept. In particular, the number of microneedle advertisements was moderate and steady before the year

2000, but since then, there has been a progressive increase year after year. An autoregressive integrated moving average model (ARIMA) study that extrapolates future trends in the short-medium term based on previous data, identified and predicted a growing trend that is currently being met (494). The number of patents registered in recent years also shows a continuous growth of MNA as drug delivery systems (495–497). The interest in MNA is related to advantages such as ease of use (can be self-administered and removed) and controlled release of drugs. Moreover, they can be considered a painless transdermal delivery system because the size of microneedles is enough to surpass the first layers of the skin, while avoiding contact with nervous terminations present in the dermis (498).

### 3.2.1. Microneedle-based transdermal delivery approaches

The success of MNA-based drug delivery is determined by critical issues, mainly concerning the design of the MNA (shape, size, geometry, and manufacturing materials and processes) and the type of active substance delivered. The different strategies can be classified as: "*poke and patch*", "*poke and flow*", "*coat and poke*", and "*poke and release*" (499).

#### *3.2.1.1. Solid MNA for "poke and patch"*

The "*poke and patch"* approach consists of the use of solid MNA to perforate the skin, creating microchannels that reach the deepest layers of the epidermis. This method significantly improves the passive transport of drugs through the skin, since the main barrier to permeability, the *stratum corneum*, is disrupted (500,501). This approach presents two steps: first, the MNA are used to pierce the epidermis and are subsequently removed; and second, the drug is applied in a conventional dosage form (solution, cream, or patch), which works as an external drug reservoir (Figure 3.7) (502). Its simplicity, from a technological point of view, makes it highly attractive, especially for its easy application in a clinical setting. However, this technique is not exempt from controversy and presents several disadvantages. One of the main drawbacks is that the micro-pores remain open only for a limited time, potentially stopping the delivery of the active

substance prematurely. It has been reported that all microneedle-treated sites recover their barrier properties within 2 h (501). Nevertheless, this period can be extended up to three days under occlusive conditions by using formulations like patches or tapes (503), although the risk of infection increases considerably in these conditions (504).

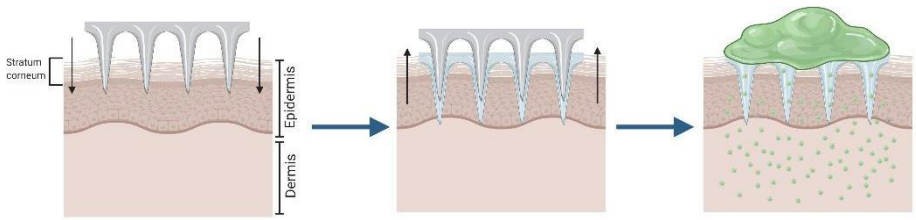


**Figure 3.7.** Schematic representation of “poke and patch” approach.

### *3.2.1.2. Coated MNA for “coat and poke”*

Another approach with solid MNA is the “*coat and poke”* technique which requires the coating of the solid microneedles’ surface with a drug or vaccine-loaded formulation (505). This strategy allows drug diffusion from the coating surface to the deeper epidermal layers after MNA insertion (Figure 3.8) (506). Certain issues, mainly related to the coating, limit the usefulness of this approach. For instance, the amount of drug which can be encapsulated in the coating layer is relatively low. Furthermore, the coating’s thickness can decrease the sharpness of the microneedles and influence their ability to perforate the skin (507). Despite this, coated MNA have shown great efficiency in vaccination, since the antigen dose needed to trigger an immune response is usually in the range of nano or micrograms (508).

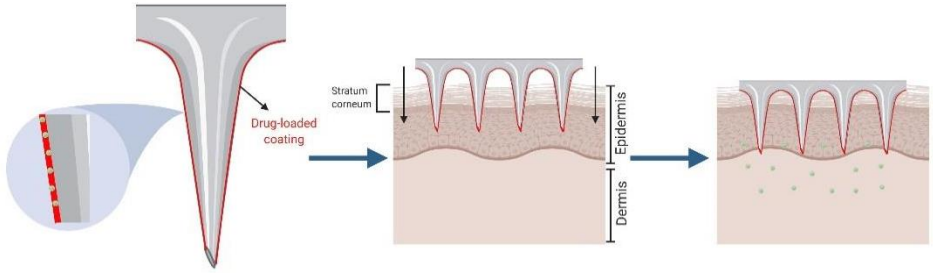


**Figure 3.8.** Schematic representation of “coat and poke” approach.

### *3.2.1.3. Dissolving and hydrogel-forming MNA for “poke and release”*

Dissolving MNA can be made from a range of water-soluble and biodegradable materials in which drugs can be loaded and released as the MNA dissolves after insertion (Figure 3.9) (509,510). The improvement seen in this approach in comparison with the *“poke and patch”* is that dissolving microneedles can maintain controlled drug release over a longer period of time, by controlling the dissolution rate of the formulation used as the MNA matrix. Another advantage is that it reduces the drug administration process to one step, as the MNA are able to pierce the skin and are kept inserted until complete dissolution (511,512). Moreover, dissolving MNA avoid the generation of sharps waste, minimising the cost related to its management and reducing needle-stick injuries. On the other hand, drawbacks include a limited drug loading and a potentially lower ability to perforate the *stratum corneum*.

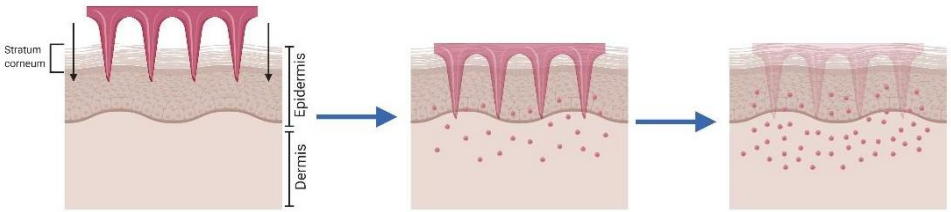


**Figure 3.9.** Schematic representation of “poke and release” approach.

Rapidly separating MNA were designed as a hybrid between coated and dissolving MNA (Figure 3.10) (513). The aim is to insert into the skin a drug-loaded water-soluble matrix encapsulating the drug, coupled with a

solid MNA composed of an insoluble polymer. This second array helps the insertion of the soft matrix that remains in the skin, while the solid MNA can be easily removed afterwards (514,515). As an evolution of these MNA, more sophisticated designs have been developed. The insertion of air bubbles in the MNA structure, between the tips and the patch base, enables the easy and rapid separation of the microneedle's tips from the backing structure after insertion, leaving the tips in the skin and generating non-sharps waste (516).

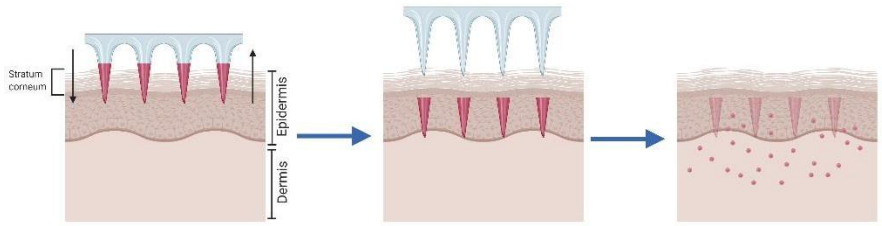


**Figure 3.10.** Schematic representation of rapidly separating MNA.

As an alternative to *"poke and patch"* approaches, hydrogel-forming MNA or swellable MNA have been developed (Figure 3.11). The aim of these devices is to imbibe skin interstitial fluid upon insertion to form continuous, unblockable microchannels amongst dermal capillaries. This approach allows the release of less potent drugs contained in an attached patch-type drug reservoir (517,518).

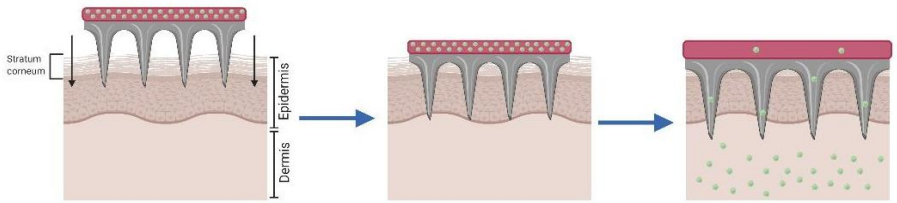


**Figure 3.11.** Schematic representation of hydrogel-forming or swelling MNA.

### *3.2.1.4. Hollow MNA for "poke and flow"*

The *"poke and flow"* approach was conceived to introduce a drug solution into the skin mimicking hypodermic injections while overcoming their limitations (519,520). In this approach, the microneedles play a similar role to hypodermic needles, through which drug formulations are administered after skin perforation (Figure 3.12). Due to their micrometric size, their manufacturing process is difficult and expensive, requiring significant technological resources. By contrast, thanks to the shorter size of these needles, the average patient's acceptance of this approach is higher than that of traditional injections.

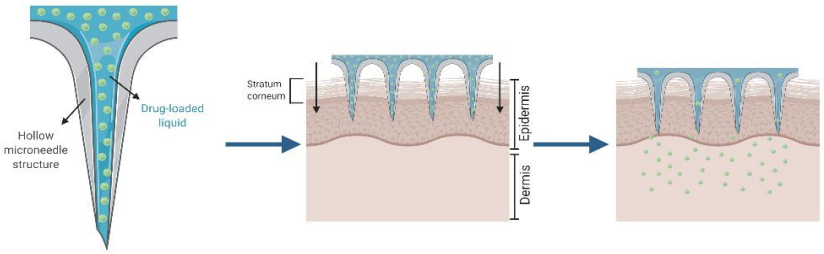


**Figure 3.12.** Schematic representation of "poke and flow" approach.

## 3.2.2. MNA fabrication: materials and manufacturing processes

MNA are produced using a wide range of materials. All of them must show key properties for the final success of this technology. Any material used for manufacturing MNA should present certain characteristics: inert nature, absence of immunogenicity, high tensile strength, mechanical strength, low corrosion rate, biocompatibility, and stability. The most common materials for making MNA are metals, silicones, ceramics, glass, sugars, and polymers (Table 3.5).

**Table 3.5.** Summary of materials and methods used to manufacture MNA.

| Material | MNA Type | Fabrication Process | Ref. |
|---|---|---|---|
| Stainless steel, Titanium, Nickel, Gold | Solid, Hollow coated | Laser cutting, laser ablation, etching, electropolishing, lithography. | (521–527) |
| Alumina, Zirconia | Ceramic | Lithography and ceramic sintering | (528–531) |
| Silicon | Solid, Hollow coated | Etching, lithography | (532–535) |
| Borosilicates | Hollow | Pulling pipettes | (519,536–538) |
| Sugars | Solid, Dissolving | Solvent casting or micromoulding | (539–542) |
| Polymers | Dissolving, Hydrogel-forming, Coated | Solvent casting or micromoulding | (513,543–552) |

The material or main component of MNA determines the most appropriate microneedle manufacturing technique. The main advantages and disadvantages are summarised in Table 3.6. In any case, the selected method should be precise, accurate, reproducible, and robust. The most commonly used techniques include laser cutting, laser ablation, electrodeposition, lithography, etching (Table 3.5) (553). However, micromoulding (also known as solvent casting) is the main trend in basic research, which consists of the use of 3D-printed structures to produce negative moulds that are filled with polymeric solutions. After solvent removal, a polymeric MNA with an identical shape and size of the 3D-printed model is obtained (554).

**Table 3.6.** Summary of advantages and disadvantages of MNA.

| MNA Type | Advantages | Disadvantages | Ref. |
|---|---|---|---|
| Stainless steel, Titanium, Nickel, Gold | Desirable mechanical properties and high tensile strength | Fractures, corrosion, and poor compatibility of some metals | (521–527) |
| Alumina, Zirconia | Good biocompatibility | Fractures | (528–531) |
| Silicon | Desirable mechanical properties | High material cost, long fabrication, and fractures | (532–535) |
| Borosilicates | Good biocompatibility | Fractures | (519,536–538) |
| Sugars | Good biocompatibility | Mechanical properties are difficult to achieve, stability problems, storage issues | (539–542) |
| Polymers | Good biocompatibility, biodegradation, and absence of waste after use | Mechanical properties are more difficult to achieve | (513,543–552) |

### 3.2.3. Safety considerations

As with any pharmaceutical formulations, MNA must be rendered safe in order to be accepted as a true alternative to classical drug delivery technologies. Three basic undesired effects could happen after the insertion of MNA: pain, infections, and local skin reactions (inflammation, erythema, irritation, etc.).

#### *3.2.3.1. Pain*

Patient's compliance and acceptance depend mainly on the pain generated by MNA in comparison with conventional injections. MNA should produce significantly less pain than a hypodermic needle, since the needle tips in MNA do not usually reach the dermis, where nerve endings are located. Several studies have demonstrated that pain depends on the length and number of needles in the MNA. Gill et al. (2007) observed that

MNA are less painful than a 26-gauge hypodermic needle and established a correlation between the pain level and the number and length of the microneedles (555,556). Particularly, the authors tested needles with lengths of 480, 700, 960, and 1450 μm, finding that the pain levels they produced varied between 5-37% of those obtained with the hypodermic needle. Additionally, a 10-fold increase in the number of projections produced a relatively small increase in pain, from 5 to 25% in comparison with a hypodermic-needle. Bal et al. (2008) tested the pain generated by microneedles below 550 μm in length, finding very low pain scores in all cases with no significant differences between them (557). However, pain and skin reactions can be produced by the breakage of the microneedles during insertion, which may be possible, and is especially associated with certain materials, such as glass and ceramics (538).

*3.2.3.2. Infections*

Open channels created by MNA can potentially become a gateway for the entry of microorganisms into the body. The development of infectious processes is directly related to disruption of the skin's barrier function. In turn, the time that the micro-pores remain open depends largely on some characteristics of the MNA, such as the length of the tips. This relationship has already been stated; for example, Kalluri et al. (2011) studied the *in vivo* kinetics of pore closure using calcein imaging, and observed that this process lasts about 15 h when exposed to the environment and up to 72 h under occlusive conditions (503). This period is similar to the estimated one for a hypodermic needle channel. The barrier function of the skin was also evaluated using the TEWL levels, indicating that the skin only needs 4 h to recover its barrier function after treatment with 550 μm long microneedles. Bal et al. (2008) reported a trend that using longer microneedles resulted in a higher increase in TEWL values, since a significant difference in response was observed between needles with lengths of 400 and 200 μm (557). Furthemore, the study of Donnelly et al. (2013) showed that microneedle puncture resulted in significantly less microbial penetration than hypodermic needle puncture and that no microorganisms crossed the

viable epidermis in microneedle-punctured skin, in contrast to needle-punctured skin. Therefore, it could be stated that the correct application of MNA to skin would not cause either local or systemic infection in normal circumstances in immune-competent patients (558). Particularly, excised porcine skin, Silescol® membranes and radiolabelled microorganisms were used in the experiments, which showed that the number of microorganisms that crossed the membranes were an order of magnitude lower when the membranes were punctured by microneedles rather than with a 21 G hypodermic needle; and the number of microorganisms penetrating the skin beyond the *stratum corneum* was approximately an order of magnitude greater than the numbers crossing Silescol® membranes in the corresponding experiment.

*3.2.3.3. Biocompatibility, immunogenicity, and local skin reactions*

The presence of strange objects or biological incompatibility of any component could trigger skin inflammation, irritation, or erythema during or after treatment with MNA. Bal et al. (2008) checked the possible impact of microneedle length on irritation, examining the redness of the skin, and blood flow (557). Both methods measure erythema, one of the fundamental indicators of inflammation. Changes in redness were observed after the application of solid metallic MNA, reaching maximum irritation values after 15 min and returning to the basal values in approximately 90 min. For those MNA, an increase in length (200, 300, and 400 μm) results in an increase in redness, although only the differences between the smaller length and the rest were statistically significant. Moreover, the treatment with MNA of various lengths did not result in significant differences in blood flow. On the other hand, Vicente–Pérez et al. (2017) did not find any significant evidence of an increase in sera biomarkers of inflammation and irritation (TNF-α and IL-1β) after a prolonged use of polymeric MNA (559).

Low biocompatibility or allergic responses are not frequent in microneedle-based approaches, especially with polymeric MNA since the manufacturing materials are commonly transferred from other fields of

pharmaceutical technology where compatibility has been guaranteed. However, other types of MNA, such as the solid and hollow ones, might be associated with some issues. For example, stainless steel MNA can suffer corrosion over time, a feature that has been clearly improved by using titanium (560). In addition, nickel MNA have been designed and used despite the fact that nickel has shown cytotoxicity and intracellular accumulation in human HaCat keratinocytes (561–563).

Some studies have demonstrated that MNA do not stimulate the humoral immune system, as shown in the work of Vicente–Pérez et al. (2017) (559). Here, they used three well known sera biomarkers such as C-reactive protein, TNF-α, and IgG to monitor possible infection and inflammatory processes associated with two dissolving MNA treatment regimens, using an *in vivo* model. TNF-α levels were undetectable in all mice, and no statistical differences were found for the other measured biomarkers, regardless of formulation type, needle density, number of applications, or mouse gender.

# Chapter 4

## Development and validation of an analytical method for cyanocobalamin

## 4.1. Materials and methods

Cyanocobalamin (B12) was quantified in all experiments by HPLC with Ultraviolet detection or UV-Vis spectroscopy. The analytical method developed is based on that previously described by Li et al. (2000), including certain modifications to adapt it to the equipment used (564).

### 4.1.1. Materials

The reagents used are listed in table 4.1.

**Table 4.1.** Reagents for validating the analytical method.

| Reagent | Quality | Supplier |
|---|---|---|
| **Water** | HPLC-grade | Milipore (Madrid, Spain) |
| **Methanol** | HPLC-grade | VWR (Radnor, PA, USA) |
| **Cyanocobalamin** | > 95% purity | Acofarma (Madrid, Spain) |

### 4.1.2. Equipment

A PerkinElmer Series 200® HPLC (PerkinElmer; Waltham, MA, USA) equipped with an automatic injector and UV-vis detector was used. TotalChrom Workstation® software was employed to process the chromatograms and determine the area of the peaks.

### 4.1.3. Stationary phase and mobile phase

The mobile phase consisted of an isocratic mixture of methanol:water (30:70). The stationary phase was a Kromasil® C18 HPLC column of 5 µm particle size, pore size 100 Å, L x I.D. 150 mm x 4.6 mm (Dr. Maisch GmbH; Ammerbuch, Germany).

### 4.1.4. Analytical conditions

The injection volume was 50 µL, and the detector was settled at 360 nm. The mobile phase was delivered at a flow rate of 0.7 mL/min, and the analysis of the samples was carried out at room temperature.

4.1.5. Validation of the analytical method

The method was validated regarding linearity, sensitivity, precision, and accuracy. To this end, the area of the peaks corresponding to the cyanocobalamin were plotted versus the concentration of the standards and fitted by least squares linear regression to the following equation (equation 4.1):

*Equation 4.1:*

$$y = b \cdot x + a$$

In which *y* is the area of the peak; *x* is the concentration (µg/mL); *b* is the slope, and *a* is the intercept with the y-axis. The software Microsoft Excel 2019® was used to perform the calculations.

*Linearity* has been expressed by the $R^2$ obtained from the straight line, which represents the linear dependency between the areas and the concentrations.

*Sensitivity* is defined as the capacity of discrimination between similar concentrations of the same substance. It has been expressed by the significance of the slope and its standard deviation (b ± SD).

The *Quantification limit* (QL) is the lowest concentration of the substance assayed that can be statistically differentiated from the blank, whereas the *detection limit* (DL) is the minimum amount of substance that can be detected under these experimental conditions. They have been calculated according to the following equations (equation 4.2 and 4.3):

*Equation 4.2:*

$$QL = \frac{10 \cdot SD}{b}$$

*Equation 4.3:*

$$DL = \frac{3 \cdot SD}{b}$$

Where *SD* stands for the standard deviation of the intercept, and *b* for the slope of the line.

The *precision* is expressed by the variation coefficient (VC) of the average concentration calculated in intraday and interday assays. Intraday VC (%) was calculated by injecting the different concentrations assayed three times during the same day, while Interday VC (%) was calculated from the areas obtained across three different days.

The *accuracy* was evaluated by the relative error (Er) from the different concentration of the three straight lines analysed across three different days, according to the mathematical expression described in the following equation (equation 4.4):

*Equation 4.4:*

$$Er\ (\%) = \frac{(Cexp - C\hat{e})}{C\hat{e}} \cdot 100$$

Where *Cexp* stands for the experimental concentration, and *Cê* for the theoretically calculated one.

## 4.2. Results and Discussion

B12-HPLC analysis under the described conditions resulted in a single and well-defined chromatographic peak with a retention time of 3.5 min. A typical chromatogram is shown in Figure S1 (Annex I).

The relationship between the chromatographic areas and cyanocobalamin concentrations was assessed in the range 10-0.039 µg/mL. The obtained results are summarised in Tables 4.2-4.5.

The linearity of the method is demonstrated by the determination coefficients, being higher than 0.999 in all cases. The graphic representations of the linear regression of the intraday and interday calibration curves are shown in Figures 4.1 and 4.2. The detection and quantification limits of the method were 0.033 µg/mL and 0.11 µg/mL

respectively, calculated from the values obtained for three different curves assayed in three different days.

**Table 4.2.** Values of cyanocobalamin intraday calibration curve (CC) from 10 to 0.039 µg/mL.

| INTRADAY CALIBRATION | | | | |
|---|---|---|---|---|
| **Concentration (µg/mL)** | **Area (CC1)** | **Area (CC 2)** | **Area (CC 3)** | **Average (mean ± SD)** |
| 10 | 541342 | 529090 | 519483 | 529971 ± 10956 |
| 5 | 285161 | 282025 | 277311 | 281499 ± 3951 |
| 2.5 | 138442 | 138583 | 141459 | 139494 ± 1702 |
| 1.25 | 72673 | 69718 | 67483 | 69958 ± 2603 |
| 0.625 | 43213 | 44089 | 45280 | 44194 ± 1037 |
| 0.312 | 23798 | 24551 | 25652 | 24667 ± 932 |
| 0.156 | 12671 | 12866 | 13355 | 13297 ± 405 |
| 0.078 | 7153 | 7589 | 7586 | 7442 ± 250 |
| 0.039 | 3524 | 3405 | 3633 | 3520 ± 114 |

**Table 4.3.** Values of cyanocobalamin interday calibration curve (CC) from 10 to 0.039 µg/mL.

| INTERDAY CALIBRATION | | | | |
|---|---|---|---|---|
| **Concentration (µg/mL)** | **Area (CC1)** | **Area (CC 2)** | **Area (CC 3)** | **Average (mean ± SD)** |
| 10 | 541342 | 529128 | 558142 | 535235 ± 14567 |
| 5 | 285161 | 261533 | 287887 | 273347 ± 14492 |
| 2.5 | 138442 | 130208 | 143989 | 134325 ± 6934 |
| 1.25 | 72673 | 65023 | 71652 | 68848 ± 4153 |
| 0.625 | 43213 | 39014 | 40799 | 41113 ± 2107 |
| 0.312 | 23798 | 22079 | 20910 | 22938 ± 1452 |
| 0.156 | 12671 | 10975 | 12845 | 11823 ± 1033 |
| 0.078 | 7153 | 6131 | 7057 | 6642 ± 564 |
| 0.039 | 3024 | 2596 | 2989 | 2810 ± 237 |

**Table 4.4.** Average of the slope (b) and intercept (a) of the intraday and interday calibration curves.

| | Intraday | Interday |
|---|---|---|
| **b** | 52900 ± 1098 | 54079 ± 1624 |
| **a** | 6419 ± 951 | 3779 ± 1644 |

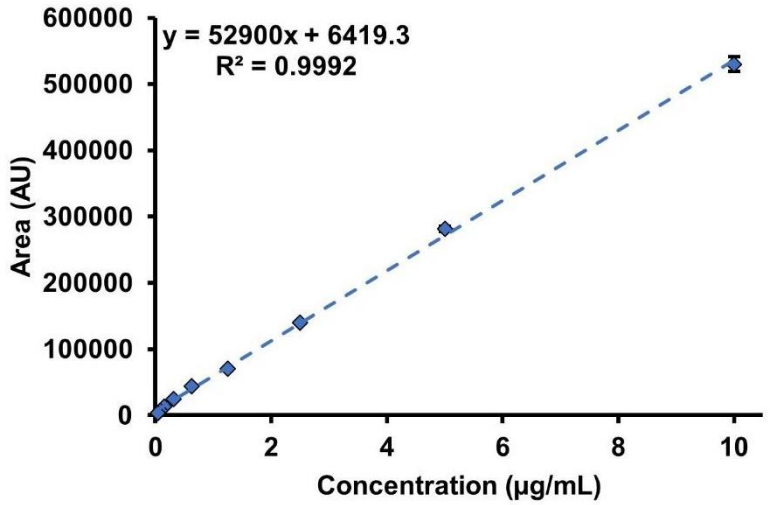


**Figure 4.1.** Average of the intraday CC with concentration values varying from 10 to 0.039 µg/mL.

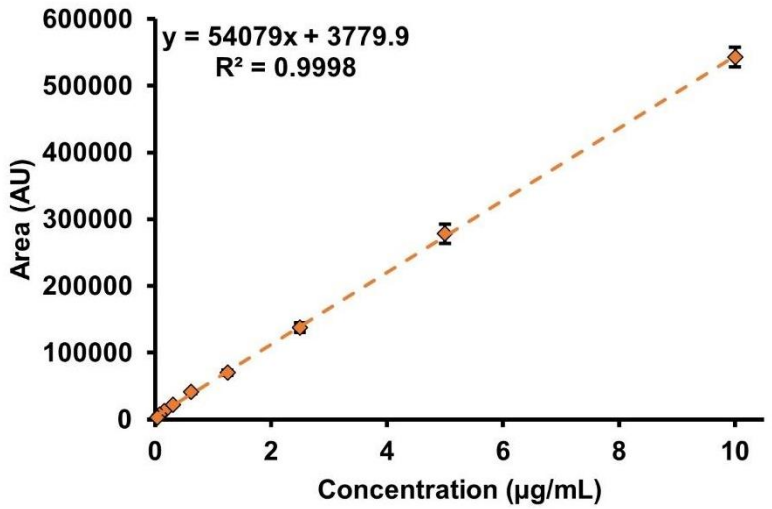


**Figure 4.2.** Average of the interday CC with concentration values varying from 10 to 0.039 µg/mL.

The precision and accuracy of the method was evaluated by the variation coefficient (VC) and the relative error (Er), respectively. Tables 4.5-4.8 show the obtained results. The validation of the method was completely satisfactory since every calculation remained under the 10% threshold, as recommended by OCDE guidelines for validation of a bioanalytical method (565). The validation of the UV-vis spectroscopy method -used in chapter 6 experiments- offered an adequate validation as well, as both share the same detection principle (data not shown).

**Table 4.5.** Intraday variation coefficients for each concentration.

**INTRADAY CALIBRATION**

| Concentration (µg/mL) | VC (%) CC1 | VC (%) CC 2 | VC (%) CC 3 | VC (%) Intraday |
|---|---|---|---|---|
| 10 | 2.02 | 2.07 | 2.10 | 2.06 ± 0.04 |
| 5 | 1.38 | 1.40 | 1.42 | 1.40 ± 0.02 |
| 2.5 | 1.22 | 1.22 | 1.20 | 1.22 ± 0.01 |
| 1.25 | 3.59 | 3.73 | 3.85 | 3.92 ± 0.13 |
| 0.625 | 2.40 | 2.35 | 2.29 | 2.34 ± 0.05 |
| 0.312 | 3.91 | 3.79 | 3.63 | 3.78 ± 0.14 |
| 0.156 | 2.96 | 3.15 | 3.03 | 3.05 ± 0.09 |
| 0.078 | 3.50 | 3.30 | 3.30 | 3.37 ± 0.11 |
| 0.039 | 3.23 | 3.34 | 3.13 | 3.23 ± 0.10 |

**Table 4.6.** Interday variation coefficients for each concentration.

**INTERDAY CALIBRATION**

| Concentration (µg/mL) | VC (%) CC1 | VC (%) CC 2 | VC (%) CC 3 | VC (%) Interday |
|---|---|---|---|---|
| 10 | 2.69 | 2.75 | 2.60 | 2.68 ± 0.07 |
| 5 | 5.08 | 5.54 | 5.03 | 5.21 ± 0.28 |
| 2.5 | 5.00 | 5.32 | 4.81 | 5.16 ± 0.25 |
| 1.25 | 5.71 | 6.38 | 5.79 | 6.03 ± 0.36 |
| 0.625 | 4.87 | 5.40 | 5.16 | 5.12 ± 0.26 |
| 0.312 | 6.10 | 6.57 | 6.94 | 6.33 ± 0.42 |
| 0.156 | 8.15 | 9.41 | 8.04 | 8.73 ± 0.76 |
| 0.078 | 7.89 | 9.20 | 7.99 | 8.49 ± 0.73 |
| 0.039 | 7.85 | 9.15 | 7.95 | 8.45 ± 0.72 |

**Table 4.7.** Intraday relative error for each concentration.

| INTRADAY CALIBRATION | | | | |
|---|---|---|---|---|
| **Concentration (µg/mL)** | **Er (%) CC1** | **Er (%) CC 2** | **Er (%) CC 3** | **Er (%) Intraday** |
| 10 | 2.14 | -0.16 | -1.98 | 0.00006 ± 2.06 |
| 5 | 1.30 | 0.18 | -1.48 | 0.0001 ± 1.39 |
| 2.5 | -0.75 | -0.65 | 1.41 | 0.001 ± 1.21 |
| 1.25 | 3.88 | -0.33 | -3.55 | 0.0002 ± 3.72 |
| 0.625 | -2.22 | -0.24 | 2.46 | 0.0001 ± 2.34 |
| 0.312 | -3.52 | -0.48 | 4.01 | 0.0005 ± 3.7 |
| 0.156 | 2.81 | -3.15 | 0.44 | 0.03 ± 3.01 |
| 0.078 | -3.89 | 2.04 | 1.88 | 0.014 ± 3.37 |
| 0.039 | 0.09 | -3.28 | 3.29 | 0.037 ± 3.28 |

**Table 4.8.** Interday relative error for each concentration.

| INTERDAY CALIBRATION | | | | |
|---|---|---|---|---|
| **Concentration (µg/mL)** | **Er (%) CC1** | **Er (%) CC 2** | **Er (%) CC 3** | **Er (%) Interday** |
| 10 | 1.14 | -1.12 | 4.32 | 1.44 ± 2.73 |
| 5 | 4.32 | -4.14 | 5.55 | 1.91 ± 5.27 |
| 2.5 | 3.06 | -2.97 | 7.42 | 2.50 ± 5.21 |
| 1.25 | 5.55 | -5.26 | 4.31 | 1.53 ± 5.91 |
| 0.625 | 5.10 | -4.85 | -0.80 | -0.18 ± 5.00 |
| 0.312 | 3.74 | -3.61 | -9.18 | -3.01 ± 6.48 |
| 0.156 | 7.17 | -6.69 | -9.31 | - 2.94 ± 8.85 |
| 0.078 | 7.69 | -7.14 | 6.76 | 2.43 ± 8.30 |
| 0.039 | 7.61 | -7.07 | 6.89 | 2.47 ± 8.27 |

## 4.3. Milestone and highlights of chapter 4

**Milestone:** An analytical HPLC method was developed to quantify B12

- **Highlight 4.1:** Calculated parameters proved the sensibility, accuracy, precision, and robustness of the method.
- **Highlight 4.2**: Detection and quantification limits of the method were below than the usual concentrations in the samples in the different studies, for being therefore an adequate method for this work

# Chapter 5

## Design, development, and characterisation of cyanocobalamin lipid vesicles

---

Chapter adapted from **Cyanocobalamin Ultraflexible Lipid Vesicles: Characterization and In Vitro Evaluation of Drug-Skin Depth Profiles,** Guillot AJ, Jornet-Mollá E, Landsberg N, Milián-Guimerá C, Montesinos MC, Garrigues TM, et al. *Pharmaceutics, 2021;* and **Exploration of Microneedle-assisted Skin Delivery of Cyanocobalamin formulated in Ultraflexible Lipid Vesicles.** Guillot AJ, Merino P, Bocchino A, O'Mahony C, Giner RM, Recio MC, et al. *European Journal of Pharmaceutics and Biopharmaceutics, 2022.*

## 5.1. Materials and methods

### 5.1.1. Materials

The reagents and materials used are listed in table 5.1.

**Table 5.1.** Reagents and materials for the preparation and characterisation of cyanocobalamin lipid vesicles.

| Reagent / Material | Information | Supplier |
|---|---|---|
| **Mili-Q Water** | Resistance > 18MΩ<br>TOC < 10 ppb | Milipore<br>(Madrid, Spain) |
| **Methanol** | HPLC-grade | VWR (Radnor, PA, USA) |
| **Phospholipon 90G®** | Soybean<br>Phosphatidyl choline | Lipoid<br>(Steinhausen, Switzerland) |
| **Cholesterol** | > 95% purity | Acofarma (Madrid, Spain) |
| **Polysorbate 80** | Tween<br>80® | Thermo Fisher Scientific<br>(Waltham, MA, USA) |
| **Cyanocobalamin** | > 95% purity | Acofarma (Madrid, Spain) |
| **NaCl** | - | Scharlab (Santmenat, Spain) |
| **KCl** | - | Scharlab (Santmenat, Spain) |
| **$KH_2PO_4$** | - | Scharlab (Santmenat, Spain) |
| **$Na_2HPO_4$** | - | Scharlab (Santmenat, Spain) |
| **Sodium dodecyl sulphate** | SDS<br>1% (w/v) | Thermo Fisher Scientific<br>(Waltham, MA, USA) |
| **Ascorbic acid** | Crystalline<br>> 99% purity | Sigma-Aldrich<br>(St. Louis, MI, USA) |
| **Ammonium molybdate** | Tetrahydrate<br>> 99% purity | Sigma-Aldrich<br>(St. Louis, MI, USA) |
| **Perchloric acid** | Aqueous solution<br>70% purity | Sigma-Aldrich<br>(St. Louis, MI, USA) |
| **Cellulose dialysis membranes** | Spectra/Por®,<br>14 kDa cut-off | Repligen<br>(Radnor, PA, USA) |
| **Lactose** | - | Guinama (Valencia, Spain) |
| **Sorbitol** | - | Guinama (Valencia, Spain) |
| **Polysulphate membrane** | Pore size:<br>200 and 100 nm | Avestin Inc.<br>(Ottawa, Canada) |
| **MTT reactive** | Thiazolyl blue<br>formazan | Sigma-Aldrich<br>(St. Louis, MI, USA) |
| **DMEM medium** | Dublecco's Modified<br>Eagle's Medium | Thermo Fisher Scientific<br>(Waltham, MA, USA) |
| **DMSO** | - | Sigma-Aldrich<br>(St. Louis, MI, USA) |

## 5.1.2. Methods

### *5.1.2.1. Preparation of liposomes, transfersomes and ethosomes*

Several formulations of liposomes (L), transfersomes (T) and ethosomes (E) were prepared by the classic film-hydration method (Figures 5.1 and 5.2) (236,566). Their quantitative composition, reconstitution conditions, and the methods used to purify them are shown in Tables 5.2-5.4. Three batches of each lipid vesicle type were prepared, blank and loaded with a variable amount of B12 which, depending on the formulation, was added to the organic phase dispersion or included in the liposomal reconstitution solution. The two B12 doses were settled at 0.2% w/w when the drug was incorporated in the organic phase, and 1% when it was incorporated in the aqueous phase. The reason for this is to avoid the bilayer saturation in the first case, which would reduce the vesicle flexibility. The 1% w/v corresponds to the 80% solubility limit of B12 in water. Briefly, Phospholipon 90G® (P90G), cholesterol (P90G:Chol molar ratio 17:1) or surfactants (P90G:Tween 15% w/w), and cyanocobalamin (except in the blank formulations and formulations reconstituted with B12-solution) were dissolved in methanol. The solvent was evaporated using a rotary evaporator (BUCHI R-210, Büchi AG; Flawil, Switzerland) under stirring at 50°C and 100 mbar. The resulting thin film was hydrated by addition of Phosphate buffer saline (PBS) pH 7.4 or B12-solution and then stirred for 1 h at 50°C to obtain a MLV dispersion. The ethosomes were prepared by the Touitou method (Figure 5.3), dissolving P90G and B12 in ethanol (199). Then, an appropriate amount of water was added at 12 ± 0.5 mL/h in a sealed beaker while stirring (710 ± 5 rpm), in a water bath tempered at 30ºC. Concurrently, the option of adding B12 dissolved in the water flow was also explored. The system was kept stirring for 5 min after the addition of the water. Once MLV were obtained, their size was reduced by sonication and membrane extrusion. In the case of liposomes and transfersomes, they were firstly sonicated at 50°C for 2 h (Elmasonic S60H, Elma; Singen, Germany), then cooled down to 4°C and extruded through a 200 μm membrane at 30°C (20 times), using a LiposoFast-Basic Extruder (Avestin;

Ottawa, Canada) (567). Ethosomes were sonicated for 1 h at room temperature and reduced by the same extrusion process. After size reduction, the samples were purified by centrifugation (12800 xg, 30 min) or washed in 2 L PBS at 4°C for 24 h (568,569). The batches were then stored at 4°C protected from light.

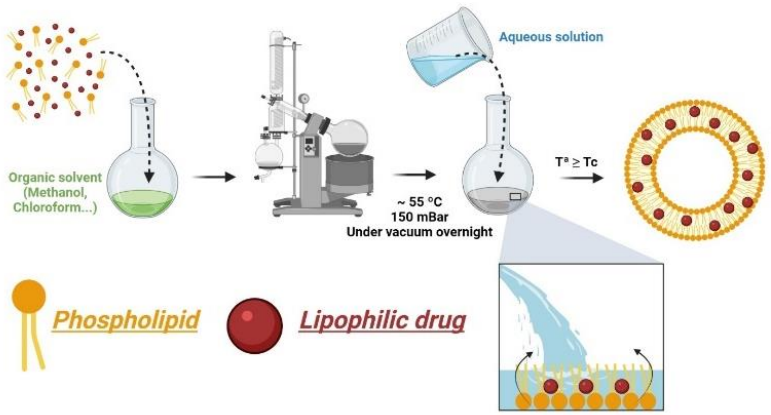


**Figure 5.1.** Lipophilic drug-loaded lipid vesicle production. Lipophilic drugs are added to the organic blend and rehydrated with an aqueous solution.

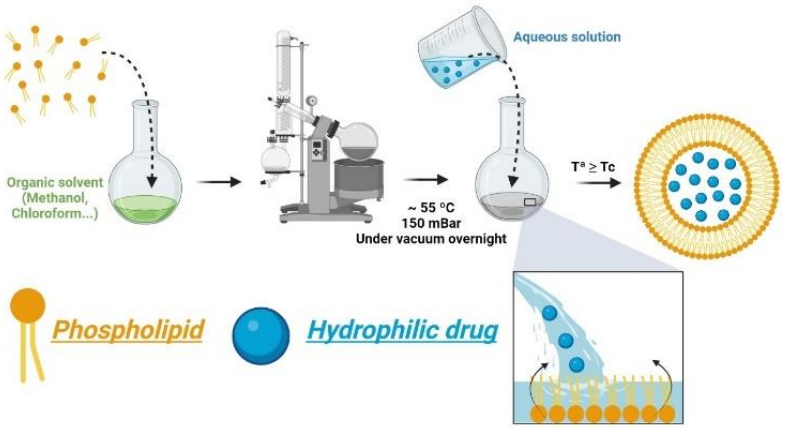


**Figure 5.2.** Hydrophilic drug-loaded lipid vesicle production. Hydrophilic drugs are included in the aqueous solution for rehydrating the thin-film.

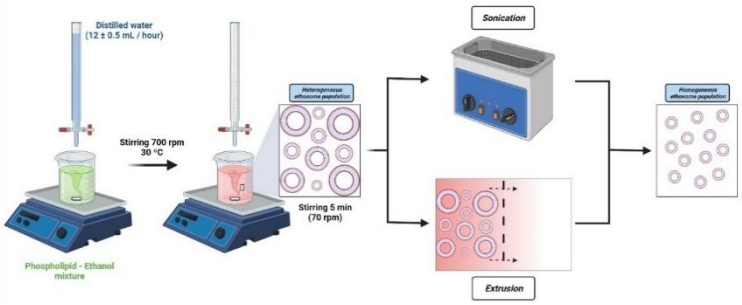


**Figure 5.3.** Touitou's method for ethosome production. Size reduction by sonication or extrusion to produce a homogeneous ethosome batch.

**Table 5.2.** Quantitative composition, reconstitution solvent and purification method of the different liposomes designed.

| Components | Liposome formulations | | | |
|---|---|---|---|---|
| | **L1** | **L2** | **L3** | **L blank** |
| **Phospholipon 90G® (g)** | 4.5 | 4.5 | 4.5 | 4.5 |
| **Cholesterol (g)** | 0.135 | 0.135 | 0.135 | 0.135 |
| **Cyanocobalamin (g)** | 1[1] | 0.2[2] | 0.2[1] | - |
| **Reconstitution Solvent (mL)** | 10 PBS | 10 PBS | 10 PBS | 10 PBS |
| **Purification method** | C | C | C | C |

[1] B12 added in reconstitution solution. [2] B12 added in the organic-lipid phase.
C: centrifugation. PBS: Phosphate Buffer Saline.

**Table 5.3.** Quantitative composition, reconstitution solvent and purification method of the different transfersomes designed.

| Components | Transfersome formulations | | | | |
|---|---|---|---|---|---|
| | **T1c** | **T2c** | **T1d** | **T2d** | **T blank** |
| **Phospholipon 90G® (g)** | 4.5 | 4.5 | 4.5 | 4.5 | 4.5 |
| **Tween 80® (g)** | 0.675 | 0.675 | 0.675 | 0.675 | 0.675 |
| **Cyanocobalamin (g)** | 1[1] | 0.2[2] | 1[1] | 0.2[2] | - |
| **Reconstitution solvent (mL)** | 10 PBS | 10 PBS | 10 PBS | 10 PBS | 10 PBS |
| **Purification method** | C | C | D | D | C+D |

[1] B12 added in reconstitution solution. [2] B12 added in the organic-lipid phase.
C: centrifugation. D: dialysis (24 h). PBS: Phosphate Buffer Saline.

**Table 5.4.** Quantitative composition, reconstitution solvent and purification method of the different ethosomes designed.

| Components | Ethosome formulations | | | |
|---|---|---|---|---|
| | **E1** | **E2** | **E3** | **E blank** |
| **Phospholipon 90G® (g)** | 3 | 3 | 3 | 3 |
| **Ethanol (mL)** | 5.55 | 5.55 | 5.55 | 5.55 |
| **Cyanocobalamin (g)** | 0.2[2] | 0.2[1] | 0.2[2] | - |
| **Reconstitution Solvent (mL)** | 10 $H_2O$ | 10 $H_2O$ | 10 $H_2O$ | 10 $H_2O$ |
| **Purification method** | C | C | - | C |

[1] B12 added in the dropped water. [2] B12 added in the organic-lipid phase.
C: centrifugation.

### *5.1.2.2. Determination of particle size, PDI and zeta-potential*

Particle size (average diameter) and PDI were measured by means of a Malvern Nano Zetasizer (Malvern Panalytical; Malvern, UK). DLS mode was used to measure the vesicular size and PDI, and laser doppler electrophoresis (LDE) to determine the zeta-potential. The temperature was set at 25ºC in all cases. Each formulation was analysed in triplicate (n=3) (570).

### *5.1.2.3. Determination of phospholipid content of vesicles*

The method of Rouser et al. (1970) was used to determine the amount of phosphatidyl choline (PC) incorporated into the different vesicles (344). Briefly, 100 µL of the liposomal aqueous samples was heated at 270ºC until complete liquid evaporation, followed by addition of 450 µL of perchloric acid (70% v/v). Next, the mixture was heated to 250ºC for 30 min. After cooling down, 3.5 mL of water, 500 µL of ammonium molybdate (2.5% w/v), and 500 µL of ascorbic acid (10% w/v) were added. The mixture was vortexed and incubated at 100ºC for 7 min. After the tubes were cooled down, the absorbance was measured at 820 nm (HITACHI U-2900 spectrophotometer, Hitachi High-Tech Corp.; Tokyo, Japan). All formulations were analysed in triplicate (n=3).

*5.1.2.4. Determination of the entrapment efficiency*

Entrapment efficiency (EE) was determined directly by calculating the amount of B12 encapsulated in lipid vesicle dispersions using the following equation (equation 5.1) (571):

*Equation 5.1:*

$$EE\ (\%) = \left(\frac{Qe}{Qt}\right) \cdot\ 100$$

Where *Qe* is the amount of B12 encapsulated, and *Qt* is the amount of B12 used for batch preparation.

For this, 0.5 mL of lipid vesicles dispersion was incubated for 1 h with a mixture of water:methanol:sodium dodecyl sulphate 1% (45:45:10) to dissolve all the vesicle components (572–574). The final mixture was filtered, and B12 content was analysed by HPLC. All formulations were analysed in triplicate (n=3).

*5.1.2.5. Differential scanning calorimetry*

DSC was carried out using a DSC 214 Polyma (Netzsch; Waldkraiburg, Germany). Temperature scans were performed from 25 to 225°C at a scan rate of 10°C/min (575). Netzsch Proteus Thermal Analysis 8.0 software (Netzsch; Waldkraiburg, Germany) was used to create baselines and thermograms, and used to determine the glass transition temperatures.

*5.1.2.6. Evaluation of lipid vesicle flexibility*

The flexibility of the different lipid vesicles was estimated indirectly by extrusion through a 100 nm membrane in cold (399). For this, 500 µL of each formulation was extruded 9 times at room temperature. The final collected volume was also recorded and the relative decrease ratio in particle size was calculated. All formulations were analysed in triplicate (n=3).

*5.1.2.7. Vesicle morphology: TEM imaging*

A drop of the vesicle dispersion was diluted (1:1000), poured into a copper grid and dried for 4 min. Excess of the dispersion was removed and a drop of phosphotungstic acid solution (2%) was applied and dried for 1 min (576). Vesicles were then visualised by means of transmission electron microscopy using a JEOL JEM 1010 -100kV- equipped with an AMT 8Mpx camera (Jeol Ltd.; Tokyo, Japan).

*5.1.2.8. Stability studies*

The physical stability of the vesicles was checked weekly for 60 days in terms of size and PDI by DLS. The stability of the vesicle suspension was determined using Turbiscan™ LAB Stability Analyzer (Formulaction SA; Toulouse, France) by checking the phenomena of coalescence, flocculation, creaming, sedimentation, and clarification during the 24 h after the suspension was formulated (577). The chemical stability of B12 was assessed by determination of drug content every week for 3 months.

*5.1.2.9. Freeze-drying*

Lipid vesicles were freeze-dried in absence and presence of lactose and sorbitol as cryoprotective agents. Lactose solutions were prepared at a molar ratio PC/sugar 1:10 and sorbitol was prepared at 2.5% v/v (442,453,578,579). Ethosomes were not lyophilised, as ethanol would be removed through the procedure (281). In all cases, 100 µL of the sample was placed together with 400 µL of cryoprotective agent, or no cryoprotectants, as control, in glass vials. Samples frozen at -80°C (Ultra Low Temperature Freezer U570, New Brunswick Scientific; Enfield, CT, USA) for 24 h and lyophilised for 48 h using a freeze-dryer (LyoQuest HT-40, Telstar; Barcelona, Spain) at -50°C and 0.08 mbar (281). Lyophilised samples were afterwards suspended in PBS and the physical stability was checked in terms of size and PDI by DLS. The chemical stability of B12 was assessed by determination of drug content after freeze-drying.

*5.1.2.10. Thermogravimetric assay*

TGA was carried out using a TG 209 F3 Tarsus (Netzsch; Waldkraiburg, Germany). Temperature scans were performed from 25 to 200°C at a scan rate of 10°C/min (575). Netzsch Proteus Thermal Analysis 8.0 software (Netzsch; Waldkraiburg, Germany) was used to create baselines and thermograms.

*5.1.2.11. Drug release study and kinetic model fitting*

*In vitro* release studies were carried out using static FDC with an effective diffusion area of 1.76 $cm^2$. 500 µL of each formulation was added to the donor chamber, and the receptor chamber was filled with 12 mL of PBS pH 7.4 (n=6). A Spectra/Por® molecular porous membrane was used to separate donor and acceptor compartments. Both the donor compartment and the sampling port were covered with Parafilm M® to avoid leakage and solvent evaporation. Samples of 400 µL were collected at 1, 2, 3, 4, 5, 6, 7, 8, 9, 10, 24, 48 and 72 h. At every sampling time, the volume was replaced with pre-warmed PBS to guarantee sink conditions (406).

The released B12 was quantified by HPLC and the cumulative amounts of B12 versus time were calculated. The total drug amount released was calculated according to the previous determination of the drug content and plotted versus time. The release profiles were fitted to different mathematical kinetic models: Higuchi, Korsmeyer-Peppas, Kim, Peppas-Sahlin, zero order and first order. For each case, the AIC was calculated to determine the optimal models to explain the experimental data. The $R^2$ of the most accurate model were reported, as an indicator of the proportion of variation of the results that can be explained by the model (415,416).

The Higuchi model assumes that the release process is carried out only by passive diffusion and is governed by the following equation (equation 5.2) (410):

*Equation 5.2:*

$$\frac{Mt}{M\infty} = k \cdot \sqrt{t}$$

Where *Mt* is the amount released at time t, *M*∞ is the maximum amount of drug released, *Mt/M*∞ is the fraction of the amount of drug released at time t, and *k* is the constant that governs the process.

The Korsmeyer-Peppas model or Power-law is described with the following equation (equation 5.3) (411,412):

*Equation 5.3:*

$$\frac{Mt}{M\infty} = k \cdot t^n$$

Where *Mt* is the amount released at time t, *M*∞ is the maximum amount of drug released, *Mt/M*∞ is the fraction of the amount of drug released at time t, *k* is the constant that governs the process and explains the characteristics of the system, and *n* is the diffusion release exponent. Values of $n < 0.5$ are indicative that the release process is explained by passive diffusion; values of $0.85 < n < 1$ show that the process is governed mainly by relaxation and intermediate values $0.5 < n < 0.85$ indicate the existence of both phenomena (anomalous transport).

As a variation of the Korsmeyer-Peppas equation, Kim et al. (1997) proposed a modification to assess the possible burst effect of the formulation (equation 5.4) (414):

*Equation 5.4:*

$$\frac{Mt}{M\infty} = k \cdot t^n + b$$

Where *b* is the parameter corresponding to the burst effect.

The Peppas-Sahlin model considers that release may occur through the processes of passive diffusion and relaxation, each represented by a constant (equation 5.5) (413):

*Equation 5.5:*

$$\frac{Mt}{M\infty} = k1 \cdot t^n + k2 \cdot t^n$$

Where *k1* and *k2* are, respectively, the constants associated to the processes of drug release by passive diffusion and relaxation, and *n* is the diffusion release exponent.

Representative theoretical models, zero order and first order are described by the following equations (equations 5.6 and 5.7) (409):

*Equation 5.6:*

$$\frac{Mt}{M\infty} = kd \cdot t$$

*Equation 5.7:*

$$\frac{Mt}{M\infty} = 1 - e^{kd \cdot t}$$

Where *kd* is the constant of diffusion release that governs the process.

### *5.1.2.12. Cellular biocompatibility*

#### *5.1.2.12.1. Cell culture*

For cell culture, RAW 264.7 cell line was used (ECACC; Salisbury, UK). The cells were maintained in Dulbecco's Modified Eagle's Medium (DMEM) supplemented with 10% foetal bovine serum (FBS), penicillin (100 IU/mL), and streptomycin (100 µg/mL) under a humidified atmosphere of 5% $CO_2$ and a temperature of 37ºC (580,581).

#### *5.1.2.12.2. Proliferation assay and cellular viability*

A suspension of cells at a density of $1 \cdot 10^6$ cells/mL was seeded onto 96-well plate (200 µL/well) in DMEM medium supplemented with 10% FBS, penicillin (100 IU/mL), and streptomycin (100 µg/mL) (581). After incubation

of 2 h, the medium was replaced with the same volume of DMEM medium supplemented with 0.5% FBS and exposed for 1 h to 10 µL of each lipid vesicle formulation at different concentrations. Then, the medium was discarded and 100 µL of MTT solution (0.5 mg/mL) was added. Supernatant was discarded after 1 h and blue deposits of coloured metabolite were dissolved in 100 µL of DMSO. Absorbance at 510 nm was measured using a VICTOR$^3$ Multilabel Plate Reader (PerkinElmer; Waltham, MA, USA) (582). Results are shown as percentage of cell viability in comparison to untreated control cells, or cells treated with blank lipid vesicles in case of observing cellular proliferation (equation 5.8).

*Equation 5.8:*

$$Cell\ viability\ (\%) = \left(\frac{Absorbance\ sample}{Absorbance\ control}\right) \cdot 100$$

Where *absorbance sample* is the absorbance of cells treated with the formulations, and *absorbance control* is the absorbance of non-treated cells or blank-treated cells, at 510 nm.

*5.1.2.13. Statistical analysis*

All data processing was performed using Microsoft Excel 2016® (Redmond, WA, USA) and SPSS version 22.0® (IBM Corp., NY, USA). Data is expressed as the mean ± standard deviation (SD) unless otherwise stated. As a previous requirement for the statistical tests, normality, homoscedasticity, and sphericity were verified if needed. Normal distribution for each data set was assessed by the Shapiro-Wilk test. Homogeneity of variances was confirmed by the Levene's test. Variances of the differences between all combinations of related groups were checked by the Mauchly's sphericity test. Statistical analysis was carried out using the T-test for simple comparisons, one-way ANOVA for tests with two variables, and two-way ANOVA for tests with three variables. All ANOVA tests were followed by the proper post hoc test. Specifically, the Games-Howell nonparametric test was used in case of heterogeneity of variances. When the homoscedasticity requirement was met, Bonferroni or Tukey

tests were used when the number of comparisons were low or high, respectively. The Gabriel test was used if the number of samples were different between the groups. Statistical differences were considered significant if p-values were below 5% ($p < 0.05$).

## 5.2. Results and Discussion

### 5.2.1. Particle size, PDI, zeta potential and phospholipid content

During the lipid vesicle design stage, different factors were considered that could potentially influence their properties, based on previous knowledge about this type of nanocarriers. In this sense, two essential factors are the composition and proportion of components, since they can affect important properties, such as the size, stability or releasing ability of the drug. It is well known that increasing the proportion of cholesterol located in the lipid bilayers, the particle size and the vesicle rigidity also increase (583–585). Considering that one of the main reasons why lipid vesicles improve drug absorption through the skin is their ability to deform and penetrate the cells of the *stratum corneum*, the initial idea was to produce flexible vesicles of the smallest possible size (586,587). For this, a low ratio of cholesterol to phospholipid (molar ratio 1:17) was chosen for conventional liposomes, since it provides small and ultraflexible vesicles with enough stability. Furthermore, 85:15% w/w lipid:surfactant ratio was used since Ahad et al. (2018) demonstrated that it is the most suitable for transdermal delivery using transfersomes based on P90G:Tween 80® (237). Also, different proportions of ethanol have been studied for preparing ethosomes (20-50% w/w). In this case, intermediate concentration (30% w/w) was used because it is the most promising ratio for transdermal absorption purposes, according to the characterisation results (588). The initial results (day 0) of size, PDI, zeta-potential, drug loading and phospholipid content are reported in Tables 5.5-5.7.

**Table 5.5.** Characterisation of the B12 liposomes. All results are expressed as mean **±** SD (n=3).

| | Liposome formulations | | | |
|---|---|---|---|---|
| | **L1** | **L2** | **L3** | **L blank** |
| **Size (nm)** | 286 ± 6 | 278 ± 13 | 275 ± 9 | 307 ± 12 |
| **PDI** | 0.26 ± 0.07 | 0.2 ± 0.01 | 0.21 ± 0.02 | 0.2 ± 0.01 |
| **Z-potential (mV)** | -11.2 ± 0.1 | -10.0 ± 3 | -9.55 ± 0.8 | -10.8 ± 0.7 |
| **P90G (%)** | 80 ± 4 | 84 ± 4 | 77 ± 2 | 79 ± 5 |

**Table 5.6.** Characterisation of the B12 transfersomes. All results are expressed as mean **±** SD (n=3).

| | Transfersome formulations | | | | |
|---|---|---|---|---|---|
| | **T1c** | **T2c** | **T1d** | **T2d** | **T blank** |
| **Size (nm)** | 175 ± 5 | 169 ± 10 | 177 ± 4 | 171 ± 3 | 185 ± 9 |
| **PDI** | 0.2 ± 0.02 | 0.26 ± 0.03 | 0.2 ± 0.02 | 0.2 ± 0.03 | 0.2 ± 0.01 |
| **Z-potential (mV)** | -4.7 ± 0.1 | -5.0 ± 0.2 | -5.5 ± 0.2 | -5.2 ± 0.4 | -4.9 ± 0.1 |
| **PG90 (%)** | 33 ± 3 | 30 ± 1 | 86 ± 8 | 82 ± 5 | 27 ± 4 |

**Table 5.7** Characterisation of the B12 ethosomes. All results are expressed as mean **±** SD (n=3).

| | Ethosome formulations | | | |
|---|---|---|---|---|
| | **E1** | **E2** | **E3** | **E blank** |
| **Size (nm)** | 150 ± 5 | 141 ± 11 | 145 ± 15 | 140 ± 9 |
| **PDI** | 0.2 ± 0.003 | 0.19 ± 0.01 | 0.201 ± 0.03 | 0.18 ± 0.3 |
| **Z-potential (mV)** | -4.63 ± 0.75 | -5.35 1.58 | -5.3 ± 0.4 | -4.2 ± 0.1 |
| **P90G (%)** | 66 ± 2 | 60 ± 5 | 97 ± 2 | 62 ± 4 |

In accordance with other works, size measurements were within the expected range for these types of lipid vesicles. Wu et al. (2019) obtained conventional liposomes in a range of 236-374 nm, depending on the percentage of cholesterol included in the formulation (227). The transfersome and ethosome particle dimension obtained in B12 lipid vesicles were smaller than in the one of conventional liposomes, because the presence of the edge-activating substances in the lipid bilayer of the vesicles causes a reduction in the surface tension (281). Transfersome sizes obtained were similar to the values previously reported by Carreras et al. (2020), and ethosome batches reproduced exactly the size described by Touitou et al. (2000), the original research for this vesicle type (30% w/w ethanol content) (199,281).

Size has a relevant impact on drug permeability through the skin. Lipid nanoparticles with a diameter of 300 nm or below can enhance their content permeability into the deeper skin layers because the smaller the size, the higher the transdermal absorption obtained (349). Based on this criterion, all vesicles formulated in this work should be able to deliver B12 in dermal or epidermal viable layers and, consequently, allow its systemic absorption. Specifically, transfersomes and ethosomes were the most promising candidates due to their size, theoretical flexibility properties and drug deposition performance. Moreover, nanoparticles with a size range of around 210 nm, as the obtained ultraflexible vesicles, also have the option to penetrate the skin through the transfollicular route (589).

PDI values as a measure of the variability in size of the particle populations were always below 0.3, which is the suggested cut-off value to consider homogeneous populations in terms of size for lipid-based carriers for drug delivery applications (349,453).

Zeta-potential values of all formulations were negative, as expected, due to the negative charge of the phospholipids. Liposomes showed the strongest charge, probably due to their bigger size and higher phospholipid amount. It has also been reported that the surface charge decreases when

increasing the level of cholesterol in a phospholipid membrane (590). Consequently, the prototypes presented lower values in comparison with other reports where lipid vesicles contain cholesterol in higher proportion (281). Regarding the transfersomes and ethosomes, they present a size reduction (probably because of an edge-activator) which implies a lower concentration in phospholipids, thus reducing the negative charge. These results are consistent with the ranges described by Ahad et al. (2017) and Touitou et al. (2000), who reported values from -5.91 to -14.0 and 4.6 to -4.3 mV for the same type of transfersomes and ethosomes, respectively (199,236). Nevertheless, none of the prototypes present a value lower than -30 mV, which predicts low long-term stability (420).

### 5.2.2. Entrapment efficiency

The entrapment efficiency percentage and total amount of encapsulated B12 are graphically presented in Figures 5.4 and 5.5.

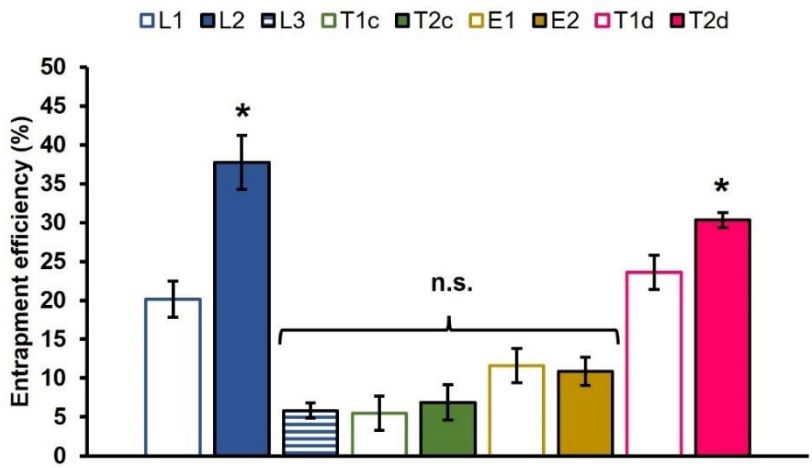


**Figure 5.4.** Entrapment efficiency of conventional liposomes, transfersomes and ethosomes prototypes (expressed as percentage). All results are expressed as mean ± SD (n=3). * means statistically significant differences ($p < 0.05$); n.s. means no statistically significant differences ($p > 0.05$).

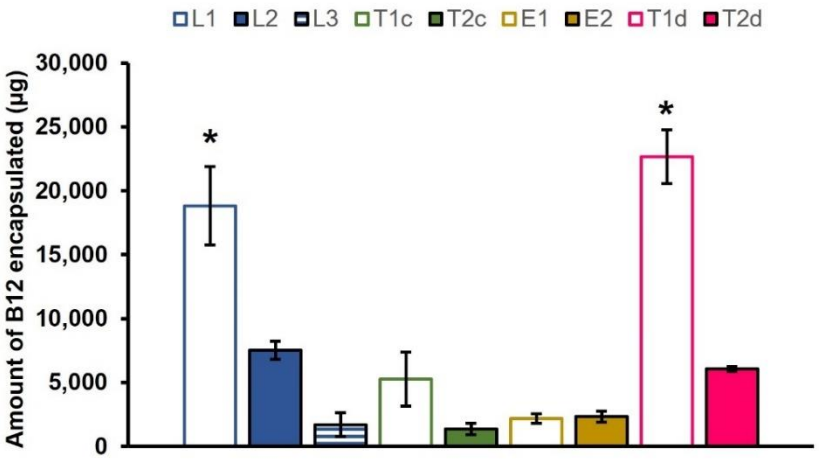


**Figure 5.5.** Total amount of B12 encapsulated in 10 mL of lipid vesicles suspension (expressed as µg). All results are expressed as mean ± SD (n=3). * means statistically significant differences ($p < 0.05$).

Usually, hydrophilic compounds show lower entrapment rates than lipophilic ones. This happens because the entrapment is more efficient if the compound is retained in the phospholipid bilayers, which depends on its primary affinity (571,591). Considering this premise, the obtained entrapment efficiency rates are in the expected range (not up to 40-50%). In addition, the ability of B12 to dissolve in water and methanol could lead to a different location of the drug in vesicle structure, leading to a different entrapment rate (Figure 5.6).

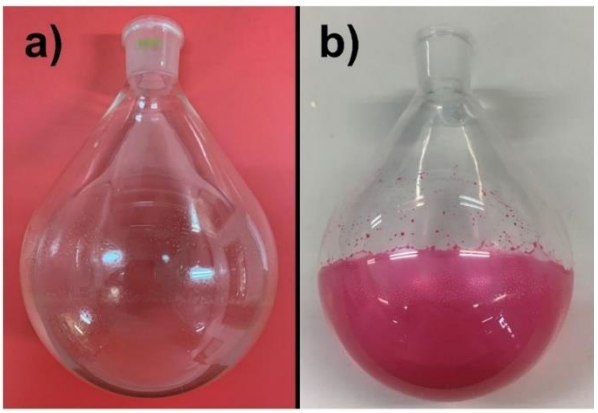


**Figure 5.6.** a) Thin-film when B12 is added after during the reconstitution stage. b) Thin-film when B12 is added with the phosphatidyl choline.

Arsalan et al. (2020) reported a maximum entrapment efficacy of 40% in B12 liposomes when maximising the amount of lipid included during the vesicle formulation (220). This result is clearly superior to L1 data (Figure 5.4). However, the L2 formulation showed the maximum efficiency in the entrapment process compared to the other prototypes, being significantly higher. The comparison between L1 and L2 analyses the effect of including B12 in each phase, and the result was higher when B12 was added to the lipid one. This comparison also suggests that the location of B12 in lipid vesicles might depend on the phase where the drug is added, which was further studied by DSC studies (Chapter 5, 5.1.7. subsection). The possible influence of differences in the initial dose was also checked by preparing L3 formulation. The poor entrapment efficiency in L3 formulation seems to indicate that lipid vesicles were unsuccessfully produced as a consequence of a destabilisation of the vesicle formation with such strategy. Thus, the L3 prototype was discarded for the rest of the experiments. T1d and T2d presented an entrapment value within the expected range. At this point, the differences between both transfersomes and L2 could be attributed either to the differences in size, which allowed the incorporation of a higher amount of B12 in the L2 vesicle core, or to the purification method used to remove the non-entrapped drug. While liposomal formulations were centrifuged, T1d and T2d were dialysed for 24 h (569). This latter reason is also checked through the EE% and PC% results of T1c and T2c. Both values were lower than expected, probably because of the unsuitability of the centrifugation method for transfersomes. In fact, the supernatant obtained after centrifugation of transfersomes was not completely clear, as it was in the conventional liposomes and contained an important amount of lipid vesicles, as demonstrated by a poor phospholipid recovery. The specific encapsulation efficiency parameter was calculated dividing EE% by PC% (Figure 5.7) (592).

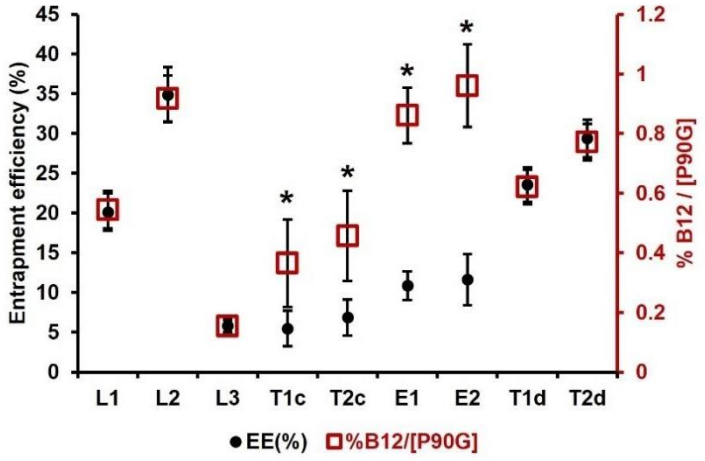


**Figure 5.7.** Specific entrapment efficiency rate of conventional liposomes, transfersomes and ethosomes prototypes. All results are expressed as mean ± SD (n=3). * means statistically significant differences ($p < 0.05$).

Consequently, T1c and T2c prototypes were also discarded for the rest of the experiments. Ethosomes were not dialysed because the dialysis process could extract the ethanol from the vesicles (281). The recovered PC% in ethosomes was around 60% of the initial amount and the EE% was reasonable for a hydrophilic molecule. As the characterisation results of E1 and E2 batches were similar, from this point ethosomal batches were considered similar in terms of characterisation (E1=E2=E3). In the other samples, phosphatidyl choline was not incorporated in a complete manner, presumably due to material loss during the manufacturing and extrusion processes (Tables 5.5-5.7). Therefore, it seems centrifugation was only suitable for liposomal formulations, as the expected amount of phospholipid was recovered after the process. However, it should be considered that the initial objective was to obtain flexible lipid vesicles with the highest possible B12 dose, as saturated systems provide highest skin permeability rates (50). Figure 5.5 represents the final amount of B12 per 10 mL of liposomal suspension. Table 5.8 shows the total amount of B12 incorporated in 1 mL of liposomal suspension. Here, it can be observed that, regardless of the encapsulation efficiency values obtained, the highest B12 load was obtained when B12 was introduced in the aqueous phase in a saturated

PBS solution (L1 and T1d) (Figure 5.5). The higher water volume entrapped by the liposome core contains higher total amounts of B12 compared to the incorporation of the drug in the thin-film layer.

**Table 5.8.** Entrapment efficiency and total amount of B12 encapsulated.

| Formulation | Drug loading (mg per mL) | Entrapment efficiency (%) |
|---|---|---|
| **L1** | 1.90 ± 0.31 | 20.01 ± 2.33 |
| **L2** | 0.75 ± 0.07 | 37.73 ± 3.45 |
| **L3** | 0.17 ± 0.09 | 5.82 ± 0.96 |
| **T1c** | 0.52 ± 0.02 | 5.47 ± 2.21 |
| **T2c** | 0.14 ± 0.04 | 6.85 ± 2.26 |
| **T1d** | 2.20 ± 0.21 | 23.6 ± 2.17 |
| **T2d** | 0.60 ± 0.02 | 30.31 ± 0.95 |
| **E1** | 0.22 ± 0.03 | 11.62 ± 2.21 |
| **E2** | 0.23 ± 0.04 | 16.87 ± 1.78 |
| **E3** | Not applicable | Not applicable |

### 5.2.3. Vesicle morphology: TEM imaging

The vesicle structure and size were assessed by TEM imaging, which has been reported to be a useful method for lipid vesicle visualisation (Figure 5.8). Multilamellar vesicles were observed, since it has been reported that the thin-film method tends to produce heterogeneous vesicles in relation to lamellae number (269). They present spherical-like shapes, although certain irregularity and ovoid-like shapes can be observed due to the drying sample process. Particle size satisfactorily meets the values reported by DLS measurements, however slight variations in size estimations can occur because of the sample preparation mentioned above (dehydration, drying).

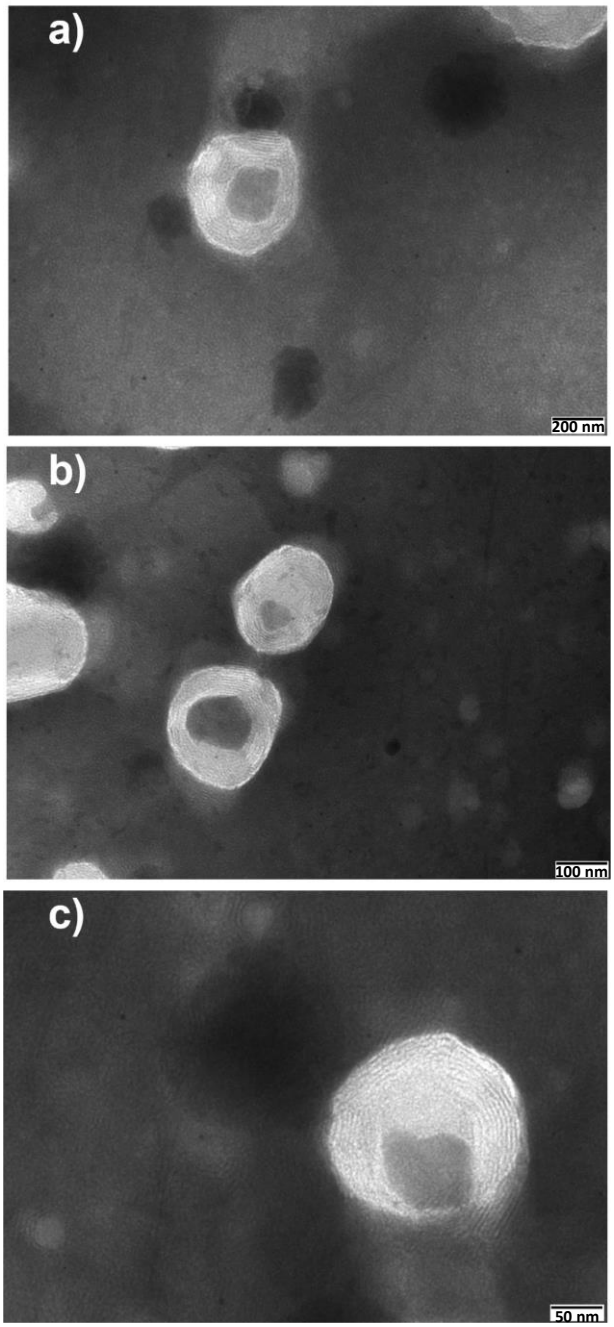


**Figure 5.8.** Representative TEM images of B12 lipid vesicles: a) liposomes; b) transfersomes; c) ethosomes.

## 5.2.4. Evaluation of lipid vesicle flexibility

Following Jain et al. (2003), the vesicle size reduction rate and volume loss after cold extrusion was used as an indirect measurement of the vesicles deformability capacity (399). Results are presented in Figures 5.9 and 5.10. Significant differences were obtained between liposomes and ultraflexible vesicles, as expected (593,594). Liposomes were retained in the 100 nm filters and forced to split into smaller particles to pass the pores. Conversely, transfersomes and ethosomes -whose initial size was higher than 100 nm-, maintained their size during the passage thanks to their flexibility. Similarly, the final volume collected after cold extrusion is inversely related to the vesicle flexibility. As such, no differences were observed in transfersome or ethosome batches, while all liposomal prototypes presented a significant reduction compared to their initial volumes. Thus, both techniques confirm the flexibility of transfersomes and ethosomes.

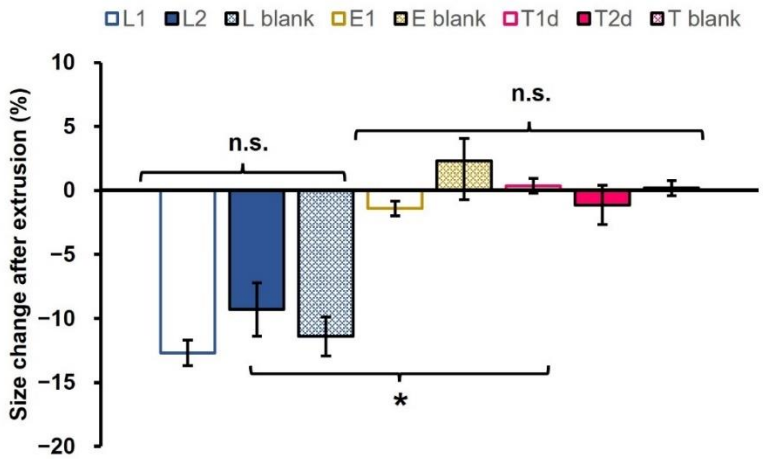


**Figure 5.9.** Size change after extrusion through 100 nm membrane. All results are expressed as mean ± SD (n=3). * means statistically significant differences ($p < 0.05$); n.s. means no statistically significant differences ($p > 0.05$).

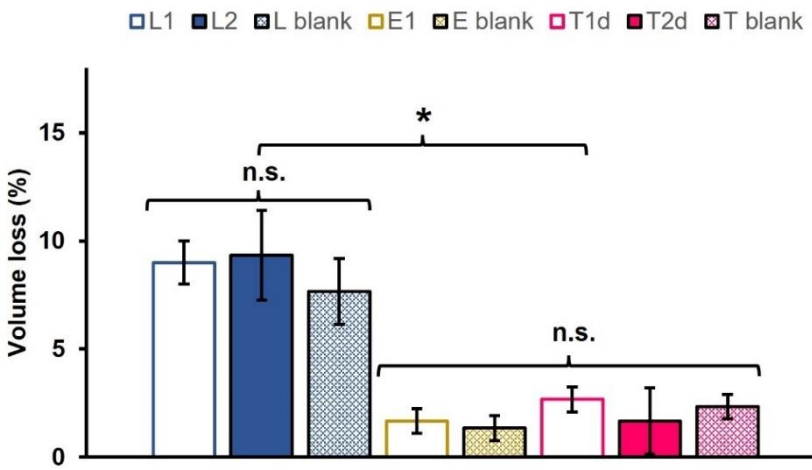


**Figure 5.10.** Volume loss after extrusion through 100 nm membrane. All results are expressed as mean ± SD (n=3). * means statistically significant differences ($p < 0.05$); n.s. means no statistically significant differences ($p > 0.05$).

## 5.2.5. Stability studies

### *5.2.5.1. Short-term stability*

The short-term stability behaviour of the formulations was studied by the TSI, a parameter offered by the Turbiscan® LAB Stability Analyzer device. TSI allows the comparison of samples that present different progression phenomena (595). Transfersomes were found to be the most stable formulation, since no changes in light transmission nor backscattering lines were reported over 24h (Figure 5.11). A flocculation phenomenon was observed for the ethosomal samples through the backscattering graph (Figure 5.12). Its evolution over the whole height of the sample proves a global increase of the particle size). Flocculates could be easily redispersed by gentle shaking. Other aggregative processes, such as coalescence, were discarded, given that no significant long-term size changes were observed after periodically redispersing the samples (Chapter 5, 5.2.5.1. subsection; Figure 5.15). Nevertheless, liposomal vesicles experienced first a sedimentation process, as the backscattering increases at the bottom of the sample, due to an increase of the concentration in the dispersed phase (sediment) and a decrease at the top

of the sample, due to a reduction of the concentration (clarified layer) (Figure 5.13). Also, the smallest particles that remained at the clarified phase showed a tiny flocculation at the end of the investigated times (yellow-red frame). Transmission and backscattering profiles in the work of Cristiano et al. (2019) were similar, and showed comparable phenomena of flocculation for ethosomes and stability for transfersomes (596).

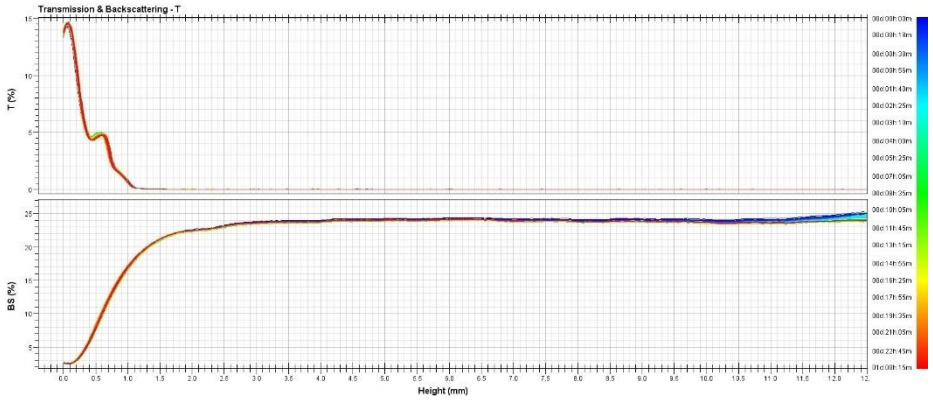


**Figure 5.11.** Ethosomes (E1) short-term stability behaviour.
T: transmittance; BS: backscattering.

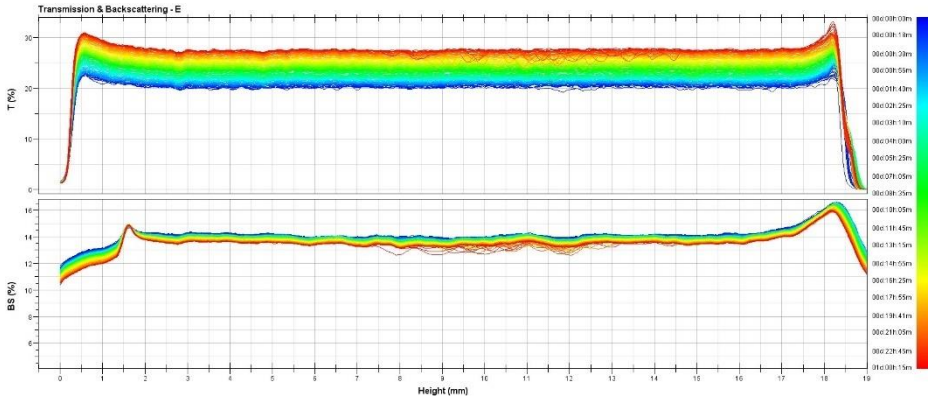


**Figure 5.12.** Transfersomes (T1d) short-term stability behaviour.
T: transmittance; BS: backscattering.

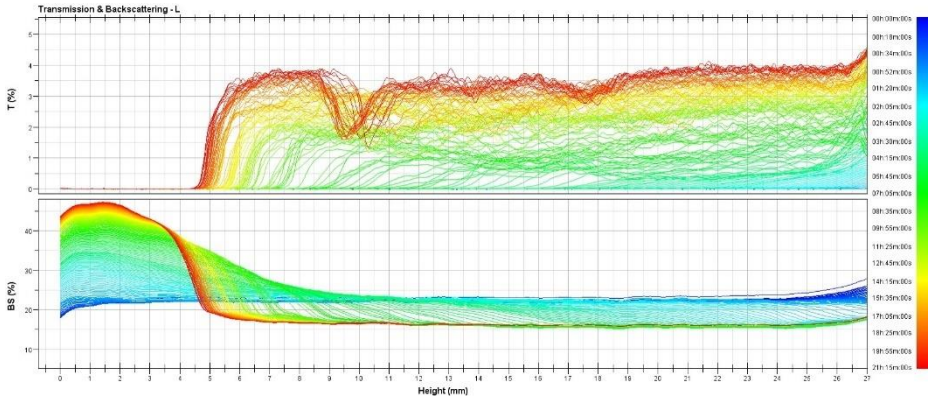


**Figure 5.13.** Conventional liposomes (L1) short-term stability behaviour.
T: transmittance; BS: backscattering.

Therefore, the global destabilisation kinetics (Figure 5.14) confirmed the stability indexes about B12 vesicles (conventional liposome < ethosome < transfersome).

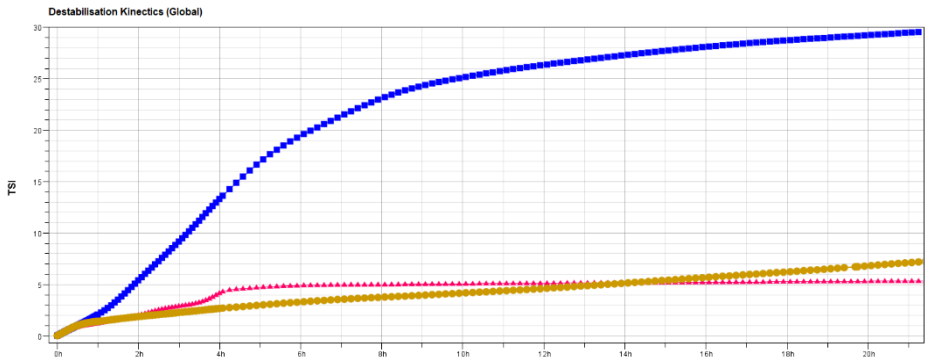


**Figure 5.14.** Global destabilisation kinetics.
L1 TSI (blue); T1d TSI (red); E1 TSI (yellow).

### *5.2.5.1. Long-term stability*

Physical and chemical long-term stability was monitored by measuring the vesicle size, PDI and EE% every week for 2 months and the drug content for 3 months. Figure 5.15 shows no significant differences in size, as a function of storage time at 4ºC, except for the liposome formulations after 4 weeks of storage. This fact has previously been

reported by other authors (426,428). On the other hand, intra-type significant changes in PDI were not observed, pointing out a homogeneous evolution in size of vesicles populations (Figure 5.16).

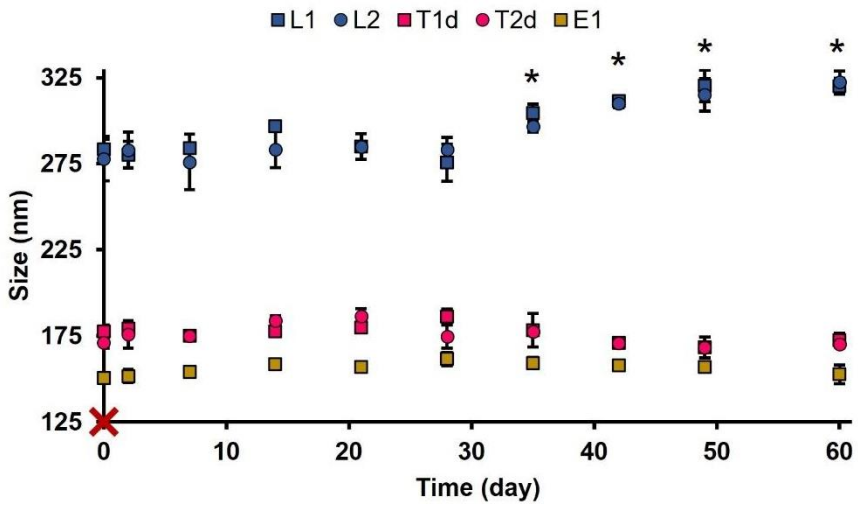


**Figure 5.15.** Vesicle size over 2 months of storage (4ºC). All results are expressed as mean ± SD (n=3). * means statistically significant differences ($p < 0.05$).

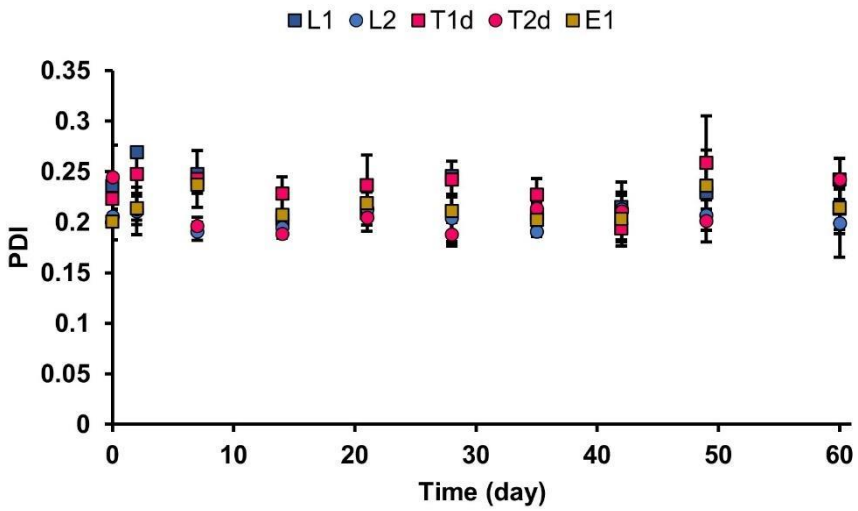


**Figure 5.16.** PDI over 2 months of storage (4ºC). All results are expressed as mean ± SD (n=3).

Significant changes in drug content related to the initial amount were detected in all prototypes between weeks 7 and 8 (Figure 5.17). Recent works have also reported a drug leakage and an effective content loss, especially for liposomes containing hydrophilic drugs, thus supporting our observations (334,428). Considering these findings, B12 lipid vesicles seem to exhibit short and medium-term stability (at least 1 month for all the parameters checked), which makes them suitable for clinical applications. However, to increase the stability for longer-term use, liposome lyophilisation has also been investigated for these B12 lipid vesicles, since it has been shown to be an excellent method for ensuring liposome long-term stability (452,597).

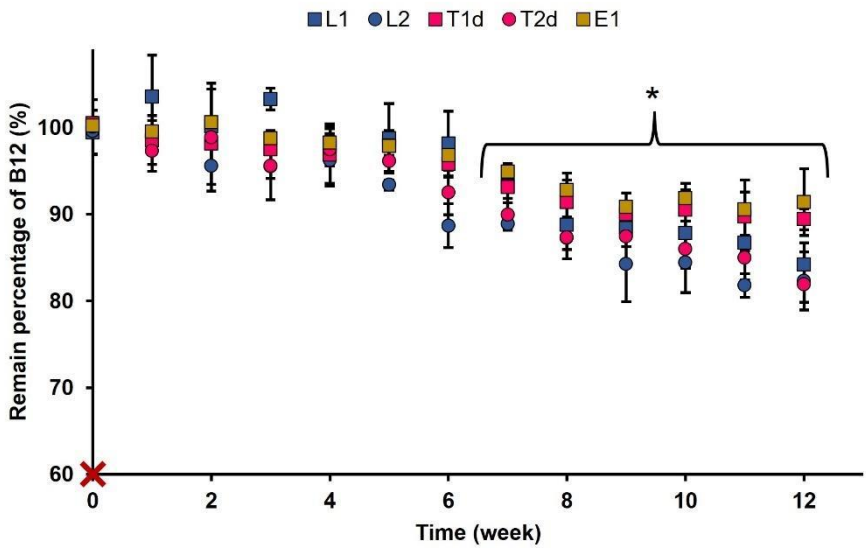


**Figure 5.17.** Remaining percentage of B12 amounts during 2 months of storage (4ºC). All results are expressed as mean ± SD (n=3). * means statistically significant differences ($p < 0.05$).

## 5.2.6. Freeze-drying

Long-term stability is one of the biggest challenges for liposome and modified-lipid vesicle production because lipid-based particles can be easily oxidised (430). When dispersed in an aqueous solution, they remain stable for between 2-3 months (79,427), although size changes could take place

from the first month (426,428). As far as physical instability is concerned, the developed B12-conventional liposomes have shown significant size changes after 1 month at 4°C storage (Figure 5.15) (79). Moreover, a significant and progressive drug leakage occurred from week 7 (Figure 5.17), as is usual for lipid vesicles containing hydrophilic drugs (428). These facts are in accordance with the zeta-potential values obtained, which did not predict long-term stability. Figure 5.18 shows pictures of the lyophilisation result using different cryoprotective agents.

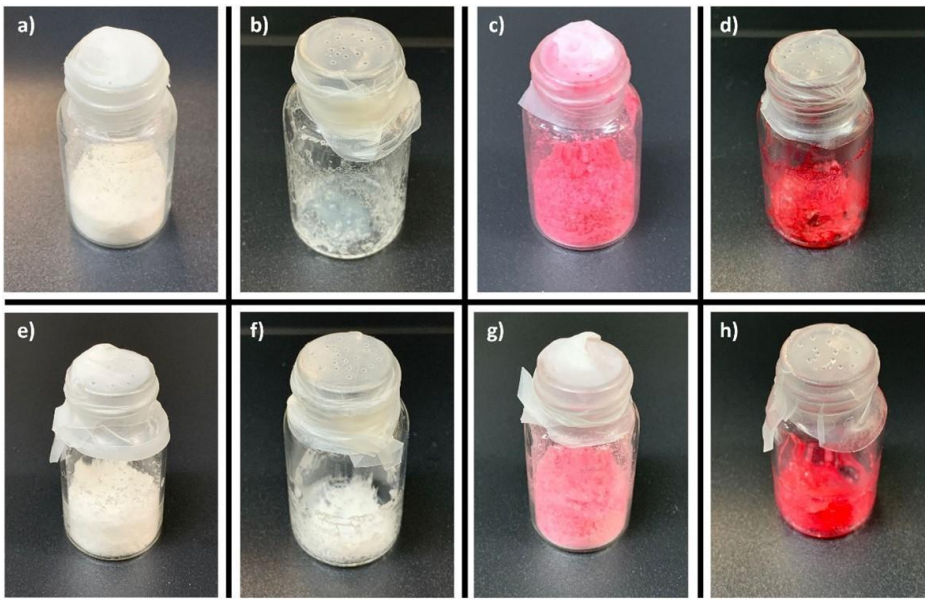


**Figure 5.18.** Representative photographs of freeze-dried B12-lipid vesicles: a) blank liposome-lactose; b) blank liposome-sorbitol; c) B12 liposome-lactose (L1); d) B12 liposome sorbitol (L1); e) blank transfersome-lactose; f) blank transfersome-sorbitol; g) B12 transfersome-lactose (T1d); h) B12 transfersome-sorbitol.

Visual inspection denotes that the use of sorbitol derived into a collapsed cake and a sub-optimal final product (Figures 5.18 b, d, f and h) (452). This collapse process implies only minor or cosmetic irregularities which do not impact patient safety or product efficacy (444,452). This way, sorbitol was considered a non-optimal cryoprotectant. Conversely, lactose achieved a uniform product with no evidence of damage (Figures 5.18 a, c, e and g). The main difference between lactose and sorbitol, regarding

lyophilisation-related properties, is their glass transition temperature of maximum freeze concentrate (*Tg'*), while the collapse temperature (*T*c) is much closer (-32°C and -27°C for lactose and sorbitol, respectively). As reported by Skrabanja et al. (1994), lactose *Tg'* is -28°C and sorbitol presents a *Tg'* of -43°C (598). Collapse may occur when the product temperature exceeds the *Tg'* during the primary drying, which corresponds to the sublimation process forced by the pressure decrease, or the *T*c during the early secondary drying, which refers to the residual water desorption process triggered by the product temperature increase under low pressure (444). This data indicates that the problem with the sorbitol-containing samples was probably that the freeze-drying equipment did not maintain a low enough temperature during the primary drying, since the temperature was settled at -50ºC just below the *Tg'* of sorbitol, and the safety margin was not guaranteed during the whole process.

Lyophilised lipid vesicles were then redispersed in water and their physical stability was assessed by size and PDI measurements. Figures 5.19 and 5.20 show the size and PDI results before and after freeze-drying. As mentioned above, the study only included liposomes and transfersomes, because ethosomal vesicles cannot be freeze-dried without ethanol loss. The results obtained show significant differences between the protected and the unprotected formulations. In terms of size, no significant differences were found when using lactose or sorbitol for transfersomes (Figure 5.19). However, a significant decrease was observed in liposomal formulations (L1 and L2) in comparison to non-freeze-dried liposomes. This event has previously been reported by different studies, where the use of high saccharide concentration leads to a size decrease after lyophilisation (441,453). Several reasons have been suggested to explain this phenomenon, but none have been generally accepted since cryoprotectants can act by different mechanisms. The water replacement theory suggests that cryoprotectants replace the water molecules that surround the particles, thus stabilising the vesicles from water removal (441,454,599). However, kosmotropic effects of stabilising excipients

support that the damage during the freeze-drying process is prevented because of a lower content in water at the membrane interface (454). This idea fits correctly with the reported findings, since the reduced size can be derived from a lower water entry into the liposomes after reconstitution. Lyophilised-lactose transfersomes did not show any differences with the non-freeze-dried formulations, probably due to their smaller initial size. Sorbitol was revealed as an ineffective cryoprotective agent for transfersomes, as size results evidenced a significant size increase after the process. Therefore, in this case, the collapsed cake suggests a loss of the 3D structure of the vesicles during the process.

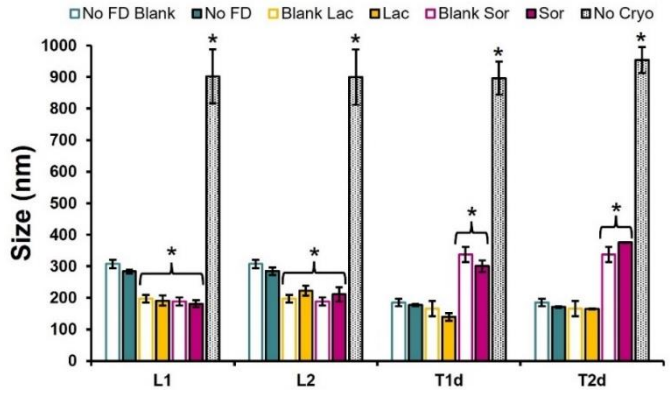


**Figure 5.19.** Vesicle size before and after freeze-drying process. All results are expressed as mean ± SD (n=3). * means statistically significant differences ($p < 0.05$).

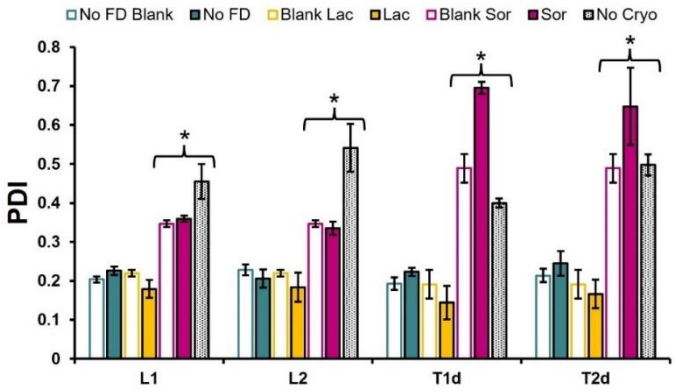


**Figure 5.20.** Vesicle PDI before and after freeze-drying process. All results are expressed as mean ± SD (n=3). * means statistically significant differences ($p < 0.05$).

Non-use of cryoprotective agents led to a typical significant increase in population heterogeneity, as shown by the PDI values (Figure 5.20) (453). The mechanical stress produced by the freezing process was properly softened by using lactose, which was able to maintain a homogeneous size distribution in all vesicles. In this sense, it is possible that the sugar molecules play a stabilising role, considering that they would help to maintain the lateral spacing between the phospholipids, as membrane stabilisers (600). In contrast, PDI values increased remarkably in liposomes and transfersomes. As discussed above, the collapse experienced by sorbitol batches could bring critical consequences to sample integrity and be responsible for this behaviour (444).

### 5.2.7. Thermogravimetric analysis

The quality of freeze-dried powders was assessed by the determination of the residual water content, which must be lower than 3%. Thermal analysis determines the remaining percentage of sample weight as function of the heat transfer (Figures 5.21 and 5.22).

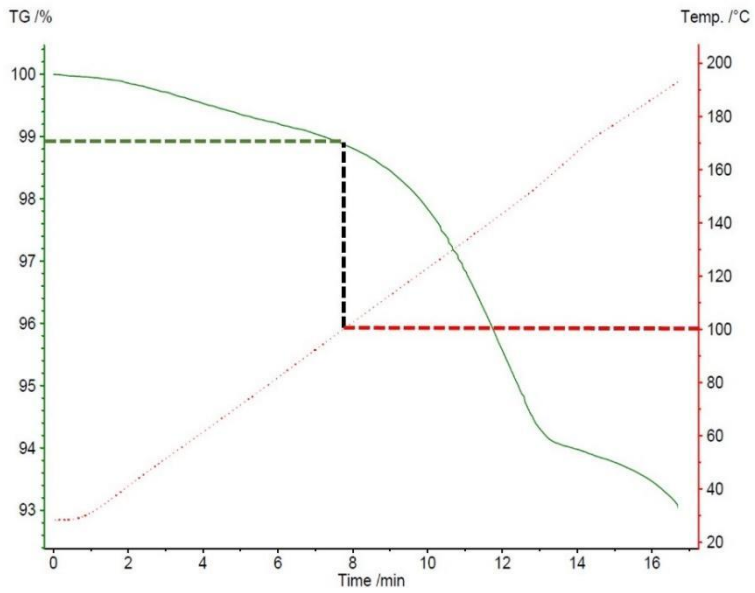


**Figure 5.21.** Thermogravimetric analysis of freeze-dried liposomes (L1).

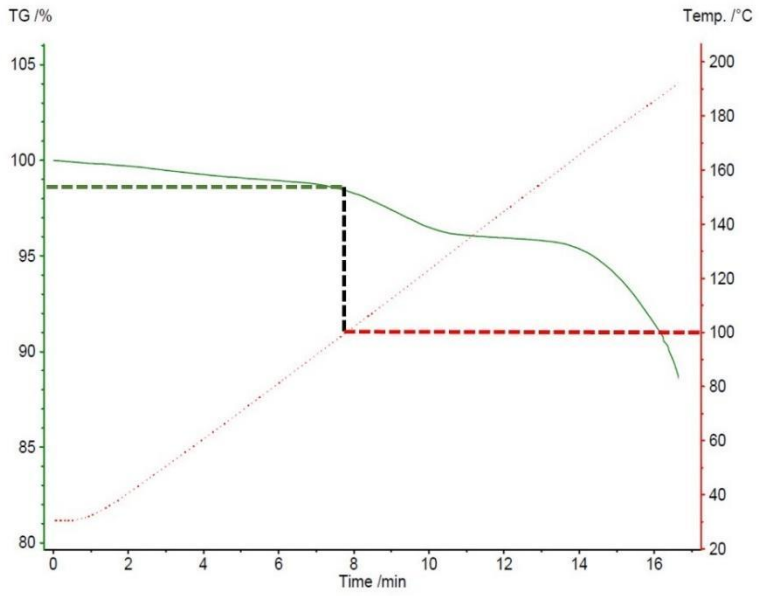


**Figure 5.22.** Thermogravimetric analysis of freeze-dried transfersomes (T1d).

As water evaporates at 100ºC, the weight loss in the first steps corresponds to residual water content, which was around 1% in both cases.

### 5.2.8. Differential scanning calorimetry

As reported before, the physicochemical properties of B12 allow its incorporation into the liposomal system dissolved either in the reconstitution solution or with the lipidic components before the organic solvent removal. This observation, linked to the differences in entrapment efficiency results, suggests a possible different liposomal assembly or structure depending on the cyanocobalamin addition step. In order to elucidate this fact, a DSC study was performed. DSC allows us to determine different thermodynamic parameters like glass transition temperature (*Tg*), degradation temperature (Td), melting temperature (*Tm*) or crystallisation temperature (*Tc*) of a powder sample or solid residue (461). While *Td*, *Tm* and *Tc* are transitions characterised by the absorption or release of latent heat carried out during the isothermal changes of matter (462), glass transition temperature (*Tg*) is defined as the change associated with variations in the molecular mobility

and relaxation time in amorphous solids, and is considered the change in the direction between the rubbery and the glassy states (601), where the latent heat and volume of the system remain constant (461).

Figures 5.23-5.27 show the thermogram of the two types of B12 and lipid vesicles that can be lyophilised and therefore studied in powder form (liposomes and transfersomes). The temperature and acquired signal are plotted in the x and y-axis, respectively. First order transitions (crystallisation, melting and degradation) are observed as well-defined peaks. At high temperatures, the system decreases its viscosity and melts. Further energy produces the degradation of the product (461). The main inconveniences of this technique are, the difficulty when analysing multicomponent preparations, and the overlapping of different signals when high heat rates are used, or weak signals when low heat rates are used (602). In this case, a 20°C/min heat rate was used even though melting and degradation are observed together.

The obtained thermograms showed a very different degradation between liposomes and transfersomes, whereas no significant differences were noticed in the degradation profiles, due to the different phases of incorporation of the drug. While L1 and L2 present two clear signals (Figures 5.24 and 5.25), before and after 160-170°C, T1 and T2 only present the complex peak of degradation after 160-170°C (Figures 5.26 and 5.27). Usually, the different coating or interaction between the components of a formulation leads to different DSC profiles (603). Analysis of the different main lipid vesicles ingredients (data not shown) results in the obtention of a peak at 150ºC for cholesterol, which can be clearly observed in liposome thermograms (Figures 5.24 and 5.25), whereas the phospholipid analysis showed a glass transition temperature of around 55ºC because of its amorphous solid nature. B12 DSC showed a peak at around 250ºC corresponding to its melting temperature (Figure 5.23). Therefore, these profiles suggest a different component assembly between both types of vesicles and as such, different vesicle structure and

properties. Moreover, there is no evidence, which implies that the incorporation of B12 in a determined phase leads to a different drug location into the vesicles and, consequently, the differences observed in the entrapment efficiency are not produced due to the drug location. It has been suggested that amphiphilic molecules that can be solubilised in organic and aqueous phases are partially embedded in the lipid bilayers and the rest in contact with the aqueous core (324). Therefore, the higher entrapment rates shown by L2 and T2 vesicles, could be produced because their encapsulation is facilitated as all the incorporated drug is surrounding and maintaining an intimate touch with the lipids, which does not happen when it is solubilised in the reconstituting solution (L1 and T1 vesicles).

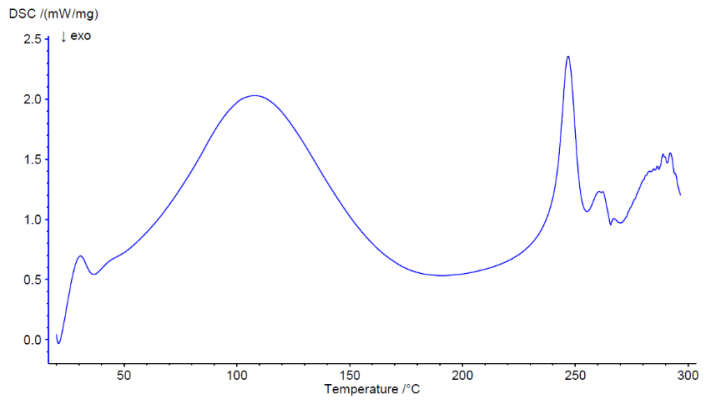


**Figure 5.23.** Thermogram obtained from the analysis of pure B12 powder.

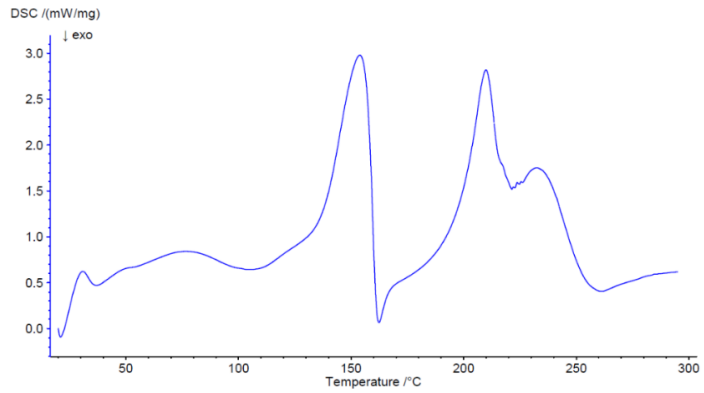


**Figure 5.24.** Thermogram obtained from the analysis of L1.

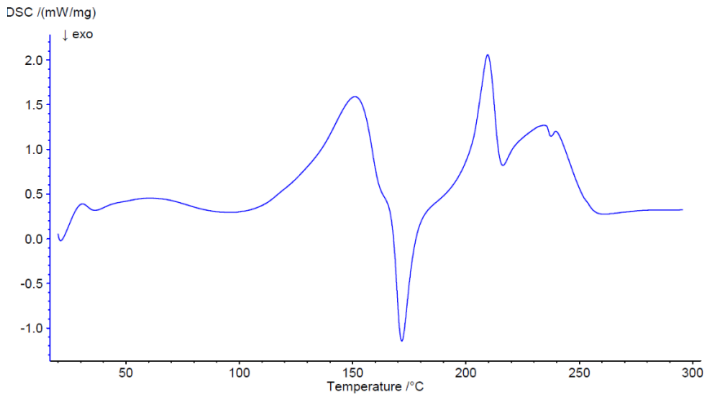


**Figure 5.25.** Thermogram obtained from the analysis of L2.

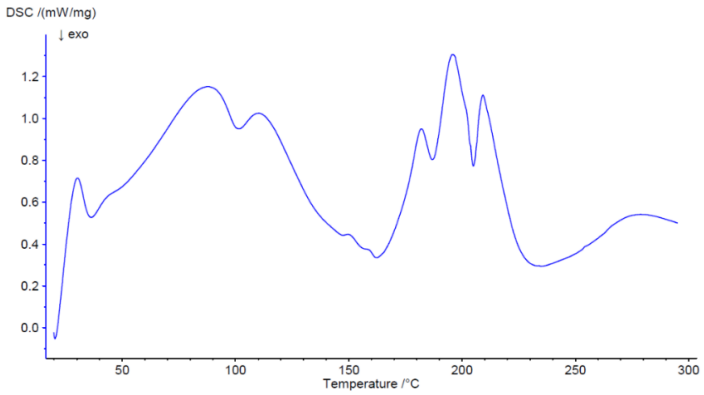


**Figure 5.26.** Thermogram obtained from the analysis of T1d.

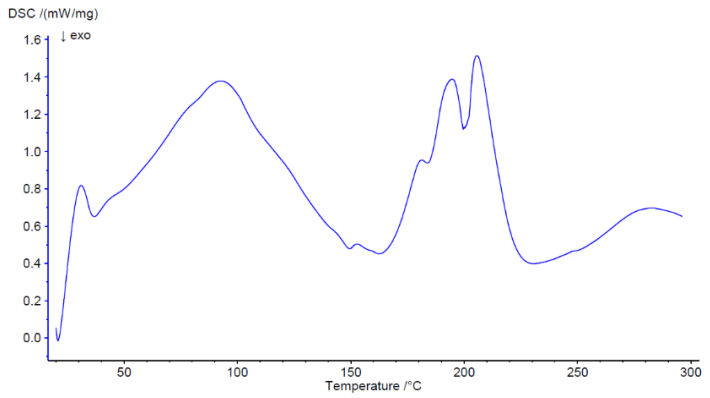


**Figure 5.27.** Thermogram obtained from the analysis of T2d.

## 5.2.9. Drug release study

*In vitro* drug release studies are regularly used in the optimisation process of pharmaceutical forms (604). The cumulative drug release profiles of the formulations were estimated by a dialysis method using the FDC set-up and presented in Figure 5.28 and 5.27 (605).

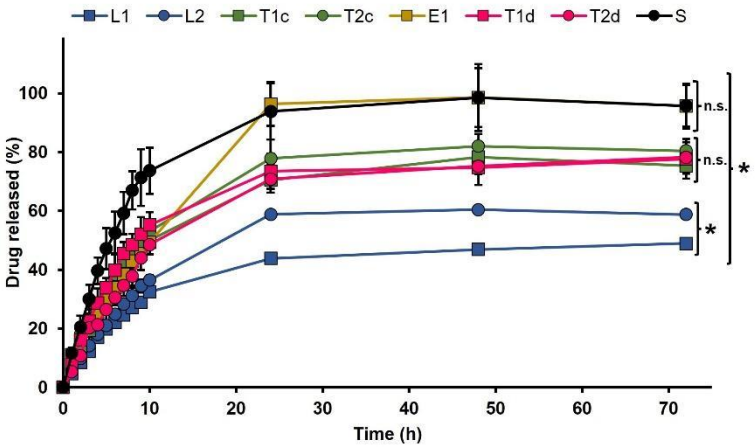


**Figure 5.28.** Release profiles from liposomes (L1 and L2), transfersomes (T1c, T2c, T1d, and T2d), ethosomes (E1), and B12 solution after 72 h. * means statistically significant differences ($p < 0.05$); n.s. means no statistically significant differences ($p > 0.05$).

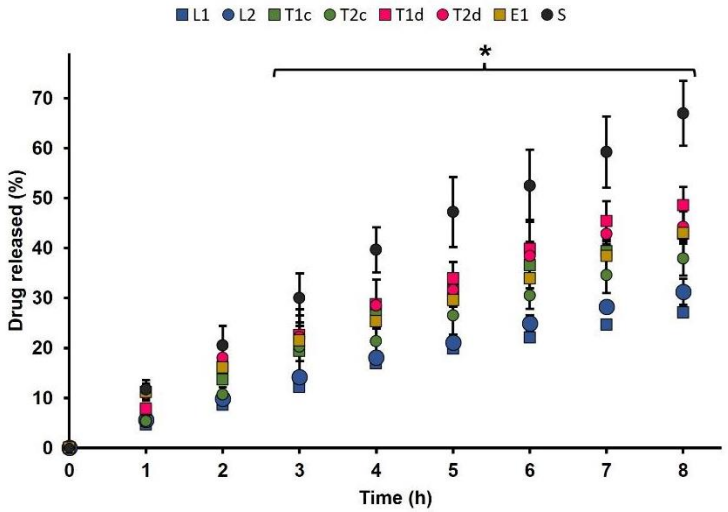


**Figure 5.29.** Release profiles from liposomes (L1 and L2), transfersomes (T1c, T2c, T1d, and T3d), ethosomes (E1), and B12 solution after 8 h. * means statistically significant differences ($p < 0.05$).

The B12 solution (S) was used as a control as it represents the drug diffusion profile without limitations. The rest of the lipid vesicle formulations showed a controlled release of the drug, as shown in Figure 5.29. The B12 release was faster during the initial hours from all the tested formulations due to the concentration gradient established between the donor and the receiver media (606). After 3 h, the amount of B12 detected in the receptor medium is significantly higher for the solution than the liposomes, transfersomes and ethosomes, as expected (607). Moreover, differences between the release from liposomal and ultraflexible vesicles were also observed, with it being lower from the liposomes, probably due to their different rigidity. It has been reported that vesicles with considerable bilayer rigidity exhibit higher resistance to drug transport through the liposomal bilayer (229). It is probably that the long-term percentage of the drug released is also affected by this vesicle property. The lowest percentage of the drug released corresponds to the liposomes and the highest to the ethosomes, which were able to release around 100% of the encapsulated B12. Nevertheless, the final percentages of released B12 between transfersomes and ethosomes were different (Figure 5.28), even though no differences were found in vesicle flexibility during the characterisation stage. Possible reasons for this are: the difference of entrapped drug amounts (higher in transfersomes than in ethosomes) that led to different gradients, and the vesicle structure and components. Similar results were found in B12 release from L1 and L2 formulation profiles at the initial stage (<10 h) even though the amount of B12 entrapped in L1 is higher than L2 formulation. Differences are observed when reaching the plateau. However, the cumulative amounts of B12 found in the last L1 samples (44%, 46% and 48% at 24, 48 and 72 h, respectively) rise, suggesting that the plateau has still not been reached and differences may be reduced if the release is extended.

### 5.2.10. Kinetic model fitting

The experimental release data were fitted to different kinetic models to better understand the release profiles: Higuchi, Korsmeyer-Peppas, Kim, Peppas-Sahlin, zero order and first order. This point is highly recommended since mathematical modelling could help to understand the further *in vivo* performance of the formulations (608). Fitting parameters of all the models using the first 10 h-data and 72 h-data are listed in Tables S1-S12 (Annex II). The AIC was used as a comparative of the goodness of fit (also listed in Tables S13 and S14, Annex II). In general, the Korsmeyer-Peppas model presented the lowest AIC values, indicating an accurate fitting, for almost all formulations. However, in certain cases (T1d 10 h, T2c 72 h, E1 72 h and S), the first order was the best model. The Kim model is a modification of Korsmeyer-Peppas, which considers a possible burst effect. This burst effect (represented by parameter "b") was neglected by the fitting, and the results of both models match. Burst release effect of drugs is frequently related to "dose dumping", an event to avoid in a controlled release system that is demonstrated not to happen in the developed prototypes (609,610).

Contrary to what was expected for ultraflexible vesicles, the Korsmeyer-Peppas model was more suitable for most of the cases, pointing out that they present a mixed release mechanism. It seems that relaxation has a stronger influence during the first steps and gets diluted during longer sampling times, in favour of passive diffusion. This behaviour can be deduced from the values of the release exponent "n" which presents intermediate values (0.5-0.85) when the initial 10 h-data is fitted, and low values (<0.5) when 72 h-data is included. Finally, the $R^2$ values from both models are also listed in Tables S17 and S18 (Annex II). We could observe from their analysis that the models used are suitable for explaining the release process (they account for > 90% of the experimental data variation) (415,416).

## 5.2.11. Cellular biocompatibility

Lipid nanocarriers are well-known as promising candidates to enhance the transdermal delivery of drugs, due to their excellent biocompatibility and ease of mixing with skin lipids (611). In certain cases, they have even shown better biocompatibility than the equivalent drug solutions (491). Biocompatibility of liposomal formulations has been tested previously in the RAW 264.7 cell line (473,474). Cell viability, expressed as percentage, is shown in Figures 5.30-5.32. Percentages above 80% were considered non-toxic and below 80% were considered cytotoxic (478).

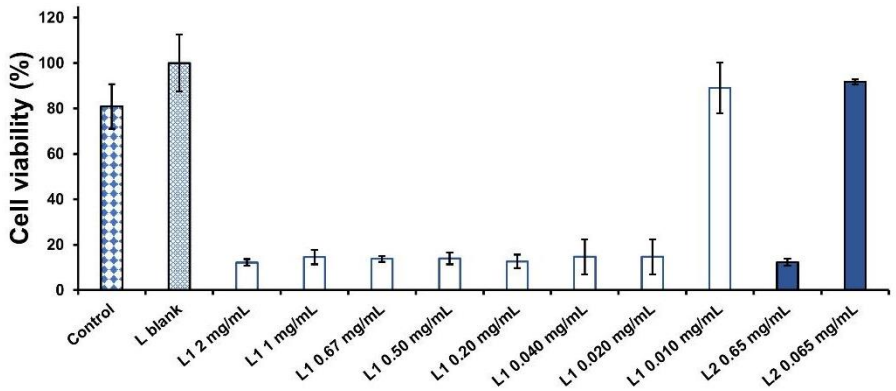


**Figure 5.30.** RAW 267.4 cell viability by MTT test after 24 h of treatment with liposomes (L blank, L1 and L2).

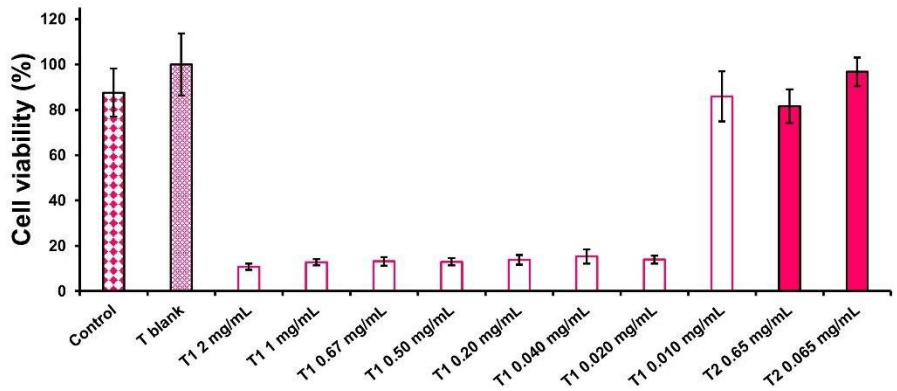


**Figure 5.31.** RAW 267.4 cell viability by MTT test after 24 h of treatment with transfersomes (T blank, T1d and T2d).

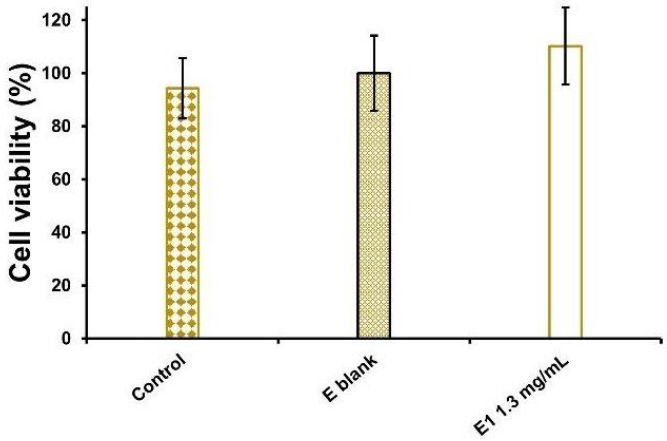


**Figure 5.32.** RAW 267.4 cell viability by MTT test after 24 h of treatment with ethosomes (E blank and E1).

The obtained data demonstrates a direct connection between the cell viability and the B12 dose-lipid carrier association. The non-diluted blank formulations showed a cell proliferative effect, especially notable in liposomes and transfersomes. This effect is one of the main inconveniences of MTT assay for testing lipid vesicles, since certain vesicle components can stimulate cell growth (479). For this reason, cell survival rates were re-calculated according to the proliferation produced by each vesicle type after 24 h. Considering that high-loaded vesicles could lead to cytotoxic effects in cells (612,613), and blank formulations had been revealed to be completely biocompatible, it seems clear that an excessive dose of B12 is mainly responsible for the observed cell death. However, the loss of cell viability could also be affected by the lipid carrier, as they provide a completely different drug release pattern and properties. For example, it should be noted that toxic concentration in liposomes and transfersomes differ from L1 and T1 to L2 and T2 respectively, with the formulations where cyanocobalamin was added in the lipid phase being more biocompatible, and is theoretically more integrated within the lipid bilayers. As Figures 5.30 and 5.31 show, the less biocompatible formulations were the liposomes, while the ethosomes were highly biocompatible. Ethosomes did not show any sign of toxicity with the initial B12 dose (1.3 mg/mL). Mönkkönen et al. (1994) stated that negatively charged vesicles provided an effective drug

delivery to cells, while neutral ones were unable to deliver their content (614). As B12 liposomes showed 2-fold lower zeta-potential values in comparison to ethosomes, they could easily lead to dose-related side-effects for cells. Transfersomes were shown to be intermediately cytotoxic carriers, as T2 vesicles presented higher cell viability than L2 with similar B12 dose. Moreover, Sguizzato et al. (2021) observed that Tween-containing vesicles induced greater cytotoxic effects in comparison to ethosomes, which did not contain any surfactant as edge activator (615), which supports the higher biocompatibility results obtained by the ethosomes here. Finally, it should be kept in mind that skin B12 concentrations will presumably be lower than those assayed in this cell viability assay and therefore, no issues of biocompatibility are expected with B12 lipid vesicle formulations in the clinic.

## 5.3. Milestone and highlights of chapter 5

**Milestone:** Three types of lipid vesicles were designed, produced and characterised: liposomes, transfersomes and ethosomes.

- **Highlight 5.1:** Size and PDI of the developed lipid vesicles were optimal for transdermal delivery purposes, being < 300 nm and < 0.3 respectively. Measurements obtained by DLS and SEM were in accordance.
- **Highlight 5.2:** Transfersome and ethosome flexibility was confirmed by neglectable size reduction and volume loss ratios after cold extrusion.
- **Highlight 5.3:** Entrapment efficiency was in the expected range for a hydrophilic drug. Final drug cargo was inversely proportional to entrapment efficiency, with the less efficient prototypes being those that contained the highest amount of drug.
- **Highlight 5.4:** Zeta-potential values were not predictive of long-term stability (liposomes < transfersomes < ethosomes). However, to preserve them during long-storage periods of time, freeze-drying

was successfully applied to conventional liposomes and transfersomes when lactose was used as a cryoprotective agent.

- **Highlight 5.5:** As a consequence of the short-term stability, it was concluded that centrifugation was an optimal method to purify liposomes, whereas transfersomes were satisfactorily purified by dialysis. Finally, ethosomes were neither centrifuged or dialysed, as they were not sedimented and ethanol could be removed as a consequence of its solubility in aqueous medium.
- **Highlight 5.7:** Drug release studies concluded that within the initial 10 h, relaxation is the main mechanism, whereas diffusion contributes to the release after this release time.
- **Highlight 5.8:** Biocompatibility of lipid vesicles was assessed using the RAW 264.7 cell line. Ethosomes showed a high biocompatibility in comparison to conventional liposomes and transfersomes, as previous reports indicate that cellular uptake of nanoparticles increases with negatively-charged surface properties.

# Chapter 6

## Design, development, and characterisation of cyanocobalamin dissolving microneedles

## 6.1. Materials and methods

### 6.1.1. Materials

The reagents and materials used are listed in table 6.1.

**Table 6.1.** Reagents and materials for the B12 MNA preparation.

| Reagent / Material | Information | Supplier |
|---|---|---|
| **Distilled water** | - | - |
| **Cyanocobalamin** | > 95% purity | Acofarma (Madrid, Spain) |
| **NaCl** | - | Scharlab (Santmenat, Spain) |
| **KCl** | - | Scharlab (Santmenat, Spain) |
| **$KH_2PO_4$** | - | Scharlab (Santmenat, Spain) |
| **$Na_2HPO_4$** | - | Scharlab (Santmenat, Spain) |
| **PVA 9-10, 38-50 kDa** | Poly (vinyl alcohol) | Sigma-Aldrich (St. Louis, MI, USA)) |
| **PVP 40 kDa** | Poly (vinyl pyrrolidone) | Sigma-Aldrich (St. Louis, MI, USA) |
| **PMDS moulds (15x15)** | 600H:200B nm (H: height B: base) | Micropoint Technologies (Singapore) |

### 6.1.2. Methods

#### *6.1.2.1. Preparation of cyanocobalamin dissolving MNA*

Several dissolving MNA were prepared by the solvent casting method using poly (vinyl alcohol) (PVA) and poly (vinyl pyrrolidone) (PVP) as biocompatible polymers. Their quantitative composition is shown in Table 6.2. The MNA preparation process is illustrated in Figure 6.1. Firstly, polymers were dissolved in water to prepare stock blends, which were used to prepare the gels at the desired polymer concentration. The gels were mixed with B12 or lyophilised T1d lipid vesicles until homogeneous. Then, the blends were centrifuged (3500 rpm, 15 min) to remove air bubbles and 0.25 g was poured into the polydimethylsiloxane moulds. Following this, the moulds were placed in a positive pressure chamber (Protima® pressure tank, TÜV Rheinland; Cologne, Germany). To fill the cavity of the moulds with the gels, a pressure of 3-4 bar was applied for 45 min (616). Finally, the microneedles were dried at room temperature for 24-48 h and removed from the moulds.

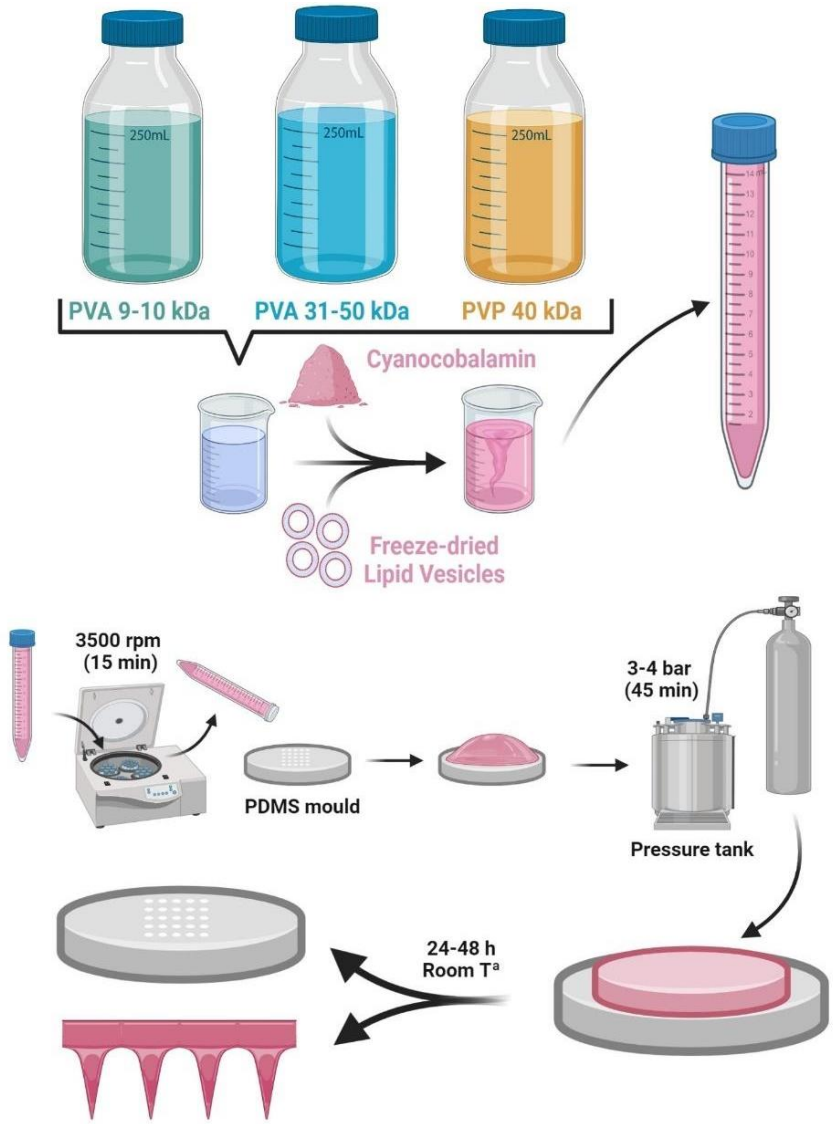


**Figure 6.1.** Manufacturing process of dissolving MNA.

**Table 6.2.** Quantitative composition of the different B12 MNA.

| Dissolving microneedle formulation | Composition (% w/w) | | | | |
|---|---|---|---|---|---|
| | **PVA 9-10 kDa** | **PVA 38-50 kDa** | **PVP 40 kDa** | **B12** | **T1d F-D** |
| **F1** | 15 | - | 5 | 1 | - |
| **F2** | 15 | - | 12.5 | 1 | - |
| **F3** | 15 | - | 20 | 1 | - |
| **F4** | 30 | - | - | 1 | - |
| **F5** | - | 15 | 5 | 1 | - |
| **F6** | - | 15 | 12.5 | 1 | - |
| **F7** | - | 15 | 20 | 1 | - |
| **F8** | - | 30 | - | 1 | - |
| **F9** | - | - | 30 | 1 | - |
| **F10** | 15 | - | 5 | - | 10 |
| **F11** | - | 15 | 5 | - | 10 |

*6.1.2.2. Microneedle morphology: SEM imaging*

The morphology of the microneedles was observed using SEM (EVO LS 15 SEM, Carl Zeiss; Jena, Germany). For this, MNA were coated with a conductive gold layer (Q150 RS sputter coater, Quorum Technologies, Lewes, UK) (617).

*6.1.2.3. Mechanical strength and insertion properties of MNA*

Mechanical strength of MNA was evaluated using a TA-TX plus Texture Analyser (Stable Microsystem; Haslemere, UK). MNA were briefly visualised before testing using a light microscope (Leica ICC50 HD, Leica Microsystems; Wetzlar, Germany) and then carefully placed on the flat plate of the equipment with the needles pointing downwards. The compression mode was applied with a force of 32 N/m for 30 sec to compress the MNA against a stainless-steel surface. Finally, MNA were observed under the light microscope to compare the decrease in size of the needles (Figure 6.2) (618).

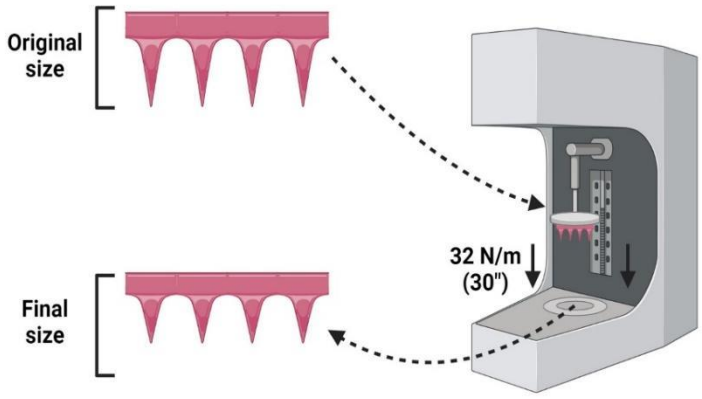


**Figure 6.2.** Standard mechanical test procedure.

The insertion depth of MNA was determined using an artificial skin model. A similar mechanical test set-up was used but MNA were pressed against eight layers of Parafilm M® (Figure 6.2). The holes created in each layer were counted using a light microscope (619).

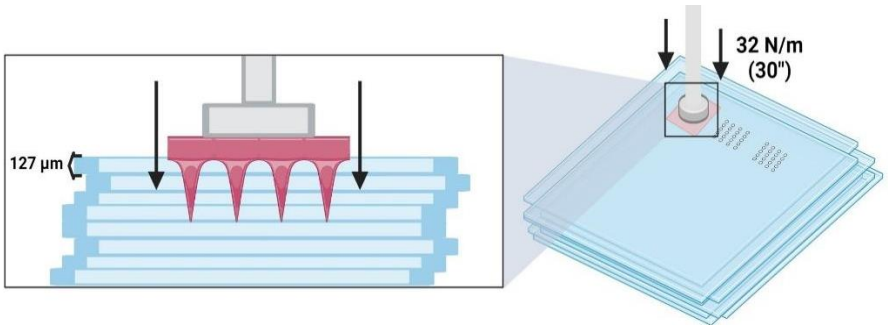


**Figure 6.3.** Parafilm M® artificial skin model to determine microneedle insertion depth.

*6.1.2.4. Thermogravimetric analysis*

TGA was carried out using a TG 209 F3 Tarsus (Netzsch; Waldkraiburg, Germany). Temperature scans were performed from 25 to 200°C at a scan rate of 10°C/mim (575). Netzsch Proteus Thermal Analysis 8.0 software (Netzsch; Waldkraiburg, Germany) was used to create baselines and thermograms.

*6.1.2.5. Differential scanning calorimetry*

DSC was carried out using a DSC 214 Polyma (Netzsch; Waldkraiburg, Germany). Temperature scans were performed from 25 to 225°C at a scan rate of 10°C/min (575). Netzsch Proteus Thermal Analysis 8.0 software (Netzsch; Waldkraiburg, Germany) was used to create baselines and thermograms, and to determine the glass transition temperatures.

*6.1.2.6. Drug release study and kinetic model fitting*

*In vitro* release studies were carried out dissolving the MNA in PBS. For this, they were placed into a 12-well plate filled with 5 mL of PBS with a temperature of 37ºC (n=3). Samples of 200 µL were collected at 5, 10, 15, 20, 30, 40, 50, 60, 90, 120, 180, and 240 min. At every sampling time, the volume was replaced with pre-warmed PBS to guarantee sink conditions (Figure 6.4) (620).

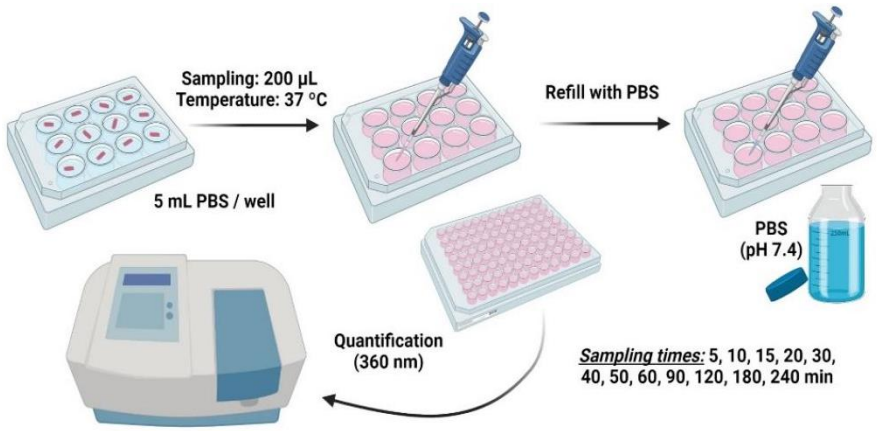


**Figure 6.4.** Scheme of the drug release experiment from dissolving MNA.

The released B12 was quantified by UV-Vis spectroscopy and the cumulative amounts of B12 versus time were calculated. The total drug amount released was calculated according to the previous determination of the drug content and was plotted versus time. The release profiles were fitted to the Korsmeyer-Peppas as it considers the passive diffusion and polymer erosion as possible drug release mechanisms. In this model,

values of release exponent $n < 0.5$ are indicative that the release process is carried out by polymer diffusion/dissolution; values of $0.85 < n < 1$ show that the process is mainly governed by relaxation/swelling and intermediate values $0.5 < n < 0.85$ indicate the existence of both phenomena. The possible burst effect was checked using the modification proposed by Kim. Both kinetic models are described in the equations 5.3 and 5.4 (Chapter 5, *5.1.2.8.* subsection).

*6.1.2.7. Statistical analysis*

All data processing was performed using Microsoft Excel 2016® (Redmond, WA, USA) and SPSS version 22.0® (IBM Corp., NY, USA). Data is expressed as the mean ± standard deviation (SD) unless otherwise stated. As a previous requirement for the statistical tests, normality, homoscedasticity, and sphericity were verified if needed. Normal distribution for each data set was assessed by the Shapiro-Wilk test. Homogeneity of variances was confirmed by the Levene's test. Variances of the differences between all combinations of related groups were checked by the Mauchly's sphericity test. Statistical analysis was carried out using the T-test for simple comparisons, one-way ANOVA for tests with two variables, and two-way ANOVA for tests with three variables. All ANOVA tests were followed by the proper post hoc test. Specifically, the Games-Howell nonparametric test was used in case of heterogeneity of variances. When the homoscedasticity requirement was met, Bonferroni or Tukey tests were used when the number of comparisons were low or high, respectively. Gabriel test was used if the number of samples were different between the groups. Statistical differences were considered significant if p-values were below 5% ($p < 0.05$).

## 6.2. Results and Discussion

### 6.2.1. Preparation of cyanocobalamin dissolving MNA

Aqueous dispersions of different biocompatible polymers were used either alone or in combination to prepare the dissolving MNA prototypes. PVA (9-10 kDa), PVA (38-50 kDa) and PVP (40 kDa) were the selected polymers, as indicated in Table 6.2. In addition, different concentrations of freeze-dried lipid vesicles were also utilised to produce a total of eleven MNA prototypes. Two formulations, F8 and F10, did not produce optimal MNA. The first one contained an excessively viscous polymer blend (30% of high-molecular weight PVA) that did not allow gel pouring into the needle moulds. The second one contained the freeze-dried lipid vesicles into the gel formulation. In this case, the low-molecular weight PVA (15% w/w) was unable to retain the lipid vesicles in the polymeric network after the centrifugation before the casting step to remove the air bubbles. Furthermore, the lipid vesicles migrated to the upper fraction of the polymeric blend as a consequence of the low density of the lyophilised powder. The rest of the formulations produced homogeneous polymer mixtures (Figure 6.5), and the resultant MNA exhibited sharp needle tips upon visual examination under light microscope.

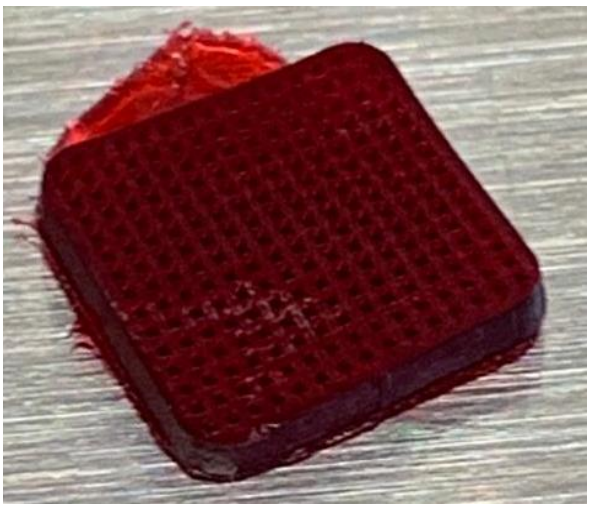

**Figure 6.5.** Image of B12-loaded MNA.

### *6.2.1.1. Thermogravimetric analysis*

MNA exhibited a discrete flexible behaviour after array demoulding. One week later, MNA were completely resistant to deformation and achieved their full strength and insertion properties. This fact was monitored by TGA analysis which showed that MNA lost a lower percentage of weight seven days after production, when compared to the recently demoulded MNA. Different TGA of representative MNA prototypes are presented in Figures 6.6-6.9. The most likely reason for this behaviour is that after 48 h the drying process is incomplete, conferring a certain degree of flexibility as the final polymer chain interactions are not completely established and polymers are more sensitive to heat degradation. Specifically, a temperature of 200ºC produces weight loss of around 7-9% and 12-14%, respectively. As a consequence, the rest of the studies involving MNA were performed after a convenient storage period.

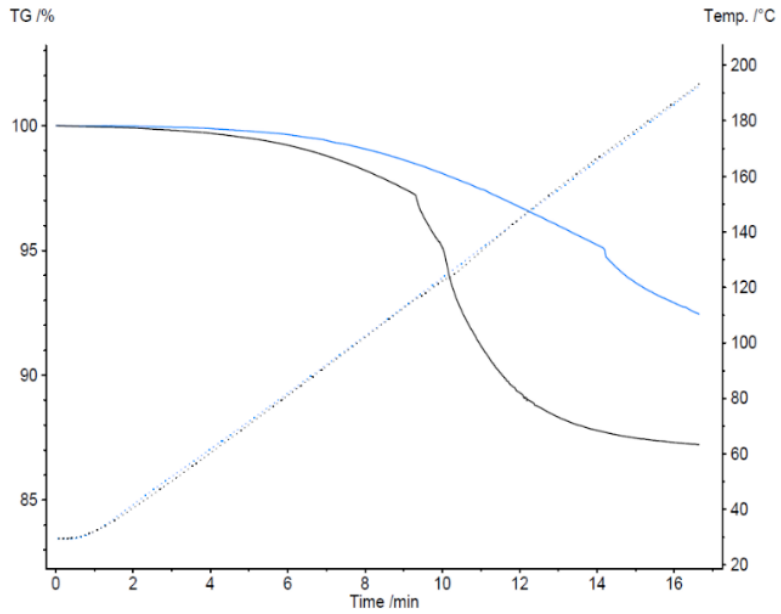


**Figure 6.6.**PVA 9-10 kDa prototype (F3): day 0 (black) and day 7 (blue).

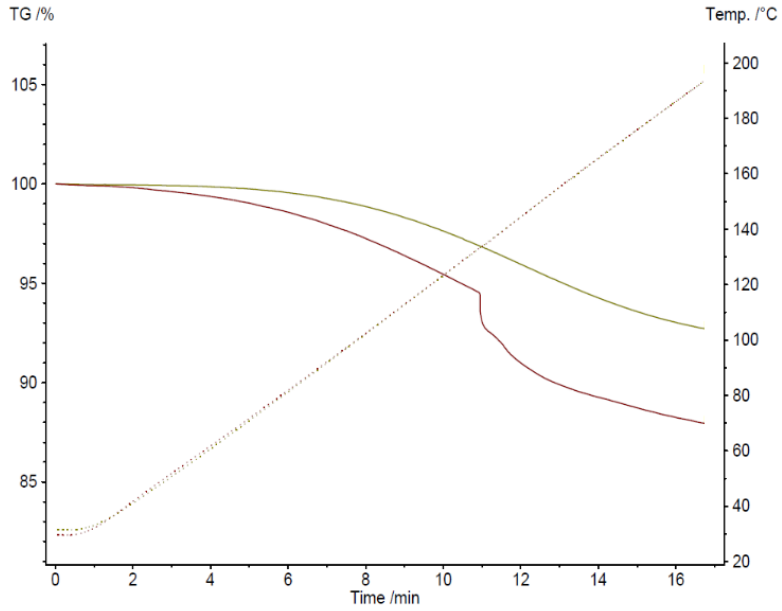


**Figure 6.7.** PVA 38-50 kDa prototype (F7): day 0 (brown) and day 7 (green).

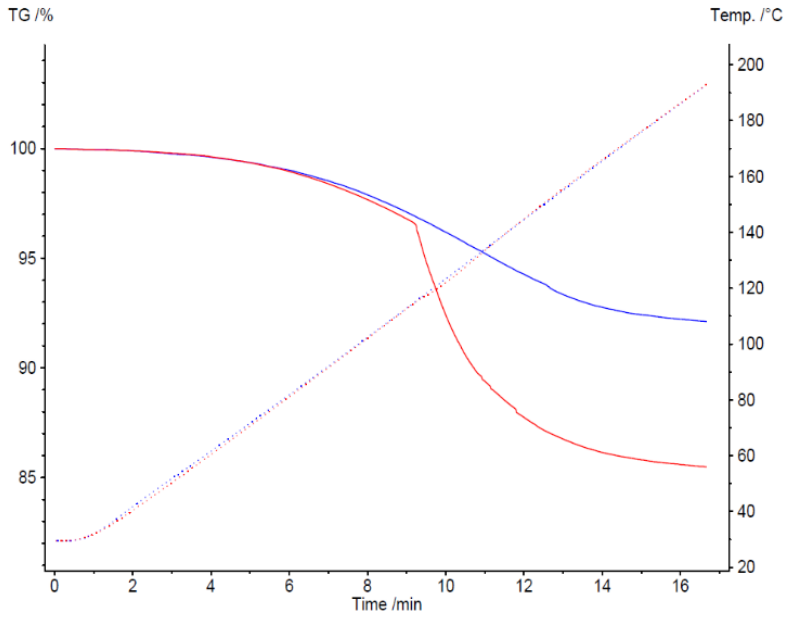


**Figure 6.8.** PVP prototype (F9): day 0 (red) and day 7 (blue).

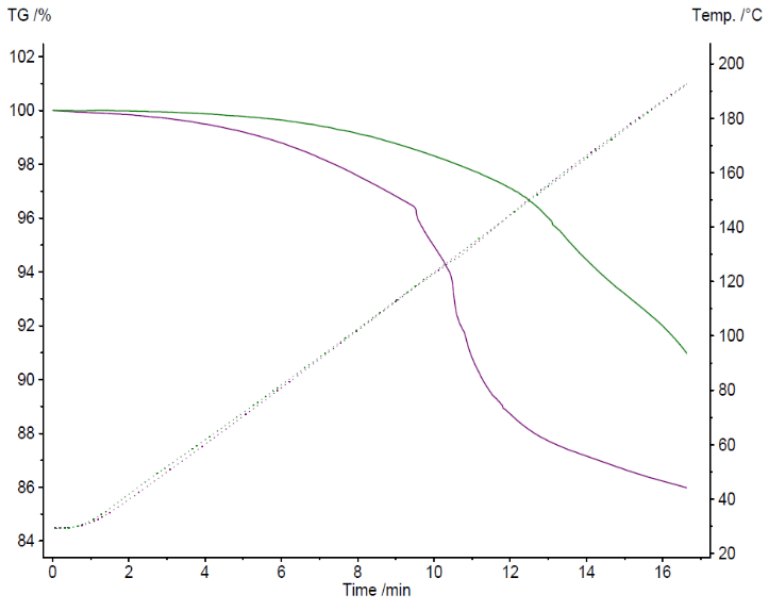


**Figure 6.9.** Lipid vesicle prototype (F11): day 0 (purple) and day 7 (green).

### *6.2.1.2. Differential scanning calorimetry*

MNA were characterised based on their constitutive materials in order to study possible polymer-polymer or polymer-drug interactions and characterise them for further scalability-processes. Depending on the main component, the thermograms showed a particular profile. The PVP-based prototype (F9) showed a considerable signal in the 50-150ºC range (Figure 6.10). This wave was also observed in the PVA 9-10 kDa-based formulations, where a notable depression was found in the baseline after around 200ºC (Figure 6.11). Finally, PVA 38-50 kDa-based formulations completely hid the PVP signal, probably as a consequence of the huge influence that this polymer exhibits in the MNA molecular structure. In addition, a recurrent peak was seen at 210-220ºC which depends on the polymer concentration, as the higher concentration, the higher the peak intensity (Figure 6.12).

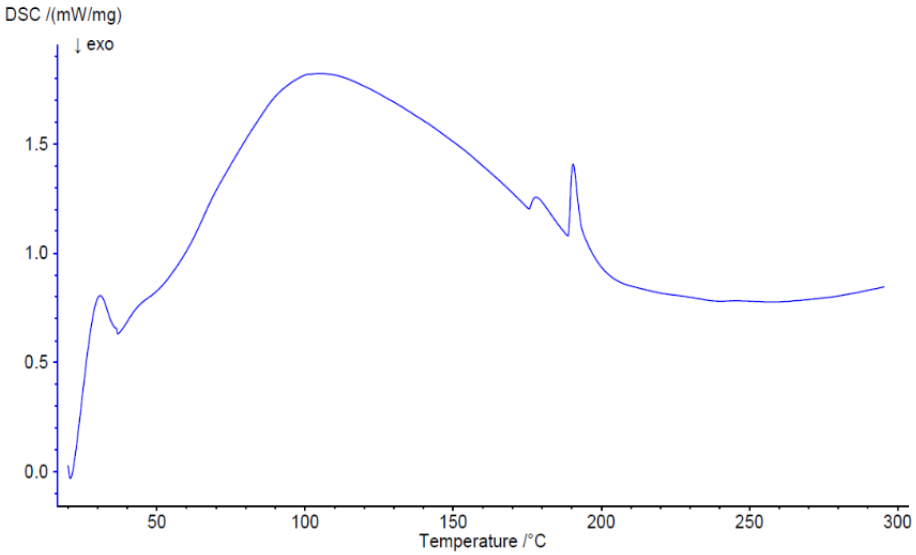


**Figure 6.10.** Thermogram obtained from the analysis PVP-based prototype (F9).

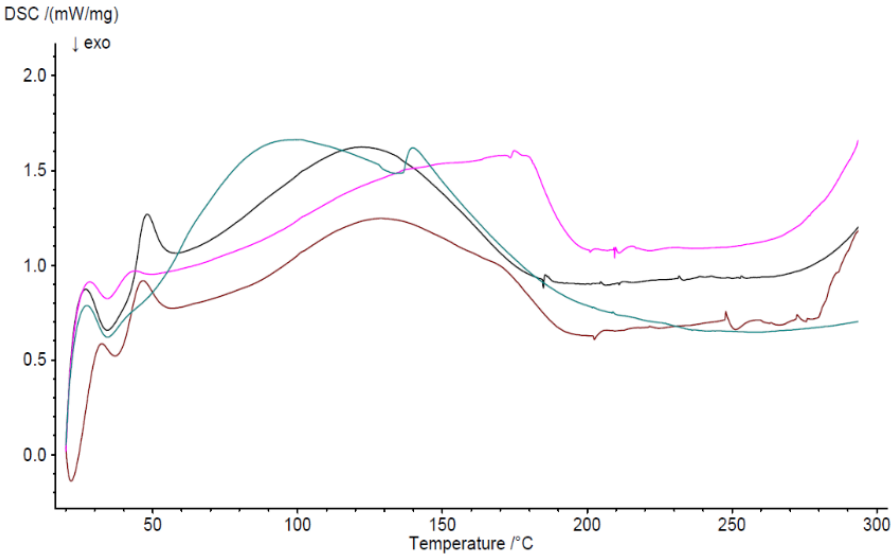


**Figure 6.11.** Thermogram obtained from the analysis PVA 9-10 kDa-based prototypes: F1 (green), F2 (black), F3 (maroon), and F4 (pink).

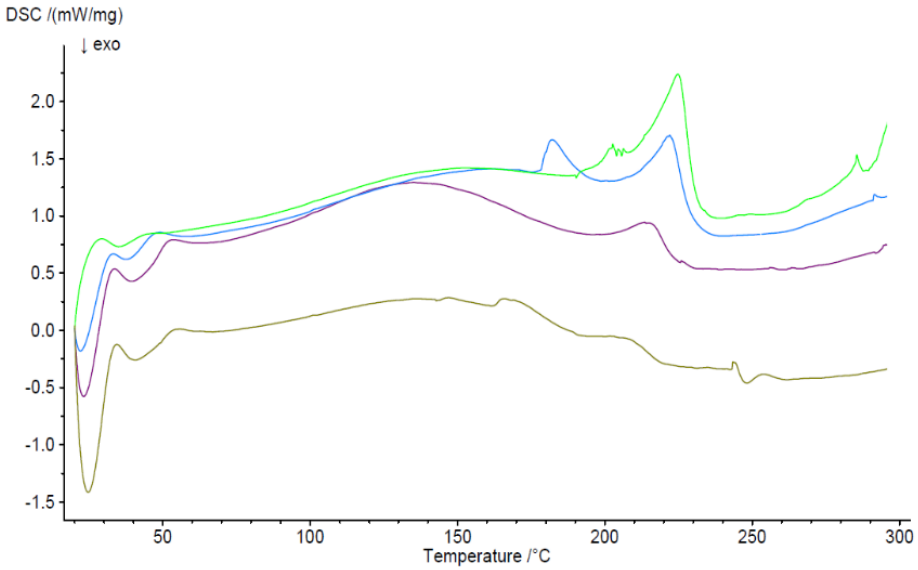


**Figure 6.12.** Thermogram obtained from the analysis PVA 38-50 kDa-based prototypes: F5 (gold), F6 (purple), F7 (blue), and F11 (green).

## 6.2.2. Microneedle morphology: optical microscopy and SEM

Representative SEM images of free drug and freeze-dried lipid vesicle-loaded formulations are presented in Figures 6.13-6.16. Two main differences can be observed between them. First, B12-loaded MNA present a smooth topography, whereas freeze-dried lipid vesicles interact with the MNA surface leading to an irregular relief. Second, the needle height of lipid vesicle-loaded MNA was significantly lower than the other MNA prototypes ($p < 0.05$). F1-F10 needle height ranged between 0.45-0.4 µm, whereas F11 was 0.31 ± 0.02 µm (Chapter 6, 6.2.3 subsection; Figure 6.20). It is probable that the high lipid-vesicle content (10% w/w) produces a different polymer behaviour with a greater trend to contraction in comparison to that produced by the free-drug (1% w/w) in the other MNA. Needle height determinations by optical microscopy were consistent with the SEM measures (Figure 6.17).

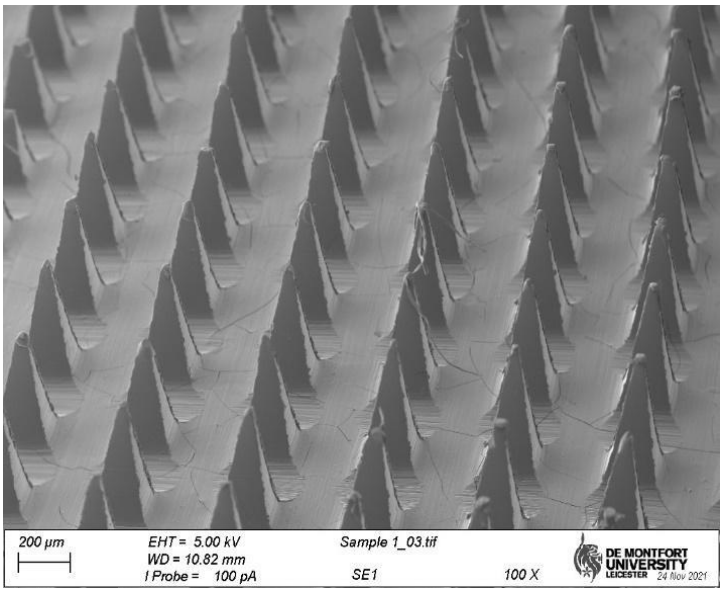


**Figure 6.13.** F7 prototype SEM image (100x magnification).

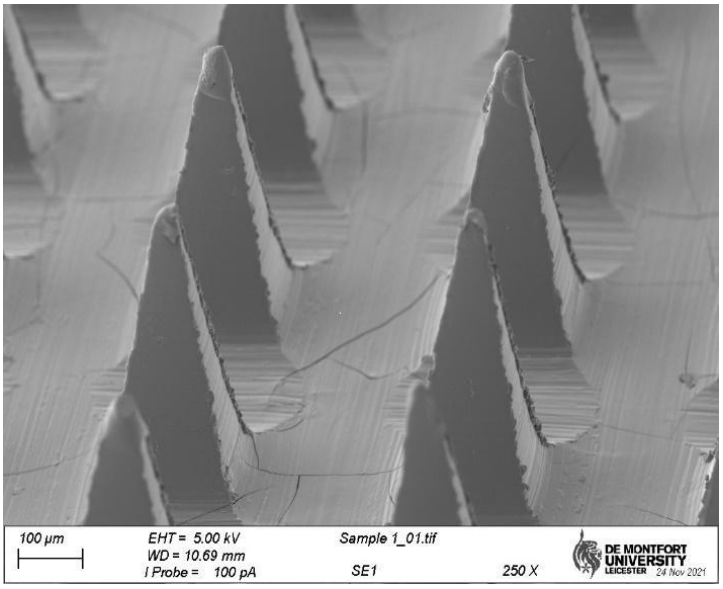


**Figure 6.14.** F7 prototype SEM image (250x magnification).

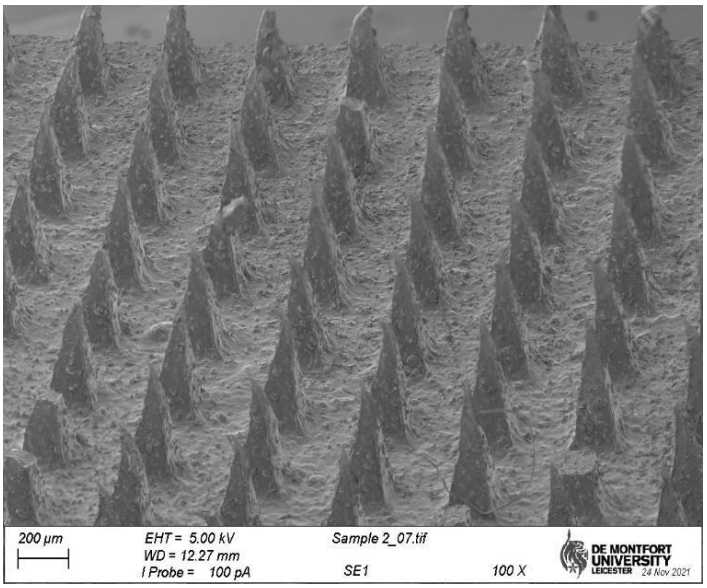


**Figure 6.15.** F11 prototype SEM image (100x magnification).

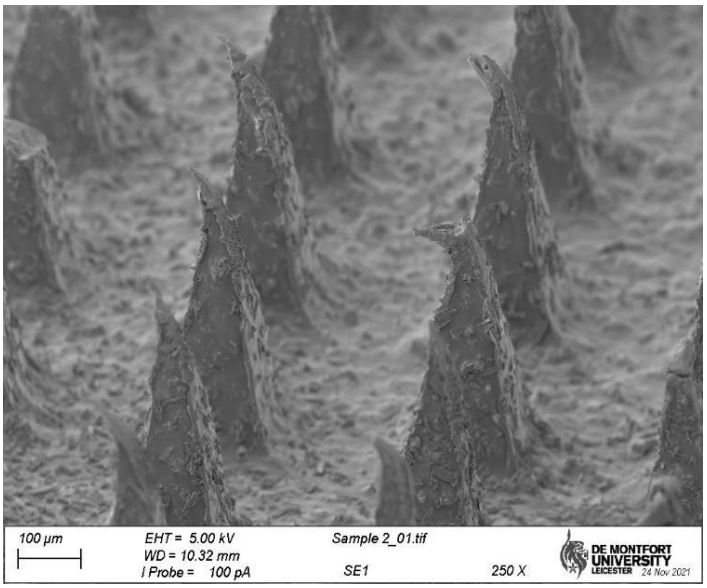


**Figure 6.16.** F11 prototype SEM image (250x magnification).

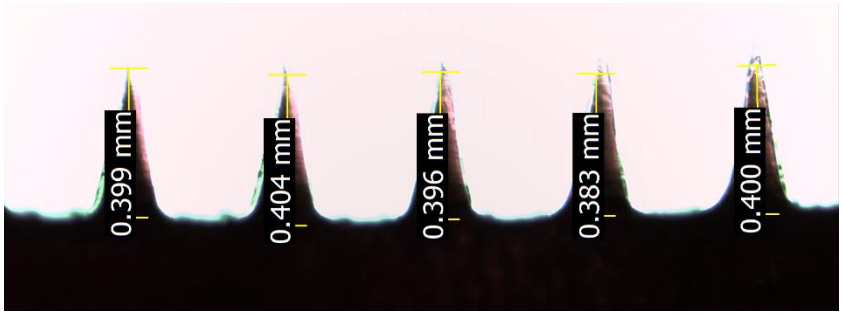


**Figure 6.17.** F3 prototype optical microscopy image.

6.2.3. Mechanical strength and insertion properties of MNA

The ability of MNA to effectively insert into the skin is crucial to its efficacy because they must completely penetrate the *stratum corneum* to deliver their 'cargo'. Mechanical strength evaluation was carried out to determine the capability of MNA arrays to resist the applied compression force when inserted into the skin. The mechanical strength of MNA was determined based on the percentage of height reduction of the needles on the arrays after the application of a force of 32 N/array, similar to manual compression force (619). The results of this experiment are presented in Figures 6.18 and 6.19. The compression of MNA produced a significant needle height reduction in all cases ($p < 0.05$) (Figure 6.18). However, the specific percentage of needle compression strongly depended on polymer combination and concentration (Figure 6.19). MNA prepared using only PVP as a polymer (F9) exhibited in some cases one of the maximum needle height reductions (36%) and needle deformation (Figures 6.20 and 6.21), representing poor mechanical properties, as previously reported (616,621). In the same way, the F4 prototype showed considerable needle height reduction (42%). In contrast, prototypes formulated with a combination of PVA and PVP (F1-F7) exhibited less compressive behaviours. PVA 9-10 kDa-based MNA did not show any difference between the different polymer proportions. On the other hand, PVA 38-

50 kDa-based prototypes were more resistant to compression, especially when the polymer concentration increased (F7). Specifically, the compression percentage of the F7 prototype was significantly lower than the other MNA ($p < 0.05$), except for the polymer combinations (F5 and F6). The observed reduction in mechanical strength in the F11 prototype can be attributed to the presence of freeze-dried nanoparticles.

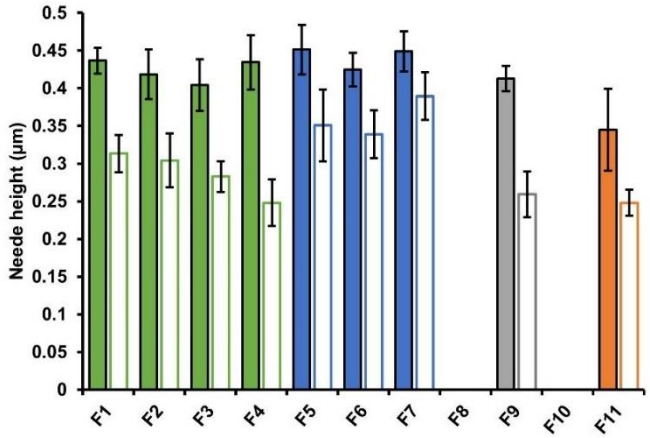


**Figure 6.18.** Needle height before and after compression of each MNA prototype. Height before (colour bars) and after compression (white bars). All results are expressed as mean ± SD (n=10).

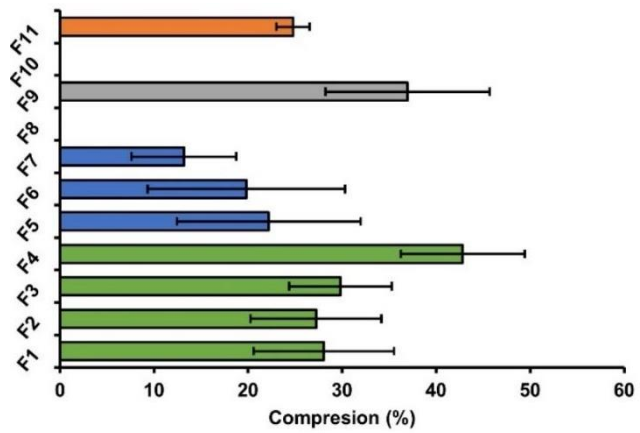


**Figure 6.19.** Height reduction percentage of needles of the different MNA. All results are expressed as mean ± SD (n=10).

This finding agrees with previously reported results where the combination of PVP and PVA increased the mechanical properties of the formulation, attributed to the hydrogen-bond interactions between −OH groups of PVA and C=O groups of PVP (621).

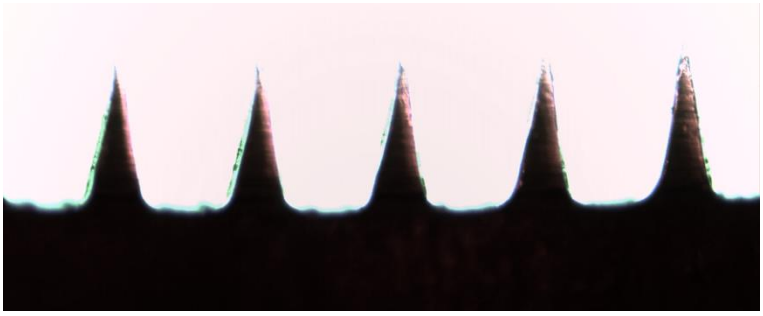

**Figure 6.20.** F9 needles before compression mechanical test.

**Figure 6.21.** F9 deformed-needles after compression mechanical test.

Parafilm® M was used as a validated artificial skin surrogate for MNA insertion studies, as previously described (619). The results of the insertion studies were in solid agreement with the mechanical strength studies. The insertion capabilities of the MNA prepared using each of nine different formulations is illustrated in Figure 6.22. The results showed that F1-F9 inserted into the third layer of Parafilm® M (Figure 6.23). The mean thickness of a Parafilm® M layer is 126 ± 7 μm, indicating that MNA were inserted up to 378 μm of the total height, approximately 83-94% of the needle height, depending on the initial needle height of each MNA. Among them, F7 reached the third layer in

a higher proportion than other prototypes ($p < 0.05$). These values were similar to previous studies focused on the insertion of other polymeric MNA into human skin (622). In contrast, the F11 prototype only penetrated the second layer of Parafilm® M, as its needles were shorter than 378 µm.

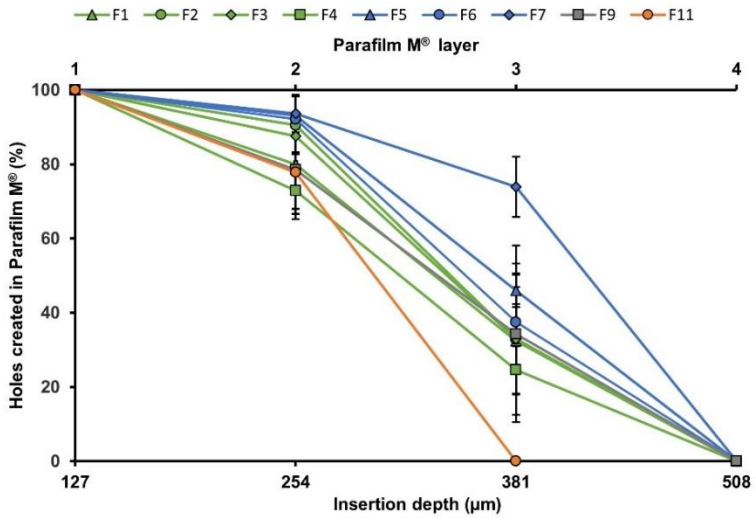


**Figure 6.22.** Percentage of holes created and insertion depth of dissolvable B12-loaded MNA in an artificial Parafilm M® skin model using a force of 32 N/array. All results are expressed as mean ± SD (n=3).

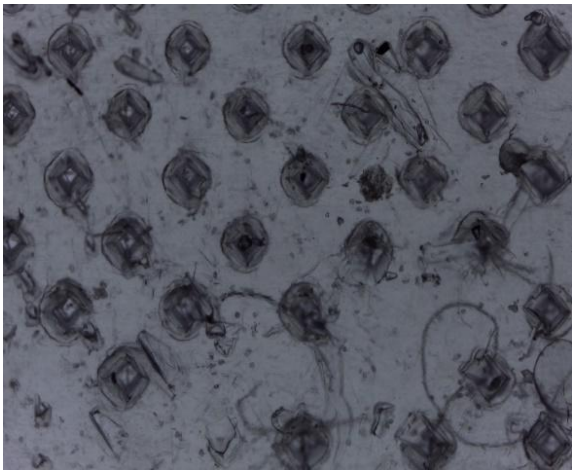

**Figure 6.23.** Holes created in a Parafilm M® layer after F5 MNA insertion visualised by optical microscopy.

## 6.2.4. Drug release study and kinetic model fitting

The use of different polymers to produce MNA leads to different mechanical and chemical properties that influence the drug release process. The different solubility properties and characteristics of the used polymers influenced the release mechanism. Although the release of active ingredients from dissolving MNA is mainly governed by the dissolution of the MNA matrix, other mechanisms are possible, for example, when polymers are insoluble in biological fluids or MNA are coupled with controlled release systems. Different methodologies have been proposed for the *in vitro* assessment of drug release. FDC set-up and the direct dissolution in a sealed beaker method are capable of discriminating release patterns. In this case, the release profiles between the developed formulations are presented in Figure 6.24.

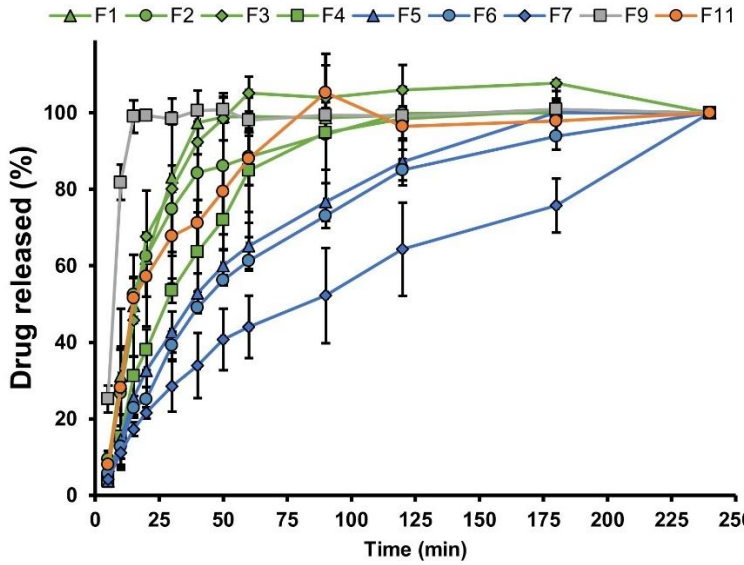


**Figure 6.24.** Release profiles from B12-MNA: PVP-based prototypes (grey), PVA 9-10 kDa-based prototypes (green), PVA 38-50 kDa prototypes (blue), freeze-dried lipid vesicles-loaded prototype (orange).

In general, the results met the findings obtained in the mechanical tests, as the PVP-based formulation showed a faster drug release than PVA/PVP-based combinations. The PVA 9-10 kDa-based prototype

exhibited a slower release in comparison to the two-polymer combination. The most probable reason for this could be that PVA is less soluble in water than PVP. PVA concentration in F4 formulation is 30% w/w while F1-F3 prototypes contain only 15% w/w of PVA, with a variable proportion of PVP. Nevertheless, the effect of polymer combination was not neglectable in PVA 38-50 kDa/PVP-based formulations. They showed the highest controlled release, probably as a consequence of the high molecular weight of the PVA. However, the increase of PVP proportion up to 20% w/w strengthened the MNA matrix and therefore the controlled release. On the contrary, the addition of the freeze-dried lipid vesicles into the MNA led to soft polymeric structures that delivered their cargo more easily (F11 prototype). In addition, as lipid vesicles present a drug loading limitation in comparison to the free-drug, the B12 dose in F11 was lower and total drug release was achieved.

At the end of the release studies, the PVA 38-50 kDa-based prototypes were the only ones that preserved the polymeric matrix (Figure 6.25), denoting a polymer relaxation/swelling alternative release mechanism to diffusion/dissolution. To confirm this, release data was adjusted to the Korsmeyer-Peppas model, which considers both mechanisms, and the F5-F7 prototypes showed intermediate values of the release exponent “n” (0.5-0.85), as expected (Tables S17 and S18, Annex II).

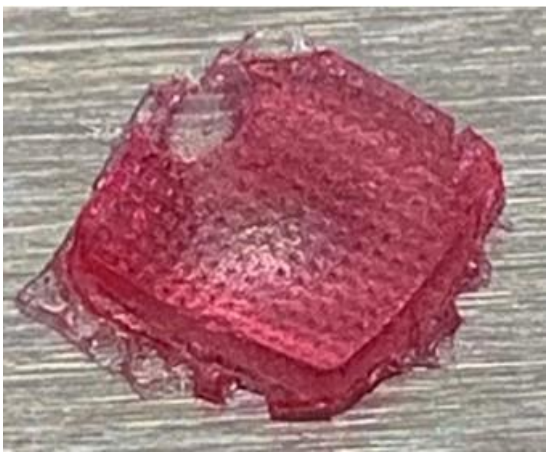

**Figure 6.25.** PVA 38-50 kDa swelled polymeric matrix after release study.

## 6.3. Milestone and highlights of chapter 6

**Milestone:** Eleven MNA loaded with freeze-dried B12-loaded lipid vesicles and free B12 were designed. PVA (9-10 and 38-50 kDa) and PVP were the polymers used in different concentrations to produce the MNA prototypes. Nine of them were successfully produced and characterised.

- **Highlight 6.1:** Lipid vesicle-loaded MNA exhibited shorter needle height as result of increased polymer contraction due to the high proportion of freeze-dried lipid vesicles in the system.
- **Highlight 6.2:** Mechanical strength was evaluated by MNA resistance to compression. The stronger resistance was shown by formulations with high polymer concentration, and PVP-PVA combination.
- **Highlight 6.3:** MNA insertion properties in an artificial skin model were correlated with their mechanical properties, reaching > 276 µm depth in all cases. Moreover, high weight polymers contributed to insertion.
- **Highlight 6.4:** Drug release was strongly dependent on the main polymeric components of the formulation. MNA manufactured with low molecular weight polymers (PVA 9-10 kDa and PVP 40 kDa) completely dissolved in the *in vitro* release test, whereas PVA 38-50 kDa-based MNA maintained the polymeric matrix after the study. In consequence, the processes that govern the release processes are diffusion/dissolution and swelling/relaxation of the polymeric matrix, respectively.

# Chapter 7

## *Ex vivo* and *in vitro* evaluation of cyanocobalamin penetration and permeability from lipid vesicles and dissolving microneedles

---

Chapter adapted from **Cyanocobalamin Ultraflexible Lipid Vesicles: Characterization and In Vitro Evaluation of Drug-Skin Depth Profiles,** Guillot AJ, Jornet-Mollá E, Landsberg N, Milián-Guimerá C, Montesinos MC, Garrigues TM, et al. *Pharmaceutics, 2021;* and **Exploration of Microneedle-assisted Skin Delivery of Cyanocobalamin formulated in Ultraflexible Lipid Vesicles.** Guillot AJ, Merino P, Bocchino A, O'Mahony C, Giner RM, Recio MC, et al. *European Journal of Pharmaceutics and Biopharmaceutics, 2022.*

## 7.1. Materials and methods

### 7.1.1. Materials

The reagents and materials used are listed in table 7.1.

**Table 7.1.** Reagents and materials for the *ex vivo* and *in vitro* studies.

| Reagent / Material | Information | Supplier |
|---|---|---|
| **Mili-Q Water** | Resistance > 18MΩ<br>TOC < 10 ppb | Millipore<br>(Madrid, Spain) |
| **Methanol** | HPLC-grade | VWR (Radnor, PA, USA) |
| **Aluminium mask** | - | 3M (Madrid, Spain) |
| **Adhesive tape** | Tesafilm kristall-klar | Tesa (Hamburg, Germany) |
| **Parafilm M®** | - | Bemis (Neenah, WI, USA) |
| **Glass beads** | Borosilicate beads<br>Diameter: 1 mm | Sigma-Aldrich<br>(St. Louis, MI, USA) |
| **NaCl** | - | Scharlab (Santmenat, Spain) |
| **KCl** | - | Scharlab (Santmenat, Spain) |
| **$KH_2PO_4$** | - | Scharlab (Santmenat, Spain) |
| **$Na_2HPO_4$** | - | Scharlab (Santmenat, Spain) |
| **Methylene Blue dye** | Powder<br>$M_w$: 319.85 g/mol | Sigma-Aldrich<br>(St. Louis, MI, USA) |
| **Solid MNA** | Needle height:<br>500 µm | Tyndall UCC<br>(Cork, Ireland) |

### 7.1.2. Methods

*Ex vivo* and *in vitro* studies were approved by the Ethical Committee of the University of Valencia, under protocol number H1540295606992 (Annex III).

#### *7.1.2.1. Drug distribution within skin layers and stratum corneum depth*

Drug penetration through the skin provided by lipid vesicles was evaluated by the tape-stripping technique. The assay was performed using porcine skin samples. Skin was removed from the connective tissues and placed onto a glass slide, with the outside layer facing upwards. An aluminium mask was placed over it, leaving the application area uncovered. 100 µL of each formulation containing lipid vesicles was applied to the delimited application area of skin. The system was then incubated at 32ºC

for 2, 4 and 6 h. Each test was performed in triplicate (n=3). After incubation, 20 strips of adhesive tape were applied sequentially to the skin using a roller, according to the standardised procedure, and then removed with a forceps (94). The amount of *stratum corneum* removed was determined by infrared densitometry (SquameScan™ 850A, Hailand electronic GmbH; Wetzlar, Germany) and strips were grouped in different pools, following the sequence: 1, 2, 3-5, 6-10, 11-15, 16-20 (623). The amount of B12 present in each sample was extracted overnight from the strips using a methanol:water mixture (50:50 v/v) as extraction solvent, since it afforded an optimal B12 recovery ratio within the established range (100 ± 20%) (95). Subsequently, B12 was quantified by HPLC with no interference with the analytical method.

*7.1.2.2. In vitro drug permeability through the skin*

The B12 skin permeability achieved by lipid vesicles and dissolving MNA was evaluated using an FDC set-up (51). The skin permeability obtained by the different nanosystems was compared with the skin permeability of a B12 solution 0.5% (w/v) (79). For those formulations, the experiments were carried out using intact or micro-pored full-thickness porcine skin (59). In the case of dissolving microneedles, skin permeability was assessed using dermatomed porcine skin (600 µm). For this, excised hairless porcine skin was obtained separating it from the cartilage using a scalpel and dermatomising it if necessary (Micro-line Wagnerd dermatome, Aesculap/Braun; Tuttlingen, Germany). The micro-pored skin samples were produced by manually inserting solid MNA with thumb force for 30 sec. Excised intact, micro-pored or dermatomed skin was placed horizontally between donor and receptor chambers, with the *stratum corneum* upwards, of the FDC (effective diffusion area of 1.76 $cm^2$). Specifically for dissolving MNA, the skin was placed onto a foam surface covered with aluminium foil and the donor chamber was strongly attached to the skin using a small amount of cyanoacrylate glue (Loctite®, Henkel; Düsseldorf, Germany). One dissolving MNA was inserted into the skin using a syringe plunger to

apply firm pressure for 30 sec. To secure the insertion of the MNA, they were affixed with Steri-Strip® adhesive bands (3M-Spain; Madrid, Spain) (624). In the case of lipid vesicles, 500 µL of each formulation was added to the donor chamber. The receptor chamber was filled with 12 mL of PBS pH 7.4 (n = 6). Temperature was maintained at 32 ± 1ºC throughout the whole experiment. The donor compartment and the sampling port were covered with Parafilm M® to avoid leakage and solvent evaporation. Samples of 200 µL were collected at prefixed times within 12-32 h, depending on the formulation tested and the skin used. At each sampling time, the volume was replaced with pre-warmed PBS to guarantee sink conditions. The released B12 was quantified using the same HPLC analytical method described above, and the cumulative amounts of B12 were plotted versus time. The cumulative amount of drug permeated through the skin was plotted as a function of time. Permeability parameters were calculated by linear regression of the steady state: *Jmax* (µg/cm$^2$ h), *Kp* (cm/h) and *tL* (h) as a simplification of the Scheuplein diffusion model.

*7.1.2.3. Visualisation of micro-pores created by solid MNA*

Dye binding studies were performed to visualise the creation of micro-pores by MNA. Microneedle-treated porcine skin was stained with methylene blue dye solution 1% (w/v) for 1 min (503). Then, the insertion site was cleaned with water to remove excess dye. Images were taken by optical microscopy, using a light microscope with a camera (Nikon digital camera DXM1200C, Nikon; Tokyo, Japan). Morphology of solid MNA was also observed by SEM imaging. The insertion depth was determined using an artificial skin model (Chapter 6, 6.1.2.3 subsection) (619).

*7.1.2.4. Statistical analysis*

All data processing was performed using Microsoft Excel 2016® (Redmond, WA, USA) and SPSS version 22.0® (IBM Corp., NY, USA). Data is expressed as the mean ± standard deviation (SD) unless otherwise stated. As a previous requirement for the statistical tests, normality, homoscedasticity, and sphericity were verified if needed. Normal

distribution for each data set was assessed by the Shapiro-Wilk test. Homogeneity of variances was confirmed by the Levene's test. Variances of the differences between all combinations of related groups were checked by the Mauchly's sphericity test. Statistical analysis was carried out using the T-test for simple comparisons, one-way ANOVA for tests with two variables, and two-way ANOVA for tests with three variables. All ANOVA tests were followed by the proper post hoc test. Specifically, the Games-Howell nonparametric test was used in case of heterogeneity of variances. When the homoscedasticity requirement was met, the Bonferroni or Tukey tests were used when the number of comparisons was low or high, respectively. The Gabriel test was used if the number of samples were different between the groups. Statistical differences were considered significant if p-values were below 5% ($p < 0.05$).

## 7.2. Results and discussion

### 7.2.1. Drug distribution within skin layers and *stratum corneum* depth

The *stratum corneum* layers depth in porcine skin was determined by infrared densitometry using a standardised procedure (623). The total thickness obtained was around 20 µm, in accordance with the standard values between 17-28 µm, previously reported by Jacobi et al. (2007) (625). Tape-stripping studies were performed using the most promising formulations according to the afore-presented data: L1, L2, T1d, T2d, E1 and E3. As incubation times, 2 h, 4 h and 6 h were selected, covering the longest time a topical formulation would be maintained on the skin. Furthermore, longer incubation times lead to overhydration of the skin and removal of the whole *stratum corneum* in a single strip (50). The B12 solution 0.5% w/v (S) was used as a reference, since it represents the free diffusion and no enhancing absorption effects are expected from the vehicle. Figures 7.1-7.3 show the progressive B12 penetration in the different layers of the *stratum corneum* at different incubation periods.

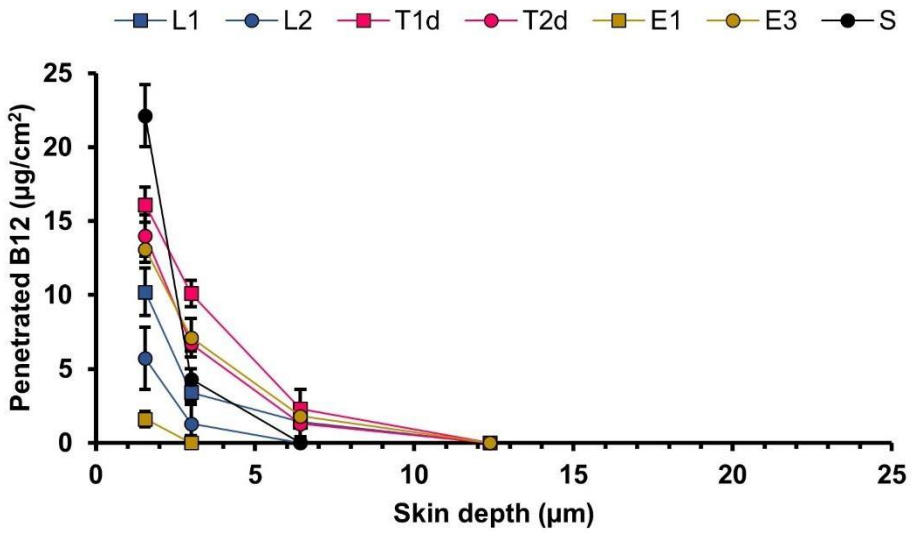


**Figure 7.1.** Penetration profiles of B12 delivered from liposomes (L1 and L2), transfersomes (T1d and T2d), ethosomes (E1 and E3), and B12 aqueous solution after 2 h. All results are expressed as mean ± SD (n=3).

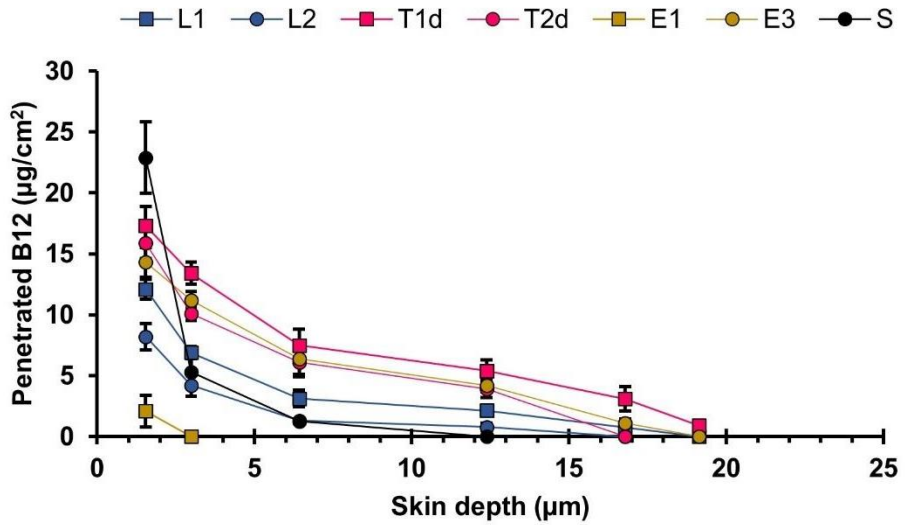


**Figure 7.2.** Penetration profiles of B12 delivered from liposomes (L1 and L2), transfersomes (T1d and T2d), ethosomes (E1 and E3), and B12 aqueous solution after 4 h. All results are expressed as mean ± SD (n=3).

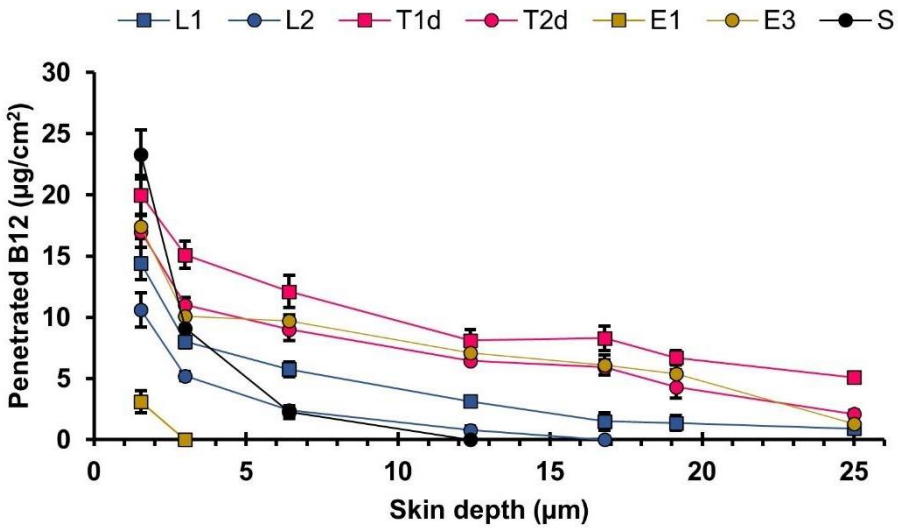


**Figure 7.3.** Penetration profiles of B12 delivered from liposomes (L1 and L2), transfersomes (T1d and T2d), ethosomes (E1 and E3), and B12 aqueous solution after 6 h. All results are expressed as mean ± SD (n=3).

In general, the amounts of B12 detected in the deeper layers of the skin increase as a function of the incubation time, as expected. As shown, the B12 solution presented the highest amount of B12 extracted in the first strip, regardless of the incubation time. Two reasons can explain this fact: the immediate availability of B12 on the skin leading to a quick distribution over the first *stratum corneum* layer, where it is retained; and a deficient cleaning of the skin surface. Concerning the latter, many authors discard this stripe because the inaccuracy of the data is typically high and considered an experimental artefact (91). However, the rest of B12 from the solution did not penetrate the *stratum corneum* nor the deeper skin layers, and only low quantifiable concentrations are detected up to the third strip, which corresponds to 6 µm depth, after 6 h. These findings confirm the inability of B12 to diffuse through intact skin. The E1 ethosome samples presented the lowest quantifiable amounts among all the vesicles tested, probably due to the low B12 load and the gradual release. Samples could have easily been under the detection and quantification limits. The L2 formulation carries less B12 amounts than the other prototypes, consequently showing considerably lower B12 penetration amounts, only

until approximately 15 µm depth (Figure 8c). Nevertheless, L1, T1d, T2d and E3 vesicles allowed B12 to reach the dermis (>25 µm). L1 and T2d contained similar B12 doses but after 4 and 6 h of incubation, the transfersomes showed higher permeation rates up to the deepest layers (Figure 8b and 8c). This means that the *stratum corneum* is saturated in B12 at that time point and a diffusion gradient to the deeper layers starts. T1d showed the highest permeation profiles. The penetration results suggest that the transfersome enhancing effect was much higher than the one of liposomes and are in agreement with Abd et al. (2016) (219), who compared the penetration of a hydrophilic drug (caffeine) delivered from liposomes, transfersomes and solution.

B12 has been delivered through the skin using chemical and physical methods by other authors. Yang et al. (2011) studied *in vitro* the effects of chemical enhancers and physical methods in topical administration of B12. Chemical enhancers (ethanol, oleic acid, and propylene glycol) allowed an effective permeability of B12 in comparison with passive diffusion. The permeability enhancement offered by iontophoresis was around 2-fold in comparison to a combination of all enhancers (50% ethanol, 10% oleic acid, and 40% propylene glycol) (626). Although these methods have proven to effectively deliver B12, they present several inconveniences in B12 delivery for atopic dermatitis. For example, they were not able to localise their effects in the epidermis and dermis, leading to an absorption of B12 in systemic circulation, which is unnecessary for psoriatic and atopic dermatitis patients. Also, local skin reactions and poor effectiveness, in combination with hydrophilic molecules, have been reported for chemical enhancers (215).

From the results presented here, it can be concluded that B12 does not diffuse through the *stratum corneum* if formulated in water media, whereas the developed formulations are able to efficiently deliver B12 to the deeper skin layers after 6 h.

### 7.2.2. *In vitro* drug permeability through the skin from lipid vesicles

Porcine skin was selected as it is a recommended surrogate of human skin for *in vitro* studies, due to the ethical considerations surrounding human sampling, and the variability associated to human skin samples as a result of differences of age, race, and anatomical donor site (59). Previous studies have determined that among all animal models, porcine skin is the most similar to human skin from the histological point of view (627). In particular, the human forearm and pig ears have a good concordance between the number of cell layers of the *stratum corneum* and whole skin thickness, which have a huge influence on drug permeability flux (628). The results obtained are even more realistic and reliable if we consider that the application area of these formulations in humans is the forearm. Systemic blood concentration parameters of a topically applied drug can be calculated using the skin penetration parameters (629,630). Cumulative amounts of permeated B12 per diffusional area of porcine skin *versus* time are presented in Figures 7.4 and 7.5. The permeability parameters calculated for each formulation and condition are presented in Tables 7.2 and 7.3, as well as the initial concentration of each sample assayed.

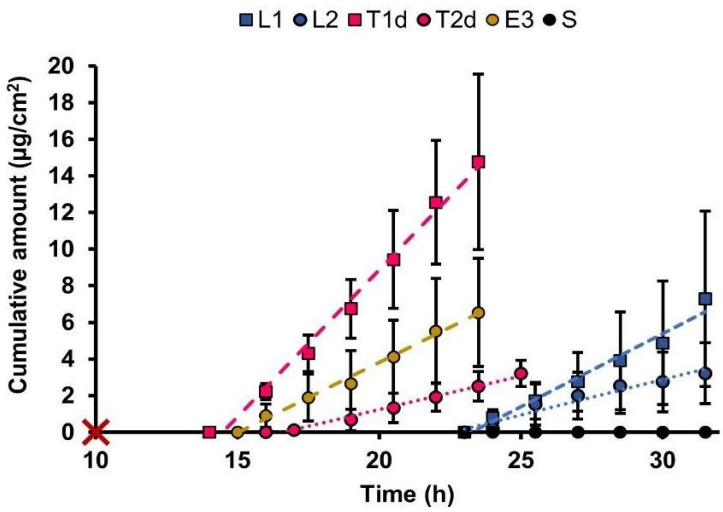


**Figure 7.4.** *In vitro* permeability profiles of B12 delivered from the different lipid vesicle prototypes through intact porcine skin. All results are expressed as mean ± SD (n=6).

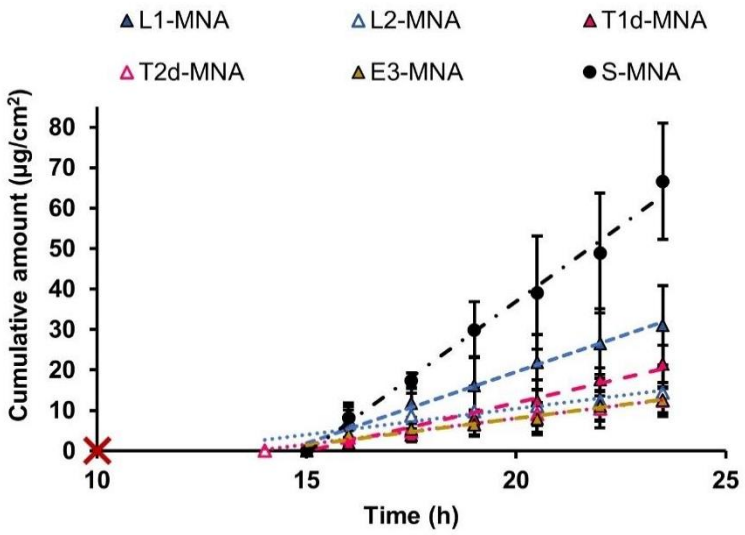


**Figure 7.5.** *In vitro* permeability profiles of B12 delivered from the different lipid vesicle prototypes through microneedle-treated porcine skin. All results are expressed as mean ± SD (n=6).

B12 diffusion for 32 h was neglectable when it was administered in an aqueous solution, obtaining drug concentrations in FDC receptor medium below the HPLC quantification limit (Figure 7.4). Moghimipour et al. (2013) reported that it is possible to achieve certain B12 *in vitro* drug permeability from an aqueous solution (631). Nevertheless, they extended the study to 80 h and used a higher concentrated solution, which causes a higher gradient difference between FDC compartments and forces the drug to pass the separating barrier. Also, they used rat skin, which is more permeable than porcine and human skin, and strongly affected by an excessive *stratum corneum* hydration after long exposure to drug-containing solutions (59).

Transdermal absorption of B12 solution can also be improved when containing chemical enhancers like ethanol, as Howe et al. (1967) studied in rat and guinea pig skin (632). The use of chemical enhancers in topical formulations is a strategy that intends to modify the drug barrier function of the skin, or to improve the drug physicochemical properties. However, they

entail certain disadvantages, such as the inability to locate the effects on the *stratum corneum* or skin reactions (irritation, inflammation and erythema) (215).

The developed lipid vesicle formulations notably increased the B12 permeability through the skin, as Figure 7.4 reflects. The calculated fluxes from all formulations tested were as follows: T1d ≥ E3 ≥ L1 > T2d ≥ L2 > S ($p < 0.05$) (Table 7.2). Thus, it can be concluded that the ability to enhance B12 diffusion by lipid vesicles increases with the incorporated dose and vesicle flexibility, while it decreases with vesicle size (633).

Among the formulations containing a similar drug amount, transfersomes and ethosomes showed higher fluxes than conventional liposomes, as expected. This trend has been observed before in several studies (588,634,635). Transfersomes and ethosomes present lower sizes in comparison to liposomes (Chapter 5, 5.1.2 subsection), and particle size has been revealed to be one of the crucial properties to consider for transdermal delivery, since the smaller the particle, the better the transdermal absorption profiles obtained (392). Additionally, different mechanisms have been proposed to explain this behaviour of ultraflexible lipid vesicles. For example: the ethanol-increased solubility of drugs in the vesicles; or their ability to squeeze along the intracellular *stratum corneum* lipids, pushed by the gradient caused by the difference in water content between the moderate dehydrated skin surface and the hydrated viable epidermis (261,636). Other researchers, like Dreier et al. (2016), consider that lipid vesicles are unable to cross intact through the *stratum corneum* layers and they disrupt the compacted intracellular lipids package (259). However, the exact mechanism is not yet completely elucidated.

*Kp* was calculated correlating the flux to the applied dose, as an efficiency measure of each vesicle (Table 7.2). Again, transfersomes and ethosomes were the most effective formulations. The comparison of the *Jmax* and *Kp* brings the role of the drug cargo that conditions the final vesicle activity to light, since the difference observed in flux between L1-L2

and T1d-T2d is mitigated when the dose is considered. Once again, ultraflexible vesicles offered a significant decrease in the lag time, showing an earlier start of the absorption in comparison to conventional liposomes.

**Table 7.2.** *In vitro* permeability parameters of B12 delivered from the different lipid vesicle prototypes through intact porcine skin. All results are expressed as mean ± SD (n=6).

| Formulation | Jmax ($\mu g/cm^2/h$) | Kp $\cdot 10^{-7}$ (cm/s) | Lag time (h) | Dose (µg/mL) |
|---|---|---|---|---|
| **Solution (S)** | - | - | - | 50000 |
| **L1** | 1.00 ± 0.56 | 1.26 ± 0.71 | 23.87 ± 0.39 | 2070 |
| **L2** | 0.44 ± 0.19 | 1.61 ± 0.68 | 22.91 ± 1.11 | 673 |
| **T1d** | 1.73 ± 0.77 | 2.41 ± 1.07 | 14.51 ± 1.63 | 2090 |
| **T2d** | 0.50 ± 0.11 | 2.23 ± 0.45 | 17.66 ± 1.55 | 610 |
| **E3** | 1.51 ± 0.35 | 2.08 ± 0.48 | 17.53 ± 2.14 | 1333 |

The skin pre-treated with solid MNA led to a further increase of B12 permeability, which was significantly higher than the ones provided by the respective lipid vesicles (Figures 7.4 and 7.5). MNA are considered one of the most promising tools to achieve systemic effects by transdermal delivery of drugs. They are designed as a minimally invasive and painless system that can physically bypass the *stratum corneum* (Figures 7.6 and 7.7) (215,637).

After MNA use, the drug solution provided the highest flux through the skin in comparison to the application of lipid vesicles (Figure 7.5). Nevertheless, it did not correspond to a higher efficiency than the rest of the tested formulations, as a consequence of the great dose administered (Table 7.3). This phenomenon could also be attributed to the vesicles' ability to control the drug released, even when they are present in the skin medium. As stated before, when the barrier function is intact, it is unclear if the drug is released from the formulations, or the vesicles carry the drug to the deeper layers, or they interact with the skin lipids, facilitating drug permeability. However, microneedles remove the barrier function, thus

opening pores of bigger size that could allow the passage of the liposomes, which can therefore still control the release of the drug.

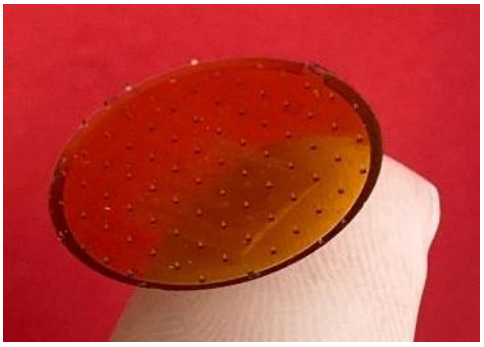

**Figure 7.6.** Solid microneedles used to create micro-pores in the porcine skin.

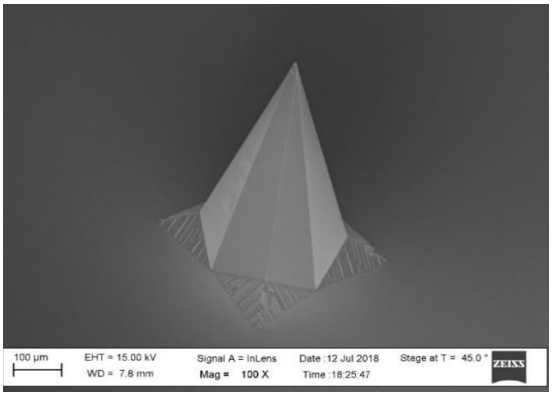


**Figure 7.7.** Needle-like projection visualised by scanning electron microscopy (SEM imaging).

In contrast to what could have been expected, the drug solution showed a similar lag time compared to the flexible vesicles (Table 7.3). Lower lag times after MNA-treatment for all formulations except T1d were observed, although the difference is not significant in this case. The possible reason for this could be that vesicles enhance the delivery of B12 through the skin, which does not happen with the B12 aqueous solution, as previously demonstrated. In the MNA-assisted cases, there are two enhancing effects happening simultaneously: the passage through the microchannels, and the passage through the intact stratum corneum. This

second effect is especially remarkable for transfersomes and ethosomes, where the lag time difference is not significant if MNA are used or not. At this point it should be considered another possible reason, since the microneedles completely perforate the *stratum corneum* as their insertion reaches the deeper skin layers, but the skin sample used also included the epidermis and the dermis. Before the drug can diffuse to the subsequent layer, the previous layer must be saturated with the drug, which is directly related to the partition coefficient for the drug in each medium (50).

**Table 7.3.** *In vitro* permeability parameters of B12 delivered from the different lipid vesicle prototypes through microneedle-treated porcine skin. All results are expressed as mean ± SD (n=6).

| Formulation | Jmax ($\mu g/cm^2/h$) | Kp $\cdot 10^{-7}$ (cm/s) | Lag time (h) | Dose (µg/mL) |
|---|---|---|---|---|
| **S-MNA** | 9.23 ± 1.65 | 5.12 ± 0.91 | 15.66 ± 0.61 | 50000 |
| **L1-MNA** | 3.65 ± 1.22 | 4.61 ± 1.53 | 14.36 ± 0.45 | 2070 |
| **L2-MNA** | 1.23 ± 0.38 | 4.51 ± 1.39 | 11.38 ± 2.60 | 673 |
| **T1d-MNA** | 3.38 ± 0.86 | 4.27 ± 1.08 | 16.27 ± 0.83 | 2090 |
| **T2d-MNA** | 1.29 ± 0.26 | 4.72 ± 0.95 | 13.83 ± 0.85 | 610 |
| **E3-MNA** | 2.44 ± 0.27 | 3.44 ±0.38 | 16.06 ± 0.97 | 1333 |

The established current posology recommends first shock doses to replenish B12 deposit, followed by maintenance doses. According to the data presented in this work, T1d transfersome formulation presents the highest transdermal flux through the skin, and therefore it can be an optimal candidate for the treatment of this vitamin deficiency. Since the recommended doses are 1 mg/day for 1 week, 1 mg/week for 4-8 weeks and 1 mg/month chronically, T1d formulation could fulfil these requirements using skin areas of around 12, 1.75 and 0.5 $cm^2$ respectively, which are perfectly feasible for the design of a transdermal patch. Solid microneedles can be used for pre-treating the skin and to achieve faster and higher cyanocobalamin concentrations, or to reduce the size of the treated skin area. This approach, usually known as “poke and patch”, is clearly delimited

and applicable to the initial stage of the treatment since the time that micro-holes remain open is nowadays under discussion (501,638).

### 7.2.3. Visualisation of micro-pores created by solid MNA

Methylene blue staining was used to assess the effectiveness of solid MNA to pierce the porcine skin (Figure 7.8). Pictures obtained by optical microscopy were similar to those obtained by Kalluri and Banga (503). Microneedle insertion effectively created microchannels in the artificial skin model (Figure 7.9). First and second skin layers (254 µm) were almost fully drilled (> 90%), which is enough to practically nullify the skin barrier function of the stratum *corneum*. Additionally, around 50% of micro-pores reached 381 µm).

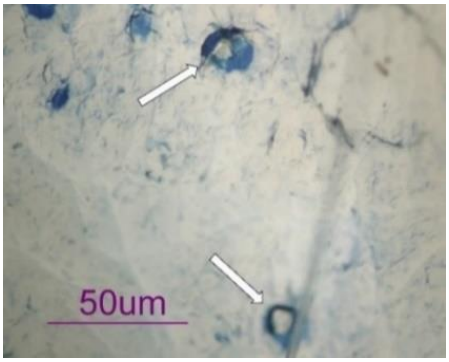


**Figure 7.8.** Micro-pores on porcine skin after MNA insertion visualised by optical microscopy.

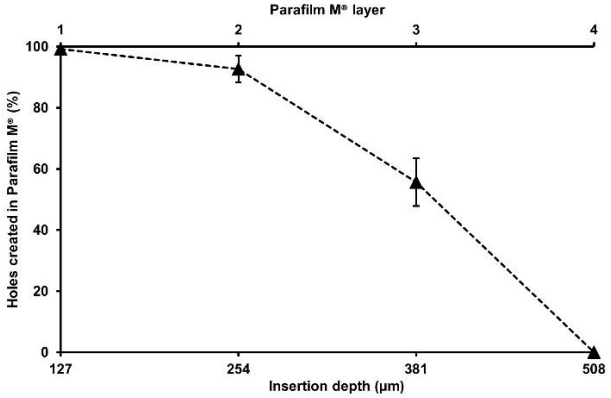


**Figure 7.9.** Percentage of holes and insertion depth of solid MNA in an Parafilm M® skin model. All results are expressed as mean ± SD (n=3).

7.2.4. *In vitro* drug absorption through the skin from dissolving MNA

To conduct these studies, porcine skin was dermatomed to 600-µm thickness, reducing the dermis layer which, not being considered as the main limiting factor to the transdermal drug absorption, could slow down the diffusion process. According to the previous results (Chapter 6, section 6.2), F3, F7, F9 and F11 prototypes were selected as representatives of MNA. The differences between them were the insertion capability, dissolving time, and drug loading. PVA 38-58 kDa-based MNA (F7) showed the highest insertion rate and non-complete dissolution of the matrix. F11 prototype (containing freeze-dried lipid vesicles) exhibited the lowest drug loading and needle height.

*In vitro* permeability profiles are presented in Figures 7.10-7.14, where a two-step process is clearly observed in all cases. It can be explained as a consequence of the transition from solid to hydrogel as a result of swelling and MNA dissolution, which increases the released B12 availability to be permeated through the skin.

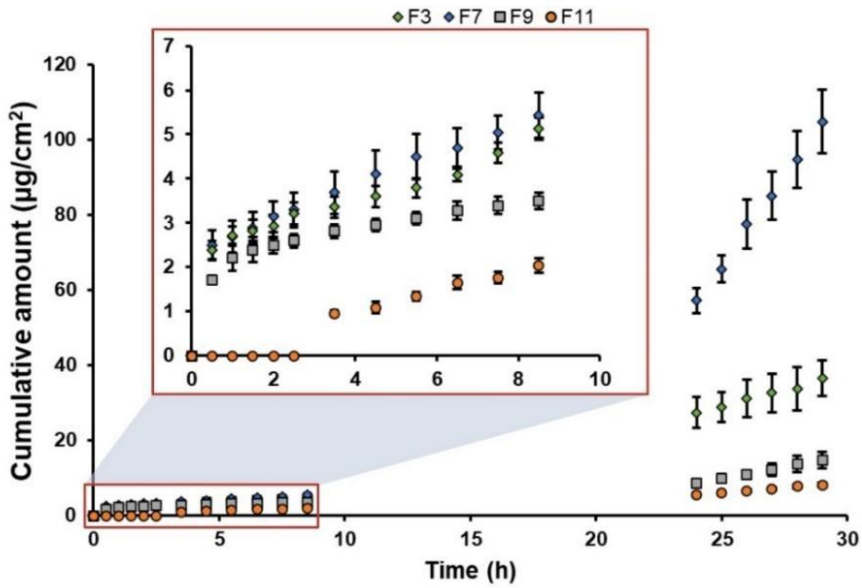


**Figure 7.10.** *In vitro* permeability profiles of B12 delivered from different dissolving MNA prototypes through dermatomed porcine skin. All results are expressed as mean ± SD (n=4).

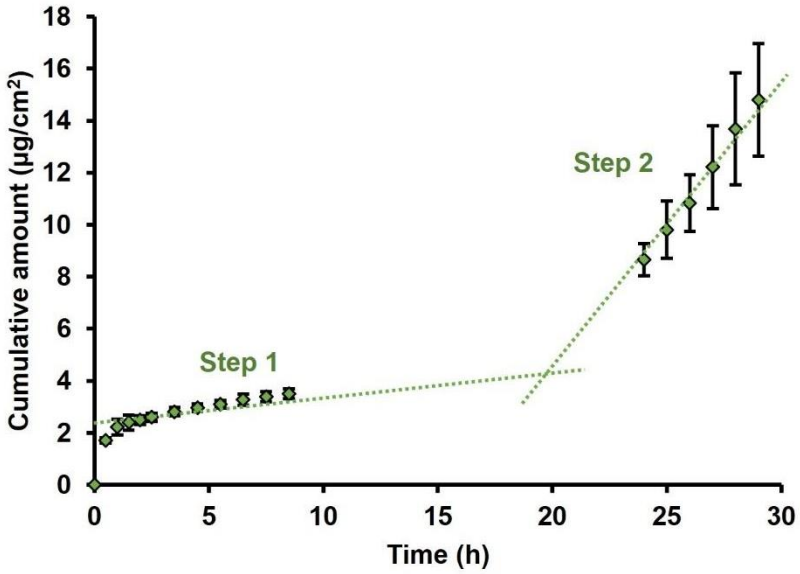


**Figure 7.11.** *In vitro* permeability profile of B12 from F3 prototype through dermatomed porcine skin. All results are expressed as mean ± SD (n=4).

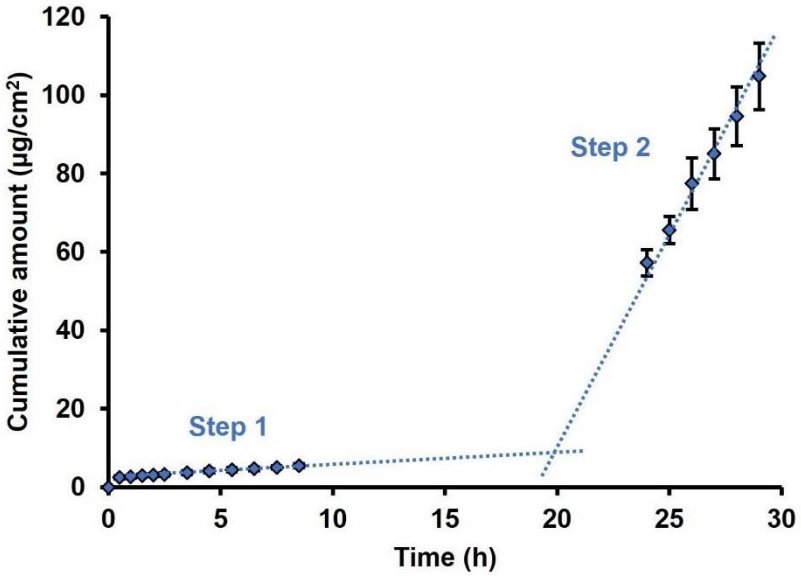


**Figure 7.12.** *In vitro* permeability profile of B12 from F7 prototype through dermatomed porcine skin. All results are expressed as mean ± SD (n=4).

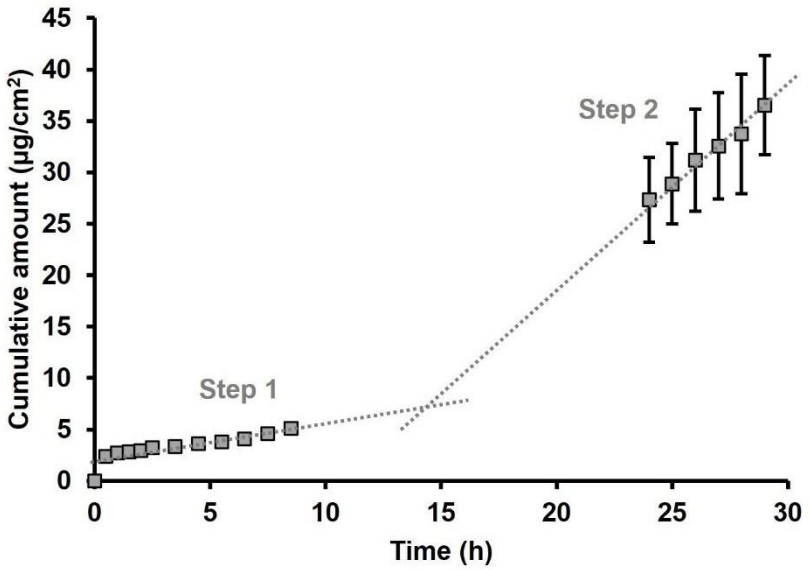


**Figure 7.13.** *In vitro* permeability profile of B12 from F9 prototype through dermatomed porcine skin. All results are expressed as mean ± SD (n=4).

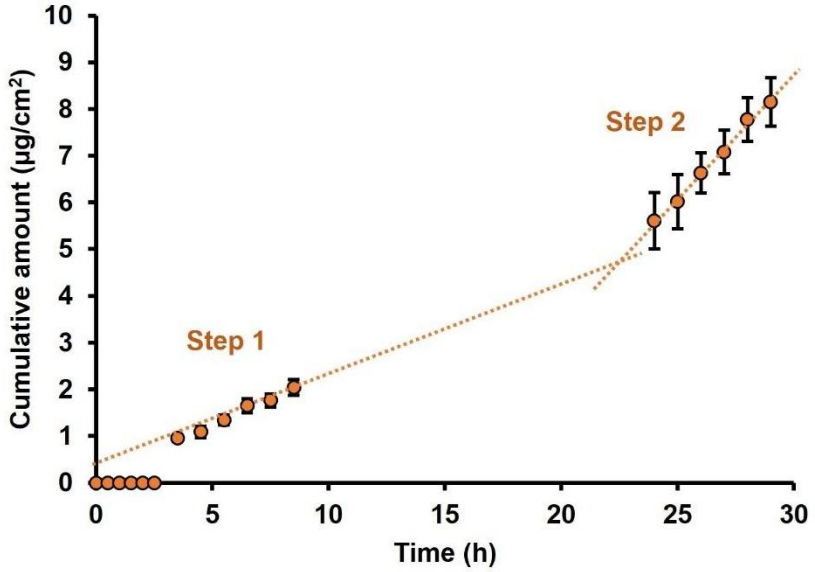


**Figure 7.14.** *In vitro* permeability profile of B12 from F11 prototype through dermatomed porcine skin. All results are expressed as mean ± SD (n=4).

The intersection of the two straight lines could be an estimation of the moment when the transition from solid MNA to hydrogel occurs, although it probably takes place gradually. PVP-based prototype (F9) showed the state-transition earlier, as expected after the release studies results (Chapter 6, 6.2.3 subsection). However, the experimental conditions are not similar and, for example, the hydration/swelling of MNA is shorter in the release studies. It should be noted here that the MNA in the release studies was immersed in the fluid, whereas it was placed in the FDC experiments onto the dry side of the skin, not directly in contact with the fluid. Therefore, the different MNA release behaviours can be compared, although not in terms of time. This could be the reason why the F11 prototype, which contains freeze-dried lipid vesicles, needed longer times to show the state-transition process. In addition, insertion depth of the F11 prototype was the most limited, and the hydration fluids coming up from the FDC receptor chamber encountered the MNA later. In this way, the insertion capability of MNA has been revealed as one of the crucial properties in achieving a maximal enhancing effect. *In vitro* permeability parameters are presented in Tables 7.4 and 7.5.

**Table 7.4.** *Jmax* of B12 delivered from the different dissolving MNA prototypes through 600-µm dermatomed porcine skin. S1: MNA dissolution step 1; S2: MNA dissolution step 2. All results are expressed as mean ± SD (n=4).

| MNA | Dose (µg/mL) | Jmax (µg/cm$^2$/h) | | |
|---|---|---|---|---|
| | | Total | S1 | S2 |
| **F3** | 1700 | 0.43 ± 0.05 | 0.39 ± 0.18 | 1.43 ± 0.48 |
| **F7** | 2000 | 4.12 ± 0.34 | 0.46 ± 0.04 | 10.80 ± 1.10 |
| **F9** | 1975 | 1.32 ± 0.22 | 0.37 ± 0.03 | 2.37 ± 0.74 |
| **F11** | 500 | 0.29 ± 0.02 | 0.47 ± 0.07 | 0.64 ± 0.04 |

**Table 7.5.** *Kp* of B12 delivered from the different dissolving MNA prototypes through 600-µm dermatomed porcine skin. S1: MNA dissolution step 1; S2: MNA dissolution step 2. All results are expressed as mean ± SD (n=4).

| MNA | Dose (µg/mL) | Kp ·10$^{-8}$ (cm/s) | | |
|---|---|---|---|---|
| | | Total | S1 | S2 |
| **F3** | 1700 | 7.1 ± 0.9 | Not applicable | 23.6 ± 7.9 |
| **F7** | 2000 | 55.6 ± 4.6 | Not applicable | 145 ± 14.8 |
| **F9** | 1975 | 18.6 ± 3.1 | Not applicable | 33.4 ± 10.4 |
| **F11** | 500 | 16.2 ± 1.1 | Not applicable | 35.1 ± 2.1 |

Transdermal fluxes were calculated for the global process and the observed steps separately (Table 7.4). S1 and S2 are the slopes obtained by linear regression of the data corresponding to each straight line drawn in the plots (Figures 7.11-7.14).

The calculated fluxes for step 1 were similar for all formulations ($p > 0.05$) since MNA remained in a solid state during the initial hours post-insertion and drug availability was quite similar in all cases. It can be concluded that the limiting step at this phase of the drug diffusion process is the release of the drug from the MNA. However, in step 2, after the experimentally observed solid-hydrogel transition, the calculated fluxes were F7 > F9 ≥ F3 > F11 ($p < 0.05$). In general, these calculated fluxes meet those obtained when both steps are considered as a single process, because step 2 has a greater impact on the drug absorption process. As mentioned above, insertion depth could be responsible for the difference between F7 and F11 transdermal fluxes, as the higher the insertion depth, the shorter the dermis path to reach the FDC receptor chamber.

*Kp* was calculated correlating the flux to the applied dose, as an efficiency measure of each MNA (Table 7.5). Nevertheless, this parameter could not be calculated for step 1 as the linear regression of straight lines intercepts with the y-axis before 0 h, offering aberrant values of the calculated parameters. It would also be inadequate, as the dose applied is

freely available for diffusion. B12 doses loaded in F3, F7 and F9 were similar, so the outcome agrees to the findings in transdermal fluxes: F7 > F9 = F3. However, F11 efficiency matched the F3 and F9 results, showing again the importance to penetrate the skin with the MNA as much as possible to improve the results. It is worth mentioning that the results of *Kp* for both dissolving and solid MNA (section 7.2.2) show comparable orders of magnitude, indicating a similar breakdown of the barrier function exerted by the *stratum corneum*.

## 7.3. Milestone and highlights of chapter 7

**Milestone:** Lipid vesicles and dissolving MNA allowed B12 penetration and permeability through the skin, which is almost neglectable when drug is administered as an aqueous solution.

- **Highlight 7.1:** B12 penetration was enhanced by the different lipid vesicles. As expected, the amounts of B12 detected in the deeper skin layers increase as a function of the incubation time and the use of ultraflexible vesicles.
- **Highlight 7.2:** B12 permeability results showed the same trend as in the penetration studies, indicating that transfersomes and ethosomes are the most effective vesicles to carry the drug to the dermis, where it can be absorbed to systemic circulation.
- **Highlight 7.3:** B12 permeability through the skin increases when skin is pre-treated with solid MNA. The micro-pores created in the *stratum corneum* almost nullified its barrier function and, consequently, increased notably the permeability rate for highly drug-loaded formulations, equalising the lag times.
- **Highlight 7.4:** B12-loaded dissolving MNA enhanced drug permeability. Absorption profiles showed two differentiated steps. In the first one, the limiting process to drug diffusion is its release from the dosage form. In the second step, the permeability profile changes, and the permeability steady state is achieved, as the arrays are completely dissolved.

- **Highlight 7.5:** Based on the obtained results, it seems that lipid vesicles are the most convenient systems to potentially treat skin disorders, whereas MNA are ideal to achieve a systemic B12 supply.

# Chapter 8

## Evaluation of cyanocobalamin lipid vesicles in a murine model of contact dermatitis

## 8.1. Materials and methods

### 8.1.1. Materials

The reagents and materials used are listed in table 8.1.

**Table 8.1.** Reagents and materials for the *in vivo* study.

| Reagent / Material | Information | Supplier |
|---|---|---|
| **Oxazolone** | > 98% purity | Sigma-Aldrich (St. Louis, MI, USA) |
| **Clobetasol** | > 99% purity | Acofarma (Madrid, Spain) |
| **Paraformaldehyde** | > 95% purity | Sigma-Aldrich (St. Louis, MI, USA) |
| **Harris' haematoxylin** | 7 g/L (w/v) | Sigma-Aldrich (St. Louis, MI, USA) |
| **Eosin stain solution** | Histological grade | Sigma-Aldrich (St. Louis, MI, USA) |
| **DPX mountant** | Histological grade | Sigma-Aldrich (St. Louis, MI, USA) |
| **Bouin's liqueur** | Acetic acid 5% Formaldehyde 9% Picric acid 0.9% | Sigma-Aldrich (St. Louis, MI, USA) |
| **Mayer's haematoxylin** | 1 g/L (w/v) | Sigma-Aldrich (St. Louis, MI, USA) |
| **Ponceau S** | - | Sigma-Aldrich (St. Louis, MI, USA) |
| **Phosphomolybdic acid** | - | Sigma-Aldrich (St. Louis, MI, USA) |
| **Aniline blue solution** | 2.5% in acetic acid (2 %) | Sigma-Aldrich (St. Louis, MI, USA) |
| **Dimethylbenzene** | > 99% purity | Sigma-Aldrich (St. Louis, MI, USA) |
| **Luminol** | Sodium salt | Sigma-Aldrich (St. Louis, MI, USA) |

### 8.1.2. Methods

#### *8.1.2.1. Animals and housing conditions*

For the DTH model experiments, a total of 42 BALB/c mice were used. Animals were conditioned to the University of Valencia facilities for 10 days. Afterwards, they were randomly assigned to an experimental group (Table 8.2). All the procedures were in accordance with the principles

of laboratory animal care and approved by the Animal Experimentation and Welfare Ethics Committee (Annex III).

**Table 8.2.** Experimental groups and number of animals included in each one.

| Group/Formulation | Number of animals |
|---|---|
| **Healthy control** | 6 |
| **Oxazolone** | 6 |
| **E blank** | 6 |
| **E3** | 6 |
| **T blank** | 6 |
| **T1d** | 6 |
| **Clobetasol** | 6 |

*8.1.2.2. Induction of DTH and evaluation of the ear oedema*

Oxazolone (OXA) was dissolved in acetone and prepared at final concentrations of 3% and 1% w/v. Abdomen of the animals was shaved (day -1), and one day later they were sensitised by a single percutaneous application of 150 µL of OXA 3% w/v solution (day 0). On day 5, the hypersensitivity reaction was triggered by applying 10 µL of OXA 1% w/v solution in each side of the right ear. In this study, 20 µL of each formulation (10 µL/side) under research was applied to the right ear after the OXA challenge, and 24 h and 48 h later. Clobetasol propionate dissolved in acetone (0.025 mg/ear) was applied topically and used as a reference drug. Experimental procedure is represented in Figure 8.1. Ear thickness was measured before the OXA challenge and days 6, 7 and 8 using a micrometre (Absolute Digimatic 2®, Mitutoyo GmbH; Neuss, Germany) (639). Afterwards, animals were euthanised by cervical dislocation and the ears were taken for the histological study.

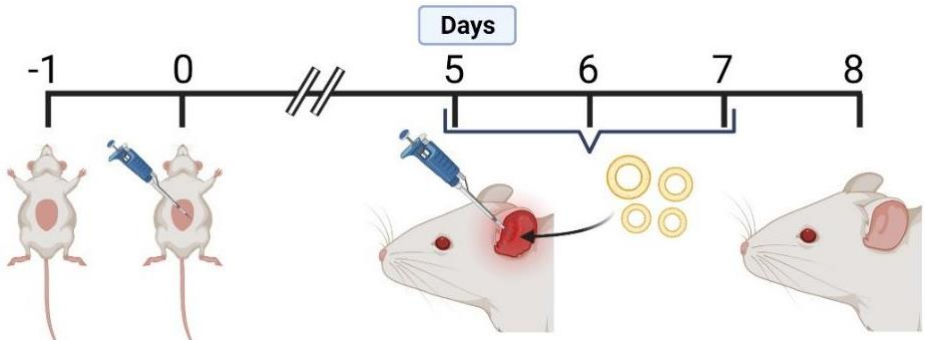


**Figure 8.1.** Schematic illustration of DTH model of acute atopic dermatitis.

*8.1.2.3. Bioluminescence imaging*

For the bioluminescence imaging (BLI), an IVIS Lumina X5 (PerkinElmer; Waltham, MA, USA) was used. Mice were treated with 0.2 mL of luminol (200 mg/kg i.p.; dissolved in PBS) and imaged 30 min after the injection under an anaesthetic protocol (isoflurane inhalation). Total photon emissions were determined at different time points (3, 6 and 24 h) (639).

*8.1.2.4. Histopathological study*

Skin-pinna biopsies were fixed in paraformaldehyde 4% w/v solution and then embedded in paraffin. Skin sections (5 µm-thickness) were stained to visualise the skin structures. For haematoxylin and eosin stains, samples were immersed in Harris' haematoxylin solution and then washed to remove the excess dye. Afterwards, they were sequentially treated with a differentiation solution and eosin ethanolic solution (50% v/v). Finally, slides were dehydrated with a sequence of alcohol solutions, mounted using DPX liquid and observed in an optical light microscope (640). Pinna sections were also stained using Masson's trichrome reagent. Briefly, samples were fixed in Bouin's liqueur overnight and then rinsed in two changes of distilled water. Skin sections were sequentially stained with Mayer's haematoxylin, 0.5% w/v hydrochloric acid ethanolic solution (0.5% w/v), acid ponceau, phosphomolybdic acid aqueous solution (1% w/v), aniline blue, and ethyl alcohol (95% w/v). Finally, samples were hyalinised

with dimethylbenzene and sealed with a neutral balsam (641). ImageJ® software (NIH; Bethesda, MD, USA) was used to process the images from histological sections and determine the skin layers thickness.

*8.1.2.5. Statistical analysis*

All data processing was performed using Microsoft Excel 2016® (Redmond, WA, USA) and SPSS version 22.0® (IBM Corp., NY, USA). Data is expressed as the mean ± standard deviation (SD) unless otherwise stated. As a previous requirement for the statistical tests, normality, homoscedasticity, and sphericity were verified if needed. Normal distribution for each data set was assessed by the Shapiro-Wilk test. Homogeneity of variances was confirmed by the Levene's test. Variances of the differences between all combinations of related groups were checked by the Mauchly's sphericity test. Statistical analysis was carried out using the T-test for simple comparisons, one-way ANOVA for tests with two variables, and two-way ANOVA for tests with three variables. All ANOVA tests were followed by the proper post hoc test. Specifically, the Games-Howell nonparametric test was used in case of heterogeneity of variances. When the homoscedasticity requirement was met, the Bonferroni or Tukey tests were used when the number of comparisons were low or high, respectively. The Gabriel test was used if the number of samples were different between the groups. Statistical differences were considered significant if p-values were below 5% ($p < 0.05$).

## 8.2. Results and Discussion

### 8.2.1. Induction of DTH and evaluation of the ear oedema

Pinna thickness increase has been proposed as a measure of ear skin oedema and vascular permeability (642,643), typically increased in atopic and contact dermatitis processes (639). For these experiments, transfersomes (T1d) and ethosomes (E3) were selected as they showed the best results regarding the B12 penetration and permeability enhancement through the skin (Chapter 7, 7.2.1 and 7.2.2 subsections).

Conventional liposomes and B12 aqueous solutions were omitted as a measure of animal reduction in compliance with the 3 Rs principle (644). Results are presented in Figures 8.2 and 8.3. Pinna thickness was increased in OXA-sensitised groups in comparison to non-sensitised (healthy control group). In addition, ear thickness did not show any increase when animals were treated with clobetasol (1.25 mg/ml w/v), proving the suitability of the model, as the pathological process can be controlled. Specifically, a slight decrease of ear thickness was noticed, probably as a consequence of steroid-induced skin thinning and atrophy (645,646). The non-treated group (OXA group) showed an ear thickness increase of 308 μm after 24 h, which subsided spontaneously over time, as animals were not exposed to the triggering agent again. B12-loaded transfersomes (T1d) significantly reduced (-172 μm) the ear thickness increase in comparison to the untreated group. Blank formulations showed a non-significant oedema reduction when compared to the untreated group. It could be attributed to the emollient properties of the lipid components and the refreshing effect produced by the aqueous vehicle. This confirms the effectiveness of B12 as a nitric oxide scavenger, since nitric oxide-mediated vasodilation, skin blushing, and pruritus are ameliorated (175). Surprisingly, ethosomes (E3) did not produce a satisfactory significant effect. A possible explanation is that the irritation produced by ethanol counteracts the neutralising effects of B12.

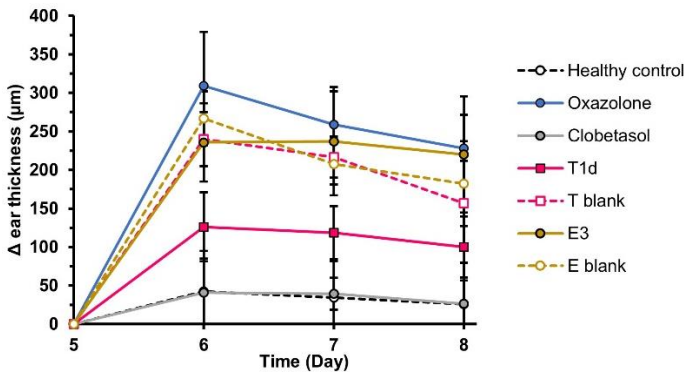


**Figure 8.2.** Ear thickness variation timeline. All results are expressed as mean ± SD (n=6).

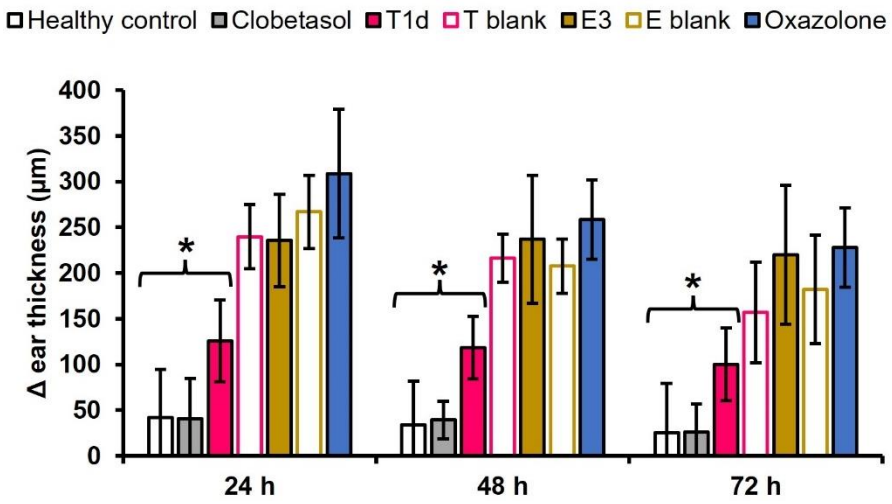


**Figure 8.3.** Ear thickness variation 24, 48 and 72 h after OXA challenge. All results are expressed as mean ± SD (n=6). * means statistically significant differences when compared to untreated group (OXA) ($p < 0.05$).

## 8.2.2. Bioluminescence imaging

The murine DTH model has long been used as a model for dermatitis, and it is well characterised that an inflammatory response via neutrophils, macrophages and T cells is generated (647). Myeloperoxidase (MPO) is an abundant protein present in the granules of neutrophils or polymorphonuclear leukocytes (PMN's). Respiratory burst, through the intervention of NADPH oxidase (Phox) and superoxide dismutase (SDS), produces hydrogen peroxide ($H_2O_2$) from molecular oxygen ($O_2$) (648). Finally, MPO catalyses the reaction of this $H_2O_2$ with chloride anions ($Cl^-$) to form hypochlorous acid (HOCl), which oxidises the luminol and triggers the chemiluminescence (Figure 8.4) (649). Eventually, MPO can also oxidise the luminol using the superoxide anion ($O_2^{\bullet}$) in a peroxidase-catalysed oxidation reaction (648,649).

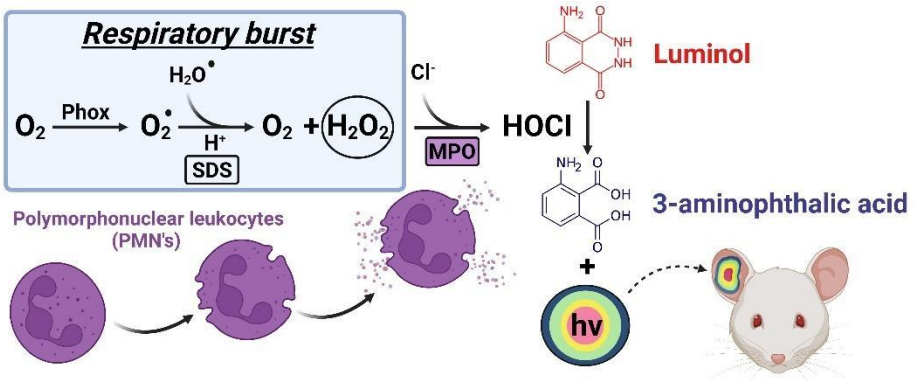


**Figure 8.4.** Luminol-oxidation BLI via neutrophilic mediation.

Therefore, a BLI assay was conducted to confirm the previous findings, and study whether neutrophils are involved in the pathological process triggered by OXA challenge, since luminol has been used for neutrophils activation and accumulation (650). Results are shown in Figure 8.5. Four groups were studied (OXA, clobetasol, T1d and T blank). Groups treated with ethosomes were discarded due to the poor results obtained in the reduction of ear thickness. The healthy control group was also discarded, since, for this study, the left ear was used as an intraindividual control in each animal.

Sensitisation to OXA generated a significant BLI between challenged (right) and non-challenged (left) ears with a maximum signal after 24 h (OXA group), confirming the existence of a certain leukocyte infiltration. As expected, luminol-induced BLI was completely normalised by clobetasol treatment, since neutrophils and macrophages are typical targets for immune suppression (647). However, contrary to ear oedema studies, T1d also showed a total photon emission attenuation, suggesting an effective mitigation of leukocyte infiltration and its activity in the inflamed area. As previously observed, blank transfersome vesicles (T blank group) reduced the BLI in comparison to the non-treated group, showing yet again a certain degree of effect produced by the aqueous vehicle.

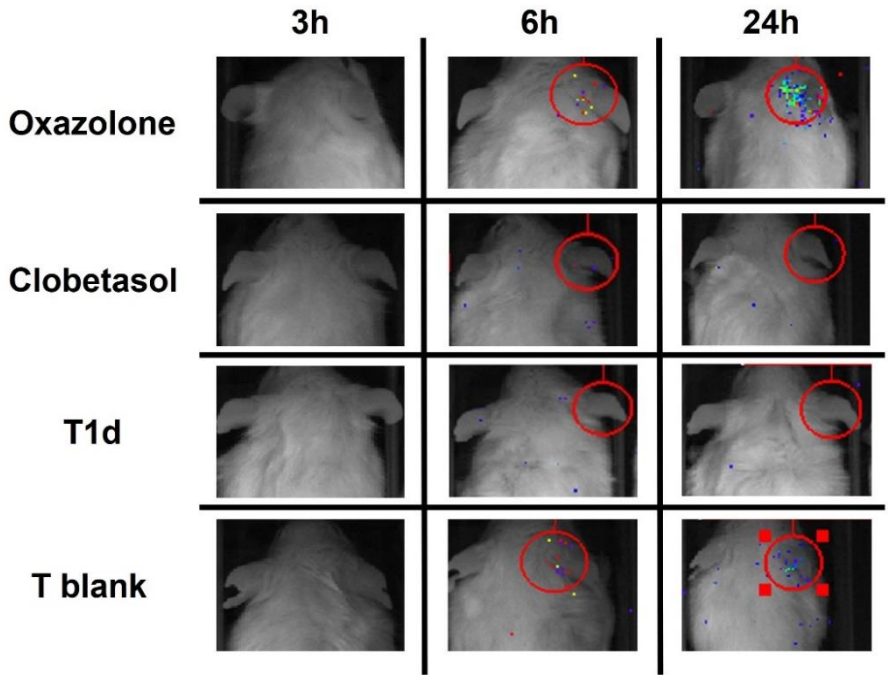


**Figure 8.5.** Representative images from the luminol-oxidation BLI experiment of the groups of interest.

### 8.2.3. Histopathological study

A histopathological study was performed to observe the anatomical differences in skin structure between groups treated with transfersomes in comparison to the healthy and non-treated animals. Representative images of eosin-haematoxylin and Masson's stains are presented in Figures 8.6 and 8.7, respectively.

Cellular infiltration as a response to the inflammatory damage after OXA challenge was noticed, like in the BLI assay, which was clearly reverted with T1d treatment (Figure 8.6). Ear thickness measurements based on the digital estimation met those obtained directly in the *in vivo* procedure and showed the same trends in terms of increase reduction when treated with transfersomes (Figure 8.8). However, this skin thickening is not only caused by the oedema -denoted by the skin structure spacing-, as the epidermis and dermis were also thickened in non-treated groups (Figure 8.7).

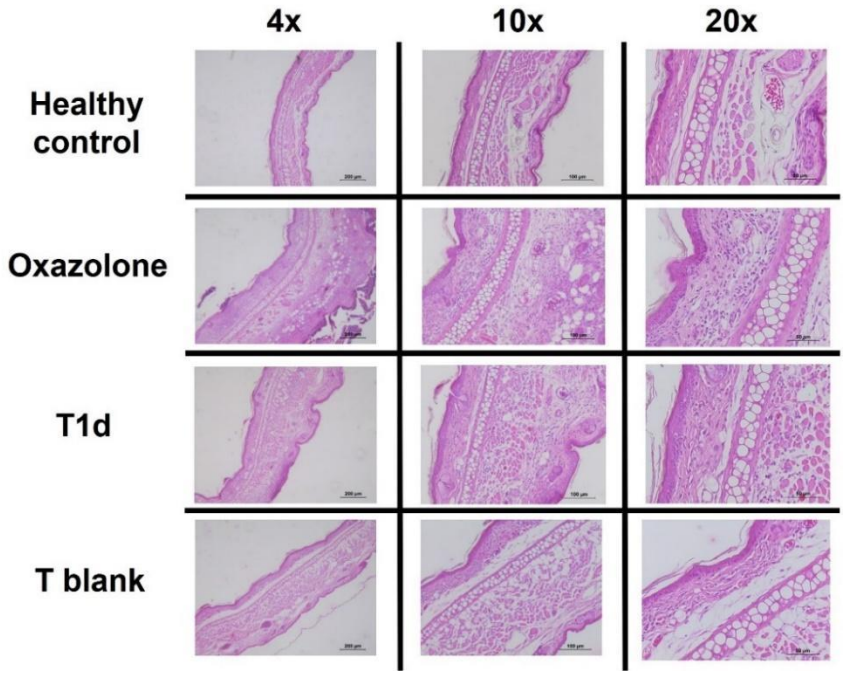


**Figure 8.6.** Representative images from the histological sections stained with eosin-haematoxylin of the groups of interest.

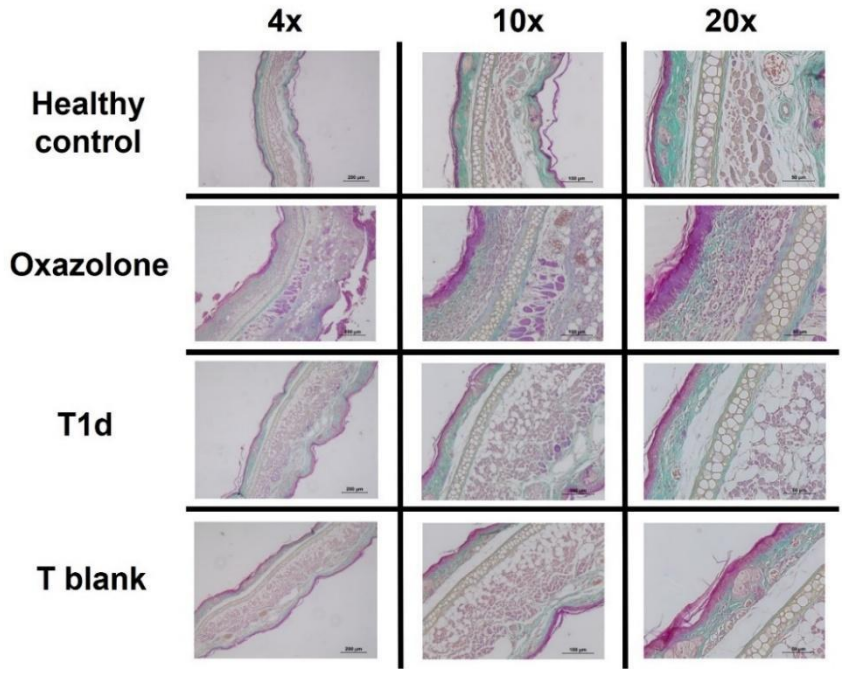


**Figure 8.7.** Representative images from the histological sections stained with Masson's trichrome reagent of the groups of interest.

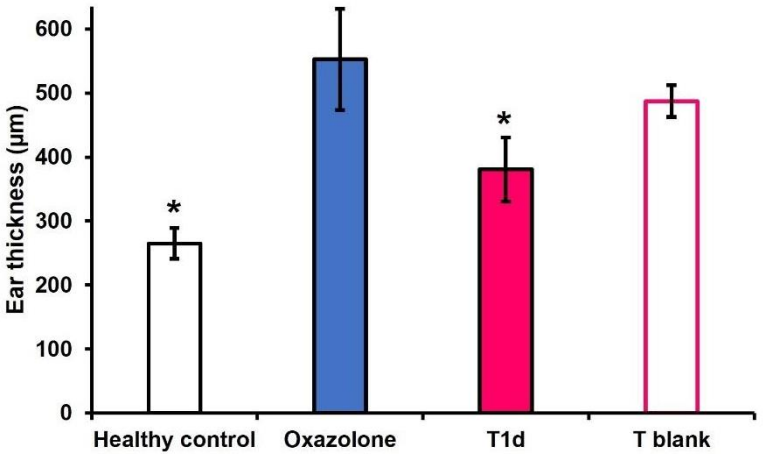


**Figure 8.8.** Ear thickness measurements based on the digital estimation of the groups of interest. * means statistically significant differences when compared to untreated group (OXA) ($p < 0.05$) (n=6).

## 8.3. Milestone and highlights of chapter 8

**Milestone:** Transfersomes (T1d) ameliorated the skin oedema measured as ear thickness in an *in vivo* delayed-type hypersensitivity murine model.

- **Highlight 8.1:** T1d formulation produced a significant reduction of 172 µm in ear thickness increase compared to the untreated control group.
- **Highlight 8.2:** T1d-treated group did not recover the baseline of healthy controls, but the difference between groups was not statistically significant. These results demonstrate that even though T1d could not fully recover the tissue from the pathological process, it contributed to reducing the damage in a considerable manner.
- **Highlight 8.3:** Blank formulations produced a non-significant reduction in ear thickness variation, probably because of the emollient properties of the vesicle-forming lipids and the refreshing ability of the aqueous vehicle. The ear thickness reduction produced by T1d was significantly higher when compared to the blank formulations, thus confirming the effectiveness of T1d.

- **Highlight 8.4:** Leukocyte implication in the pathological process triggered by the OXA challenge was confirmed through BLI assay as an indirect measure of MPO activity. The T1d-treated group showed a similar mitigation to the clobetasol-treated group. Transfersome blank vesicles also produce a partial reduction of cellular infiltration.
- **Highlight 8.5:** Histopathological study of skin sections confirmed the decreased oedema, reduced skin layers thickening, and no increased leukocyte infiltration when contact dermatitis is treated with T1d.

# Chapter 9

## Conclusions

The most relevant conclusions derived from the data obtained in this work are:

**Conclusion 1:** B12 can be detected and quantified by HPLC and spectrophotometry UV-vis.

**Conclusion 2:** Lipid vesicles can be produced and loaded with B12, showing optimal properties for topical and transdermal delivery purposes.

**Conclusion 3:** B12 and freeze-dried lipid vesicles can be successfully formulated as dissolvable MNA devices that present adequate mechanical and insertion properties to effectively bypass the *stratum corneum* and deliver the drug in the dermis.

**Conclusion 4:** *Ex vivo* and *in vitro* penetration and permeability of B12 through the skin can be enhanced using advanced transdermal delivery systems: dissolvable MNA > solid MNA-lipid vesicles combination > transfersomes > ethosomes > conventional liposomes > aqueous solution

**Conclusion 5:** Contact dermatitis and eczema can be ameliorated by the administration of B12-loaded transfersomes which boost the nitric oxide scavenger properties of B12.

# References

1. Prausnitz MR, Mitragotri S, Langer R. Current status and future potential of transdermal drug delivery. Nat Rev Drug Discov. 2004 Feb;3(2):115–24.

2. Alkilani AZ, McCrudden MTC, Donnelly RF. Transdermal Drug Delivery: Innovative Pharmaceutical Developments Based on Disruption of the Barrier Properties of the Stratum Corneum. Pharmaceutics. 2015 Dec;7(4):438–70.

3. Bruce J, Wong I. Parenteral Drug Administration Errors by Nursing Staff on an Acute Medical Admissions Ward During Day Duty. Drug-Safety. 2001 Sep 1;24(11):855–62.

4. Kydonieus AF, Wille JJ. Biochemical Modulation of Skin Reactions: Transdermals, Topicals, Cosmetics. CRC Press; 1999. 352 p.

5. Bruno BJ, Miller GD, Lim CS. Basics and recent advances in peptide and protein drug delivery. Therapeutic Delivery. 2013 Nov 1;4(11):1443–67.

6. Hua S. Physiological and Pharmaceutical Considerations for Rectal Drug Formulations. Frontiers in Pharmacology. 2019;10:1196.

7. Kathe K, Kathpalia H. Film forming systems for topical and transdermal drug delivery. Asian Journal of Pharmaceutical Sciences. 2017 Nov 1;12(6):487–97.

8. Melero A, Guillot A, Carneiro C, Nuñez-Sanchez H, Rodríguez-Martí L, Chiari-Andréo BG, et al. Caffeine analysis and extraction from a topical cream intended for UV-skin protection. Journal of Dispersion Science and Technology. 2020 Nov 27;0(0):1–7.

9. Megna M, Fabbrocini G, Marasca C, Monfrecola G. Photodynamic Therapy and Skin Appendage Disorders: A Review. SAD. 2016;2(3–4):166–76.

10. Lodén M. Role of Topical Emollients and Moisturizers in the Treatment of Dry Skin Barrier Disorders. Am J Clin Dermatol. 2003 Nov 1;4(11):771–88.

11. Lundborg M, Wennberg CL, Narangifard A, Lindahl E, Norlén L. Predicting drug permeability through skin using molecular dynamics simulation. Journal of Controlled Release. 2018 Aug 10;283:269–79.

12. Slominski AT, Zmijewski MA, Skobowiat C, Zbytek B, Slominski RM, Steketee JD. Sensing the environment: regulation of local and global homeostasis by the skin's neuroendocrine system. Adv Anat Embryol Cell Biol. 2012;212:v, vii, 1–115.

13. Sparr E, Millecamps D, Isoir M, Burnier V, Larsson Å, Cabane B. Controlling the hydration of the skin though the application of occluding barrier creams. Journal of The Royal Society Interface. 2013 Mar 6;10(80):20120788.

14. Brenner M, Hearing VJ. The Protective Role of Melanin Against UV Damage in Human Skin†. Photochemistry and Photobiology. 2008;84(3):539–49.

15. Owens DM, Lumpkin EA. Diversification and Specialization of Touch Receptors in Skin. Cold Spring Harb Perspect Med. 2014 Jan 6;4(6):a013656.

16. Kobayashi S. Temperature receptors in cutaneous nerve endings are thermostat molecules that induce thermoregulatory behaviors against thermal load. Temperature (Austin). 2015 Apr 27;2(3):346–51.

17. Foldvari M. Non-invasive administration of drugs through the skin: challenges in delivery system design. Pharmaceutical Science & Technology Today. 2000 Dec 1;3(12):417–25.

18. Koster MI. Making an Epidermis. Annals of the New York Academy of Sciences. 2009;1170(1):7–10.

19. Kim E, Rebecca V, Fedorenko IV, Messina JL, Mathew R, Maria-Engler SS, et al. Senescent Fibroblasts in Melanoma Initiation and Progression: An Integrated Theoretical, Experimental, and Clinical Approach. Cancer Res. 2013 Dec 1;73(23):6874–85.

20. Chantasart D, Li SK. Structure Enhancement Relationship of Chemical Penetration Enhancers in Drug Transport across the Stratum Corneum. Pharmaceutics. 2012 Mar;4(1):71–92.

21. Geyer SH, Nöhammer MM, Tinhofer IE, Weninger WJ. The dermal arteries of the human thumb pad. Journal of Anatomy. 2013;223(6):603–9.

22. Kennedy WR, Wendelschafer-Crabb G. The innervation of human epidermis. Journal of the Neurological Sciences. 1993 Apr 1;115(2):184–90.

23. Aziz J, Shezali H, Radzi Z, Yahya NA, Kassim NHA, Czernuszka J, et al. Molecular Mechanisms of Stress-Responsive Changes in Collagen and Elastin Networks in Skin. SPP. 2016;29(4):190–203.

24. Green EM, Mansfield JC, Bell JS, Winlove CP. The structure and micromechanics of elastic tissue. Interface Focus. 2014 Apr 6;4(2):20130058.

25. Muiznieks LD, Keeley FW. Molecular assembly and mechanical properties of the extracellular matrix: A fibrous protein perspective. Biochim Biophys Acta. 2013 Jul;1832(7):866–75.

26. Roger M, Fullard N, Costello L, Bradbury S, Markiewicz E, O'Reilly S, et al. Bioengineering the microanatomy of human skin. Journal of Anatomy. 2019;234(4):438–55.

27. Yanez DA, Lacher RK, Vidyarthi A, Colegio OR. The role of macrophages in skin homeostasis. Pflugers Arch - Eur J Physiol. 2017 Apr 1;469(3):455–63.

28. Pérez-Sánchez A, Barrajón-Catalán E, Herranz-López M, Micol V. Nutraceuticals for Skin Care: A Comprehensive Review of Human Clinical Studies. Nutrients. 2018 Apr;10(4):403.

29. Mittal B. Subcutaneous adipose tissue & visceral adipose tissue. Indian J Med Res. 2019 May;149(5):571–3.

30. Cassisa A. Pathophysiology of subcutaneous fat. G Ital Dermatol Venereol. 2013 Aug;148(4):315–23.

31. Hwang K, Kim H, Kim DJ. Thickness of skin and subcutaneous tissue of the free flap donor sites: A histologic study. Microsurgery. 2016;36(1):54–8.

32. Weng T, Wu P, Zhang W, Zheng Y, Li Q, Jin R, et al. Regeneration of skin appendages and nerves: current status and further challenges. Journal of Translational Medicine. 2020 Feb 3;18(1):53.

33. Kraft J, Freiman A. Management of acne. CMAJ. 2011 Apr 19;183(7):E430–5.

34. Sardesai VR, Prasad S, Agarwal TD. A Study to Evaluate the Efficacy of Various Topical Treatment Modalities for Alopecia Areata. Int J Trichology. 2012;4(4):265–70.

35. Barry BW. Drug delivery routes in skin: a novel approach. Advanced Drug Delivery Reviews. 2002 Nov 1;54:S31–40.

36. Lademann J, Richter H, Schaefer UF, Blume-Peytavi U, Teichmann A, Otberg N, et al. Hair Follicles – A Long-Term Reservoir for Drug Delivery. SPP. 2006;19(4):232–6.

37. Patzelt A, Lademann J. Recent advances in follicular drug delivery of nanoparticles. Expert Opinion on Drug Delivery. 2020 Jan 2;17(1):49–60.

38. Baroni A, Buommino E, De Gregorio V, Ruocco E, Ruocco V, Wolf R. Structure and function of the epidermis related to barrier properties. Clinics in Dermatology. 2012 May 1;30(3):257–62.

39. Sakabe J ichi, Yamamoto M, Hirakawa S, Motoyama A, Ohta I, Tatsuno K, et al. Kallikrein-related Peptidase 5 Functions in Proteolytic Processing of Profilaggrin in Cultured Human Keratinocytes*. Journal of Biological Chemistry. 2013 Jun 14;288(24):17179–89.

40. Deckers J, Hammad H, Hoste E. Langerhans Cells: Sensing the Environment in Health and Disease. Frontiers in Immunology. 2018;9:93.

41. Mustafa FEZA, Abdel-maksoud FM, Hassan AHS, Mokhtar DM. Melatonin induces a stimulatory action on the scrotal skin components of Soay ram in the non-breeding season. Sci Rep. 2020 Jun 23;10(1):10154.

42. N'Da DD. Prodrug Strategies for Enhancing the Percutaneous Absorption of Drugs. Molecules. 2014 Dec;19(12):20780–807.

43. Mathes C, Melero A, Conrad P, Vogt T, Rigo L, Selzer D, et al. Nanocarriers for optimizing the balance between interfollicular permeation and follicular uptake of topically applied clobetasol to minimize adverse effects. Journal of Controlled Release. 2016 Feb 10;223:207–14.

44. Fox LT, Gerber M, Plessis JD, Hamman JH. Transdermal Drug Delivery Enhancement by Compounds of Natural Origin. Molecules. 2011 Dec;16(12):10507–40.

45. Hadgraft J. Skin, the final frontier. International Journal of Pharmaceutics. 2001 Aug 14;224(1):1–18.

46. Mitragotri S, Anissimov YG, Bunge AL, Frasch HF, Guy RH, Hadgraft J, et al. Mathematical models of skin permeability: An overview. International Journal of Pharmaceutics. 2011 Oct 10;418(1):115–29.

47. Singh S, Singh J. Transdermal drug delivery by passive diffusion and iontophoresis: A review. Medicinal Research Reviews. 1993;13(5):569–621.

48. Bos JD, Meinardi MMHM. The 500 Dalton rule for the skin penetration of chemical compounds and drugs. Experimental Dermatology. 2000;9(3):165–9.

49. Andrews SN, Jeong E, Prausnitz MR. Transdermal Delivery of Molecules is Limited by Full Epidermis, Not Just Stratum Corneum. Pharm Res. 2013 Apr 1;30(4):1099–109.

50. Melero A, Garrigues TM, Almudever P, Villodre AMN, Lehr CM, Schäfer U. Nortriptyline hydrochloride skin absorption: development of a transdermal patch. Eur J Pharm Biopharm. 2008 Jun;69(2):588–96.

51. Melero A, Garrigues TM, Alós M, Kostka KH, Lehr CM, Schaefer UF. Nortriptyline for smoking cessation: release and human skin diffusion from patches. Int J Pharm. 2009 Aug 13;378(1–2):101–7.

52. Baert B, Boonen J, Burvenich C, Roche N, Stillaert F, Blondeel P, et al. A new discriminative criterion for the development of Franz diffusion tests for transdermal pharmaceuticals. J Pharm Pharm Sci. 2010;13(2):218–30.

53. Pineau A, Guillard O, Favreau F, Marty MH, Gaudin A, Vincent CM, et al. In vitro study of percutaneous absorption of aluminum from antiperspirants through human skin in the Franz™ diffusion cell. J Inorg Biochem. 2012 May;110:21–6.

54. Intarakumhaeng R, Wanasathop A, Li SK. Effects of solvents on skin absorption of nonvolatile lipophilic and polar solutes under finite dose conditions. International Journal of Pharmaceutics. 2018 Jan 30;536(1):405–13.

55. Coderch L, Collini I, Carrer V, Barba C, Alonso C. Assessment of Finite and Infinite Dose In Vitro Experiments in Transdermal Drug Delivery. Pharmaceutics. 2021 Mar;13(3):364.

56. Bartosova L, Bajgar J. Transdermal drug delivery in vitro using diffusion cells. Curr Med Chem. 2012;19(27):4671–7.

57. Klein S. Influence of different test parameters on in vitro drug release from topical diclofenac formulations in a vertical diffusion cell setup. Pharmazie. 2013 Jul;68(7):565–71.

58. Ng SF, Rouse JJ, Sanderson FD, Meidan V, Eccleston GM. Validation of a static Franz diffusion cell system for in vitro permeation studies. AAPS PharmSciTech. 2010 Sep;11(3):1432–41.

59. Todo H. Transdermal Permeation of Drugs in Various Animal Species. Pharmaceutics. 2017 Sep 6;9(3):E33.

60. Southwell D, Barry BW, Woodford R. Variations in permeability of human skin within and between specimens. International Journal of Pharmaceutics. 1984 Feb 1;18(3):299–309.

61. Akomeah FK, Martin GP, Brown MB. Variability in human skin permeability in vitro: comparing penetrants with different physicochemical properties. J Pharm Sci. 2007 Apr;96(4):824–34.

62. Qvist MH, Hoeck U, Kreilgaard B, Madsen F, Frokjaer S. Evaluation of Göttingen minipig skin for transdermal in vitro permeation studies. Eur J Pharm Sci. 2000 Jul;11(1):59–68.

63. Khiao In M, Richardson KC, Loewa A, Hedtrich S, Kaessmeyer S, Plendl J. Histological and functional comparisons of four anatomical regions of porcine skin with human abdominal skin. Anat Histol Embryol. 2019 May;48(3):207–17.

64. Debeer S, Le Luduec JB, Kaiserlian D, Laurent P, Nicolas JF, Dubois B, et al. Comparative histology and immunohistochemistry of porcine versus human skin. Eur J Dermatol. 2013 Aug;23(4):456–66.

65. Simon GA, Maibach HI. The pig as an experimental animal model of percutaneous permeation in man: qualitative and quantitative observations--an overview. Skin Pharmacol Appl Skin Physiol. 2000 Oct;13(5):229–34.

66. van Ravenzwaay B, Leibold E. A comparison between in vitro rat and human and in vivo rat skin absorption studies. Hum Exp Toxicol. 2004 Aug;23(9):421–30.

67. Takeuchi H, Mano Y, Terasaka S, Sakurai T, Furuya A, Urano H, et al. Usefulness of rat skin as a substitute for human skin in the in vitro skin permeation study. Exp Anim. 2011;60(4):373–84.

68. Bartek MJ, LaBudde JA, Maibach HI. Skin permeability in vivo: comparison in rat, rabbit, pig and man. J Invest Dermatol. 1972 Mar;58(3):114–23.

69. Takeuchi H, Ishida M, Furuya A, Todo H, Urano H, Sugibayashi K. Influence of skin thickness on the in vitro permeabilities of drugs through Sprague-Dawley rat or Yucatan micropig skin. Biol Pharm Bull. 2012;35(2):192–202.

70. Kligman AM, Christophers E. Preparation of isolated sheets of human stratum corneum. Arch Dermatol. 1963 Dec;88:702–5.

71. Zaman M, Khalid U, Abdul Ghafoor Raja M, Siddique W, Sultana K, Amjad MW, et al. Fabrication and Characterization of Matrix-Type Transdermal Patches Loaded with Ramipril and Repaglinide Through Cellulose-based Hydrophilic and Hydrophobic Polymers: In Vitro and Ex Vivo Permeation Studies. Polymer-Plastics Technology and Engineering. 2017 Nov 2;56(16):1713–22.

72. Ng SF, Rouse J, Sanderson D, Eccleston G. A Comparative Study of Transmembrane Diffusion and Permeation of Ibuprofen across Synthetic Membranes Using Franz Diffusion Cells. Pharmaceutics. 2010 May 18;2(2):209–23.

73. Simon A, Amaro MI, Healy AM, Cabral LM, de Sousa VP. Comparative evaluation of rivastigmine permeation from a transdermal system in the Franz cell using synthetic membranes and pig ear skin with in vivo-in vitro correlation. Int J Pharm. 2016 Oct 15;512(1):234–41.

74. Van Gele M, Geusens B, Brochez L, Speeckaert R, Lambert J. Three-dimensional skin models as tools for transdermal drug delivery: challenges and limitations. Expert Opin Drug Deliv. 2011 Jun;8(6):705–20.

75. Netzlaff F, Lehr CM, Wertz PW, Schaefer UF. The human epidermis models EpiSkin, SkinEthic and EpiDerm: an evaluation of morphology and their suitability for testing phototoxicity, irritancy, corrosivity, and substance transport. Eur J Pharm Biopharm. 2005 Jul;60(2):167–78.

76. Hou X, Liu S, Wang M, Wiraja C, Huang W, Chan P, et al. Layer-by-Layer 3D Constructs of Fibroblasts in Hydrogel for Examining Transdermal Penetration Capability of Nanoparticles. SLAS Technol. 2017 Aug;22(4):447–53.

77. Rapalli VK, Singhvi G. Dermato-pharmacokinetic: assessment tools for topically applied dosage forms. Expert Opinion on Drug Delivery. 2021 Apr 3;18(4):423–6.

78. Wachsman W, Morhenn V, Palmer T, Walls L, Hata T, Zalla J, et al. Noninvasive genomic detection of melanoma. British Journal of Dermatology. 2011;164(4):797–806.

79. Guillot AJ, Jornet-Mollá E, Landsberg N, Milián-Guimerá C, Montesinos MC, Garrigues TM, et al. Cyanocobalamin Ultraflexible Lipid Vesicles: Characterization and In Vitro Evaluation of Drug-Skin Depth Profiles. Pharmaceutics. 2021 Mar;13(3):418.

80. Lademann J, Jacobi U, Surber C, Weigmann HJ, Fluhr JW. The tape stripping procedure – evaluation of some critical parameters. European Journal of Pharmaceutics and Biopharmaceutics. 2009 Jun 1;72(2):317–23.

81. Voegeli R, Heiland J, Doppler S, Rawlings AV, Schreier T. Efficient and simple quantification of stratum corneum proteins on tape strippings by infrared densitometry. Skin Res Technol. 2007 Aug;13(3):242–51.

82. Klang V, Schwarz JC, Lenobel B, Nadj M, Auböck J, Wolzt M, et al. In vitro vs. in vivo tape stripping: validation of the porcine ear model and penetration assessment of novel sucrose stearate emulsions. Eur J Pharm Biopharm. 2012 Apr;80(3):604–14.

83. Wagner H, Kostka KH, Lehr CM, Schaefer UF. Drug distribution in human skin using two different in vitro test systems: comparison with in vivo data. Pharm Res. 2000 Dec;17(12):1475–81.

84. de Oliveira D, de Andrade DF, de Oliveira EG, Beck RCR. Liquid chromatography method to assay tretinoin in skin layers: validation and application in skin penetration/retention studies. Heliyon. 2020 Jan 1;6(1):e03098.

85. Hoppel M, Baurecht D, Holper E, Mahrhauser D, Valenta C. Validation of the combined ATR-FTIR/tape stripping technique for monitoring the distribution of surfactants in the stratum corneum. Int J Pharm. 2014 Sep 10;472(1–2):88–93.

86. Khurana S, Jain NK, Bedi PMS. Nanoemulsion based gel for transdermal delivery of meloxicam: Physico-chemical, mechanistic investigation. Life Sciences. 2013 Mar 14;92(6):383–92.

87. Hussain A, Samad A, Singh SK, Ahsan MN, Haque MW, Faruk A, et al. Nanoemulsion gel-based topical delivery of an antifungal drug: in vitro activity and in vivo evaluation. Drug Delivery. 2016 Feb 12;23(2):642–57.

88. Förster M, Bolzinger MA, Rovere MR, Damour O, Montagnac G, Briançon S. Confocal Raman microspectroscopy for evaluating the stratum corneum removal by 3 standard methods. Skin Pharmacol Physiol. 2011;24(2):103–12.

89. Baby A, Lacerda A, Kawano Y, Velasco M, Kaneko T. PAS-FTIR and FT-Raman qualitative characterization of sodium dodecyl sulfate interaction with an alternative stratum corneum model membrane. Die Pharmazie. 2007 Nov 1;62:727–31.

90. Löffler H, Dreher F, Maibach H i. Stratum corneum adhesive tape stripping: influence of anatomical site, application pressure, duration and removal. British Journal of Dermatology. 2004;151(4):746–52.

91. Surber C, Schwarb FP, Smith EW. Tape-stripping technique. Journal of Toxicology: Cutaneous and Ocular Toxicology. 2001 Jan 1;20(4):461–74.

92. Teichmann A, Jacobi U, Ossadnik M, Richter H, Koch S, Sterry W, et al. Differential Stripping: Determination of the Amount of Topically Applied Substances Penetrated into the Hair Follicles. Journal of Investigative Dermatology. 2005 Aug 1;125(2):264–9.

93. Raber AS, Mittal A, Schäfer J, Bakowsky U, Reichrath J, Vogt T, et al. Quantification of nanoparticle uptake into hair follicles in pig ear and human forearm. Journal of Controlled Release. 2014 Apr 10;179:25–32.

94. Carolina Oliveira dos Santos L, Spagnol CM, Guillot AJ, Melero A, Corrêa MA. Caffeic acid skin absorption: Delivery of microparticles to hair follicles. Saudi Pharmaceutical Journal. 2019 Sep 1;27(6):791–7.

95. Melero A, Ferreira Ourique A, Stanisçuaski Guterres S, Raffin Pohlmann A, Lehr CM, Ruver Beck RC, et al. Nanoencapsulation in lipid-core nanocapsules controls mometasone furoate skin permeability rate and its penetration to the deeper skin layers. Skin Pharmacol Physiol. 2014;27(4):217.

96. Cevc G, Schätzlein A, Richardsen H. Ultradeformable lipid vesicles can penetrate the skin and other semi-permeable barriers unfragmented. Evidence from double label CLSM experiments and direct size measurements. Biochimica et Biophysica Acta (BBA) - Biomembranes. 2002 Aug 19;1564(1):21–30.

97. Abdel-Hafez SM, Hathout RM, Sammour OA. Tracking the transdermal penetration pathways of optimized curcumin-loaded chitosan nanoparticles via confocal laser scanning microscopy. Int J Biol Macromol. 2018 Mar;108:753–64.

98. Kirjavainen M, Urtti A, Jääskeläinen I, Suhonen TM, Paronen P, Valjakka-Koskela R, et al. Interaction of liposomes with human skin in vitro--the influence of lipid composition and structure. Biochim Biophys Acta. 1996 Dec 13;1304(3):179–89.

99. Kathuria H, Handral HK, Cha S, Nguyen DTP, Cai J, Cao T, et al. Enhancement of Skin Delivery of Drugs Using Proposome Depends on Drug Lipophilicity. Pharmaceutics. 2021 Sep;13(9):1457.

100. Ilie MA, Caruntu C, Lupu M, Lixandru D, Tampa M, Georgescu SR, et al. Current and future applications of confocal laser scanning microscopy imaging in skin oncology. Oncol Lett. 2019 May;17(5):4102–11.

101. Krammer S, Krammer C, Vladimirova G, Salzer S, Ruini C, Sattler E, et al. Ex vivo Confocal Laser Scanning Microscopy: A Potential New Diagnostic Imaging Tool in Onychomycosis Comparable With Gold Standard Techniques. Front Med (Lausanne). 2020 Nov 6;7:586648.

102. Niu XQ, Zhang DP, Bian Q, Feng XF, Li H, Rao YF, et al. Mechanism investigation of ethosomes transdermal permeation. International Journal of Pharmaceutics: X. 2019 Dec 1;1:100027.

103. Holmgaard R, Nielsen JB, Benfeldt E. Microdialysis Sampling for Investigations of Bioavailability and Bioequivalence of Topically Administered Drugs: Current State and Future Perspectives. SPP. 2010;23(5):225–43.

104. Baumann KY, Church MK, Clough GF, Quist SR, Schmelz M, Skov PS, et al. Skin microdialysis: methods, applications and future opportunities—an EAACI position paper. Clinical and Translational Allergy. 2019 Apr 10;9(1):24.

105. Voelkner NMF, Voelkner A, Derendorf H. Determination of Dermal Pharmacokinetics by Microdialysis Sampling in Rats. Curr Protoc Pharmacol. 2019 Jun;85(1):e58.

106. Davies MI, Cooper JD, Desmond SS, Lunte CE, Lunte SM. Analytical considerations for microdialysis sampling. Advanced Drug Delivery Reviews. 2000 Dec 15;45(2):169–88.

107. Kho CM, Enche Ab Rahim SK, Ahmad ZA, Abdullah NS. A Review on Microdialysis Calibration Methods: the Theory and Current Related Efforts. Mol Neurobiol. 2017 Jul;54(5):3506–27.

108. Groth L. Cutaneous microdialysis. Methodology and validation. Acta Derm Venereol Suppl (Stockh). 1996;197:1–61.

109. Matsumoto K, Kitaoka M, Kuroda Y, Ikawa K, Morikawa N, Sasaki J, et al. Pharmacokinetics and skin-tissue penetration of daptomycin in rats. Clin Pharmacol. 2015;7:79–82.

110. Parasuraman S, Raveendran R, Kesavan R. Blood sample collection in small laboratory animals. J Pharmacol Pharmacother. 2010;1(2):87–93.

111. Kim HJ, Kim B, Park BM, Jeon JE, Lee SH, Mann S, et al. Topical cannabinoid receptor 1 agonist attenuates the cutaneous inflammatory responses in oxazolone-induced atopic dermatitis model. International Journal of Dermatology. 2015;54(10):e401–8.

112. Li Q, Liu W, Gao S, Mao Y, Xin Y. Application of imiquimod-induced murine psoriasis model in evaluating interleukin-17A antagonist. BMC Immunology. 2021 Jan 28;22(1):11.

113. Lelliott EJ, Cullinane C, Martin CA, Walker R, Ramsbottom KM, Souza-Fonseca-Guimaraes F, et al. A novel immunogenic mouse model of melanoma for the preclinical assessment of combination targeted and immune-based therapy. Sci Rep. 2019 Feb 4;9(1):1225.

114. Fang JY, Lin CH, Huang TH, Chuang SY. In Vivo Rodent Models of Type 2 Diabetes and Their Usefulness for Evaluating Flavonoid Bioactivity. Nutrients. 2019 Feb 28;11(3):530.

115. Ahad A, Aqil M, Kohli K, Sultana Y, Mujeeb M. Nano vesicular lipid carriers of angiotensin II receptor blocker: Anti-hypertensive and skin toxicity study in focus. Artif Cells Nanomed Biotechnol. 2016 May;44(3):1002–7.

116. Clemensen J, Rasmussen LV, Abelson KSP. Transdermal Fentanyl Solution Provides Long-term Analgesia in the Hind-paw Incisional Model of Postoperative Pain in Male Rats. In Vivo. 2018 Aug;32(4):713–9.

117. Roseboom IC, Rosing H, Beijnen JH, Dorlo TPC. Skin tissue sample collection, sample homogenization, and analyte extraction strategies for liquid chromatographic mass spectrometry quantification of pharmaceutical compounds. Journal of Pharmaceutical and Biomedical Analysis. 2020 Nov 30;191:113590.

118. Rujimongkon K, Ampawong S, Reamtong O, Buaban T, Aramwit P. The therapeutic effects of Bombyx mori sericin on rat skin psoriasis through modulated epidermal immunity and attenuated cell proliferation. J Tradit Complement Med. 2021 Jul 1;11(6):587–97.

119. Hood BL, Grahovac J, Flint MS, Sun M, Charro N, Becker D, et al. Proteomic Analysis of Laser Microdissected Melanoma Cells from Skin Organ Cultures. J Proteome Res. 2010 Jul 2;9(7):3656–63.

120. Brannan JL, Holman PJ, Olafson PU, Pruett JH, Riggs PK. Evaluation of methods for the isolation of high quality RNA from bovine and cervine hide biopsies. J Parasitol. 2013 Feb;99(1):19–23.

121. Lerche CM, Olsen P, Nissen CV, Philipsen PA, Wulf HC. A novel LC-MS/MS method to quantify eumelanin and pheomelanin and their relation to UVR sensitivity - A study on human skin biopsies. Pigment Cell Melanoma Res. 2019 Nov;32(6):809–16.

122. Nirogi R, Padala NSP, Boggavarapu RK, Kalaikadhiban I, Ajjala DR, Bhyrapuneni G, et al. Skin sample preparation by collagenase digestion for diclofenac quantification using LC–MS/MS after topical application. Bioanalysis. 2016 Jun 1;8(12):1251–63.

123. Wingfield PT. Protein Precipitation Using Ammonium Sulfate. Curr Protoc Protein Sci. 2001 May;APPENDIX 3:Appendix-3F.

124. Green R. Vitamin B12 deficiency from the perspective of a practicing hematologist. Blood. 2017 May 11;129(19):2603–11.

125. Bottiglieri T. Folate, vitamin B12, and neuropsychiatric disorders. Nutr Rev. 1996 Dec;54(12):382–90.

126. Lachner C, Steinle NI, Regenold WT. The neuropsychiatry of vitamin B12 deficiency in elderly patients. J Neuropsychiatry Clin Neurosci. 2012;24(1):5–15.

127. Rannelli L, Watterson R, Pandya R, Leung AA. Vitamin B12 deficiency with combined hematological and neuropsychiatric derangements: a case report. J Med Case Rep. 2014 Aug 15;8:277.

128. Langan RC, Goodbred AJ. Vitamin B12 Deficiency: Recognition and Management. Am Fam Physician. 2017 Sep 15;96(6):384–9.

129. Green R, Allen LH, Bjørke-Monsen AL, Brito A, Guéant JL, Miller JW, et al. Vitamin B 12 deficiency. Nat Rev Dis Primers. 2017 Jun 29;3(1):1–20.

130. Green R, Kinsella LJ. Current concepts in the diagnosis of cobalamin deficiency. Neurology. 1995 Aug;45(8):1435–40.

131. Sharma GS, Kumar T, Singh LR. N-homocysteinylation induces different structural and functional consequences on acidic and basic proteins. PLoS One. 2014;9(12):e116386.

132. Shipton MJ, Thachil J. Vitamin B12 deficiency - A 21st century perspective. Clin Med (Lond). 2015 Apr;15(2):145–50.

133. Guéant JL, Safi A, Aimone-Gastin I, Rabesona H, Bronowicki JP, Plénat F, et al. Autoantibodies in pernicious anemia type I patients recognize sequence 251-256 in human intrinsic factor. Proc Assoc Am Physicians. 1997 Sep;109(5):462–9.

134. Schjønsby H. Vitamin B12 absorption and malabsorption. Gut. 1989 Dec;30(12):1686–91.

135. Merchant JL. Parietal Cell Death by Cytokines. Cell Mol Gastroenterol Hepatol. 2018 Feb 15;5(4):636–7.

136. Behrend C, Jeppesen PB, Mortensen PB. Vitamin B12 absorption after ileorectal anastomosis for Crohn's disease: effect of ileal resection and time span after surgery. Eur J Gastroenterol Hepatol. 1995 May;7(5):397–400.

137. Streeter AM, Duraiappah B, Boyle R, O'Neill BJ, Pheils MT. Malabsorption of vitamin B12 after vagotomy. The American Journal of Surgery. 1974 Sep 1;128(3):340–3.

138. Duerksen DR, Fallows G, Bernstein CN. Vitamin B12 malabsorption in patients with limited ileal resection. Nutrition. 2006 Dec;22(11–12):1210–3.

139. Ward MG, Kariyawasam VC, Mogan SB, Patel KV, Pantelidou M, Sobczyńska-Malefora A, et al. Prevalence and Risk Factors for Functional Vitamin B12 Deficiency in Patients with Crohn's Disease. Inflamm Bowel Dis. 2015 Dec;21(12):2839–47.

140. Sharma K, Wijarnpreecha K, Merrell N. Diphyllobothrium latum Mimicking Subacute Appendicitis. Gastroenterology Res. 2018 Jun;11(3):235–7.

141. Rizzo G, Laganà AS, Rapisarda AMC, La Ferrera GMG, Buscema M, Rossetti P, et al. Vitamin B12 among Vegetarians: Status, Assessment and Supplementation. Nutrients. 2016 Nov 29;8(12):767.

142. Pawlak R, Lester SE, Babatunde T. The prevalence of cobalamin deficiency among vegetarians assessed by serum vitamin B12: a review of literature. Eur J Clin Nutr. 2014 May;68(5):541–8.

143. Sebastiani G, Herranz Barbero A, Borrás-Novell C, Alsina Casanova M, Aldecoa-Bilbao V, Andreu-Fernández V, et al. The Effects of Vegetarian and Vegan Diet during Pregnancy on the Health of Mothers and Offspring. Nutrients. 2019 Mar 6;11(3):557.

144. Ünal Ş, Rupar T, Yetgin S, Yaralı N, Dursun A, Gürsel T, et al. Transcobalamin II Deficiency in Four Cases with Novel Mutations. Turk J Haematol. 2015 Dec;32(4):317–22.

145. Mohn ES, Kern HJ, Saltzman E, Mitmesser SH, McKay DL. Evidence of Drug–Nutrient Interactions with Chronic Use of Commonly Prescribed Medications: An Update. Pharmaceutics. 2018 Mar 20;10(1):36.

146. Miller JW. Proton Pump Inhibitors, H2-Receptor Antagonists, Metformin, and Vitamin B-12 Deficiency: Clinical Implications. Adv Nutr. 2018 Jul 1;9(4):511S-518S.

147. Allen LH. How common is vitamin B-12 deficiency? Am J Clin Nutr. 2009 Feb;89(2):693S-6S.

148. Koenig V, Stanga Z, Zerlauth M, Bernasconi L, Risch M, Huber A, et al. Prevalence of vitamin B12 depletion and deficiency in Liechtenstein. Public Health Nutrition. 2014 Feb;17(2):241–7.

149. Carmel R. How I treat cobalamin (vitamin B12) deficiency. Blood. 2008 Sep 15;112(6):2214–21.

150. Ungley CC. Absorption of vitamin B12 in pernicious anaemia. I. Oral administration without a source of intrinsic factor. Br Med J. 1950 Oct 21;2(4685):905–8.

151. Elia M. Oral or parenteral therapy for B12 deficiency. Lancet. 1998 Nov 28;352(9142):1721–2.

152. Chan CQH, Low LL, Lee KH. Oral Vitamin B12 Replacement for the Treatment of Pernicious Anemia. Front Med (Lausanne). 2016 Aug 23;3:38.

153. Oh R, Brown DL. Vitamin B12 deficiency. Am Fam Physician. 2003 Mar 1;67(5):979–86.

154. Rodger MA, King L. Drawing up and administering intramuscular injections: a review of the literature. J Adv Nurs. 2000 Mar;31(3):574–82.

155. Shah BS, Yarbrough C, Price A, Biswas R. An unfortunate injection. BMJ Case Rep. 2016 Mar 1;2016:bcr2015211127.

156. Soliman E, Ranjan S, Xu T, Gee C, Harker A, Barrera A, et al. A narrative review of the success of intramuscular gluteal injections and its impact in psychiatry. Biodes Manuf. 2018;1(3):161–70.

157. Adler-Neal AL, Cline A, Frantz T, Strowd L, Feldman SR, Taylor S. Complementary and Integrative Therapies for Childhood Atopic Dermatitis. Children (Basel). 2019 Oct 30;6(11):E121.

158. Kapur S, Watson W, Carr S. Atopic dermatitis. Allergy Asthma Clin Immunol. 2018;14(Suppl 2):52.

159. Hirabayashi T, Anjo T, Kaneko A, Senoo Y, Shibata A, Takama H, et al. PNPLA1 has a crucial role in skin barrier function by directing acylceramide biosynthesis. Nat Commun. 2017 Mar 1;8:14609.

160. Agrawal R, Woodfolk JA. Skin barrier defects in atopic dermatitis. Curr Allergy Asthma Rep. 2014 May;14(5):433.

161. Zaniboni MC, Samorano LP, Orfali RL, Aoki V. Skin barrier in atopic dermatitis: beyond filaggrin. An Bras Dermatol. 2016 Aug;91(4):472–8.

162. Kolb L, Ferrer-Bruker SJ. Atopic Dermatitis. In: StatPearls [Internet]. Treasure Island (FL): StatPearls Publishing; 2022 [cited 2022 Mar 30]. Available from: http://www.ncbi.nlm.nih.gov/books/NBK448071/

163. Parisi R, Symmons DPM, Griffiths CEM, Ashcroft DM, Identification and Management of Psoriasis and Associated ComorbidiTy (IMPACT) project team. Global epidemiology of psoriasis: a systematic review of incidence and prevalence. J Invest Dermatol. 2013 Feb;133(2):377–85.

164. Arima K, Ohta S, Takagi A, Shiraishi H, Masuoka M, Ontsuka K, et al. Periostin contributes to epidermal hyperplasia in psoriasis common to atopic dermatitis. Allergol Int. 2015 Jan;64(1):41–8.

165. Heidenreich R, Röcken M, Ghoreschi K. Angiogenesis drives psoriasis pathogenesis. Int J Exp Pathol. 2009 Jun;90(3):232–48.

166. Nussbaum L, Chen YL, Ogg GS. Role of regulatory T cells in psoriasis pathogenesis and treatment. Br J Dermatol. 2021 Jan;184(1):14–24.

167. Badri T, Kumar P, Oakley AM. Plaque Psoriasis. In: StatPearls [Internet]. Treasure Island (FL): StatPearls Publishing; 2022 [cited 2022 Mar 30]. Available from: http://www.ncbi.nlm.nih.gov/books/NBK430879/

168. Thomsen SF. Atopic dermatitis: natural history, diagnosis, and treatment. ISRN Allergy. 2014;2014:354250.

169. Fiore M, Leone S, Maraolo AE, Berti E, Damiani G. Liver Illness and Psoriatic Patients. Biomed Res Int. 2018;2018:3140983.

170. Grandinetti V, Baraldi O, Comai G, Corradetti V, Aiello V, Bini C, et al. Renal dysfunction in psoriatic patients. G Ital Nefrol. 2020 Feb 12;37(1):2020-vol1.

171. Jindal N, Arora K, Jindal P, Jain VK, Ghosh S. Inflamed psoriatic plaques: Drug toxicity or disease exacerbation? Indian Journal of Pharmacology. 2013 Jan 7;45(4):410.

172. Oray M, Abu Samra K, Ebrahimiadib N, Meese H, Foster CS. Long-term side effects of glucocorticoids. Expert Opinion on Drug Safety. 2016 Apr 2;15(4):457–65.

173. Siegfried EC, Jaworski JC, Hebert AA. Topical Calcineurin Inhibitors and Lymphoma Risk: Evidence Update with Implications for Daily Practice. Am J Clin Dermatol. 2013 Jun 1;14(3):163–78.

174. Sirsjö A, Karlsson M, Gidlöf A, Rollman O, Törmä H. Increased expression of inducible nitric oxide synthase in psoriatic skin and cytokine-stimulated cultured keratinocytes. Br J Dermatol. 1996 Apr;134(4):643–8.

175. Akdeniz N, Aktaş A, Erdem T, Akyüz M, Özdemir Ş. Nitric oxide levels in atopic dermatitis. The Pain Clinic. 2004 Oct 1;16(4):401–5.

176. Brescoll J, Daveluy S. A review of vitamin B12 in dermatology. Am J Clin Dermatol. 2015 Feb;16(1):27–33.

177. Baker H, Comaish JS. Is Vitamin B12 of Value in Psoriasis? Br Med J. 1962 Dec 29;2(5321):1729–30.

178. Januchowski R. Evaluation of Topical Vitamin B12 for the Treatment of Childhood Eczema. The Journal of Alternative and Complementary Medicine. 2009 Apr;15(4):387–9.

179. Stücker M, Memmel U, Hoffmann M, Hartung J, Altmeyer P. Vitamin B(12) cream containing avocado oil in the therapy of plaque psoriasis. Dermatology. 2001;203(2):141–7.

180. Del Duca E, Farnetani F, De Carvalho N, Bottoni U, Pellacani G, Nisticò SP. Superiority of a vitamin B12-containing emollient compared to a standard emollient in the maintenance treatment of mild-to-moderate plaque psoriasis. Int J Immunopathol Pharmacol. 2017 Dec;30(4):439–44.

181. Wilkinson JB, Moore RJ. Harry's cosmeticology [Internet]. Longman Scientific & Technical; 1982 [cited 2022 Mar 31]. Available from: http://localhost:8080/xmlui/handle/123456789/784

182. Paudel KS, Milewski M, Swadley CL, Brogden NK, Ghosh P, Stinchcomb AL. Challenges and opportunities in dermal/transdermal delivery. Ther Deliv. 2010 Jul;1(1):109–31.

183. Reginster JY, Donazzolo Y, Brion N, Lins R. Estradiol pharmacokinetics after transdermal application of patches to postmenopausal women: matrix versus reservoir patches. Climacteric. 2000 Jan 1;3(3):168–75.

184. Bertonazzi A, Nelson B, Salvador J, Umland E. The Smallest Available Estradiol Transdermal Patch: A New Treatment Option for the Prevention of Postmenopausal Osteoporosis. Womens Health (Lond Engl). 2015 Nov 1;11(6):815–24.

185. Grissinger M. Fentanyl Transdermal Patches. P T. 2009 Jul;34(7):343–90.

186. Chai SH, Leventhal AM, Kirkpatrick MG, Eisenlohr-Moul TA, Rapkin AJ, D'Orazio L, et al. Effectiveness of transdermal nicotine patch in premenopausal female smokers is moderated by within-subject severity of negative affect and physical symptoms. Psychopharmacology. 2020 Jun 1;237(6):1737–44.

187. Wasley MA, McNagny SE, Phillips VL, Ahluwalia JS. The Cost-Effectiveness of the Nicotine Transdermal Patch for Smoking Cessation. Preventive Medicine. 1997 Mar 1;26(2):264–70.

188. Alexander A, Dwivedi S, Ajazuddin, Giri TK, Saraf S, Saraf S, et al. Approaches for breaking the barriers of drug permeation through transdermal drug delivery. Journal of Controlled Release. 2012 Nov 28;164(1):26–40.

189. Ramadon D, McCrudden MTC, Courtenay AJ, Donnelly RF. Enhancement strategies for transdermal drug delivery systems: current trends and applications. Drug Deliv Transl Res. 2022 Apr;12(4):758–91.

190. Kim B, Cho HE, Moon SH, Ahn HJ, Bae S, Cho HD, et al. Transdermal delivery systems in cosmetics. Biomedical Dermatology. 2020 Apr 7;4(1):10.

191. Asbill CS, El-Kattan AF, Michniak B. Enhancement of transdermal drug delivery: chemical and physical approaches. Crit Rev Ther Drug Carrier Syst. 2000;17(6):621–58.

192. Hadgraft J, Lane ME. Passive transdermal drug delivery systems. Am J Drug Deliv. 2006 Sep 1;4(3):153–60.

193. Williams AC, Barry BW. Penetration enhancers. Advanced Drug Delivery Reviews. 2004 Mar 27;56(5):603–18.

194. Jeevanandam J, Barhoum A, Chan YS, Dufresne A, Danquah MK. Review on nanoparticles and nanostructured materials: history, sources, toxicity and regulations. Beilstein J Nanotechnol. 2018 Apr 3;9(1):1050–74.

195. Park K. Nanotechnology: What it can do for drug delivery. J Control Release. 2007 Jul 16;120(1–2):1–3.

196. Bangham AD, Standish MM, Watkins JC. Diffusion of univalent ions across the lamellae of swollen phospholipids. J Mol Biol. 1965 Aug;13(1):238–52.

197. Bangham AD. Liposomes: the Babraham connection. Chem Phys Lipids. 1993 Sep;64(1–3):275–85.

198. Cevc G, Blume G. Lipid vesicles penetrate into intact skin owing to the transdermal osmotic gradients and hydration force. Biochim Biophys Acta. 1992 Feb 17;1104(1):226–32.

199. Touitou E, Dayan N, Bergelson L, Godin B, Eliaz M. Ethosomes — novel vesicular carriers for enhanced delivery: characterization and skin penetration properties. Journal of Controlled Release. 2000 Apr 3;65(3):403–18.

200. Albash R, Abdelbary AA, Refai H, El-Nabarawi MA. Use of transethosomes for enhancing the transdermal delivery of olmesartan medoxomil: in vitro, ex vivo, and in vivo evaluation. Int J Nanomedicine. 2019;14:1953–68.

201. Manca ML, Zaru M, Manconi M, Lai F, Valenti D, Sinico C, et al. Glycerosomes: a new tool for effective dermal and transdermal drug delivery. Int J Pharm. 2013 Oct 15;455(1–2):66–74.

202. Casula E, Manca ML, Perra M, Pedraz JL, Lopez-Mendez TB, Lozano A, et al. Nasal Spray Formulations Based on Combined Hyalurosomes and Glycerosomes Loading Zingiber officinalis Extract as Green and Natural Strategy for the Treatment of Rhinitis and Rhinosinusitis. Antioxidants. 2021 Jul;10(7):1109.

203. Prasanthi D, Lakshmi PK. Effect of chemical enhancers in transdermal permeation of alfuzosin hydrochloride. ISRN Pharm. 2012;2012:965280.

204. Huang YB, Tsai YH, Chang JS, Liu JC, Tsai MJ, Wu PC. Effect of antioxidants and anti-irritants on the stability, skin irritation and penetration capacity of captopril gel. International Journal of Pharmaceutics. 2002 Jul 25;241(2):345–51.

205. Vasyuchenko EP, Orekhov PS, Armeev GA, Bozdaganyan ME. CPE-DB: An Open Database of Chemical Penetration Enhancers. Pharmaceutics. 2021 Jan;13(1):66.

206. Ita KB. Prodrugs for transdermal drug delivery – trends and challenges. Journal of Drug Targeting. 2016 Sep 13;24(8):671–8.

207. Dhote V, Bhatnagar P, Mishra PK, Mahajan SC, Mishra DK. Iontophoresis: A Potential Emergence of a Transdermal Drug Delivery System. Sci Pharm. 2012;80(1):1–28.

208. Roustit M, Blaise S, Cracowski JL. Trials and tribulations of skin iontophoresis in therapeutics. British Journal of Clinical Pharmacology. 2014;77(1):63–71.

209. Prausnitz MR, Bose VG, Langer R, Weaver JC. Electroporation of mammalian skin: a mechanism to enhance transdermal drug delivery. Proc Natl Acad Sci U S A. 1993 Nov 15;90(22):10504–8.

210. Lin CH, Aljuffali IA, Fang JY. Lasers as an approach for promoting drug delivery via skin. Expert Opinion on Drug Delivery. 2014 Apr 1;11(4):599–614.

211. Rich KT, Hoerig CL, Rao MB, Mast TD. Relations between acoustic cavitation and skin resistance during intermediate- and high-frequency sonophoresis. Journal of Controlled Release. 2014 Nov 28;194:266–77.

212. Barolet D, Benohanian A. Current trends in needle-free jet injection: an update. CCID. 2018 May 1;11:231–8.

213. Hoffman PN, Abuknesha RA, Andrews NJ, Samuel D, Lloyd JS. A model to assess the infection potential of jet injectors used in mass immunisation. Vaccine. 2001 Jul 16;19(28–29):4020–7.

214. Lee JW, Park JH, Prausnitz MR. Dissolving microneedles for transdermal drug delivery. Biomaterials. 2008 May 1;29(13):2113–24.

215. Guillot AJ, Cordeiro AS, Donnelly RF, Montesinos MC, Garrigues TM, Melero A. Microneedle-Based Delivery: An Overview of Current Applications and Trends. Pharmaceutics. 2020 Jun 19;12(6).

216. Singh R, Vyas SP. Topical liposomal system for localized and controlled drug delivery. Journal of Dermatological Science. 1996 Nov 1;13(2):107–11.

217. Chacko IA, Ghate VM, Dsouza L, Lewis SA. Lipid vesicles: A versatile drug delivery platform for dermal and transdermal applications. Colloids and Surfaces B: Biointerfaces. 2020 Nov 1;195:111262.

218. Mohammed AR, Weston N, Coombes AGA, Fitzgerald M, Perrie Y. Liposome formulation of poorly water soluble drugs: optimisation of drug loading and ESEM analysis of stability. International Journal of Pharmaceutics. 2004 Nov 5;285(1):23–34.

219. Abd E, Roberts MS, Grice JE. A Comparison of the Penetration and Permeation of Caffeine into and through Human Epidermis after Application in Various Vesicle Formulations. Skin Pharmacol Physiol. 2016;29(1):24–30.

220. Arsalan A, Ahmad I, Ali SA, Qadeer K, Mahmud S, Humayun F, et al. The kinetics of photostabilization of cyanocobalamin in liposomal preparations. International Journal of Chemical Kinetics. 2020;52(3):207–17.

221. Sercombe L, Veerati T, Moheimani F, Wu SY, Sood AK, Hua S. Advances and Challenges of Liposome Assisted Drug Delivery. Frontiers in Pharmacology. 2015;6:286.

222. Henriksen-Lacey M, Bramwell VW, Christensen D, Agger EM, Andersen P, Perrie Y. Liposomes based on dimethyldioctadecylammonium promote a depot effect and enhance immunogenicity of soluble antigen. Journal of Controlled Release. 2010 Mar 3;142(2):180–6.

223. Puri A, Loomis K, Smith B, Lee JH, Yavlovich A, Heldman E, et al. Lipid-based nanoparticles as pharmaceutical drug carriers: from concepts to clinic. Crit Rev Ther Drug Carrier Syst. 2009;26(6):523–80.

224. Tian C an, Chiu C cheng. Importance of Hydrophilic Groups on Modulating the Structural, Mechanical, and Interfacial Properties of Bilayers: A Comparative Molecular Dynamics Study of Phosphatidylcholine and Ion Pair Amphiphile Membranes. International Journal of Molecular Sciences. 2018 Jun;19(6):1552.

225. Perumal Chandran S, Natarajan S, Rajan D, Prabakaran L. Phospholipids as versatile polymer in drug delivery systems. International Journal of Pharmacy and Pharmaceutical Sciences. 2014 Jan 1;6:8–11.

226. Ahmad A, Ahsan H. Lipid-based formulations in cosmeceuticals and biopharmaceuticals. Biomedical Dermatology. 2020 May 6;4(1):12.

227. Wu IY, Bala S, Škalko-Basnet N, di Cagno MP. Interpreting non-linear drug diffusion data: Utilizing Korsmeyer-Peppas model to study drug release from liposomes. European Journal of Pharmaceutical Sciences. 2019 Oct 1;138:105026.

228. Ali MH, Kirby DJ, Mohammed AR, Perrie Y. Solubilisation of drugs within liposomal bilayers: alternatives to cholesterol as a membrane stabilising agent. Journal of Pharmacy and Pharmacology. 2010 Nov 1;62(11):1646–55.

229. Leite NB, Martins DB, Fazani VE, Vieira MR, Dos Santos Cabrera MP. Cholesterol modulates curcumin partitioning and membrane effects. Biochim Biophys Acta Biomembr. 2018 Nov;1860(11):2320–8.

230. Lee EH, Kim A, Oh YK, Kim CK. Effect of edge activators on the formation and transfection efficiency of ultradeformable liposomes. Biomaterials. 2005 Jan 1;26(2):205–10.

231. Gupta R, Kumar A. Transfersomes: The Ultra-Deformable Carrier System for Non-Invasive Delivery of Drug. Curr Drug Deliv. 2021;18(4):408–20.

232. Gupta A, Aggarwal G, Singla S, Arora R. Transfersomes: A Novel Vesicular Carrier for Enhanced Transdermal Delivery of Sertraline: Development, Characterization, and Performance Evaluation. Scientia Pharmaceutica. 2012 Dec;80(4):1061–80.

233. Rai S, Pandey V, Rai G. Transfersomes as versatile and flexible nano-vesicular carriers in skin cancer therapy: the state of the art. Nano Reviews & Experiments. 2017 Jan 1;8(1):1325708.

234. Singh S, Vardhan H, Kotla NG, Maddiboyina B, Sharma D, Webster TJ. The role of surfactants in the formulation of elastic liposomal gels containing a synthetic opioid analgesic. IJN. 2016 Apr 8;11:1475–82.

235. Zdziennicka A, Szymczyk K, Krawczyk J, Jańczuk B. Critical micelle concentration of some surfactants and thermodynamic parameters of their micellization. Fluid Phase Equilibria. 2012 May 25;322–323:126–34.

236. Ahad A, Al-Saleh AA, Al-Mohizea AM, Al-Jenoobi FI, Raish M, Yassin AEB, et al. Formulation and characterization of novel soft nanovesicles for enhanced transdermal delivery of eprosartan mesylate. Saudi Pharmaceutical Journal. 2017 Nov 1;25(7):1040–6.

237. Ahad A, Al-Saleh AA, Al-Mohizea AM, Al-Jenoobi FI, Raish M, Yassin AEB, et al. Formulation and characterization of Phospholipon 90 G and tween 80 based transfersomes for transdermal delivery of eprosartan mesylate. Pharmaceutical Development and Technology. 2018 Sep 14;23(8):787–93.

238. Touitou E, Godin B. Ethosomes for skin delivery. Journal of Drug Delivery Science and Technology. 2007 Jan 1;17(5):303–8.

239. Yang L, Wu L, Wu D, Shi D, Wang T, Zhu X. Mechanism of transdermal permeation promotion of lipophilic drugs by ethosomes. IJN. 2017 Apr 26;12:3357–64.

240. Manca ML, Cencetti C, Matricardi P, Castangia I, Zaru M, Sales OD, et al. Glycerosomes: Use of hydrogenated soy phosphatidylcholine mixture and its effect on vesicle features and diclofenac skin penetration. International Journal of Pharmaceutics. 2016 Sep 10;511(1):198–204.

241. Gupta P, Mazumder R, Padhi S. Glycerosomes: Advanced Liposomal Drug Delivery System. Indian Journal of Pharmaceutical Sciences. 2020 Jun 3;82(3):385–97.

242. El-Refaie WM, Elnaggar YSR, El-Massik MA, Abdallah OY. Novel curcumin-loaded gel-core hyaluosomes with promising burn-wound healing potential: Development, in-vitro appraisal and in-vivo studies. International Journal of Pharmaceutics. 2015 May 30;486(1):88–98.

243. Awasthi VD, Garcia D, Klipper R, Goins BA, Phillips WT. Neutral and Anionic Liposome-Encapsulated Hemoglobin: Effect of Postinserted Poly(ethylene glycol)-distearoylphosphatidylethanolamine on Distribution and Circulation Kinetics. J Pharmacol Exp Ther. 2004 Apr 1;309(1):241–8.

244. Shim G, Kim MG, Park JY, Oh YK. Application of cationic liposomes for delivery of nucleic acids. Asian Journal of Pharmaceutical Sciences. 2013 Apr 1;8(2):72–80.

245. Joo KI, Xiao L, Liu S, Liu Y, Lee CL, Conti PS, et al. Crosslinked multilamellar liposomes for controlled delivery of anticancer drugs. Biomaterials. 2013 Apr 1;34(12):3098–109.

246. Joshi S, Hussain MT, Roces CB, Anderluzzi G, Kastner E, Salmaso S, et al. Microfluidics based manufacture of liposomes simultaneously entrapping hydrophilic and lipophilic drugs. International Journal of Pharmaceutics. 2016 Nov 30;514(1):160–8.

247. Patil YP, Jadhav S. Novel methods for liposome preparation. Chemistry and Physics of Lipids. 2014 Jan 1;177:8–18.

248. Vuillemard JC. Recent advances in the large-scale production of lipid vesicles for use in food products: microfluidization. Journal of Microencapsulation. 1991 Jan 1;8(4):547–62.

249. Giuliano CB, Cvjetan N, Ayache J, Walde P. Multivesicular Vesicles: Preparation and Applications. ChemSystemsChem. 2021;3(2):e2000049.

250. Maja L, Željko K, Mateja P. Sustainable technologies for liposome preparation. The Journal of Supercritical Fluids. 2020 Nov 1;165:104984.

251. Kulkarni CV. Lipid crystallization: from self-assembly to hierarchical and biological ordering. Nanoscale. 2012 Sep 13;4(19):5779–91.

252. Akbarzadeh A, Rezaei-Sadabady R, Davaran S, Joo SW, Zarghami N, Hanifehpour Y, et al. Liposome: classification, preparation, and applications. Nanoscale Res Lett. 2013 Feb 22;8(1):102.

253. Pierre MBR, dos Santos Miranda Costa I. Liposomal systems as drug delivery vehicles for dermal and transdermal applications. Arch Dermatol Res. 2011 Jul 30;303(9):607.

254. Mufamadi MS, Pillay V, Choonara YE, Du Toit LC, Modi G, Naidoo D, et al. A Review on Composite Liposomal Technologies for Specialized Drug Delivery. Journal of Drug Delivery. 2011 Feb 8;2011:e939851.

255. Ganesan MG, Weiner ND, Flynn GL, Ho NFH. Influence of liposomal drug entrapment on percutaneous absorption. International Journal of Pharmaceutics. 1984 Jan 1;20(1):139–54.

256. Hofland HEJ, Bouwstra JA, Boddé HE, Spies F, Junginger HE. Interactions between liposomes and human stratum corneum in vitro: freeze fracture electron microscopical visualization and small angle X-ray scattering studies. British Journal of Dermatology. 1995;132(6):853–66.

257. Souto EB, Macedo AS, Dias-Ferreira J, Cano A, Zielińska A, Matos CM. Elastic and Ultradeformable Liposomes for Transdermal Delivery of Active Pharmaceutical Ingredients (APIs). International Journal of Molecular Sciences. 2021 Jan;22(18):9743.

258. Foldvari M, Gesztes A, Mezei M. Dermal drug delivery by liposome encapsulation: Clinical and electron microscopic studies. Journal of Microencapsulation. 1990 Jan 1;7(4):479–89.

259. Dreier J, Sørensen JA, Brewer JR. Superresolution and Fluorescence Dynamics Evidence Reveal That Intact Liposomes Do Not Cross the Human Skin Barrier. PLoS One. 2016 Jan 11;11(1):e0146514.

260. He H, Lu Y, Qi J, Zhu Q, Chen Z, Wu W. Adapting liposomes for oral drug delivery. Acta Pharmaceutica Sinica B. 2019 Jan 1;9(1):36–48.

261. Rajan R, Jose S, Mukund VPB, Vasudevan DT. Transferosomes - A vesicular transdermal delivery system for enhanced drug permeation. J Adv Pharm Technol Res. 2011 Jul;2(3):138–43.

262. Manconi M, Caddeo C, Sinico C, Valenti D, Mostallino MC, Biggio G, et al. Ex vivo skin delivery of diclofenac by transcutol containing liposomes and suggested mechanism of vesicle–skin interaction. European Journal of Pharmaceutics and Biopharmaceutics. 2011 May 1;78(1):27–35.

263. Verma P, Pathak K. Therapeutic and cosmeceutical potential of ethosomes: An overview. J Adv Pharm Technol Res. 2010;1(3):274–82.

264. Paiva-Santos AC, Silva AL, Guerra C, Peixoto D, Pereira-Silva M, Zeinali M, et al. Ethosomes as Nanocarriers for the Development of Skin Delivery Formulations. Pharm Res. 2021 Jun;38(6):947–70.

265. Jain S, Umamaheshwari RB, Bhadra D, Jain N. Ethosomes: A novel vesicular carrier for enhanced transdermal delivery of an antiHIV agent. Indian Journal of Pharmaceutical Sciences. 2004 Jan 1;66:72–81.

266. Elsayed MMA, Abdallah OY, Naggar VF, Khalafallah NM. Deformable liposomes and ethosomes: Mechanism of enhanced skin delivery. International Journal of Pharmaceutics. 2006 Sep 28;322(1):60–6.

267. Huang Z, Li X, Zhang T, Song Y, She Z, Li J, et al. Progress involving new techniques for liposome preparation. Asian Journal of Pharmaceutical Sciences. 2014 Aug 1;9(4):176–82.

268. Mozafari MR. Liposomes: an overview of manufacturing techniques. Cell Mol Biol Lett. 2005;10(4):711–9.

269. Zhang H. Thin-Film Hydration Followed by Extrusion Method for Liposome Preparation. Methods Mol Biol. 2017;1522:17–22.

270. López-Pinto JM, González-Rodríguez ML, Rabasco AM. Effect of cholesterol and ethanol on dermal delivery from DPPC liposomes. International Journal of Pharmaceutics. 2005 Jul 14;298(1):1–12.

271. Perra M, Lozano-Sánchez J, Leyva-Jiménez FJ, Segura-Carretero A, Pedraz JL, Bacchetta G, et al. Extraction of the antioxidant phytocomplex from wine-making by-products and sustainable loading in phospholipid vesicles specifically tailored for skin protection. Biomedicine & Pharmacotherapy. 2021 Oct 1;142:111959.

272. Maestrelli F, Capasso G, González-Rodríguez ML, Rabasco AM, Ghelardini C, Mura P. Effect of preparation technique on the properties and in vivo efficacy of benzocaine-loaded ethosomes. Journal of Liposome Research. 2009 Dec 1;19(4):253–60.

273. Zhaowu Z, Xiaoli W, Yangde Z, Nianfeng L. Preparation of matrine ethosome, its percutaneous permeation in vitro and anti-inflammatory

activity in vivo in rats. Journal of Liposome Research. 2009 Jun 1;19(2):155–62.

274. Chapman CJ, Erdahl WE, Taylor RW, Pfeiffer DR. Effects of solute concentration on the entrapment of solutes in phospholipid vesicles prepared by freeze-thaw extrusion. Chem Phys Lipids. 1991 Dec;60(2):201–8.

275. Bhalaria MK, Naik S, Misra AN. Ethosomes: a novel delivery system for antifungal drugs in the treatment of topical fungal diseases. Indian J Exp Biol. 2009 May;47(5):368–75.

276. Güven A, Ortiz M, Constanti M, O'Sullivan CK. Rapid and efficient method for the size separation of homogeneous fluorescein-encapsulating liposomes. Journal of Liposome Research. 2009 Jun 1;19(2):148–54.

277. Dimov N, Kastner E, Hussain M, Perrie Y, Szita N. Formation and purification of tailored liposomes for drug delivery using a module-based micro continuous-flow system. Sci Rep. 2017 Sep 21;7(1):12045.

278. Adamala K, Engelhart AE, Kamat NP, Jin L, Szostak JW. Construction of a liposome dialyzer for the preparation of high-value, small-volume liposome formulations. Nat Protoc. 2015 Jun;10(6):927–38.

279. Hua S. Comparison of in vitro dialysis release methods of loperamide-encapsulated liposomal gel for topical drug delivery. IJN. 2014 Jan 30;9(1):735–44.

280. Shariat S, Badiee A, Jaafari MR, Mortazavi SA. Optimization of a Method to Prepare Liposomes Containing HER2/Neu- Derived Peptide as a Vaccine Delivery System for Breast Cancer. Iran J Pharm Res. 2014;13(Suppl):15–25.

281. Carreras JJ, Tapia-Ramirez WE, Sala A, Guillot AJ, Garrigues TM, Melero A. Ultraflexible lipid vesicles allow topical absorption of cyclosporin A. Drug Deliv Transl Res. 2020 Apr;10(2):486–97.

282. Khattak MIK, Ahmed N, Umer MF, Riaz A, Ahmad NM, Khan GM. Chloroform-Injection (CI) and Spontaneous-Phase-Transition (SPT) Are Novel Methods, Simplifying the Fabrication of Liposomes with Versatile Solution to Cholesterol Content and Size Distribution. Pharmaceutics. 2020 Nov;12(11):1065.

283. Khan I, Yousaf S, Subramanian S, Alhnan MA, Ahmed W, Elhissi A. Proliposome Powders for the Generation of Liposomes: the Influence of Carbohydrate Carrier and Separation Conditions on Crystallinity and Entrapment of a Model Antiasthma Steroid. AAPS PharmSciTech. 2018 Jan 1;19(1):262–74.

284. Sánchez-López V, Fernández-Romero JM, Gómez-Hens A. Evaluation of liposome populations using a sucrose density gradient centrifugation approach coupled to a continuous flow system. Analytica Chimica Acta. 2009 Jul 10;645(1):79–85.

285. Gonzalez Gomez A, Syed S, Marshall K, Hosseinidoust Z. Liposomal Nanovesicles for Efficient Encapsulation of Staphylococcal Antibiotics. ACS Omega. 2019 Jun 30;4(6):10866–76.

286. Marques SS, Ramos II, Fernandes SR, Barreiros L, Lima SAC, Reis S, et al. Insights on Ultrafiltration-Based Separation for the Purification and Quantification of Methotrexate in Nanocarriers. Molecules. 2020 Jan;25(8):1879.

287. Calle D, Negri V, Ballesteros P, Cerdán S. Magnetoliposomes Loaded with Poly-Unsaturated Fatty Acids as Novel Theranostic Anti-Inflammatory Formulations. Theranostics. 2015 Feb 15;5(5):489–503.

288. Wagner A, Vorauer-Uhl K, Katinger H. Liposomes produced in a pilot scale: production, purification and efficiency aspects. European Journal of Pharmaceutics and Biopharmaceutics. 2002 Sep 1;54(2):213–9.

289. Magin RL, Chan HC. Rapid separation of liposomes using ultrafiltration. Biotechnol Tech. 1987 Sep 1;1(3):185–8.

290. Fekete S, Beck A, Veuthey JL, Guillarme D. Theory and practice of size exclusion chromatography for the analysis of protein aggregates. Journal of Pharmaceutical and Biomedical Analysis. 2014 Dec 1;101:161–73.

291. Ruysschaert T, Marque A, Duteyrat JL, Lesieur S, Winterhalter M, Fournier D. Liposome retention in size exclusion chromatography. BMC Biotechnology. 2005 May 10;5(1):11.

292. Grabielle-Madelmont C, Lesieur S, Ollivon M. Characterization of loaded liposomes by size exclusion chromatography. Journal of Biochemical and Biophysical Methods. 2003 Jun 30;56(1):189–217.

293. Afergan E, Ben David M, Epstein H, Koroukhov N, Gilhar D, Rohekar K, et al. Liposomal Simvastatin Attenuates Neointimal Hyperplasia in Rats. AAPS J. 2010 Jun 1;12(2):181–7.

294. Xu R, Fitts A, Li X, Fernandes J, Pochampally R, Mao J, et al. Quantification of Small Extracellular Vesicles by Size Exclusion Chromatography with Fluorescence Detection. Anal Chem. 2016 Nov 1;88(21):10390–4.

295. Elamir A, Ajith S, Sawaftah NA, Abuwatfa W, Mukhopadhyay D, Paul V, et al. Ultrasound-triggered herceptin liposomes for breast cancer therapy. Sci Rep. 2021 Apr 6;11(1):7545.

296. Watwe RM, Bellare JR. Manufacture of liposomes: A review. Current Science. 1995;68(7):715–24.

297. Šturm L, Poklar Ulrih N. Basic Methods for Preparation of Liposomes and Studying Their Interactions with Different Compounds, with the Emphasis on Polyphenols. International Journal of Molecular Sciences. 2021 Jan;22(12):6547.

298. Leekumjorn S, Sum AK. Molecular studies of the gel to liquid-crystalline phase transition for fully hydrated DPPC and DPPE bilayers. Biochimica et Biophysica Acta (BBA) - Biomembranes. 2007 Feb 1;1768(2):354–65.

299. M'Baye G, Mély Y, Duportail G, Klymchenko AS. Liquid ordered and gel phases of lipid bilayers: fluorescent probes reveal close fluidity but different hydration. Biophys J. 2008 Aug;95(3):1217–25.

300. Wagner A, Vorauer-Uhl K. Liposome Technology for Industrial Purposes. Journal of Drug Delivery. 2010 Dec 5;2011:e591325.

301. Bagatolli L, Kumar PBS. Phase behavior of multicomponent membranes: Experimental and computational techniques. Soft Matter. 2009 Aug 18;5(17):3234–48.

302. Bochicchio S, Dalmoro A, Lamberti G, Barba AA. Advances in Nanoliposomes Production for Ferrous Sulfate Delivery. Pharmaceutics. 2020 May;12(5):445.

303. Nam JH, Kim SY, Seong H. Investigation on Physicochemical Characteristics of a Nanoliposome-Based System for Dual Drug Delivery. Nanoscale Research Letters. 2018 Apr 13;13(1):101.

304. de Freitas CF, Calori IR, Tessaro AL, Caetano W, Hioka N. Rapid formation of Small Unilamellar Vesicles (SUV) through low-frequency sonication: An innovative approach. Colloids and Surfaces B: Biointerfaces. 2019 Sep 1;181:837–44.

305. Barba AA, Bochicchio S, Lamberti G, Dalmoro A. Ultrasonic energy in liposome production: process modelling and size calculation. Soft Matter. 2014 Mar 19;10(15):2574–81.

306. Vitrac H, Courrègelongue M, Couturier M, Collin F, Thérond P, Rémita S, et al. Radiation-induced peroxidation of small unilamellar vesicles of phosphatidylcholine generated by sonication. Can J Physiol Pharmacol. 2004 Feb 1;82(2):153–60.

307. Yamaguchi T, Nomura M, Matsuoka T, Koda S. Effects of frequency and power of ultrasound on the size reduction of liposome. Chemistry and Physics of Lipids. 2009 Jul 1;160(1):58–62.

308. Ribeiro LN de M, Couto VM, Fraceto LF, de Paula E. Use of nanoparticle concentration as a tool to understand the structural properties of colloids. Sci Rep. 2018 Jan 17;8(1):982.

309. Berger N, Sachse A, Bender J, Schubert R, Brandl M. Filter extrusion of liposomes using different devices: comparison of liposome size, encapsulation efficiency, and process characteristics. International Journal of Pharmaceutics. 2001 Jul 31;223(1):55–68.

310. Olson F, Hunt CA, Szoka FC, Vail WJ, Papahadjopoulos D. Preparation of liposomes of defined size distribution by extrusion through polycarbonate membranes. Biochim Biophys Acta. 1979 Oct 19;557(1):9–23.

311. Szoka F, Olson F, Heath T, Vail W, Mayhew E, Papahadjopoulos D. Preparation of unilamellar liposomes of intermediate size (0.1-0.2 mumol) by a combination of reverse phase evaporation and extrusion through polycarbonate membranes. Biochim Biophys Acta. 1980 Oct 2;601(3):559–71.

312. Schiffelers RM, Metselaar JM, Fens MHAM, Janssen APCA, Molema G, Storm G. Liposome-Encapsulated Prednisolone Phosphate Inhibits Growth of Established Tumors in Mice. Neoplasia. 2005 Feb 1;7(2):118–27.

313. Ong SGM, Chitneni M, Lee KS, Ming LC, Yuen KH. Evaluation of Extrusion Technique for Nanosizing Liposomes. Pharmaceutics. 2016 Dec;8(4):36.

314. Hinna A, Steiniger F, Hupfeld S, Stein P, Kuntsche J, Brandl M. Filter-extruded liposomes revisited: a study into size distributions and morphologies in relation to lipid-composition and process parameters. Journal of Liposome Research. 2016 Jan 2;26(1):11–20.

315. Brandl M, Bachmann D, Drechsler M, Bauer KH. Liposome Preparation by a New High Pressure Homogenizer Gaulin Micron Lab 40. Drug Development and Industrial Pharmacy. 1990 Jan 1;16(14):2167–91.

316. Hamilton RL, Goerke J, Guo LS, Williams MC, Havel RJ. Unilamellar liposomes made with the French pressure cell: a simple preparative and semiquantitative technique. Journal of Lipid Research. 1980 Nov 1;21(8):981–92.

317. Bachmann D, Brandl M, Gregoriadis G. Preparation of liposomes using a Mini-Lab 8.30 H high-pressure homogenizer. International Journal of Pharmaceutics. 1993 Apr 5;91(1):69–74.

318. Lajunen T, Hisazumi K, Kanazawa T, Okada H, Seta Y, Yliperttula M, et al. Topical drug delivery to retinal pigment epithelium with microfluidizer produced small liposomes. European Journal of Pharmaceutical Sciences. 2014 Oct 1;62:23–32.

319. Shelar SB, Dey A, Gawali SL, Dhinakaran S, Barick KC, Basu M, et al. Spontaneous Formation of Cationic Vesicles in Aqueous DDAB-Lecithin Mixtures for Efficient Plasmid DNA Complexation and Gene Transfection. ACS Appl Bio Mater. 2021 Aug 16;4(8):6005–15.

320. Magome N, Takemura T, Yoshikawa K. Spontaneous Formation of Giant Liposomes from Neutral Phospholipids. Chem Lett. 1997 Mar 1;26(3):205–6.

321. Mayer LD, Bally MB, Hope MJ, Cullis PR. Techniques for encapsulating bioactive agents into liposomes. Chemistry and Physics of Lipids. 1986 Jun 1;40(2):333–45.

322. Schwendener RA, Schott H. Liposome formulations of hydrophobic drugs. Methods Mol Biol. 2010;605:129–38.

323. Tamam H, Park J, Gadalla HH, Masters AR, Abdel-Aleem JA, Abdelrahman SI, et al. Development of Liposomal Gemcitabine with High Drug Loading Capacity. Mol Pharmaceutics. 2019 Jul 1;16(7):2858–71.

324. Maherani B, Arab-Tehrany E, Mozafari M, Gaiani C, M L. Liposomes: A Review of Manufacturing Techniques and Targeting Strategies. Current Nanoscience. 2011 Jun 1;7:436–52.

325. Sur S, Fries AC, Kinzler KW, Zhou S, Vogelstein B. Remote loading of preencapsulated drugs into stealth liposomes. PNAS. 2014 Feb 11;111(6):2283–8.

326. Mayer LD, Bally MB, Cullis PR. Uptake of adriamycin into large unilamellar vesicles in response to a pH gradient. Biochim Biophys Acta. 1986 May 9;857(1):123–6.

327. Llu L, Yonetani T. Preparation and Characterization of Liposome-Encapsulated Haemoglobin by a Freeze-Thaw Method. Journal of Microencapsulation. 1994 Jan 1;11(4):409–21.

328. Ohsawa T, Miura H, Harada K. Improvement of Encapsulation Efficiency of Water-Soluble Drugs in Liposomes Formed by the Freeze-Thawing Method. Chemical & Pharmaceutical Bulletin. 1985;33(9):3945–52.

329. Costa AP, Xu X, Burgess DJ. Freeze-Anneal-Thaw Cycling of Unilamellar Liposomes: Effect on Encapsulation Efficiency. Pharm Res. 2014 Jan 1;31(1):97–103.

330. Colletier JP, Chaize B, Winterhalter M, Fournier D. Protein encapsulation in liposomes: efficiency depends on interactions between protein and phospholipid bilayer. BMC Biotechnology. 2002 May 10;2(1):9.

331. Zhao YZ, Lu CT. Increasing the Entrapment of Protein-Loaded Liposomes with a Modified Freeze–Thaw Technique: A Preliminary Experimental Study. Drug Development and Industrial Pharmacy. 2009 Feb 1;35(2):165–71.

332. Mayer LD, Tai LC, Ko DS, Masin D, Ginsberg RS, Cullis PR, et al. Influence of vesicle size, lipid composition, and drug-to-lipid ratio on the biological activity of liposomal doxorubicin in mice. Cancer Res. 1989 Nov 1;49(21):5922–30.

333. Johnston MJW, Semple SC, Klimuk SK, Edwards K, Eisenhardt ML, Leng EC, et al. Therapeutically optimized rates of drug release can be achieved by varying the drug-to-lipid ratio in liposomal vincristine formulations. Biochim Biophys Acta. 2006 Jan;1758(1):55–64.

334. Muppidi K, Pumerantz AS, Wang J, Betageri G. Development and stability studies of novel liposomal vancomycin formulations. ISRN Pharm. 2012;2012:636743.

335. Jaafar-Maalej C, Diab R, Andrieu V, Elaissari A, Fessi H. Ethanol injection method for hydrophilic and lipophilic drug-loaded liposome preparation. Journal of Liposome Research. 2010 Sep 1;20(3):228–43.

336. Nii T, Ishii F. Encapsulation efficiency of water-soluble and insoluble drugs in liposomes prepared by the microencapsulation vesicle method. International Journal of Pharmaceutics. 2005 Jul 14;298(1):198–205.

337. Cullis PR, Mayer LD, Bally MB, Madden TD, Hope MJ. Generating and loading of liposomal systems for drug-delivery applications. Advanced Drug Delivery Reviews. 1989 May 1;3(3):267–82.

338. Gubernator J. Active methods of drug loading into liposomes: recent strategies for stable drug entrapment and increased in vivo activity. Expert Opinion on Drug Delivery. 2011 May 1;8(5):565–80.

339. Cui F, Zhang L, Zheng J, Kawashima Y. A study of insulin-chitosan complex nanoparticles used for oral administration. Journal of Drug Delivery Science and Technology. 2004 Jan 1;14(6):435–9.

340. Gulati M, Grover M, Singh M, Singh S. Study of azathioprine encapsulation into liposomes. Journal of Microencapsulation. 1998 Jan 1;15(4):485–94.

341. Pleguezuelos-Villa M, Mir-Palomo S, Díez-Sales O, Buso MAOV, Sauri AR, Nácher A. A novel ultradeformable liposomes of Naringin for anti-inflammatory therapy. Colloids and Surfaces B: Biointerfaces. 2018 Feb 1;162:265–70.

342. Volodkin D, Mohwald H, Voegel JC, Ball V. Coating of negatively charged liposomes by polylysine: Drug release study. Journal of Controlled Release. 2007 Jan 22;117(1):111–20.

343. Hein R, Uzundal CB, Hennig A. Simple and rapid quantification of phospholipids for supramolecular membrane transport assays. Org Biomol Chem. 2016 Feb 9;14(7):2182–5.

344. Rouser G, Fleischer S, Yamamoto A. Two dimensional thin layer chromatographic separation of polar lipids and determination of phospholipids by phosphorus analysis of spots. Lipids. 1970;5(5):494–6.

345. Bartlett GR. Phosphorus Assay in Column Chromatography. Journal of Biological Chemistry. 1959 Mar 1;234(3):466–8.

346. Grohganz H, Ziroli V, Massing U, Brandl M. Quantification of various phosphatidylcholines in liposomes by enzymatic assay. AAPS PharmSciTech. 2003 Dec 1;4(4):500–5.

347. Tejera-Garcia R, Connell L, Shaw WA, Kinnunen PKJ. Gravimetric determination of phospholipid concentration. Chemistry and Physics of Lipids. 2012 Sep 1;165(6):689–95.

348. Siriwardane DA, Wang C, Jiang W, Mudalige T. Quantification of phospholipid degradation products in liposomal pharmaceutical formulations by ultra performance liquid chromatography-mass spectrometry (UPLC-MS). International Journal of Pharmaceutics. 2020 Mar 30;578:119077.

349. Danaei M, Dehghankhold M, Ataei S, Hasanzadeh Davarani F, Javanmard R, Dokhani A, et al. Impact of Particle Size and Polydispersity Index on the Clinical Applications of Lipidic Nanocarrier Systems. Pharmaceutics. 2018 Jun;10(2):57.

350. Verma DD, Verma S, Blume G, Fahr A. Liposomes increase skin penetration of entrapped and non-entrapped hydrophilic substances into human skin: a skin penetration and confocal laser scanning microscopy study. Eur J Pharm Biopharm. 2003 May;55(3):271–7.

351. Boakye CHA, Patel K, Singh M. Doxorubicin liposomes as an investigative model to study the skin permeation of nanocarriers. International Journal of Pharmaceutics. 2015 Jul 15;489(1):106–16.

352. Pawar A. Transfersome: A Novel Technique Which Improves Transdermal Permeability. 2016;

353. Sentjurc M, Vrhovnik K, Kristl J. Liposomes as a topical delivery system: the role of size on transport studied by the EPR imaging method. J Control Release. 1999 May 1;59(1):87–97.

354. Hua S. Lipid-based nano-delivery systems for skin delivery of drugs and bioactives. Frontiers in Pharmacology. 2015;6:219.

355. Geusens B, Strobbe T, Bracke S, Dynoodt P, Sanders N, Gele MV, et al. Lipid-mediated gene delivery to the skin. European Journal of Pharmaceutical Sciences. 2011 Jul 17;43(4):199–211.

356. Prima GD, Librizzi F, Carrotta R. Light Scattering as an Easy Tool to Measure Vesicles Weight Concentration. Membranes. 2020 Sep;10(9):222.

357. Robson AL, Dastoor PC, Flynn J, Palmer W, Martin A, Smith DW, et al. Advantages and Limitations of Current Imaging Techniques for Characterizing Liposome Morphology. Frontiers in Pharmacology. 2018;9:80.

358. Nguyen TL, Nguyen TH, Nguyen DH. Development and In Vitro Evaluation of Liposomes Using Soy Lecithin to Encapsulate Paclitaxel. International Journal of Biomaterials. 2017 Feb 26;2017:e8234712.

359. Hupfeld S, Holsæter AM, Skar M, Frantzen CB, Brandl M. Liposome Size Analysis by Dynamic/Static Light Scattering upon Size Exclusion-/Field Flow-Fractionation. Journal of Nanoscience and Nanotechnology. 2006 Sep 1;6(9–10):3025–31.

360. Nallamothu R, Wood GC, Pattillo CB, Scott RC, Kiani MF, Moore BM, et al. A tumor vasculature targeted liposome delivery system for combretastatin A4: Design, characterization, and in vitro evaluation. AAPS PharmSciTech. 2006 Jun 1;7(2):E7–16.

361. Akashi K, Miyata H, Itoh H, Kinosita K. Preparation of giant liposomes in physiological conditions and their characterization under an optical microscope. Biophys J. 1996 Dec;71(6):3242–50.

362. Fernandez RM, Riske KA, Amaral LQ, Itri R, Lamy MT. Influence of salt on the structure of DMPG studied by SAXS and optical microscopy. Biochim Biophys Acta. 2008 Apr;1778(4):907–16.

363. Bucana C, Hoyer LC, Plentovich D. Preservation of multilamellar lipid vesicles (liposomes) for ultrastructural studies. Scan Electron Microsc. 1983;(Pt 3):1329–37.

364. Ruozi B, Belletti D, Tombesi A, Tosi G, Bondioli L, Forni F, et al. AFM, ESEM, TEM, and CLSM in liposomal characterization: a comparative study. IJN. 2011 Mar 14;6:557–63.

365. Adler K, Schiemann J. Characterization of liposomes by scanning electron microscopy and the freeze-fracture technique. Micron and Microscopica Acta. 1985 Jan 1;16(2):109–13.

366. Sabeti B, Noordine MIB, Javar HA, Davoudi ET, Kadivar A. Characterization of Diclofenac Liposomes Formulated with Palm Oil Fractions. Tropical Journal of Pharmaceutical Research. 2014 Feb 25;13(2):185–90.

367. Ishii F, Takamura A, Noro S. Observation of Liposomes by Scanning Electron Microscope. membrane. 1982;7(5):307–8.

368. Lujan H, Griffin WC, Taube JH, Sayes CM. Synthesis and characterization of nanometer-sized liposomes for encapsulation and microRNA transfer to breast cancer cells. Int J Nanomedicine. 2019 Jul 11;14:5159–73.

369. Muscariello L, Rosso F, Marino G, Giordano A, Barbarisi M, Cafiero G, et al. A critical overview of ESEM applications in the biological field. Journal of Cellular Physiology. 2005;205(3):328–34.

370. Bibi S, Kaur R, Henriksen-Lacey M, McNeil SE, Wilkhu J, Lattmann E, et al. Microscopy imaging of liposomes: From coverslips to environmental SEM. International Journal of Pharmaceutics. 2011 Sep 30;417(1):138–50.

371. Kodama T, Tomita N, Horie S, Sax N, Iwasaki H, Suzuki R, et al. Morphological study of acoustic liposomes using transmission electron microscopy. Journal of Electron Microscopy. 2010 Jun 1;59(3):187–96.

372. De Carlo S, Harris JR. Negative staining and cryo-negative staining of macromolecules and viruses for TEM. Micron. 2011 Feb 1;42(2):117–31.

373. Gallagher JR, Kim AJ, Gulati NM, Harris AK. Negative-Stain Transmission Electron Microscopy of Molecular Complexes for Image Analysis by 2D Class Averaging. Current Protocols in Microbiology. 2019;54(1):e90.

374. Gulik-Krzywicki T. Freeze-fracture transmission electron microscopy. Current Opinion in Colloid & Interface Science. 1997 Apr 1;2(2):137–44.

375. Blancett CD, Monninger MK, Nguessan CA, Kuehl KA, Rossi CA, Olschner SP, et al. Utilization of Capsules for Negative Staining of Viral Samples within Biocontainment. J Vis Exp. 2017 Jul 19;(125).

376. Winey M, Meehl JB, O'Toole ET, Giddings TH. Conventional transmission electron microscopy. MBoC. 2014 Feb 1;25(3):319–23.

377. Carson JL. Fundamental Technical Elements of Freeze-fracture/Freeze-etch in Biological Electron Microscopy. J Vis Exp. 2014 Sep 11;(91):51694.

378. Severs NJ. Freeze-fracture electron microscopy. Nat Protoc. 2007 Mar;2(3):547–76.

379. Fox CB, Mulligan SK, Sung J, Dowling QM, Fung HWM, Vedvick TS, et al. Cryogenic transmission electron microscopy of recombinant tuberculosis vaccine antigen with anionic liposomes reveals formation of flattened liposomes. IJN. 2014 Mar 11;9(1):1367–77.

380. Helvig S, Azmi IDM, Moghimi SM, Yaghmur A, Helvig S, Azmi IDM, et al. Recent Advances in Cryo-TEM Imaging of Soft Lipid Nanoparticles. AIMSBPOA. 2015;2(2):116–30.

381. Li T, Nowell CJ, Cipolla D, Rades T, Boyd BJ. Direct Comparison of Standard Transmission Electron Microscopy and Cryogenic-TEM in Imaging Nanocrystals Inside Liposomes. Mol Pharmaceutics. 2019 Apr 1;16(4):1775–81.

382. Nordström R, Zhu L, Härmark J, Levi-Kalisman Y, Koren E, Barenholz Y, et al. Quantitative Cryo-TEM Reveals New Structural Details of Doxil-Like PEGylated Liposomal Doxorubicin Formulation. Pharmaceutics. 2021 Jan;13(1):123.

383. Anabousi S, Laue M, Lehr CM, Bakowsky U, Ehrhardt C. Assessing transferrin modification of liposomes by atomic force microscopy and transmission electron microscopy. European Journal of Pharmaceutics and Biopharmaceutics. 2005 Jul 1;60(2):295–303.

384. Takechi-Haraya Y, Goda Y, Sakai-Kato K. Atomic Force Microscopy Study on the Stiffness of Nanosized Liposomes Containing Charged Lipids. Langmuir. 2018 Jul 3;34(26):7805–12.

385. Spyratou E, Mourelatou EA, Makropoulou M, Demetzos C. Atomic force microscopy: a tool to study the structure, dynamics and stability of liposomal drug delivery systems. Expert Opinion on Drug Delivery. 2009 Mar 1;6(3):305–17.

386. Sebinelli HG, Borin IA, Ciancaglini P, Bolean M. Topographical and mechanical properties of liposome surfaces harboring Na,K-ATPase by

means of atomic force microscopy. Soft Matter. 2019 Mar 27;15(13):2737–45.

387. Sitterberg J, Özcetin A, Ehrhardt C, Bakowsky U. Utilising atomic force microscopy for the characterisation of nanoscale drug delivery systems. European Journal of Pharmaceutics and Biopharmaceutics. 2010 Jan 1;74(1):2–13.

388. Liang X, Mao G, Ng KYS. Mechanical properties and stability measurement of cholesterol-containing liposome on mica by atomic force microscopy. Journal of Colloid and Interface Science. 2004 Oct 1;278(1):53–62.

389. Beltrán-Gracia E, López-Camacho A, Higuera-Ciapara I, Velázquez-Fernández JB, Vallejo-Cardona AA. Nanomedicine review: clinical developments in liposomal applications. Cancer Nanotechnology. 2019 Dec 19;10(1):11.

390. Ishida T, Takanashi Y, Kiwada H. Safe and Efficient Drug Delivery System with Liposomes for Intrathecal Application of an Antivasospastic Drug, Fasudil. Biological and Pharmaceutical Bulletin. 2006;29(3):397–402.

391. Alhajlan M, Alhariri M, Omri A. Efficacy and safety of liposomal clarithromycin and its effect on Pseudomonas aeruginosa virulence factors. Antimicrob Agents Chemother. 2013 Jun;57(6):2694–704.

392. Verma DD, Verma S, Blume G, Fahr A. Particle size of liposomes influences dermal delivery of substances into skin. International Journal of Pharmaceutics. 2003 Jun 4;258(1):141–51.

393. Refai H, Hassan D, Abdelmonem R. Development and characterization of polymer-coated liposomes for vaginal delivery of sildenafil citrate. Drug Delivery. 2017 Jan 1;24(1):278–88.

394. Woodbury DJ, Richardson ES, Grigg AW, Welling RD, Knudson BH. Reducing Liposome Size with Ultrasound: Bimodal Size Distributions. Journal of Liposome Research. 2006 Jan 1;16(1):57–80.

395. Ibišević M, Smajlović A, Arsić I. Optimization of high pressure homogenization in the production of liposomal dispersions. Technologica Acta. 2020 Feb 5;12(2):7–10.

396. Maulucci G, De Spirito M, Arcovito G, Boffi F, Castellano AC, Briganti G. Particle Size Distribution in DMPC Vesicles Solutions Undergoing Different Sonication Times. Biophysical Journal. 2005 May 1;88(5):3545–50.

397. Cho NJ, Hwang LY, Solandt JJR, Frank CW. Comparison of Extruded and Sonicated Vesicles for Planar Bilayer Self-Assembly. Materials. 2013 Aug;6(8):3294–308.

398. González-Rodríguez ML, Arroyo CM, Cózar-Bernal MJ, González-R PL, León JM, Calle M, et al. Deformability properties of timolol-loaded transfersomes based on the extrusion mechanism. Statistical optimization of the process. Drug Development and Industrial Pharmacy. 2016 Oct 2;42(10):1683–94.

399. Jain S, Jain P, Umamaheshwari RB, Jain NK. Transfersomes—A Novel Vesicular Carrier for Enhanced Transdermal Delivery: Development, Characterization, and Performance Evaluation. Drug Development and Industrial Pharmacy. 2003 Jan 1;29(9):1013–26.

400. Raza K, Singh B, Mahajan A, Negi P, Bhatia A, Katare OP. Design and evaluation of flexible membrane vesicles (FMVs) for enhanced topical delivery of capsaicin. Journal of Drug Targeting. 2011 May 1;19(4):293–302.

401. Ahmed TA, El-Say KM, Aljaeid BM, Fahmy UA, Abd-Allah FI. Transdermal glimepiride delivery system based on optimized ethosomal nano-vesicles: Preparation, characterization, in vitro, ex vivo and clinical evaluation. International Journal of Pharmaceutics. 2016 Mar 16;500(1):245–54.

402. Lin H, Xie Q, Huang X, Ban J, Wang B, Wei X, et al. Increased skin permeation efficiency of imperatorin via charged ultradeformable lipid vesicles for transdermal delivery. IJN. 2018 Feb 8;13:831–42.

403. Cipolla D, Wu H, Eastman S, Redelmeier T, Gonda I, Chan H. Development and Characterization of an In Vitro Release Assay for Liposomal Ciprofloxacin for Inhalation. Journal of Pharmaceutical Sciences. 2014 Jan 1;103(1):314–27.

404. Solomon D, Gupta N, Mulla NS, Shukla S, Guerrero YA, Gupta V. Role of In Vitro Release Methods in Liposomal Formulation Development: Challenges and Regulatory Perspective. AAPS J. 2017 Nov 1;19(6):1669–81.

405. Miao ZL, Deng YJ, Du HY, Suo XB, Wang XY, Wang X, et al. Preparation of a liposomal delivery system and its in vitro release of rapamycin. Experimental and Therapeutic Medicine. 2015 Mar 1;9(3):941–6.

406. Nava G, Piñón E, Mendoza L, Mendoza N, Quintanar D, Ganem A. Formulation and in Vitro, ex Vivo and in Vivo Evaluation of Elastic Liposomes for Transdermal Delivery of Ketorolac Tromethamine. Pharmaceutics. 2011 Dec;3(4):954–70.

407. Milon A, Lazrak T, Albrecht AM, Wolff G, Weill G, Ourisson G, et al. Osmotic swelling of unilamellar vesicles by the stopped-flow light scattering method. Influence of vesicle size, solute, temperature, cholesterol and three α,ω-dihydroxycarotenoids. Biochimica et Biophysica Acta (BBA) - Biomembranes. 1986 Jul 10;859(1):1–9.

408. Briuglia ML, Rotella C, McFarlane A, Lamprou DA. Influence of cholesterol on liposome stability and on in vitro drug release. Drug Deliv and Transl Res. 2015 Jun 1;5(3):231–42.

409. Jain A, Jain SK. In vitro release kinetics model fitting of liposomes: An insight. Chemistry and Physics of Lipids. 2016 Dec 1;201:28–40.

410. Higuchi T. Rate of Release of Medicaments from Ointment Bases Containing Drugs in Suspension. Journal of Pharmaceutical Sciences. 1961 Oct 1;50(10):874–5.

411. Ritger PL, Peppas NA. A simple equation for description of solute release I. Fickian and non-fickian release from non-swellable devices in the form of slabs, spheres, cylinders or discs. Journal of Controlled Release. 1987 Jun 1;5(1):23–36.

412. Ritger PL, Peppas NA. A simple equation for description of solute release II. Fickian and anomalous release from swellable devices. Journal of Controlled Release. 1987 Jun 1;5(1):37–42.

413. Peppas NA, Sahlin JJ. A simple equation for the description of solute release. III. Coupling of diffusion and relaxation. International Journal of Pharmaceutics. 1989 Dec 22;57(2):169–72.

414. Kim H, Fassihi R. Application of binary polymer system in drug release rate modulation. 2. Influence of formulation variables and hydrodynamic conditions on release kinetics. J Pharm Sci. 1997 Mar;86(3):323–8.

415. Hamilton DF, Ghert M, Simpson AHRW. Interpreting regression models in clinical outcome studies. Bone & Joint Research. 2015 Sep 1;4(9):152–3.

416. Akaike H. Information Theory and an Extension of the Maximum Likelihood Principle. In: Parzen E, Tanabe K, Kitagawa G, editors. Selected Papers of Hirotugu Akaike. New York, NY: Springer; 1998. p. 199–213. (Springer Series in Statistics).

417. van Maanen L, Katsimpokis D, van Campen AD. Fast and slow errors: Logistic regression to identify patterns in accuracy–response time relationships. Behav Res. 2019 Oct 1;51(5):2378–89.

418. Taira MC, Chiaramoni NS, Pecuch KM, Alonso-Romanowski S. Stability of Liposomal Formulations in Physiological Conditions for Oral Drug Delivery. Drug Delivery. 2004 Jan 1;11(2):123–8.

419. Müller RH, Mäder K, Gohla S. Solid lipid nanoparticles (SLN) for controlled drug delivery – a review of the state of the art. European Journal of Pharmaceutics and Biopharmaceutics. 2000 Jul 3;50(1):161–77.

420. Iqbal MA, Md S, Sahni JK, Baboota S, Dang S, Ali J. Nanostructured lipid carriers system: recent advances in drug delivery. J Drug Target. 2012 Dec;20(10):813–30.

421. Yücel Ç, Değim Z, Yılmaz Ş. Development of Cisplatin-loaded Liposome and Evaluation of Transport Properties Through Caco-2 Cell Line. Turkish Journal of Pharmaceutical Sciences. 2016 Apr 1;13:95–108.

422. Stano P, Bufali S, Domazou AS, Luisi PL. Effect of Tryptophan Oligopeptides on the Size Distribution of POPC Liposomes: A Dynamic Light Scattering and Turbidimetric Study. Journal of Liposome Research. 2005 Jan 1;15(1–2):29–47.

423. Urbanija J, Tomsic N, Lokar M, Ambrozic A, Cucnik S, Rozman B, et al. Coalescence of phospholipid membranes as a possible origin of anticoagulant effect of serum proteins. Chem Phys Lipids. 2007 Nov;150(1):49–57.

424. Dimitrova MN, Tsekov R, Matsumura H, Furusawa K. Size Dependence of Protein-Induced Flocculation of Phosphatidylcholine Liposomes. J Colloid Interface Sci. 2000 Jun 1;226(1):44–50.

425. Vargha-Butler EI, Foldvari M, Mezei M. Study of the sedimentation behaviour of liposomal drug delivery system. Colloids and Surfaces. 1989 Jan 1;42(2):375–89.

426. Elsana H, Olusanya TOB, Carr-Wilkinson J, Darby S, Faheem A, Elkordy AA. Evaluation of novel cationic gene based liposomes with cyclodextrin prepared by thin film hydration and microfluidic systems. Sci Rep. 2019 Oct 22;9(1):15120.

427. Samuni AM, Lipman A, Barenholz Y. Damage to liposomal lipids: protection by antioxidants and cholesterol-mediated dehydration. Chem Phys Lipids. 2000 Apr;105(2):121–34.

428. Liang T, Guan R, Quan Z, Tao Q, Liu Z, Hu Q. Cyanidin-3-o-glucoside liposome: Preparation via a green method and antioxidant activity in GES-1 cells. Food Res Int. 2019 Nov;125:108648.

429. Nowak D, Jakubczyk E. The Freeze-Drying of Foods—The Characteristic of the Process Course and the Effect of Its Parameters on the Physical Properties of Food Materials. Foods. 2020 Oct 18;9(10):1488.

430. Schnitzer E, Pinchuk I, Bor A, Leikin-Frenkel A, Lichtenberg D. Oxidation of liposomal cholesterol and its effect on phospholipid peroxidation. Chem Phys Lipids. 2007 Mar;146(1):43–53.

431. Pikal MJ, Shah S. The collapse temperature in freeze drying: Dependence on measurement methodology and rate of water removal from the glassy phase. International Journal of Pharmaceutics. 1990 Jul 31;62(2):165–86.

432. Lewis LM, Johnson RE, Oldroyd ME, Ahmed SS, Joseph L, Saracovan I, et al. Characterizing the Freeze–Drying Behavior of Model Protein Formulations. AAPS PharmSciTech. 2010 Nov 6;11(4):1580–90.

433. Alhalaweh A, Alzghoul A, Mahlin D, Bergström CAS. Physical stability of drugs after storage above and below the glass transition temperature: Relationship to glass-forming ability. International Journal of Pharmaceutics. 2015 Nov 10;495(1):312–7.

434. Červinka C, Fulem M. Structure and Glass Transition Temperature of Amorphous Dispersions of Model Pharmaceuticals with Nucleobases from Molecular Dynamics. Pharmaceutics. 2021 Aug 13;13(8):1253.

435. Kunz C, Gieseler H. Factors Influencing the Retention of Organic Solvents in Products Freeze-Dried From Co-Solvent Systems. J Pharm Sci. 2018 Aug;107(8):2005–12.

436. Patel SM, Doen T, Pikal MJ. Determination of end point of primary drying in freeze-drying process control. AAPS PharmSciTech. 2010 Mar;11(1):73–84.

437. Schneid SC, Gieseler H, Kessler WJ, Luthra SA, Pikal MJ. Optimization of the secondary drying step in freeze drying using TDLAS technology. AAPS PharmSciTech. 2011 Mar;12(1):379–87.

438. Merivaara A, Zini J, Koivunotko E, Valkonen S, Korhonen O, Fernandes FM, et al. Preservation of biomaterials and cells by freeze-drying: Change of paradigm. Journal of Controlled Release. 2021 Aug 10;336:480–98.

439. Tian Y, Li Y, Xu X, Jin Z. Starch retrogradation studied by thermogravimetric analysis (TGA). Carbohydrate Polymers. 2011 Mar 17;84(3):1165–8.

440. Wang Y, Kawano Y, Aubuchon SR, Palmer RA. TGA and Time-Dependent FTIR Study of Dehydrating Nafion−Na Membrane. Macromolecules. 2003 Feb 1;36(4):1138–46.

441. Guimarães D, Noro J, Silva C, Cavaco-Paulo A, Nogueira E. Protective Effect of Saccharides on Freeze-Dried Liposomes Encapsulating Drugs. Front Bioeng Biotechnol. 2019;7:424.

442. Stark B, Pabst G, Prassl R. Long-term stability of sterically stabilized liposomes by freezing and freeze-drying: Effects of cryoprotectants on structure. European Journal of Pharmaceutical Sciences. 2010 Nov 20;41(3):546–55.

443. van Winden EC, Zhang W, Crommelin DJ. Effect of freezing rate on the stability of liposomes during freeze-drying and rehydration. Pharm Res. 1997 Sep;14(9):1151–60.

444. Patel SM, Nail SL, Pikal MJ, Geidobler R, Winter G, Hawe A, et al. Lyophilized Drug Product Cake Appearance: What Is Acceptable? J Pharm Sci. 2017 Jul;106(7):1706–21.

445. Patel SM, Pikal MJ. Emerging Freeze-Drying Process Development and Scale-up Issues. AAPS PharmSciTech. 2011 Feb 23;12(1):372–8.

446. Izutsu K ichi, Yonemochi E, Yomota C, Goda Y, Okuda H. Studying the morphology of lyophilized protein solids using X-ray micro-CT: effect of post-freeze annealing and controlled nucleation. AAPS PharmSciTech. 2014 Oct;15(5):1181–8.

447. Kumar KN, Mallik S, Sarkar K. Role of freeze-drying in the presence of mannitol on the echogenicity of echogenic liposomes. J Acoust Soc Am. 2017 Dec;142(6):3670–6.

448. Mohammed AR, Coombes AGA, Perrie Y. Amino acids as cryoprotectants for liposomal delivery systems. Eur J Pharm Sci. 2007 Apr;30(5):406–13.

449. Wilkhu JS, McNeil SE, Anderson DE, Kirchmeier M, Perrie Y. Development of a solid dosage platform for the oral delivery of bilayer vesicles. European Journal of Pharmaceutical Sciences. 2017 Oct 15;108:71–7.

450. Crowe JH, Hoekstra FA, Nguyen KH, Crowe LM. Is vitrification involved in depression of the phase transition temperature in dry phospholipids? Biochim Biophys Acta. 1996 Apr 26;1280(2):187–96.

451. Koster KL, Webb MS, Bryant G, Lynch DV. Interactions between soluble sugars and POPC (1-palmitoyl-2-oleoylphosphatidylcholine) during dehydration: vitrification of sugars alters the phase behavior of the phospholipid. Biochim Biophys Acta. 1994 Jul 13;1193(1):143–50.

452. Franzé S, Selmin F, Samaritani E, Minghetti P, Cilurzo F. Lyophilization of Liposomal Formulations: Still Necessary, Still Challenging. Pharmaceutics. 2018 Aug 28;10(3):E139.

453. Chen C, Han D, Cai C, Tang X. An overview of liposome lyophilization and its future potential. J Control Release. 2010 Mar 19;142(3):299–311.

454. Ingvarsson PT, Yang M, Nielsen HM, Rantanen J, Foged C. Stabilization of liposomes during drying. Expert Opin Drug Deliv. 2011 Mar;8(3):375–88.

455. Levine H, Slade L. Thermomechanical properties of small-carbohydrate–water glasses and 'rubbers'. Kinetically metastable systems at sub-zero temperatures. J Chem Soc, Faraday Trans 1. 1988 Jan 1;84.

456. Demetzos C. Differential Scanning Calorimetry (DSC): a tool to study the thermal behavior of lipid bilayers and liposomal stability. J Liposome Res. 2008;18(3):159–73.

457. Neunert G, Tomaszewska-Gras J, Witkowski S, Polewski K. Tocopheryl Succinate-Induced Structural Changes in DPPC Liposomes: DSC and ANS Fluorescence Studies. Molecules. 2020 Jun 16;25(12):E2780.

458. Moeller EH, Holst B, Nielsen LH, Pedersen PS, Østergaard J. Stability, liposome interaction, and in vivo pharmacology of ghrelin in liposomal suspensions. International Journal of Pharmaceutics. 2010 May 5;390(1):13–8.

459. González N, Custal M, Rodríguez D, Riba JR, Armelin E. Influence of ZnO and TiO2 Particle Sizes in the Mechanical and Dielectric Properties of Vulcanized Rubber. Materials Research. 2017 Jul 1;20.

460. Németh Z, Pallagi E, Dobó DG, Kozma G, Kónya Z, Csóka I. An Updated Risk Assessment as Part of the QbD-Based Liposome Design and Development. Pharmaceutics. 2021 Jul 13;13(7):1071.

461. Leyva-Porras C, Cruz-Alcantar P, Espinosa-Solís V, Martínez-Guerra E, Balderrama CIP, Martínez IC, et al. Application of Differential Scanning Calorimetry (DSC) and Modulated Differential Scanning Calorimetry (MDSC) in Food and Drug Industries. Polymers (Basel). 2019 Dec 18;12(1):E5.

462. Liu Y, Bhandari B, Zhou W. Glass transition and enthalpy relaxation of amorphous food saccharides: a review. J Agric Food Chem. 2006 Aug 9;54(16):5701–17.

463. Rahman SMA, Islam MR, Mujumdar AS. A Study of Coupled Heat and Mass Transfer in Composite Food Products during Convective Drying. Drying Technology. 2007 Aug 1;25(7–8):1359–68.

464. van Hoogevest P, Wendel A. The use of natural and synthetic phospholipids as pharmaceutical excipients. European Journal of Lipid Science and Technology. 2014;116(9):1088–107.

465. Inglut CT, Sorrin AJ, Kuruppu T, Vig S, Cicalo J, Ahmad H, et al. Immunological and Toxicological Considerations for the Design of Liposomes. Nanomaterials. 2020 Feb;10(2):190.

466. Smistad G, Jacobsen J, Sande SA. Multivariate toxicity screening of liposomal formulations on a human buccal cell line. International Journal of Pharmaceutics. 2007 Feb 7;330(1):14–22.

467. Mayhew E, Ito M, Lazo R. Toxicity of non-drug-containing liposomes for cultured human cells. Experimental Cell Research. 1987 Jul 1;171(1):195–202.

468. da Silva CMG, Franz-Montan M, Limia CEG, Ribeiro LN de M, Braga MA, Guilherme VA, et al. Encapsulation of ropivacaine in a combined (donor-acceptor, ionic-gradient) liposomal system promotes extended anesthesia time. PLoS One. 2017;12(10):e0185828.

469. Lau KG, Hattori Y, Chopra S, O'Toole EA, Storey A, Nagai T, et al. Ultra-deformable liposomes containing bleomycin: In vitro stability and toxicity on human cutaneous keratinocyte cell lines. International Journal of Pharmaceutics. 2005 Aug 26;300(1):4–12.

470. Skóra B, Piechowiak T, Szychowski KA, Gmiński J. Entrapment of silver nanoparticles in L-α-phosphatidylcholine/cholesterol-based liposomes mitigates the oxidative stress in human keratinocyte (HaCaT) cells. European Journal of Pharmaceutics and Biopharmaceutics. 2021 Sep 1;166:163–74.

471. Bokrova J, Marova I, Matouskova P, Pavelkova R. Fabrication of novel PHB-liposome nanoparticles and study of their toxicity in vitro. J Nanopart Res. 2019 Mar 5;21(3):49.

472. Fens MH a. M, Hill KJ, Issa J, Ashton SE, Westwood FR, Blakey DC, et al. Liposomal encapsulation enhances the antitumour efficacy of the vascular disrupting agent ZD6126 in murine B16.F10 melanoma. Br J Cancer. 2008 Oct;99(8):1256–64.

473. Chiong HS, Yong YK, Ahmad Z, Sulaiman MR, Zakaria ZA, Yuen KH, et al. Cytoprotective and enhanced anti-inflammatory activities of liposomal

piroxicam formulation in lipopolysaccharide-stimulated RAW 264.7 macrophages. IJN. 2013 Mar 22;8(1):1245–55.

474. Vicario de la Torre M, Benítez del Castillo JM, Vico E, Guzmán M, de las Heras B, Herrero-Vanrell R, et al. Design and characterization of an ocular topical liposomal preparation to replenish the lipids of the tear film. Invest Ophthalmol Vis Sci. 2014 Nov 6;55(12):7839–47.

475. Bardania H, Shojaosadati SA, Kobarfard F, Morshedi D, Aliakbari F, Tahoori MT, et al. RGD-Modified Nano-Liposomes Encapsulated Eptifibatide with Proper Hemocompatibility and Cytotoxicity Effect. Iranian Journal of Biotechnology. 2019 Jun 1;17(2):8–13.

476. Rashidi M, Ahmadzadeh A, Ziai SA, Narenji M, Jamshidi H. Evaluating cytotoxic effect of nanoliposomes encapsulated with umbelliprenin on 4T1 cell line. In Vitro CellDevBiol-Animal. 2017 Jan 1;53(1):7–11.

477. Abud MB, Louzada RN, Isaac DLC, Souza LG, dos Reis RG, Lima EM, et al. In vivo and in vitro toxicity evaluation of liposome-encapsulated sirolimus. International Journal of Retina and Vitreous. 2019 Sep 24;5(1):35.

478. López-García J, Lehocký M, Humpolíček P, Sáha P. HaCaT Keratinocytes Response on Antimicrobial Atelocollagen Substrates: Extent of Cytotoxicity, Cell Viability and Proliferation. J Funct Biomater. 2014 May 8;5(2):43–57.

479. Angius F, Floris A. Liposomes and MTT cell viability assay: An incompatible affair. Toxicology in Vitro. 2015 Mar 1;29(2):314–9.

480. Parnham MJ, Wetzig H. Toxicity screening of liposomes. Chemistry and Physics of Lipids. 1993 Sep 1;64(1):263–74.

481. Kato S, Itagaki H, Chiyoda I, Hagino S, Kobayashi T, Fujiyama Y, et al. Liposomes as an in vitro model for predicting the eye irritancy of chemicals. Toxicology in Vitro. 1988 Jan 1;2(2):125–30.

482. Taniguchi K, Yamamoto Y, Itakura K, Miichi H, Hayashi S. Assessment of Ocular Irritability of Liposome Preparations. Journal of Pharmacobio-Dynamics. 1988;11(9):607–11.

483. Budai P, Lehel J, Tavaszi J, Kormos É. HET-CAM test for determining the possible eye irritancy of pesticides. Acta Veterinaria Hungarica. 2010 Aug 16;58(3):369–77.

484. Guillot AJ, Petalas D, Skondra P, Rico H, Garrigues TM, Melero A. Ciprofloxacin self-dissolvable Soluplus based polymeric films: a novel

proposal to improve the management of eye infections. Drug Deliv and Transl Res. 2021 Apr 1;11(2):608–25.

485. Schrage A, Kolle SN, Moreno MCR, Norman K, Raabe H, Curren R, et al. The Bovine Corneal Opacity and Permeability Test in Routine Ocular Irritation Testing and its Improvement within the Limits of OECD Test Guideline 437. Altern Lab Anim. 2011 Mar 1;39(1):37–53.

486. Verstraelen S, Maglennon G, Hollanders K, Boonen F, Adriaens E, Alépée N, et al. Reprint of "CON4EI: Bovine Corneal Opacity and Permeability (BCOP) test for hazard identification and labelling of eye irritating chemicals". Toxicology in Vitro. 2018 Jun 1;49:53–64.

487. Kalweit S, Besoke R, Gerner I, Spielmann H. A national validation project of alternative methods to the Draize rabbit eye test. Toxicology in Vitro. 1990 Jan 1;4(4):702–6.

488. Gilleron L, Coecke S, Sysmans M, Hansen E, van Oproy S, Marzin D, et al. Evaluation of the HET-CAM-TSA method as an alternative to the draize eye irritation test. Toxicology in Vitro. 1997 Oct 1;11(5):641–4.

489. McKenzie B, Kay G, Matthews KH, Knott RM, Cairns D. The hen's egg chorioallantoic membrane (HET-CAM) test to predict the ophthalmic irritation potential of a cysteamine-containing gel: Quantification using Photoshop® and ImageJ. International Journal of Pharmaceutics. 2015 Jul 25;490(1):1–8.

490. Lorenzo-Veiga B, Sigurdsson HH, Loftsson T, Alvarez-Lorenzo C. Cyclodextrin–Amphiphilic Copolymer Supramolecular Assemblies for the Ocular Delivery of Natamycin. Nanomaterials. 2019 May;9(5):745.

491. Zhang YT, Shen LN, Wu ZH, Zhao JH, Feng NP. Comparison of ethosomes and liposomes for skin delivery of psoralen for psoriasis therapy. International Journal of Pharmaceutics. 2014 Aug 25;471(1):449–52.

492. Rzhevskiy AS, Singh TRR, Donnelly RF, Anissimov YG. Microneedles as the technique of drug delivery enhancement in diverse organs and tissues. J Control Release. 2018 Jan 28;270:184–202.

493. Bhatnagar S, Dave K, Venuganti VVK. Microneedles in the clinic. J Control Release. 2017 Aug 28;260:164–82.

494. Cheung K, Das DB. Microneedles for drug delivery: trends and progress. Drug Deliv. 2016 Sep;23(7):2338–54.

495. Singh TRR, Dunne NJ, Cunningham E, Donnelly RF. Review of patents on microneedle applicators. Recent Pat Drug Deliv Formul. 2011 Jan;5(1):11–23.

496. Lhernould MS, Tailler S, Deleers M, Delchambre A. Review of patents for microneedle application devices allowing fluid injections through the skin. Recent Pat Drug Deliv Formul. 2015;9(2):146–57.

497. Bariya SH, Gohel MC, Mehta TA, Sharma OP. Microneedles: an emerging transdermal drug delivery system. Journal of Pharmacy and Pharmacology. 2012 Jan 1;64(1):11–29.

498. Escobar-Chávez JJ, Bonilla-Martínez D, Villegas-González MA, Molina-Trinidad E, Casas-Alancaster N, Revilla-Vázquez AL. Microneedles: a valuable physical enhancer to increase transdermal drug delivery. J Clin Pharmacol. 2011 Jul;51(7):964–77.

499. Prausnitz MR. Engineering Microneedle Patches for Vaccination and Drug Delivery to Skin. Annu Rev Chem Biomol Eng. 2017 Jun 7;8:177–200.

500. Li WZ, Huo MR, Zhou JP, Zhou YQ, Hao BH, Liu T, et al. Super-short solid silicon microneedles for transdermal drug delivery applications. Int J Pharm. 2010 Apr 15;389(1–2):122–9.

501. Gupta J, Gill HS, Andrews SN, Prausnitz MR. Kinetics of skin resealing after insertion of microneedles in human subjects. J Control Release. 2011 Sep 5;154(2):148–55.

502. Larrañeta E, Lutton REM, Woolfson AD, Donnelly RF. Microneedle arrays as transdermal and intradermal drug delivery systems: Materials science, manufacture and commercial development. Materials Science and Engineering: R: Reports. 2016 Jun 1;104:1–32.

503. Kalluri H, Banga AK. Formation and closure of microchannels in skin following microporation. Pharm Res. 2011 Jan;28(1):82–94.

504. Donnelly RF, Singh TRR, Alkilani AZ, McCrudden MTC, O'Neill S, O'Mahony C, et al. Hydrogel-forming microneedle arrays exhibit antimicrobial properties: potential for enhanced patient safety. Int J Pharm. 2013 Jul 15;451(1–2):76–91.

505. Chen Y, Chen BZ, Wang QL, Jin X, Guo XD. Fabrication of coated polymer microneedles for transdermal drug delivery. J Control Release. 2017 Nov 10;265:14–21.

506. Li S, Li W, Prausnitz M. Individually coated microneedles for co-delivery of multiple compounds with different properties. Drug Deliv Transl Res. 2018 Oct;8(5):1043–52.

507. Iliescu F, Dimitrescu-iones D, Petrescu M, Iliescu C. A Review on Transdermal Drug Delivery Using Microneedles: Current Research and Perspective. Annals of Academy of Romanian Scientists Series on Science and Technology of Information. 2014 Jul 1;7:7–34.

508. Koutsonanos DG, del Pilar Martin M, Zarnitsyn VG, Sullivan SP, Compans RW, Prausnitz MR, et al. Transdermal influenza immunization with vaccine-coated microneedle arrays. PLoS One. 2009;4(3):e4773.

509. Rodgers AM, McCrudden MTC, Vincente-Perez EM, Dubois AV, Ingram RJ, Larrañeta E, et al. Design and characterisation of a dissolving microneedle patch for intradermal vaccination with heat-inactivated bacteria: A proof of concept study. Int J Pharm. 2018 Oct 5;549(1–2):87–95.

510. Lee WJ, Han MR, Kim JS, Park JH. A tearable dissolving microneedle system for shortening application time. Expert Opin Drug Deliv. 2019 Mar;16(3):199–206.

511. Ito Y, Yoshimitsu JI, Shiroyama K, Sugioka N, Takada K. Self-dissolving microneedles for the percutaneous absorption of EPO in mice. J Drug Target. 2006 Jun;14(5):255–61.

512. Hong X, Wei L, Wu F, Wu Z, Chen L, Liu Z, et al. Dissolving and biodegradable microneedle technologies for transdermal sustained delivery of drug and vaccine. DDDT. 2013 Sep 4;7:945–52.

513. Zhu DD, Wang QL, Liu XB, Guo XD. Rapidly separating microneedles for transdermal drug delivery. Acta Biomater. 2016 Sep 1;41:312–9.

514. Chen MC, Huang SF, Lai KY, Ling MH. Fully embeddable chitosan microneedles as a sustained release depot for intradermal vaccination. Biomaterials. 2013 Apr 1;34(12):3077–86.

515. Zhu DD, Zhang XP, Shen CB, Cui Y, Guo XD. The maximum possible amount of drug in rapidly separating microneedles. Drug Deliv Transl Res. 2019 Dec;9(6):1133–42.

516. Li W, Terry RN, Tang J, Feng MR, Schwendeman SP, Prausnitz MR. Rapidly separable microneedle patch for the sustained release of a contraceptive. Nat Biomed Eng. 2019 Mar;3(3):220–9.

517. Raj Singh TR, Garland MJ, Migalska K, Salvador EC, Shaikh R, McCarthy HO, et al. Influence of a pore-forming agent on swelling, network parameters, and permeability of poly(ethylene glycol)-crosslinked poly(methyl vinyl ether-co-maleic acid) hydrogels: Application in transdermal delivery systems. Journal of Applied Polymer Science. 2012;125(4):2680–94.

518. Donnelly RF, Singh TRR, Garland MJ, Migalska K, Majithiya R, McCrudden CM, et al. Hydrogel-Forming Microneedle Arrays for Enhanced Transdermal Drug Delivery. Adv Funct Mater. 2012 Dec 5;22(23):4879–90.

519. Norman JJ, Choi SO, Tong NT, Aiyar AR, Patel SR, Prausnitz MR, et al. Hollow microneedles for intradermal injection fabricated by sacrificial micromolding and selective electrodeposition. Biomed Microdevices. 2013 Apr;15(2):203–10.

520. Martanto W, Moore JS, Kashlan O, Kamath R, Wang PM, O'Neal JM, et al. Microinfusion Using Hollow Microneedles. Pharm Res. 2006 Jan 1;23(1):104–13.

521. Rajabi M, Roxhed N, Shafagh RZ, Haraldson T, Fischer AC, Wijngaart W van der, et al. Flexible and Stretchable Microneedle Patches with Integrated Rigid Stainless Steel Microneedles for Transdermal Biointerfacing. PLOS ONE. 2016 Dec 9;11(12):e0166330.

522. Verbaan FJ, Bal SM, van den Berg DJ, Groenink WHH, Verpoorten H, Lüttge R, et al. Assembled microneedle arrays enhance the transport of compounds varying over a large range of molecular weight across human dermatomed skin. J Control Release. 2007 Feb 12;117(2):238–45.

523. Jiang J, Gill HS, Ghate D, McCarey BE, Patel SR, Edelhauser HF, et al. Coated microneedles for drug delivery to the eye. Invest Ophthalmol Vis Sci. 2007 Sep;48(9):4038–43.

524. Li J, Liu B, Zhou Y, Chen Z, Jiang L, Yuan W, et al. Fabrication of a Ti porous microneedle array by metal injection molding for transdermal drug delivery. PLoS One. 2017;12(2):e0172043.

525. Parker ER, Rao M, Foster K, Meinhart C, MacDonald NC. Bulk Micromachined Titanium Microneedles. Microelectromechanical Systems, Journal of. 2007 May 1;16:289–95.

526. Şenel M, Dervisevic M, Voelcker N. Gold microneedles fabricated by casting of gold ink used for urea sensing. Materials Letters. 2019;

527. Davis SP, Martanto W, Allen MG, Prausnitz MR. Hollow metal microneedles for insulin delivery to diabetic rats. IEEE Trans Biomed Eng. 2005 May;52(5):909–15.

528. Indermun S, Luttge R, Choonara YE, Kumar P, du Toit LC, Modi G, et al. Current advances in the fabrication of microneedles for transdermal delivery. J Control Release. 2014 Jul 10;185:130–8.

529. Verhoeven M, Bystrova S, Winnubst L, Qureshi H, de Gruijl TD, Scheper RJ, et al. Applying ceramic nanoporous microneedle arrays as a transport interface in egg plants and an ex-vivo human skin model. Microelectronic Engineering. 2012 Oct 1;98:659–62.

530. van der Maaden K, Luttge R, Vos PJ, Bouwstra J, Kersten G, Ploemen I. Microneedle-based drug and vaccine delivery via nanoporous microneedle arrays. Drug Deliv Transl Res. 2015 Aug;5(4):397–406.

531. Ita K. Ceramic microneedles and hollow microneedles for transdermal drug delivery: Two decades of research. Journal of Drug Delivery Science and Technology. 2018 Apr 1;44:314–22.

532. Wilke N, Mulcahy A, Ye S, Morrissey A. Process optimization and characterization of silicon microneedles fabricated by wet etch technology. Microelectron J. 2005;

533. Das A, Singha C, Bhattacharyya A. Development of silicon microneedle arrays with spontaneously generated micro-cavity ring for transdermal drug delivery. Microelectronic Engineering. 2019 Apr 1;210:14–8.

534. Li Y, Zhang H, Yang R, Laffitte Y, Schmill U, Hu W, et al. Fabrication of sharp silicon hollow microneedles by deep-reactive ion etching towards minimally invasive diagnostics. Microsyst Nanoeng. 2019;5:41.

535. Kim H, Theogarajan L, Pennathur S. A repeatable and scalable fabrication method for sharp, hollow silicon microneedles. 2018;

536. McAllister DV, Wang PM, Davis SP, Park JH, Canatella PJ, Allen MG, et al. Microfabricated needles for transdermal delivery of macromolecules and nanoparticles: fabrication methods and transport studies. Proc Natl Acad Sci U S A. 2003 Nov 25;100(24):13755–60.

537. Gupta J, Park SS, Bondy B, Felner EI, Prausnitz MR. Infusion pressure and pain during microneedle injection into skin of human subjects. Biomaterials. 2011 Oct;32(28):6823–31.

538. Sivamani RK, Liepmann D, Maibach HI. Microneedles and transdermal applications. Expert Opinion on Drug Delivery. 2007 Jan 1;4(1):19–25.

539. Miyano T, Tobinaga Y, Kanno T, Matsuzaki Y, Takeda H, Wakui M, et al. Sugar micro needles as transdermic drug delivery system. Biomed Microdevices. 2005 Sep;7(3):185–8.

540. Lee JW, Choi SO, Felner EI, Prausnitz MR. Dissolving microneedle patch for transdermal delivery of human growth hormone. Small. 2011 Feb 18;7(4):531–9.

541. Raphael AP, Crichton ML, Falconer RJ, Meliga S, Chen X, Fernando GJP, et al. Formulations for microprojection/microneedle vaccine delivery: Structure, strength and release profiles. J Control Release. 2016 Mar 10;225:40–52.

542. Donnelly RF, Morrow DIJ, Singh TRR, Migalska K, McCarron PA, O'Mahony C, et al. Processing difficulties and instability of carbohydrate microneedle arrays. Drug Dev Ind Pharm. 2009 Oct;35(10):1242–54.

543. Sun W, Inayathullah M, Manoukian MAC, Malkovskiy AV, Manickam S, Marinkovich MP, et al. Transdermal Delivery of Functional Collagen Via Polyvinylpyrrolidone Microneedles. Ann Biomed Eng. 2015 Dec;43(12):2978–90.

544. Castañeda PS, Domínguez Delgado CL, Cruz IMR, Contreras LMM, Trinidad EMM, Cervantes ML, et al. Development of Poly (Methyl vinyl ether-alt-maleic acid) Microneedles for Transdermal Delivery of Atorvastatin Calcium. Curr Pharm Biotechnol. 2020;21(9):852–61.

545. Gittard SD, Ovsianikov A, Akar H, Chichkov B, Monteiro-Riviere NA, Stafslien S, et al. Two Photon Polymerization-Micromolding of Polyethylene Glycol-Gentamicin Sulfate Microneedles. Adv Eng Mater. 2010 Apr;12(4):B77–82.

546. Oh JH, Park HH, Do KY, Han M, Hyun DH, Kim CG, et al. Influence of the delivery systems using a microneedle array on the permeation of a hydrophilic molecule, calcein. Eur J Pharm Biopharm. 2008 Aug;69(3):1040–5.

547. Nguyen HX, Bozorg BD, Kim Y, Wieber A, Birk G, Lubda D, et al. Poly (vinyl alcohol) microneedles: Fabrication, characterization, and application for transdermal drug delivery of doxorubicin. Eur J Pharm Biopharm. 2018 Aug;129:88–103.

548. Xiang Z, Wang H, Pant A, Pastorin G, Lee C. Development of vertical SU-8 microneedles for transdermal drug delivery by double drawing lithography technology. Biomicrofluidics. 2013 Dec 6;7(6):066501.

549. Kim JY, Han MR, Kim YH, Shin SW, Nam SY, Park JH. Tip-loaded dissolving microneedles for transdermal delivery of donepezil hydrochloride for treatment of Alzheimer's disease. Eur J Pharm Biopharm. 2016 Aug;105:148–55.

550. Choi JT, Park SJ, Park JH. Microneedles containing cross-linked hyaluronic acid particulates for control of degradation and swelling behaviour after administration into skin. J Drug Target. 2018 Dec;26(10):884–94.

551. Park YH, Ha SK, Choi I, Kim K, Park J, Choi N, et al. Fabrication of degradable carboxymethyl cellulose (CMC) microneedle with laser writing and replica molding process for enhancement of transdermal drug delivery. Biotechnology and Bioprocess Engineering. 2016 Jan 1;21:110–8.

552. Nguyen HX, Banga AK. Delivery of Methotrexate and Characterization of Skin Treated by Fabricated PLGA Microneedles and Fractional Ablative Laser. Pharm Res. 2018 Feb 21;35(3):68.

553. Dharadhar S, Majumdar A, Dhoble S, Patravale V. Microneedles for transdermal drug delivery: a systematic review. Drug Dev Ind Pharm. 2019 Feb;45(2):188–201.

554. de Oliveira RS, Fantaus SS, Guillot AJ, Melero A, Beck RCR. 3D-Printed Products for Topical Skin Applications: From Personalized Dressings to Drug Delivery. Pharmaceutics. 2021 Nov;13(11):1946.

555. Gill HS, Denson DD, Burris BA, Prausnitz MR. Effect of Microneedle Design on Pain in Human Subjects. Clin. J. Pain. 2008 Sep;24 (7): 585–594.

556. Gill HS, Prausnitz MR. Does needle size matter? J Diabetes Sci Technol. 2007 Sep;1(5):725-9.557.

557. Bal SM, Caussin J, Pavel S, Bouwstra JA. In vivo assessment of safety of microneedle arrays in human skin. Eur J Pharm Sci. 2008 Oct 2;35(3):193–202.

558. Donnelly RF, Singh TRR, Tunney MM, Morrow DIJ, McCarron PA, O'Mahony C, et al. Microneedle arrays allow lower microbial penetration than hypodermic needles in vitro. Pharm Res. 2009 Nov;26(11):2513–22.

559. Vicente-Perez EM, Larrañeta E, McCrudden MTC, Kissenpfennig A, Hegarty S, McCarthy HO, et al. Repeat application of microneedles does not alter skin appearance or barrier function and causes no measurable disturbance of serum biomarkers of infection, inflammation or immunity in mice in vivo. Eur J Pharm Biopharm. 2017 Aug;117:400–7.

560. Serhan H, Slivka M, Albert T, Kwak SD. Is galvanic corrosion between titanium alloy and stainless steel spinal implants a clinical concern? Spine J. 2004 Aug;4(4):379–87.

561. Jung P, Lee T, Oh D, Hwang S, Jung I, Lee S, et al. Nickel microneedles fabricated by sequential copper and nickel electroless plating and copper chemical wet etching. Sensors and Materials. 2008 Jan 1;20:45–53.

562. Ermolli M, Menné C, Pozzi G, Serra MA, Clerici LA. Nickel, cobalt and chromium-induced cytotoxicity and intracellular accumulation in human hacat keratinocytes. Toxicology. 2001 Feb 21;159(1–2):23–31.

563. Jeong HR, Lee HS, Choi IJ, Park JH. Considerations in the use of microneedles: pain, convenience, anxiety and safety. J Drug Target. 2017 Jan;25(1):29–40.

564. Li HB, Chen F, Jiang Y. Determination of vitamin B12 in multivitamin tablets and fermentation medium by high-performance liquid chromatography with fluorescence detection. Journal of Chromatography A. 2000 Sep 8;891(2):243–7.

565. Bioanalytical method validation | European Medicines Agency [Internet]. [cited 2022 Jan 11]. Available from: https://www.ema.europa.eu/en/bioanalytical-method-validation

566. Castoldi A, Herr C, Niederstraßer J, Labouta HI, Melero A, Gordon S, et al. Calcifediol-loaded liposomes for local treatment of pulmonary bacterial infections. Eur J Pharm Biopharm. 2017 Sep;118:62–7.

567. El Maghraby GM, Williams AC, Barry BW. Oestradiol skin delivery from ultradeformable liposomes: refinement of surfactant concentration. Int J Pharm. 2000 Feb 25;196(1):63–74.

568. Ong SGM, Ming LC, Lee KS, Yuen KH. Influence of the Encapsulation Efficiency and Size of Liposome on the Oral Bioavailability of Griseofulvin-Loaded Liposomes. Pharmaceutics. 2016 Aug 26;8(3):25.

569. Lin M, Xianrong Q. Purification Method of Drug-Loaded Liposome. In 2019. p. 1–11.

570. Sabeti B, Noordin MI, Mohd S, Hashim R, Dahlan A, Javar HA. Development and characterization of liposomal doxorubicin hydrochloride with palm oil. Biomed Res Int. 2014;2014:765426.

571. Panwar P, Pandey B, Lakhera PC, Singh KP. Preparation, characterization, and in vitro release study of albendazole-encapsulated nanosize liposomes. Int J Nanomedicine. 2010 Mar 9;5:101–8.

572. Keller S, Heerklotz H, Jahnke N, Blume A. Thermodynamics of Lipid Membrane Solubilization by Sodium Dodecyl Sulfate. Biophys J. 2006 Jun 15;90(12):4509–21.

573. Hernández-Borrell J, Pons M, Juarez JC, Estelrich J. The action of Triton X-100 and sodium dodecyl sulphate on lipid layers. Effect on monolayers and liposomes. J Microencapsul. 1990 Jun;7(2):255–9.

574. Igarashi T, Shoji Y, Katayama K. Anomalous solubilization behavior of dimyristoylphosphatidylcholine liposomes induced by sodium dodecyl sulfate micelles. Anal Sci. 2012;28(4):345–50.

575. Sabín J, Prieto X, Sennato S, Blanco E, Messina P, Ruso J, et al. Examination of the influence of F6H10 fluorinated diblocks on DPPC liposomes. Journal of Thermal Analysis and Calorimetry - J THERM ANAL CALORIM. 2007 Jan 1;87:301–4.

576. Baxa U. Imaging of Liposomes by Transmission Electron Microscopy. Methods Mol Biol. 2018;1682:73–88.

577. Celia C, Trapasso E, Cosco D, Paolino D, Fresta M. Turbiscan lab expert analysis of the stability of ethosomes and ultradeformable liposomes containing a bilayer fluidizing agent. Colloids Surf B Biointerfaces. 2009 Aug 1;72(1):155–60.

578. Franzè S, Selmin F, Rocco P, Colombo G, Casiraghi A, Cilurzo F. Preserving the Integrity of Liposomes Prepared by Ethanol Injection upon Freeze-Drying: Insights from Combined Molecular Dynamics Simulations and Experimental Data. Pharmaceutics. 2020 Jun 9;12(6):530.

579. Amis TM, Renukuntla J, Bolla PK, Clark BA. Selection of Cryoprotectant in Lyophilization of Progesterone-Loaded Stearic Acid Solid Lipid Nanoparticles. Pharmaceutics. 2020 Sep 19;12(9):892.

580. Marín M, Gimeno C, Giner RM, Ríos JL, Máñez S, Recio MC. Influence of Dimerization of Apocynin on Its Effects in Experimental Colitis. J Agric Food Chem. 2017 May 24;65(20):4083–91.

581. Bas E, Recio MC, Máñez S, Giner RM, Escandell JM, López-Ginés C, et al. New insight into the inhibition of the inflammatory response to experimental delayed-type hypersensitivity reactions in mice by scropolioside A. Eur J Pharmacol. 2007 Jan 26;555(2–3):199–210.

582. Escandell JM, Recio MC, Máñez S, Giner RM, Cerdá-Nicolás M, Ríos JL. Cucurbitacin R reduces the inflammation and bone damage associated with adjuvant arthritis in lewis rats by suppression of tumor necrosis factor-alpha in T lymphocytes and macrophages. J Pharmacol Exp Ther. 2007 Feb;320(2):581–90.

583. Shaker S, Gardouh AR, Ghorab MM. Factors affecting liposomes particle size prepared by ethanol injection method. Res Pharm Sci. 2017 Oct;12(5):346–52.

584. Lee SC, Lee KE, Kim JJ, Lim SH. The Effect of Cholesterol in the Liposome Bilayer on the Stabilization of Incorporated Retinol. Journal of Liposome Research. 2005 Jan 1;15(3–4):157–66.

585. Coderch L, Fonollosa J, De Pera M, Estelrich J, De La Maza A, Parra JL. Influence of cholesterol on liposome fluidity by EPR. Relationship with percutaneous absorption. J Control Release. 2000 Jul 31;68(1):85–95.

586. Opatha SAT, Titapiwatanakun V, Chutoprapat R. Transfersomes: A Promising Nanoencapsulation Technique for Transdermal Drug Delivery. Pharmaceutics. 2020 Sep 9;12(9):855.

587. Fernández-García R, Lalatsa A, Statts L, Bolás-Fernández F, Ballesteros MP, Serrano DR. Transferosomes as nanocarriers for drugs across the skin: Quality by design from lab to industrial scale. Int J Pharm. 2020 Jan 5;573:118817.

588. Ascenso A, Raposo S, Batista C, Cardoso P, Mendes T, Praça FG, et al. Development, characterization, and skin delivery studies of related ultradeformable vesicles: transfersomes, ethosomes, and transethosomes. Int J Nanomedicine. 2015;10:5837–51.

589. Zeb A, Qureshi OS, Kim HS, Cha JH, Kim HS, Kim JK. Improved skin permeation of methotrexate via nanosized ultradeformable liposomes. Int J Nanomedicine. 2016;11:3813–24.

590. Magarkar A, Dhawan V, Kallinteri P, Viitala T, Elmowafy M, Róg T, et al. Cholesterol level affects surface charge of lipid membranes in saline solution. Sci Rep. 2014 May 21;4:5005.

591. Xu X, Khan MA, Burgess DJ. Predicting hydrophilic drug encapsulation inside unilamellar liposomes. International Journal of Pharmaceutics. 2012 Feb 28;423(2):410–8.

592. Kirby C, Gregoriadis G. Dehydration-Rehydration Vesicles: A Simple Method for High Yield Drug Entrapment in Liposomes. Nat Biotechnol. 1984 Nov;2(11):979–84.

593. Abdulbaqi IM, Darwis Y, Khan NAK, Assi RA, Khan AA. Ethosomal nanocarriers: the impact of constituents and formulation techniques on ethosomal properties, in vivo studies, and clinical trials. Int J Nanomedicine. 2016;11:2279–304.

594. Iskandaryah I, Masrijal C, Harmita H. Effects of sonication on size distribution and entrapment of lynestrenol transfersome. International Journal of Applied Pharmaceutics. 2020 Mar 23;245–7.

595. Wu CS, Guo JH, Lin MJ. Stability Evaluation of pH-Adjusted Goat Milk for Developing Ricotta Cheese with a Mixture of Cow Cheese Whey and Goat Milk. Foods. 2020 Mar 21;9(3):E366.

596. Cristiano MC, Froiio F, Spaccapelo R, Mancuso A, Nisticò SP, Udongo BP, et al. Sulforaphane-Loaded Ultradeformable Vesicles as A Potential Natural Nanomedicine for the Treatment of Skin Cancer Diseases. Pharmaceutics. 2019 Dec 19;12(1):E6.

597. Chen M, Liu X, Fahr A. Skin penetration and deposition of carboxyfluorescein and temoporfin from different lipid vesicular systems: In vitro study with finite and infinite dosage application. Int J Pharm. 2011 Apr 15;408(1–2):223–34.

598. Skrabanja AT, de Meere AL, de Ruiter RA, van den Oetelaar PJ. Lyophilization of biotechnology products. PDA J Pharm Sci Technol. 1994 Dec;48(6):311–7.

599. Mensink MA, Frijlink HW, van der Voort Maarschalk K, Hinrichs WLJ. How sugars protect proteins in the solid state and during drying: Mechanisms of stabilization in relation to stress conditions. European Journal of Pharmaceutics and Biopharmaceutics. 2017 May 1;114:288–95.

600. Garvey CJ, Lenné T, Koster KL, Kent B, Bryant G. Phospholipid Membrane Protection by Sugar Molecules during Dehydration—Insights into Molecular Mechanisms Using Scattering Techniques. Int J Mol Sci. 2013 Apr 12;14(4):8148–63.

601. Rahman MS. Food stability determination by macro–micro region concept in the state diagram and by defining a critical temperature. Journal of Food Engineering. 2010 Aug 1;99(4):402–16.

602. Verdonck E, Schaap K, Thomas LC. A discussion of the principles and applications of Modulated Temperature DSC (MTDSC). Int J Pharm. 1999 Dec 1;192(1):3–20.

603. Lopes L, Scarpa M, Pereira N, Oliveira L, Oliveira A. Interaction of sodium diclofenac with freeze-dried soya phosphatidylcholine and unilamellar liposomes. Revista Brasileira De Ciencias Farmaceuticas - RBCF. 2006 Oct 1;42.

604. Cunha S, Costa CP, Loureiro JA, Alves J, Peixoto AF, Forbes B, et al. Double Optimization of Rivastigmine-Loaded Nanostructured Lipid Carriers (NLC) for Nose-to-Brain Delivery Using the Quality by Design (QbD) Approach: Formulation Variables and Instrumental Parameters. Pharmaceutics. 2020 Jun 28;12(7):E599.

605. Spagnol CM, Zaera AM, Isaac VLB, Corrêa MA, Salgado HRN. Release and permeation profiles of spray-dried chitosan microparticles containing caffeic acid. Saudi Pharm J. 2018 Mar;26(3):410–5.

606. Gulati K, Kant K, Findlay D, Losic D. Periodically tailored titania nanotubes for enhanced drug loading and releasing performances. J Mater Chem B. 2015 Mar 28;3(12):2553–9.

607. Nounou MM, El-Khordagui LK, Khalafallah NA, Khalil SA. In vitro release of hydrophilic and hydrophobic drugs from liposomal dispersions and gels. Acta Pharm. 2006 Sep;56(3):311–24.

608. Lu T, Ten Hagen TLM. A novel kinetic model to describe the ultra-fast triggered release of thermosensitive liposomal drug delivery systems. J Control Release. 2020 Aug 10;324:669–78.

609. Kaur G, Grewal J, Jyoti K, Jain UK, Chandra R, Madan J. Oral controlled and sustained drug delivery systems: Concepts, advances, preclinical, and clinical status. In: Grumezescu AM, editor. Drug Targeting and Stimuli Sensitive Drug Delivery Systems. William Andrew Publishing; 2018. p. 567–626. Available from: https://www.sciencedirect.com/science/article/pii/B978012813689800015X

610. Brazel CS, Huang X. The Cost of Optimal Drug Delivery: Reducing and Preventing the Burst Effect in Matrix Systems. In: Carrier-Based Drug Delivery [Internet]. American Chemical Society; 2004 [cited 2022 Mar 31]. p. 267–82. (ACS Symposium Series; vol. 879). Available from: https://doi.org/10.1021/bk-2004-0879.ch019

611. Chourasia MK, Kang L, Chan SY. Nanosized ethosomes bearing ketoprofen for improved transdermal delivery. Results in Pharma Sciences. 2011 May 1;1(1):60–7.

612. Orlando A, Re F, Sesana S, Rivolta I, Panariti A, Brambilla D, et al. Effect of nanoparticles binding β-amyloid peptide on nitric oxide production by cultured endothelial cells and macrophages. Int J Nanomedicine. 2013;8:1335–47.

613. Cristiano MC, Mancuso A, Giuliano E, Cosco D, Paolino D, Fresta M. EtoGel for Intra-Articular Drug Delivery: A New Challenge for Joint Diseases Treatment. Journal of Functional Biomaterials. 2021 Jun;12(2):34.

614. Mönkkönen J, Valjakka R, Hakasalo M, Urtti A. The effects of liposome surface charge and size on the intracellular delivery of clodronate and gallium in vitro. International Journal of Pharmaceutics. 1994 Jul 11;107(3):189–97.

615. Sguizzato M, Ferrara F, Hallan SS, Baldisserotto A, Drechsler M, Malatesta M, et al. Ethosomes and Transethosomes for Mangiferin Transdermal Delivery. Antioxidants. 2021 May;10(5):768.

616. Permana AD, Tekko IA, McCrudden MTC, Anjani QK, Ramadon D, McCarthy HO, et al. Solid lipid nanoparticle-based dissolving microneedles: A promising intradermal lymph targeting drug delivery system with potential for enhanced treatment of lymphatic filariasis. Journal of Controlled Release. 2019 Dec 28;316:34–52.

617. Liao JF, Lee JC, Lin CK, Wei KC, Chen PY, Yang HW. Self-Assembly DNA Polyplex Vaccine inside Dissolving Microneedles for High-Potency Intradermal Vaccination. Theranostics. 2017;7(10):2593–605.

618. Donnelly RF, Majithiya R, Singh TRR, Morrow DIJ, Garland MJ, Demir YK, et al. Design, optimization and characterisation of polymeric microneedle arrays prepared by a novel laser-based micromoulding technique. Pharm Res. 2011 Jan;28(1):41–57.

619. Larrañeta E, Moore J, Vicente-Pérez EM, González-Vázquez P, Lutton R, Woolfson AD, et al. A proposed model membrane and test method for microneedle insertion studies. International Journal of Pharmaceutics. 2014 Sep 10;472(1):65–73.

620. Larrañeta E, Stewart S, Fallows SJ, Birkhäuer LL, McCrudden MTC, Woolfson AD, et al. A facile system to evaluate in vitro drug release from dissolving microneedle arrays. Int J Pharm. 2016 Jan 30;497(1–2):62–9.

621. Teodorescu M, Bercea M, Morariu S. Biomaterials of PVA and PVP in medical and pharmaceutical applications: Perspectives and challenges. Biotechnol Adv. 2019 Feb;37(1):109–31.

622. Donnelly RF, Moffatt K, Alkilani AZ, Vicente-Pérez EM, Barry J, McCrudden MTC, et al. Hydrogel-forming microneedle arrays can be effectively inserted in skin by self-application: a pilot study centred on pharmacist intervention and a patient information leaflet. Pharm Res. 2014 Aug;31(8):1989–99.

623. Melero A, Hahn T, Schaefer UF, Schneider M. In vitro human skin segmentation and drug concentration-skin depth profiles. Methods Mol Biol. 2011;763:33–50.

624. Permana AD, McCrudden MTC, Donnelly RF. Enhanced Intradermal Delivery of Nanosuspensions of Antifilariasis Drugs Using Dissolving Microneedles: A Proof of Concept Study. Pharmaceutics. 2019 Jul 17;11(7):346.

625. Jacobi U, Kaiser M, Toll R, Mangelsdorf S, Audring H, Otberg N, et al. Porcine ear skin: an in vitro model for human skin. Skin Res Technol. 2007 Feb;13(1):19–24.

626. Yang Y, Kalluri H, Banga AK. Effects of chemical and physical enhancement techniques on transdermal delivery of cyanocobalamin (vitamin B12) in vitro. Pharmaceutics. 2011 Aug 10;3(3):474–84.

627. Gray GM, Yardley HJ. Lipid compositions of cells isolated from pig, human, and rat epidermis. J Lipid Res. 1975 Nov;16(6):434–40.

628. Jung EC, Maibach HI. Animal models for percutaneous absorption. J Appl Toxicol. 2015 Jan;35(1):1–10.

629. Nakamura A, Mori D, Tojo K. Evaluation of the predicted time-concentration profile of serum tulobuterol in human after transdermal application. Chem Pharm Bull (Tokyo). 2012;60(3):300–5.

630. Hatanaka T, Yoshida S, Kadhum WR, Todo H, Sugibayashi K. In Silico Estimation of Skin Concentration Following the Dermal Exposure to Chemicals. Pharm Res. 2015 Dec;32(12):3965–74.

631. Moghimipour E, Salimi A, Zadeh BSM. Effect of the Various Solvents on the In Vitro Permeability of Vitamin B12 through Excised Rat Skin. Tropical Journal of Pharmaceutical Research. 2013 Oct 29;12(5):671–7.

632. Howe EE, Dooley CL, Geoffroy RF, Rosenblum C. Percutaneous absorption of vitamin B12 in the rat and guinea pig. J Nutr. 1967 Jun;92(2):261–6.

633. El Maghraby GM. Occlusive and Non-Occlusive Application of Microemulsion for Transdermal Delivery of Progesterone: Mechanistic Studies. Sci Pharm. 2012;80(3):765–78.

634. Defraeye T, Bahrami F, Ding L, Malini RI, Terrier A, Rossi RM. Predicting Transdermal Fentanyl Delivery Using Mechanistic Simulations for Tailored Therapy. Front Pharmacol. 2020 Sep 29;11:585393.

635. Bragagni M, Mennini N, Maestrelli F, Cirri M, Mura P. Comparative study of liposomes, transfersomes and ethosomes as carriers for improving topical delivery of celecoxib. Drug Deliv. 2012 Oct;19(7):354–61.

636. Romero EL, Morilla MJ. Highly deformable and highly fluid vesicles as potential drug delivery systems: theoretical and practical considerations. Int J Nanomedicine. 2013;8:3171–86.

637. Guo L, Chen J, Qiu Y, Zhang S, Xu B, Gao Y. Enhanced transcutaneous immunization via dissolving microneedle array loaded with liposome encapsulated antigen and adjuvant. International Journal of Pharmaceutics. 2013 Apr 15;447(1):22–30.

638. Ogunjimi AT, Lawson C, Carr J, Patel KK, Ferguson N, Brogden NK. Micropore Closure Rates following Microneedle Application at Various Anatomical Sites in Healthy Human Subjects. Skin Pharmacol Physiol. 2021;34(4):214–28.

639. Hofmann MCJ, Schmidt M, Arne O, Geisslinger G, Parnham MJ, de Bruin NMWJ. Non-invasive bioluminescence imaging as a standardized assessment measure in mouse models of dermal inflammation. J Dermatol Sci. 2018 Apr 23;S0923-1811(18)30187-7.

640. Heo YS, Song HJ. Characterizing cutaneous elastic fibers by eosin fluorescence detected by fluorescence microscopy. Ann Dermatol. 2011 Feb;23(1):44–52.

641. Mao H, Su P, Qiu W, Huang L, Yu H, Wang Y. The use of Masson's trichrome staining, second harmonic imaging and two-photon excited fluorescence of collagen in distinguishing intestinal tuberculosis from Crohn's disease. Colorectal Dis. 2016 Dec;18(12):1172–8.

642. Qin W, Wang RK. Assessment of edema volume in skin upon injury in a mouse ear model with optical coherence tomography. Lasers Med Sci. 2016 Sep;31(7):1351–61.

643. Hartono SP, Bedell VM, Alam SkK, O'Gorman M, Serres M, Hall SR, et al. Vascular Endothelial Growth Factor as an Immediate-Early Activator of Ultraviolet-Induced Skin Injury. Mayo Clinic Proceedings. 2022 Jan 1;97(1):154–64.

644. Aske KC, Waugh CA. Expanding the 3R principles. EMBO Rep. 2017 Sep;18(9):1490–2.

645. Abraham A, Roga G. Topical Steroid-Damaged Skin. Indian J Dermatol. 2014;59(5):456–9.

646. Barnes L, Kaya G, Rollason V. Topical corticosteroid-induced skin atrophy: a comprehensive review. Drug Saf. 2015 May;38(5):493–509.

647. Tuckermann JP, Kleiman A, Moriggl R, Spanbroek R, Neumann A, Illing A, et al. Macrophages and neutrophils are the targets for immune suppression by glucocorticoids in contact allergy. J Clin Invest. 2007 May;117(5):1381–90.

648. Alshetaiwi HS, Balivada S, Shrestha TB, Pyle M, Basel MT, Bossmann SH, et al. Luminol-based bioluminescence imaging of mouse mammary tumors. J Photochem Photobiol B. 2013 Oct 5;127:223–8.

649. Gross S, Gammon ST, Moss BL, Rauch D, Harding J, Heinecke JW, et al. Bioluminescence imaging of myeloperoxidase activity in vivo. Nat Med. 2009 Apr;15(4):455–61.

650. Zhang N, Francis KP, Prakash A, Ansaldi D. Enhanced detection of myeloperoxidase activity in deep tissues through luminescent excitation of near-infrared nanoparticles. Nat Med. 2013 Apr;19(4):500–5.

# Annex I

## Cyanocobalamin HPLC chromatogram

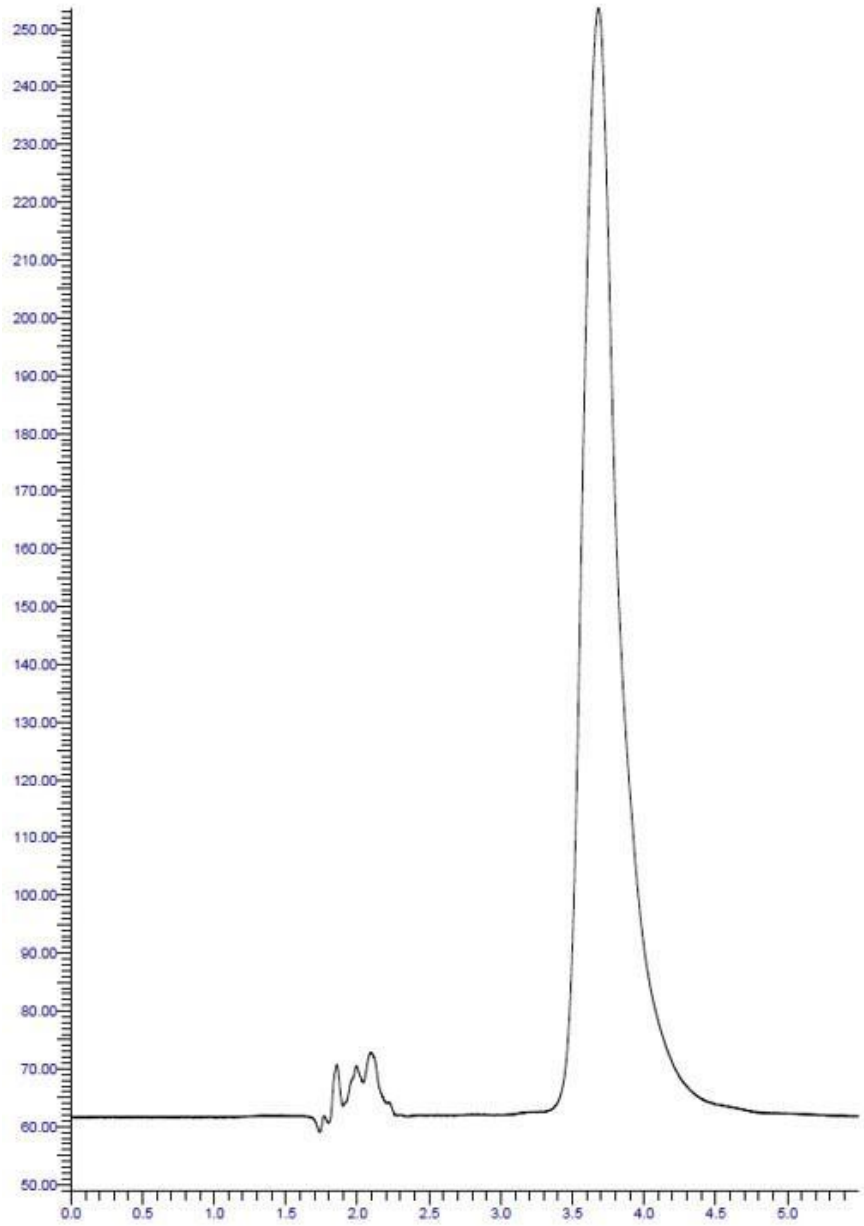


**Figure S1.** Chromatogram obtained from a B12 standard.

# Annex II

## Kinetic model fitting parameters

**Table S1.** Lipid vesicle release parameters (10 h) for Higuchi kinetic model.
All results are expressed as mean ± SD (n=6).

| | Higuchi model | | | | | | | |
|---|---|---|---|---|---|---|---|---|
| | **L1** | **L2** | **T1c** | **T2c** | **T1d** | **T2d** | **E1** | **S** |
| **k** | 9.12 ± 0.51 | 10.36 ± 0.63 | 14.51 ± 0.65 | 11.30 ± 0.76 | 16.70 ± 1.56 | 11.30 ± 0.87 | 14.31 ± 1.30 | 21.80 ± 1.50 |

**Table S2.** Lipid vesicle release parameters (72 h) Higuchi for kinetic model.
All results are expressed as mean ± SD (n=6).

| | Higuchi model | | | | | | | |
|---|---|---|---|---|---|---|---|---|
| | **L1** | **L2** | **T1c** | **T2c** | **T1d** | **T2d** | **E1** | **S** |
| **k** | 7.32 ± 0.13 | 8.92 ± 0.35 | 11.68 ± 0.36 | 13.03 ± 0.59 | 12.19 ± 0.97 | 13.03 ± 0.45 | 13.83 ± 1.08 | 15.85 ± 2.97 |

**Table S3.** Lipid vesicle release parameters (10 h) for Korsmeyer-Peppas kinetic model.
All results are expressed as mean ± SD (n=6).

| | Korsmeyer-Peppas model | | | | | | | |
|---|---|---|---|---|---|---|---|---|
| | **L1** | **L2** | **T1c** | **T2c** | **T1d** | **T2d** | **E1** | **S** |
| **kd** | 5.41 ± 0.33 | 5.85 ± 0.65 | 9.07 ± 2.40 | 10.87 ± 0.54 | 9.96 ± 1.63 | 6.57 ± 1.26 | 9.93 ± 1.27 | 13.35 ± 2.65 |
| **n** | 0.77 ± 0.02 | 0.80 ± 0.03 | 0.75 ± 0.08 | 0.68 ± 0.02 | 0.76 ± 0.04 | 0.86 ± 0.11 | 0.69 ± 0.03 | 0.76 ± 0.05 |

**Table S4.** Lipid vesicle release parameters (72 h) for Korsmeyer-Peppas kinetic model. All results are expressed as mean ± SD (n=6).

| | Korsmeyer-Peppas model | | | | | | | |
|---|---|---|---|---|---|---|---|---|
| | **L1** | **L2** | **T1c** | **T2c** | **T1d** | **T2d** | **E1** | **S** |
| **kd** | 11.31 ± 0.34 | 12.59 ± 0.72 | 18.18 ± 1.08 | 19.75 ± 1.29 | 21.07 ± 2.05 | 15.23 ± 1.23 | 16.75 ± 2.50 | 29.22 ± 4.55 |
| **n** | 0.36 ± 0.05 | 0.39 ± 0.01 | 0.36 ± 0.01 | 0.36 ± 0.01 | 0.33 ± 0.02 | 0. 41 ± 0.01 | 0.44 ± 0.03 | 0.31 ± 0.02 |

**Table S5.** Lipid vesicle release parameters (10 h) for Kim kinetic model.
All results are expressed as mean ± SD (n=6).

| | Kim model | | | | | | | |
|---|---|---|---|---|---|---|---|---|
| | **L1** | **L2** | **T1c** | **T2c** | **T1d** | **T2d** | **E1** | **S** |
| **kd** | 5.41 ± 0.33 | 5.85 ± 0.65 | 9.07 ± 2.40 | 10.87 ± 0.54 | 9.90 ± 1.63 | 6.57 ± 1.26 | 9.93 ± 1.27 | 13.35 ± 2.65 |
| **n** | 0.77 ± 0.02 | 0.80 ± 0.03 | 0.75 ± 0.08 | 0.68 ± 0.02 | 0.76 ± 0.76 | 0.86 ± 0.11 | 0.69 ± 0.03 | 0.76 ± 0.05 |
| **b** | 0 ± 0 | 0 ± 0 | 0 ± 0 | 0 ± 0 | 0 ± 0 | 0 ± 0 | 0 ± 0 | 0 ± 0 |

**Table S6.** Lipid vesicle release parameters (72 h) for Kim kinetic model.
All results are expressed as mean ± SD (n=6).

| | Kim model | | | | | | | |
|---|---|---|---|---|---|---|---|---|
| | **L1** | **L2** | **T1c** | **T2c** | **T1d** | **T2d** | **E1** | **S** |
| **kd** | 11.31 ± 0.34 | 12.59 ± 0.72 | 18.18 ± 1.08 | 19.75 ± 1.29 | 21.07 ± 2.05 | 15.23 ± 1.23 | 16.75 ± 2.50 | 29.22 ± 4.55 |
| **n** | 0.36 ± 0.05 | 0.39 ± 0.01 | 0.36 ± 0.01 | 0.36 ± 0.01 | 0.33 ± 0.02 | 0. 41 ± 0.01 | 0.44 ± 0.03 | 0.31 ± 0.02 |
| **b** | 0 ± 0 | 0 ± 0 | 0 ± 0 | 0 ± 0 | 0 ± 0 | 0 ± 0 | 0 ± 0 | 0 ± 0 |

**Table S7.** Lipid vesicle release parameters (10 h) for Peppas-Sahlin kinetic model.
All results are expressed as mean ± SD (n=6).

| | Peppas-Sahlin model | | | | | | | |
|---|---|---|---|---|---|---|---|---|
| | **L1** | **L2** | **T1c** | **T2c** | **T1d** | **T2d** | **E1** | **S** |
| **$K_1$** | 2.89 ± 0.31 | 2.68 ± 0.15 | 0 ± 0 | 6.15 ± 1.45 | 0 ± 0 | 3.42 ± 1.86 | 5.63 ± 0.52 | 13.33 ± 2.65 |
| **$K_2$** | 2.99 ± 0.45 | 3.49 ± 0.58 | 9.07 ± 2.13 | 5.26 ± 1.17 | 9.90 ± 1.50 | 3.64 ± 2.20 | 4.77 ± 3.45 | 0 ± 0 |
| **n** | 0.45 ± 0.02 | 0.46 ± 0.02 | 0.37 ± 0.03 | 0.42 ± 0.03 | 0.38 ± 0.02 | 0.50 ± 0.07 | 0.48 ± 0.09 | 0.38 ± 0.02 |

**Table S8.** Lipid vesicle release parameters (72 h) for Peppas-Sahlin kinetic model.
All results are expressed as mean ± SD (n=6).

| | Peppas-Sahlin model | | | | | | | |
|---|---|---|---|---|---|---|---|---|
| | **L1** | **L2** | **T1c** | **T2c** | **T1d** | **T2d** | **E1** | **S** |
| **$K_1$** | 3.78 ± 0.32 | 5.71 ± 1.07 | 7.78 ± 0.26 | 7.92 ± 0.04 | 8.97 ± 0.86 | 6.56 ± 0.41 | 6.60 ± 0.91 | 17.14 ± 2.29 |
| **$K_2$** | 4.34 ± 0.44 | 7.45 ± 1.58 | 11.05 ± 0.85 | 12.48 ± 0.64 | 12.72 ± 1.72 | 9.34 ± 0.88 | 10.93 ± 1.60 | 3.30 ± 0.83 |
| **n** | 0.25 ± 0.007 | 0.23 ± 0.24 | 0.21 ± 0.007 | 0.20 ± 0.006 | 0.19 ± 0.01 | 0.23 ± 0.008 | 0.24 ± 0.02 | 0.43 ± 0.02 |

**Table S9.** Lipid vesicle release parameters (10 h) for zero order kinetic model.
All results are expressed as mean ± SD (n=6).

| | Zero order model | | | | | | | |
|---|---|---|---|---|---|---|---|---|
| | **L1** | **L2** | **T1c** | **T2c** | **T1d** | **T2d** | **E1** | **S** |
| **Kd** | 3.46 ± 0.06 | 3.90 ± 0.02 | 5.49 ± 0.29 | 5.80 ± 0.31 | 6.12 ± 0.58 | 4.97 ± 0.35 | 5.39 ± 0.05 | 8.26 ± 0.09 |

**Table S10.** Lipid vesicle release parameters (72 h) for zero order kinetic model.
All results are expressed as mean ± SD (n=6).

| | Zero order model | | | | | | | |
|---|---|---|---|---|---|---|---|---|
| | **L1** | **L2** | **T1c** | **T2c** | **T1d** | **T2d** | **E1** | **S** |
| **Kd** | 0.96 ± 0.86 | 1.19 ± 0.04 | 1.53 ± 0.07 | 1.63 ± 0.09 | 1.57 ± 0.12 | 1.52 ± 0.05 | 1.89 ± 0.01 | 2.02 ± 0.02 |

**Table S11.** Lipid vesicle release parameters (10 h) for zero order kinetic model.
All results are expressed as mean ± SD (n=6).

| | First order model | | | | | | | |
|---|---|---|---|---|---|---|---|---|
| | **L1** | **L2** | **T1c** | **T2c** | **T1d** | **T2d** | **E1** | **S** |
| **Kd** | 0.04 ± 0.001 | 0.04 ± 0.008 | 0.07 ± 0.004 | 0.07 ± 0.005 | 0.08 ± 0.01 | 0.06 ± 0.005 | 0.07 ± 0.009 | 0.13 ± 0.002 |

**Table S12.** Lipid vesicle release parameters (72 h) for zero order kinetic model.
All results are expressed as mean ± SD (n=6).

| | First order model | | | | | | | |
|---|---|---|---|---|---|---|---|---|
| | **L1** | **L2** | **T1c** | **T2c** | **T1d** | **T2d** | **E1** | **S** |
| **Kd** | 0.02 ± 0.001 | 0.03 ± 0.002 | 0.06 ± 0.005 | 0.07 ± 0.007 | 0.07 ± 0.01 | 0.05 ± 0.006 | 0.07 ± 0.01 | 0.12 ± 0.02 |

**Table S13.** AIC values of the different kinetic models for lipid vesicles release data (10 h). All results are expressed as mean (n=6).

| | AIC 10 h | | | | | | | |
|---|---|---|---|---|---|---|---|---|
| | **L1** | **L2** | **T1c** | **T2c** | **T1d** | **T2d** | **E1** | **S** |
| **Higuchi** | 44.75 | 52.77 | 48.21 | 47.88 | 55.28 | 56.56 | 46.57 | 61.35 |
| **Korsmeyer- Peppas** | 18.06 | 48.21 | 31.89 | 24.95 | 30.15 | 32.51 | 17.21 | 37.41 |
| **Kim** | 18.06 | 48.21 | 31.89 | 24.95 | 30.15 | 32.51 | 17.21 | 37.41 |
| **Peppas- Sahlin** | 22.84 | 14.33 | 33.89 | 27.67 | 32.15 | 35.20 | 14.33 | 39.41 |
| **Zero order** | 37.44 | 36.38 | 49.60 | 54.18 | 50.43 | 38.80 | 14.33 | 56.48 |
| **First order** | 26.30 | 17.75 | 34.32 | 39.01 | 18.20 | 32.76 | 38.46 | 35.17 |

**Table S14.** AIC values of the different kinetic models for lipid vesicles release data (72 h). All results are expressed as mean (n=6).

| | AIC 72 h | | | | | | | |
|---|---|---|---|---|---|---|---|---|
| | **L1** | **L2** | **T1c** | **T2c** | **T1d** | **T2d** | **E1** | **S** |
| **Higuchi** | 80.90 | 95.75 | 87.80 | 87.24 | 100.90 | 91.28 | 96.13 | 110.50 |
| **Korsmeyer- Peppas** | 76.04 | 87.80 | 89.00 | 89.30 | 91.98 | 89.04 | 96.59 | 100.60 |
| **Kim** | 76.04 | 87.80 | 89.00 | 89.30 | 91.98 | 89.04 | 96.59 | 100.60 |
| **Peppas- Sahlin** | 91.91 | 87.81 | 91.85 | 92.08 | 34.69 | 91.93 | 99.22 | 97.46 |
| **Zero order** | 107.29 | 111.64 | 119.71 | 121.45 | 122.57 | 116.72 | 99.22 | 130.60 |
| **First order** | 108.83 | 99.58 | 92.05 | 86.75 | 93.82 | 89.29 | 73.66 | 52.81 |

**Table S15.** $R^2$ values of Korsmeyer-Peppas and First order kinetic models for lipid vesicles release data (10 h). All results are expressed as mean (n=6).

| | $R^2$ 10 h | | | | | | | |
|---|---|---|---|---|---|---|---|---|
| | **L1** | **L2** | **T1c** | **T2c** | **T1d** | **T2d** | **E1** | **S** |
| **Korsmeyer- Peppas** | 0.996 | 0.999 | 0.994 | 0.997 | 0.996 | 0.993 | 0.998 | 0.996 |
| **First order** | 0.995 | 0.998 | 0.994 | 0.994 | 0.997 | 0.992 | 0.994 | 0.997 |

**Table S16.** $R^2$ values of Korsmeyer-Peppas and First order kinetic models for lipid vesicles release data (72 h). All results are expressed as mean (n=6).

| | $R^2$ 72 h | | | | | | | |
|---|---|---|---|---|---|---|---|---|
| | **L1** | **L2** | **T1c** | **T2c** | **T1d** | **T2d** | **E1** | **S** |
| **Korsmeyer- Peppas** | 0.916 | 0.899 | 0.911 | 0.917 | 0.890 | 0.916 | 0.908 | 0.868 |
| **First order** | 0.879 | 0.884 | 0.891 | 0.915 | 0.881 | 0.915 | 0.917 | 0.935 |

**Table S-17.** MNA release parameters for Korsmeyer-Peppas model. All results are expressed as mean ± SD (n=3).

| | Korsmeyer-Peppas | | | | | | | | |
|---|---|---|---|---|---|---|---|---|---|
| | **F1** | **F2** | **F3** | **F4** | **F5** | **F6** | **F7** | **F9** | **F11** |
| **kd** | 28.05 ± 8.92 | 24.09 ± 7.05 | 25.87 ± 3.64 | 12.79 ± 2.61 | 7.22 ± 0.72 | 7.07 ± 1.05 | 3.45 ± 1.57 | 59.22 ± 1.43 | 21.52 ± 3.01 |
| **n** | 0.27 ± 0.06 | 0.29 ± 0.03 | 0.28 ± 0.01 | 0.40 ± 0.03 | 0.50 ± 0.02 | 0.50 ± 0.02 | 0.62 ± 0.06 | 0.11 ± 0.01 | 0.30 ± 0.02 |

**Table S18.** MNA release parameters for K*im* model. All results are expressed as mean ± SD (n=3).

| | Kim | | | | | | | | |
|---|---|---|---|---|---|---|---|---|---|
| | **F1** | **F2** | **F3** | **F4** | **F5** | **F6** | **F7** | **F9** | **F11** |
| **kd** | 28.05 ± 8.92 | 24.09 ± 7.05 | 25.87 ± 3.64 | 12.79 ± 2.61 | 7.22 ± 0.72 | 7.07 ± 1.05 | 3.45 ± 1.57 | 59.22 ± 1.43 | 21.52 ± 3.01 |
| **n** | 0.27 ± 0.06 | 0.29 ± 0.03 | 0.28 ± 0.01 | 0.40 ± 0.03 | 0.50 ± 0.02 | 0.50 ± 0.02 | 0.62 ± 0.06 | 0.11 ± 0.01 | 0.30 ± 0.02 |
| **b** | 0 ± 0 | 0 ± 0 | 0 ± 0 | 0 ± 0 | 0 ± 0 | 0 ± 0 | 0 ± 0 | 0 ± 0 | 0 ± 0 |

# Annex III

## Experimental protocol authorizations

VNIVERSITAT DE VALÈNCIA

**Vicerectorat d'Investigació**

D. José María Montiel Company, Profesor Contratado Doctor del departamento de Estomatología, y secretario del Comité Ético de Investigación en Humanos de la Comisión de Ética en Investigación Experimental de la Universitat de Valencia,

CERTIFICA:

Que el Comité Ético de Investigación en Humanos, en la reunión celebrada el día 8 de noviembre de 2018, una vez estudiado el proyecto de investigación titulado:

"Estudio de la absorción de activos cosméticos y farmacéuticos a través de piel humana y porcina" número de procedimiento H1540295606992 cuyo responsable es Ana Melero Zaera ha acordado informar favorablemente el mismo dado que se respetan los principios fundamentales establecidos en la Declaración de Helsinki, en el Convenio del Consejo de Europa relativo a los derechos humanos y cumple los requisitos establecidos en la legislación española en el ámbito de la investigación biomédica, la protección de datos de carácter personal y la bioética.

Y para que conste, se firma el presente certificado en Valencia, a doce de noviembre de dos mil dieciocho.

GENERALITAT VALENCIANA
Conselleria de Agricultura, Desarrollo Rural, Emergencia Climática y Transición Ecológica

**Dirección General de Agricultura, Ganadería y Pesca**
Ciudad Administrativa 9 de Octubre Calle de La Democracia, 77 · 46018 Valencia
www.gva. es

UNIÓN EUROPEA

**AUTORIZACION PROCEDIMIENTO 2021/VSC/PEA/0182**

Vista la solicitud realizada en fecha **08/07/21** con nº reg. entrada **1755239** por D/Dª. **Carlos Hermenegildo Caudevilla**, **Vicerrector de Investigación y Política Científica**, centro usuario **ES460780001001**, para realizar el procedimiento:

***"Tratamiento de la dermatitis atópica mediante vesículas lipídicas ultraflexibles de ciclosporina y cianocobalamina"***

Teniendo en cuenta la documentación aportada, según se indica en el artículo 33, punto 5 y 6, y puesto que dicho procedimiento se halla sujeto a autorización en virtud de lo dispuesto en el artículo 31 del Real Decreto 53/2013, de 1 de febrero,

Vista la propuesta del jefe del servicio de Producción y Sanidad Animal.

**AUTORIZO:**

la realización de dicho procedimiento al que se le asigna el código: **2021/VSC/PEA/0182** tipo **2,** de acuerdo con las características descritas en la propia documentación para el número de animales, especie y periodo de tiempo solicitado. Todo ello sin menoscabo de las autorizaciones pertinentes, por otras Administraciones y entidades, y llevándose a cabo en las siguientes condiciones:

Usuario: **Universitat de València**

Responsable del proyecto: **Ana Melero Zaera**

Establecimiento: **Sección de Producción Animal SCSIE-Campus Burjassot**

Necesidad de evaluación restrospectiva:

Condiciones específicas:

Observaciones:

Valencia a, fecha de la firma electrónica
El director general de Agricultura, Ganadería y Pesca

Firmado por Antonio Quintana Martínez el 10/08/2021 11:39:32
Cargo: Director General de Agricultura, Ganadería y Pesca